CANCER CHEMOTHERAPY REPORTS

Part 1

July/Aug 1975
Vol. 59, No. 4

Cancer Chemotherapy Reports

National Cancer Institute

Frank J. Rauscher, Jr., *Director*

Division of Cancer Treatment

Vincent T. DeVita, Jr., *Director*

SCIENTIFIC EDITORS

J.A.R. Mead *Editor in Chief*
Richard H. Adamson
Vincent H. Bono, Jr.
Bruce A. Chabner
Patrick J. Creaven
Peter H. Wiernik

EDITORIAL STAFF

Pamela W. Hutchins, *Managing Editor*
Assistant Editors:
Cynthia K. Muse
Jean M. Griffin
Editorial Assistants:
Virginia T. Ascosi
Elaine P. Beck

EDITORIAL POLICY

Original contributions are welcome on all aspects of the treatment of cancer. Preliminary reports of work in progress are acceptable to facilitate the prompt exchange of information among investigators in this field. Letters pertinent to published articles, commentaries, and reviews may also be submitted. Requests for the publication of symposia will be considered provided a complete edited transcript of the proceedings is submitted.

Manuscripts should be addressed to: Managing Editor, Cancer Chemotherapy Reports, National Cancer Institute, Bethesda, Maryland 20014

INSTRUCTIONS TO AUTHORS

Summary
Begin the article with a short summary.

Text
Submit an original and three copies of the manuscript, typed double spaced. Each page should begin with a new paragraph. Use accepted spelling, abbreviation, and hyphenation found in *Webster's New International Dictionary*. Footnotes should be typed at the bottom of the page on which they appear.

Tables
Submit each table on a separate page, typed double spaced. Please use standard abbreviations; otherwise spell out.

References
Submit references typed double spaced. Follow the standard form of *Index Medicus:* author, title, name of journal, volume number, page or inclusive pages, and year. In book references, give author, title of book, edition (if more than one), city, name of publisher, date of book,volume number, and pages cited. References in text should begin with number 1 and continue consecutively.

Illustrations
Photographs and graphs preferably should be clear, glossy prints. Original artwork should be done in black ink for good reproduction. Please send 2 copies of each print.

Nomenclature
Names of compounds should conform to American usage. See *Chemical Abstracts* for proper nomenclature.

Abbreviations
Only standard abbreviations are acceptable. If a new or coined abbreviation is used, it must be defined when first mentioned.

Reprints
Supplied free of charge: 250 reprints will be sent to the senior author about three weeks after publication of the article.

SUBSCRIPTIONS

Cancer Chemotherapy Reports is for sale by the Superintendent of Documents, US Government Printing Office, Washington, DC 20402. The yearly subscription rate is $38.35 domestic, with an additional $9.60 for foreign mailing. The prices vary for individual issues. Payment is required in advance; check or money order should be made payable to the Superintendent of Documents. Please specify List ID "CAN" when requesting a subscription.

Contents

Cancer Chemotherapy Reports
Vol. 59, No. 4
July/Aug 1975

Page

LETTER

Contact Dermatitis Associated With Adriamycin (NSC-123127) and Daunorubicin (NSC-82151) 677
Steven D. Reich and Nicholas R. Bachur
Baltimore Cancer Research Center, Maryland

COMMENTARY

The Role of Structure-Activity Studies in the Design of Antitumor Agents 679
Bruce F. Cain
Cancer Chemotherapy Laboratory, Auckland, New Zealand

ARTICLES

Chemical Assay for the Antitumor Agent Inosine Dialdehyde (NSC-118994) in Biologic Fluids 685
Richard L. Cysyk
National Cancer Institute, Bethesda, Maryland

Enhancement of the Effectiveness of Daunorubicin (NSC-82151) or Adriamycin (NSC-123127) Against Early Mouse L1210 Leukemia With ICRF-159 (NSC-129943) 689
R. J. Woodman, R. L. Cysyk, I. Kline, M. Gang, and J. M. Venditti
Microbiological Associates, Inc., Bethesda, Maryland

Effects of Levamisole (NSC-177023) and Tetramisole (NSC-102063) in Experimental Tumor Systems 697
Randall K. Johnson, David P. Houchens, Marilyn R. Gaston, and Abraham Goldin
National Cancer Institute, Bethesda, Maryland

Toxicologic Screening of Daunorubicin (NSC-82151), Adriamycin (NSC-123127), and Their Derivatives in Rats 707
Gerhard Zbinden and Elisabeth Brändle
University of Zurich, Switzerland

Inhibition of Deamination of ^{14}C-Cytosine Arabinoside (NSC-63878): A Useful Biologic Assay for Tetrahydrouridine (NSC-112907) 717
R. L. Furner and L. B. Mellett
Southern Research Institute, Birmingham, Alabama

Potential Biologic Markers in Burkitt's Lymphoma 721
T. Phillip Waalkes, Charles W. Gehrke, Werner A. Bleyer, Robert W. Zumwalt, Charles L. M. Olweny, Kenneth C. Kuo, Duane B. Lakings, and Samuel A. Jacobs
National Cancer Institute, Bethesda, Maryland

Review of Selected Experimental Brain Tumor Models Used in Chemotherapy Experiments 729
Philip C. Merker, Isidore Wodinsky, and Ruth I. Geran
Arthur D. Little, Inc., Cambridge, Massachusetts

Clinical Study of the New Podophyllotoxin Derivative, 4'-Demethylepipodophyllotoxin 9-(4,6-*O*-ethylidene-β-D-glucopyranoside) (NSC-141540; VP-16-213), in Solid Tumors in Man 737
Walter Felix Jungi and Hans Joerg Senn
Medizinische Klinik C Kantonsspital, St. Gallen, Switzerland

4'-Demethylepipodophyllotoxin 9-(4,6-*O*-2-thenylidene-β D-glucopyranoside) (NSC-122819; VM-26) and 4'-Demethylepipodophyllotoxin 9-(4,6-*O*-ethylidene-β-D-glucopyranoside) (NSC-141540; VP-16-213) in Childhood Cancer: Preliminary Observations 743
Gaston Rivera, Thomas Avery, and Charles Pratt
St. Jude Children's Research Hospital, Memphis, Tennessee

Phase I Clinical Trial of Isophosphamide (NSC-109724) 751
M. H. Cohen, P. J. Creaven, F. Tejada, H. H. Hansen, F. Muggia, A. Mittelman, and O. S. Selawry
National Cancer Institute-Veterans' Administration Medical Oncology Branch, Washington, DC

Daunorubicin (NSC-82151), Vincristine (NSC-67574), Cytosine Arabinoside (NSC-63878), and Prednisone (NSC-10023) Combination Therapy for Advanced Adult Acute Leukemia 757
C. Patrick Burns
University of Iowa College of Medicine, Iowa City

BRIEF REPORTS AND PRELIMINARY COMMUNICATIONS

Phase II Study of ICRF-159 (NSC-129943) in Advanced Colorectal Carcinoma 761
T. A. Marciniak, C. G. Moertel, A. J. Schutt, R. G. Hahn, and R. J. Reitemeier
Mayo Clinic, Rochester, Minnesota

Cardiac Uptake of Adriamycin (NSC-123127) Not Affected by Strophanthin G (NSC-25485) 765
Nicholas R. Bachur, William Reiter, and Emanuela Arena
Baltimore Cancer Research Center, Maryland

Treatment of Malignant Melanoma With Vinblastine (NSC-49842), Procarbazine (NSC-77213), and Actinomycin D (NSC-3053) 767
Elliott Perlin, James Engeler, James W. Reid, Julian L. Lokey, and John Kostinas
National Naval Medical Center, Bethesda, Maryland

Combination Chemotherapy With CCNU (NSC-79037) and 5-[3,3-Bis(2-chloroethyl)-1-triazeno]imidazole-4-carboxamide (NSC-82196) 769
Hui-Yen Chang, Emil J Freireich, Abdul Khaliq, Lawrence Einhorn, and Jeffrey A. Gottlieb
M. D. Anderson Hospital and Tumor Institute, Houston, Texas

Proceedings of the Symposium on PHARMACOKINETIC MODELING OF ANTICANCER DRUGS: November 10-14, 1974

Opening Remarks 775
Ti Li Loo
University of Texas System Cancer Center, Houston

Some Fundamental Considerations of the Applications of Pharmacokinetics to Cancer Chemotherapy 777
Kenneth B. Bischoff
Cornell University, Ithaca, New York

Pharmacokinetic Considerations on Resistance to Anticancer Drugs 795
Robert L. Dedrick, Daniel S. Zaharko, Richard A. Bender, W. Archie Bleyer, and Robert J. Lutz
National Institutes of Health, Bethesda, Maryland

Cytokinetic Aspects of Clinical Drug Resistance 805
Richard A. Bender and Robert L. Dedrick
National Cancer Institute, Bethesda, Maryland

Kinetic Model for the Disposition and Metabolism of Moderate and High-Dose Methotrexate (NSC-740) in Man 811
Paulo R. Leme, Patrick J. Creaven, Larry M. Allen, and Mones Berman
National Cancer Institute- Veterans' Administration Medical Oncology Branch, Washington, DC

Preliminary Pharmacokinetic Model for Adriamycin (NSC-123127) 819
Phillip A. Harris and Joseph F. Gross
University of California, Los Angeles

Mathematic Models for Cancer Chemotherapy: Pharmacokinetic and Cell Kinetic Considerations 827
Shui-Nan Chuang
Southern Research Institute, Birmingham, Alabama

Stochastic Compartmental Modeling of the Disposition of 5-(3,3-Dimethyl-1-triazeno)imidazole-4-carboxamide (NSC-45388) 843
Bayliss McInnis, Asha Kapadia, Souhail El-Asfouri, and Ti Li Loo
University of Houston, Texas

Analysis of the Effects of Antitumor Drugs on Cell Cycle Kinetics 847
Kwang B. Woo, Larry B. Brenkus, and Karl M. Wiig
National Cancer Institute, Bethesda, Maryland

Disposition of Cytosine Arabinoside (NSC-63878) and its Metabolites: A Pharmacokinetic Simulation 861
P. F. Morrison, T. L. Lincoln, and J. Aroesty
The Rand Corporation, Santa Monica, California

Human Pharmacokinetic Model for Isophosphamide (NSC-109724) 877
Larry M. Allen and Patrick J. Creaven
National Cancer Institute-Veterans' Administration Medical Oncology Branch, Washington, DC

Medical Oncology Course

Memorial Sloan-Kettering Cancer Center Nursing Symposium

Symposium on Modern Concepts in Brain Tumor Therapy: Laboratory and Clinical Investigation

Postgraduate Course on "Immunology for the Practicing Physician"

The Secretary of Health, Education, and Welfare has determined that the publication of this periodical is necessary in the transaction of the public business required by law of this Department. Use of funds for printing this periodical has been approved by the Director of the Office of Management and Budget through November 30, 1976.

LETTER

Contact Dermatitis Associated With Adriamycin (NSC-123127) and Daunorubicin (NSC-82151)[1]

Adriamycin and daunorubicin are two potent anthracycline antibiotics which, because of their dramatic action against cancer, are the subjects of vigorous research studies. The systemic toxic and adverse reactions to the anthracycline antibiotics are well known (1,2). Previous reports have described skin reactions resulting from systemic drug administration (3,4), but we are not aware of any report of a case of contact dermatitis associated with these agents. Since more researchers and clinicians are coming into direct contact with these drugs, we feel it is important to report a case of dermatitis in a laboratory technician.

CASE REPORT

This 29-year-old white male technician, whose job involved handling adriamycin and daunorubicin, complained of areas of red, sore, dry, cracking skin. These areas included the anterolateral aspect of the middle segment of the right third and fourth and the left third fingers, the anterolateral aspect of the proximal portion of the left fourth finger, and the posterior aspect of the middle segment of the right third finger. The technician described a nonspecific dermatitis on the posterior aspect of the right middle finger and a contact dermatitis secondary to a gold ring on the left fourth finger. Both of these fingers had a mild ongoing process with no symptoms other than dry scaly skin. However, when the laboratory worker started handling organic solvents including chloroform, methanol, and acid alcohol (95% ethanol and 5% concentrated hydrochloric acid), he noted progression of the dermatitis to previously uninvolved areas. Symptoms included persistent redness and dry, cracking skin which burned on contact with organic solvents. The anterolateral aspect of the right third finger had the worst symptoms. The patient treated himself with sporadic applications of steroid cream (Cordran, 0.05%) with some beneficial effect.

The technician had been working with adriamycin and daunorubicin for approximately 4 months, which also coincided with the onset of the skin reaction, when he noticed red-orange fluorescence under ultraviolet light in the areas of dermatitis. This led to the suspicion that the anthracycline antibiotics were causing the dermatitis. The worker then began wearing plastic gloves when handling the drugs. After 2 weeks with no steroid therapy, the fingers were much improved; however, fluorescence was still present. The technician then stopped using gloves because of the improvement and the dermatitis returned. He now uses gloves intermittently despite repeated warnings and continues to have a low-grade inflammatory reaction with dry cracked skin. Steroids were permanently discontinued.

COMMENTS

Adriamycin and daunorubicin along with many of their derivatives have a characteristic red-orange fluorescence when activated with ultraviolet light with a wavelength of 2537 Å. This fluorescence is also seen in drug-DNA complexes in vitro and in vivo. In fact, photomicrographs of cells viewed with fluorescent techniques show the nuclear localization of these anthracycline drugs (5). The proteinaceous layer of keratin apparently is impervious to the anthracycline drugs in organic or aqueous solution since these drugs are easily removed from the hands. By adequate washing with soap and water, little or no fluorescence remains. Other workers in this laboratory report fluorescence lasting 3-4 days, usually in hard-to-wash areas such as the nail beds. No other worker complained of a dermatitis. It is presumed that in this particular technician, the pre-existing dermatitis caused breaks in the keratin and allowed the drugs to penetrate the nucleated cells below. It is postulated that contact with a wide variety of organic solvents caused dry cracking skin on the previously uninvolved fingers which then allowed the drugs to penetrate to the cellular layers. We noted that the prominent points of contact with a round tube or flask were the anteriolateral aspects of the middle segments of the third and fourth fingers.

Because this technician repeatedly comes into contact with adriamycin and daunorubicin it is impossible to tell how long the fluorescence lasts. The long-range effects of a chronic dermatitis secondary to these potent anthracycline drugs are not known. We recommend that any person with a dermatitis avoid contact with adriamycin, daunorubicin, or their derivatives. Scanning hands under ultraviolet light for red-orange fluorescence aids in localizing anthracycline antibiotic deposits and consequential contact dermatitis.

REFERENCES

1. Bonadonna G, Monfardini S, De Lena M, et al. Phase I and preliminary phase II evaluation of adriamycin (NSC 123127). Cancer Res 30:2572-2582, 1970.
2. Serpick AA, and Henderson ES. Observations on toxicity and clinical trials with daunomycin. Pathol Biol 15:909-912, 1967.

[1]Adriamycin: CAS reg. No. 23214-92-8.
Daunorubicin: CAS reg. No. 23541-50-6.

3. Rothberg H, Place CH, and Shteir O. Adriamycin (NSC-123127) toxicity: unusual melanotic reaction. Cancer Chemother Rep 58:749-751, 1974.

4. Etcubanas E, and Wilbur JR. Letter: Uncommon side effects of adriamycin (NSC-123127). Cancer Chemother Rep 58:757-758, 1974.

5. Egorin MJ, Hildebrand RC, Cimino EF, et al. Cytofluorescence localization of adriamycin and daunorubicin. Cancer Res 34:2243-2245, 1974.

Steven D. Reich
Nicholas R. Bachur

Biochemistry Section
Baltimore Cancer Research Center
Division of Cancer Treatment
National Cancer Institute
3100 Wyman Park Dr
Baltimore, Md 21211

April 11, 1975

COMMENTARY

The Role of Structure-Activity Studies in the Design of Antitumor Agents

Bruce F. Cain[1,2]

In recent years it has been demonstrated that important drug-macromolecular interactions and many chemical structure-biologic activity relationships (SAR) can be described by relatively simple mathematical equations (1,2). In large measure these successes can be credited to Corwin Hansch, who laid the conceptual framework for modern SAR analysis (3). While successful SAR analyses have revealed a gratifying degree of order in large volumes of raw screening data, the mathematical relationships uncovered have also provided medicinal chemists with a new perspective. From these recently provided insights there is the prospect of being able to manipulate chemical structure to provide a required set of biologic properties, a prospect of fundamental importance to cancer chemotherapy.

Physicochemical Drug Properties

In very early attempts to derive meaningful SAR, researchers pinpointed the critical role of the lipophilic-hydrophilic balance of drugs, as measured by partitioning of these between immiscible solvents (4,5).

In recent studies Hansch and co-workers have espoused *n*-octanol and water as the immiscible solvents, and the logarithms of the partition coefficients of drugs in these solvents (log P) are now extensively used in the derivation of SAR (6). Data from drug partitioning in other immiscible solvent systems, or partition chromatography, can provide alternate measures of lipophilic-hydrophilic balance of equivalent utility (7). An example given in figure 1 shows the often-observed relationship between log P and log (biologic activity). The biologic activity plotted in this diagram stems from L1210 screening data obtained with certain homologous series of recently developed acridines (8). As often found, a parabolic relationship best correlates log P with measures of activity (fig 1) (9). Biologic data from animal screening tests have usually been found to correlate with parabolic functions of log P when the drug congeners examined have covered a sufficiently wide range of log P values.

It has been suggested that log P factors in SAR relate to the rate of drug migration to the site of action (10). Drug movement is visualized as a partition-type progress of the drug through alternate lipid-rich and lipid-poor biophases; compounds of optimum log P pass most rapidly to site while suboptimal and supraoptimal log P compounds tend to reside longer in aqueous and lipid phases respectively (10).

By using biologic data from homologous drug series it is possible to derive curves (see curve A, fig 1) which, provided certain necessary requirements are met (8), show directly the log P-biologic activity dependence. When attempting to obtain maximum biologic activity by modifying the molecular structure of a lead chemical, the early demonstration of such a relationship (fig 1) can considerably facilitate the process (8).

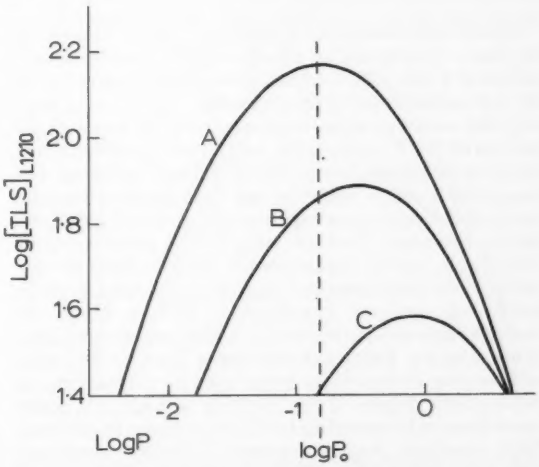

FIGURE 1.—Antileukemic activity (L1210) as a function of log P and site of tumor implantation. Log P = logarithm (*n*-octanol-water partition coefficient) of the drugs used. Log $[ILS]_{L1210}$ = logarithm (percent increase in lifespan in L1210 tests at the optimum dose). Full details of the animal test procedures and the agents used have been described (8,25). The results depicted in curves A, B, and C were obtained when the L1210 tumor was implanted ip, sc, and ic respectively, using the same drugs and standardized conditions of dosing.

[1]Cancer Chemotherapy Laboratory, Auckland, New Zealand.

[2]*Reprint requests to:* Dr. Bruce F. Cain, Cancer Chemotherapy Laboratory, PO Box 1724, Auckland, New Zealand.

Log P Dominates

The relationship expressed by curve A (fig 1) shows that any change in drug structure which provides an agent of altered log P automatically produces a change in biologic activity. As a generality the following can be stated: Until the relationship between biologic activity and log P is known no unequivocal statement may be made about the importance of drug structural features for biologic activity. The observation that biologic activity is abolished when certain drug structural features are removed or masked is not sufficient by itself to conclude that those drug features are essential for biologic activity. Particular care is necessary if, when functions are masked or removed, large changes in log P result. Compilations of the approximately constant changes in log P produced by common drug substituents (Hansch's π values) are available (11). Substituent changes in log P have been shown to be additive within certain limits and are extremely valuable for predicting the approximate partition coefficients of putative agents (12). As an example, replacement of a nitrogen atom by carbon in a six-membered ring of a drug would result in a molecule with a log P value higher than the original by: log P (benzene) — log P (pyridine) = 2.13—0.69 = 1.44. With the drugs considered in figure 1 this increase in log P would have alone ensured that the most active drug of the series would be converted to an inactive derivative. What conclusion about the importance of the ring nitrogen atom can then be made?

Site "Fit" Factors

Once a reference curve such as A (fig 1) is available, the importance of site-fit effects can be ascertained and the SAR further unravelled. The activity of any substituted drug congener can be compared with the activity expected from it on the basis of its measured log P; ie, biologic activity comparisons are made at isolipophilicity. The difference between the measured biologic activity and that predicted on the basis of the reference curve should provide a quantitative measure of other substituent contributions (electronic, steric, hydrophobic, etc) to biologic activity. Note that computer assistance is not a prerequisite for such an approach to SAR analysis although such assistance can provide useful computational checks. There are now many factors (36!) other than log P that have been used in attempting to improve the degree of correlations in SAR, and these have been well described in the extensive review that SAR analysis has attracted (1,13-15). However, there are many possible manipulations of log P effects alone which are potentially valuable yet remain unexplored.

Optimum Log P

What is the significance of the optimum log P (log P_o) value (fig 1) associated with maximum activity in the usual intraperitoneal (ip) L1210 tests? Does this provide information about some property of L1210 cells, the drug series, the host animal, or some combination of factors? If log P_o values specify maximum rate of drug migration to the site of action, is this then a necessary property for drugs to penetrate L1210 cells at the most advantageous rate? Will log P_o for most L1210-active drug series be the same?

L1210 leukemia cells examined in vitro, using members of a single drug series, should provide an optimum log P figure. However, this latter figure will not necessarily reflect the optimum observed in animal studies for the following reasons:

1. **Host Toxicity:** In animal tests permissible drug levels are dictated by host toxicity. Cells of host tissues that provide dose limitation will have their own (different?) log P_o's. Whole animal-determined log P values will therefore be the resultant figures, balancing maximum sparing of host-sensitive tissues while retaining the maximum possible tumor cell kill. The most sensitive, dose-limiting, host tissue may vary with different drug series and the log P_o's observed can then be expected to change also.
2. **Pharmacodynamic Properties:** While several of these properties are catalogued separately, the dynamic situation in animals dictates that none should be considered in isolation.
   a. *Drug distribution and excretion.*—The partitioning of a drug dose into various body compartments will be governed by pharmacodynamic factors. Concentrations and effective contact times of drugs reaching the host's sensitive tissues will alter with changing drug log P.
   b. *Metabolic effects.*—If a drug class has a common structural feature which is essential for biologic activity but this feature is readily recognized and degraded by, for example, the host's microsomal enzyme systems, then the more lipophilic members of the drug series can be expected to be enzymatically degraded more rapidly (16). Resultant log P_o's would be lower.
   c. *Drug reactivity.*—Many tumor-active drugs bear reactive functionality which leads to rapid decay of the active principle in vivo. Current theories state that more hydrophilic drugs move more slowly to sites of action so that these, with their longer residence times in polar biophases, have a greater opportunity for decay. Accordingly, there may be drug concentration gradients to sites of action for hydrophilic drugs, and higher log P_o figures could result.
3. **Dosage Schedule Dependence:** Drug half-life in vivo lengthens as binding to plasma proteins increases (17); drug binding to macromolecules increases linearly with log P (2). When there is a marked dependence of drug half-life for activity, more lipophilic drugs may then appear more active. If congeners of cycle-selective agents, such

as cytosine arabinoside,[3] were screened using a single daily dosage schedule, the need for long drug contact times for effective tumor cell kill could force the selection of agents with longer half-lives (more lipophilic) (18-20). Log P_0 would then be observed at higher figures.

4. **Tumor Site:** It has been repeatedly observed that ip administered drugs are less effective against subcutaneously (sc) than ip implanted L1210. The agents providing the data for figure 1 proved no exception and gave less effect against sc L1210 as summarized in curve B (fig 1). Intracerebrally (ic) implanted L1210 was even less affected under the same dosing conditions (curve C, fig 1). It is known that impressing the requirement that drugs pass the blood-brain barrier tends to select the more lipophilic agents; there is a consequent shift in the most favorable log P to higher figures. The log P_0 recorded for sc L1210 appears to lie in an intermediate position between those recorded for ip and ic tumor. Further factors can be envisaged that will alter not only the log P_0 values found in animal experiments but also those found in tissue culture studies.

5. **Intracellular Site Location:** In penetrating to intracellular sites of action, drugs with different modes of action may pass varying numbers of extracellular and intracellular barriers of different compositions. The log P_0 found for any drug series would then reflect the number and nature of the barriers surmounted to reach the various sites of action.

6. **Drug Structural Features:** Components of drug-site binding due to hydrophobic forces are generally accepted to be proportional to the log P of that portion of the drug which is binding hydrophobically (21). If in a series of drugs there was a common structural feature, eg, a benzene ring, which was involved in hydrophobic site binding, then a further log P factor would be impressed into the SAR and there would be a corresponding displacement of log P_0 to higher figures. Clearly, as so often found when attempting to measure drug effects in a tumor-bearing animal, the measured log P_0 values are influenced by drug, host, and tumor factors.

Unfortunately the various factors listed above (points 1-6) hinder attempts to answer the interesting queries: Do different tumors have distinguishable log P_0 values? Do different tumor log P_0 values contribute to drug-tumor spectra of action? A knowledge of the comparative drug permeability of tumor cell populations, as a function of log P, could be valuable, particularly when the latentiation strategies discussed below are considered.

[3]Cytosine arabinoside: NSC-63878; CAS reg. No. 69-74-9; 1-β-D-arabinofuranosyl-, monohydrochloride.

Latentiation Strategies

When drugs are administered ip, ip implanted L1210 provides a better approximation to in vitro conditions than does either sc or ic implanted tumor. Therefore, the log P_0 observed in the ip case approaches the optimum more closely than would be found in in vitro tests. Clearly, we may conclude from figure 1 that the log P gate-controlling entry of this series of drugs into L1210 cells lies in hydrophilic regions. It has already been pointed out that L1210 leukemia appears to have a penchant for selecting hydrophilic agents (22). The rate of drug entry into cerebral spaces is governed by a parabolic relationship in log P; the entry rate increases with increasing log P but so does the protein binding which finally provides a cut-off when the quantity of diffusable nonbound drug drops below significant levels. Examination of drugs acting on the central nervous system shows these to have log P_0's close to 2 (23). A diagrammatic representation (fig 2) shows how superposition of the two opposing requirements for ic activity (ability of drug to pass the blood-brain barrier and agent log P values within acceptable ranges for L1210 activity) can explain the observed result (curve C, fig 1). If such a compromise (fig 2) provides the reason for the low degree of drug effectiveness against ic tumor, an alternate strategy of attack could provide superior results. If a latentiated, ie, masked or pro-drug, form having a log P of about 2 was prepared, this then should provide maximum drug concentration, albeit latentiated, in the brain spaces. If the active core molecule, having a log P_0 matched to the sensitivity of the L1210, was then released from the latentiated form, one of the

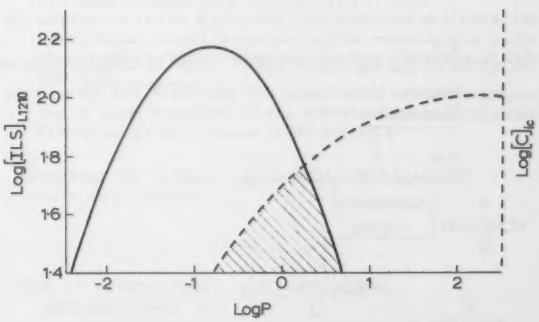

FIGURE 2.—Depiction of how the limited drug inhibitions recorded with ic L1210 (curve C, fig 1) could result from the combination of a low log P dependence of the L1210 population and a high log P requirement for drug passage of the blood-brain barrier. The parabola in the solid line is a duplicate of curve A from fig 1. The curve in the broken line shows the parabolic relationship expected between log P and log $[C]_{ic}$ = logarithm (maximum ic drug concentration reached following ip administration of a standard drug dose). The central shaded area, approximating a parabola, would delineate the apparent log P dependence of ic L1210 following ip drug administration.

most active drugs of the series would have been delivered to the central nervous system in high concentration. The liberation step to provide active drug could possibly be enzymatic but it is difficult to find a suitable candidate enzyme which will satisfactorily accomplish this step in brain fluids. Alternatively, unmasking could be a spontaneous process with chemical instability in body fluids providing a continuous liberation of active species. Such instability would certainly prove vexatious to any chemist, biologist, or clinician forced to handle the agent. However, addition of yet another drug-masking group could provide stability in selected cases. A simple example is provided and shows how an ester group may function as a stabilizing function in the correct situation (fig 3). There appears to be no reason why the doubly masked agent *1* (fig 3) should not be acceptably stable and readily handled. Following administration of agent 1 to an animal, ubiquitous serum esterases should readily cleave the ester function liberating the relatively unstable hydroxylic component *2* (fig 3). Provided this liberated fragment has a log P ~ 2 it should pass the blood-brain barrier. Fragment *2* contains a lactone unit in open-chain form and it is the drive to reclose the lactone ring that is the reason for the inherent instability and the consequent cleavage which liberates the core-active molecule and reforms the ring lactone *5*. The active core molecule will therefore be liberated ic at a rate determined by the kinetics of the cleavage reaction and the ic concentration of the hydroxylic component *2*. Dimethanesulfonate[4] (*3*) was selected as the core-active molecule for the example given; this alkylating agent is hydrophilic, having a low log P value (-1.71) in the area we associate with high L1210 activity.

The example shown (fig 3) provides the medicinal chemist with the necessary flexibility to be able to

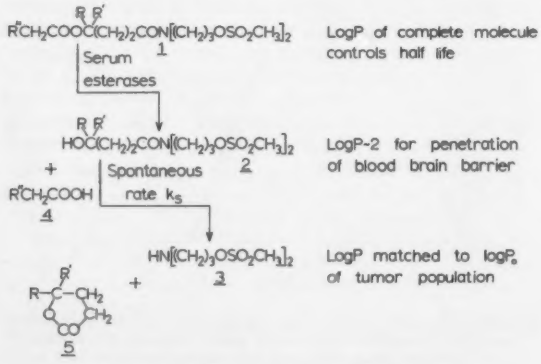

FIGURE 3.—Cascade latentiation.

control the important variables of drug action. Drug half-life in vivo can be varied by altering the log P of the fully latentiated drug *1*, and this could allow matching the half-life with the mode of drug action and the pharmacokinetic properties of the target tumor. The substituents R and R′ allow control of the log P of the unstable fragment *2*, thereby influencing the rate of penetration to the central nervous system and, additionally, exerting steric control on the rate of lactone closure and therefore the rate of liberation of the active principle *3*. Altering the size of the potential lactone ring will also influence th rate of the final liberation step. Multiple drug masking as described, with a necessary cascade of events before the active agent is liberated, might well be termed cascade latentiation. Possibly, the considerable clinical success seen with cyclophosphamide[5] is due to the latentiated nature of this alkylating agent. Cyclophosphamide provides an example of a slightly different cascade sequence. The initially stable form of the agent, as administered, is hydroxylated by the host's liver oxidases and it is this hydroxyl derivative which is unstable under physiologic conditions (24). Spontaneous breakdown of the distributed hydroxy-cyclophosphamide provides a tumor-active species at site (24).

The "Most Active" Drug?

In modern SAR analysis the correlations resulting from the deliberations of a computer sometimes allow a structure for the "most active" drug to be predicted. Such predicted agents inevitably prove deficient in some of their biologic and pharmacodynamic properties. Clearly, the discovery of the "most active" drug should not be regarded as an end point but more as a starting point. From the "most active" drug it will be the further deliberations of the medicinal chemist that will lead to latentiated derivatives and ultimately the "most desirable" agent.

Extensions and Questions

The L1210 system has been referred to throughout this paper merely as a convenient example for discussion, the ideas propounded being capable of extension to other tumor systems. Certainly, the strategy proposed for tackling ic L1210 should be directed towards brain tumors. If the chemotherapeutic sensitivity of a brain tumor, having a log P_o for drug penetration below -2, was examined and ip drug administration was used so that a need to penetrate the blood-brain barrier (log P ~ 2) was impressed, the tumor would appear "naturally drug resistant" (*see* fig 2). The methods of measuring log P_o for brain tumors pose several difficulties. Similar measurement problems must be faced with many of our other

[4]Dimethanesulfonate: NSC-102627; CAS reg. No. 3458-22-8; 1-propanol, 3,3′-iminodi-, dimethanesulfonate (ester), hydrochloride.

[5]Cyclophosphamide: NSC-26271; CAS reg. No. 6055-19-2; 2*H*-1,-3,2-oxazaphosphorine, 2-[bis(2-chloroethyl)amino]tetrahydro-, 2-oxide, monohydrate.

current solid tumor models which are used as sc implants. A comparison of curves A and B (fig 1) suggests that by screening against sc implanted tumors an unnecessary and possibly disadvantageous compromise may have already been accepted. Would an alternate approach, determination of log P_o and then preparation of latentiated derivatives, provide superior results? Is the different chemotherapeutic sensitivity of the primary tumor compared to the distant matastases another facet of the same problem?

Screening against L1210 implanted at different sites (ip, sc, and ic) could select as "most active" three different drugs from a congeneric series (compare curves A, B, and C; fig 1). Which of these drugs most warrants clinical trial? Should we continue to rank congeneric drugs using ip L1210 tests?

While a consideration of the importance of log P effects has given rise to many queries about our current tumor screening models and the way we use them, the essential core question is of course, "What is the relationship between the log P_o values of the tumors used in screening and those confronted in the clinic?"

REFERENCES

1. Hansch C. Quantitative structure-activity relationships. *In* Drug Design (Ariëns EJ, ed). New York, Academic Press, 1971, vol 1, pp 271-343.
2. Hansch C, and Anderson SM. The structure-activity relationship in barbiturates and its similarity to that in other narcotics. J Med Chem 10:745-753, 1967.
3. Hansch C, and Fujita T. ρ - π- σ Analysis: a method for the correlation of biological activity and chemical structure. J Am Chem Soc 86:1616-1626, 1964.
4. Overton E. Studien uber die Narkose. Jena, Fischer, 1901, p 45.
5. Ferguson J. The discovery of the anaesthetic halothane. Chem Ind (London), 1964, pp 818-824.
6. Leo A, Hansch C, and Elkins D. Partition coefficients and their uses. Chem Rev 71:525-616, 1971.
7. Iwasa J, Fujita T, and Hansch C. Substituent constants for aliphatic functions obtained from partition coefficients. J Med Chem 8:150-153, 1965.
8. Cain BF, Seelye RN, and Atwell GJ. Potential antitumor agents. Part 14. Acridylmethanesulfonanilides. J Med Chem 17:922-930, 1974.
9. Hansch C, Steward AR, and Iwasa J. The correlation of localisation rates of benzeneboronic acids in brain and tumor tissue with substituent constants. Mol Pharmacol 1:87-92, 1965.
10. Penniston JT, Beckett L, Bentley DL, et al. Passive permeation of organic compounds through biological tissue: a non-steady state theory. Mol Pharmacol 5:333-341, 1969.
11. Hansch C, Nikaitani D, and Lien EJ. Aromatic substituent constants for structure-activity correlations. J Med Chem 16:1207-1216, 1973.
12. Hansch C. A quantitative approach to biochemical structure-activity relationships. Accounts Chem Res 2:232-239, 1969.
13. Tute MS. Guide to structure-activity correlation for the medicinal chemist. *In* Advances in Drug Research (Harper NJ, and Simmonds AB, eds). New York, Academic Press, 1971, vol 6, pp 1-78.
14. Hansch C. Quantitative Approaches to Pharmacological Structure-Activity Relationships (Cavallito CJ, ed). New York, Pergamon Press, 1973, vol 1.
15. Redl G, Cramer RD, and Berkoff CE. Quantitative drug design. Chem Soc Rev 3:273-292, 1974.
16. Martin Y, and Hansch C. The influence of hydrophobic character on the relative rate of oxidation of drugs by rat liver microsomes. J Med Chem 14:777-779, 1971.
17. Helmer F, Kiehs K, and Hansch C. The linear free-energy relationship between partition coefficients and the binding and conformational perturbation of macromolecules by small organic compounds. Biochemistry 7:2858-2863, 1968.
18. Moffatt JG, Hamamura EK, Russell AF, et al. Synthesis and biologic examination of some derivatives of 2,2′-anhydro-1-(β-D-arabinofuranosyl)cytosine hydrochloride (NSC-145668). Cancer Chemother Rep 58:451-469, 1974.
19. Montgomery JA, and Thomas HJ. Acyl derivatives of 1-β-D-arabinofuranosylcytosine. J Med Chem 15:116-118, 1972.
20. Warner DT, Neil GL, Taylor AJ, et al. 3′*O*- and 2′*O*-esters of 1-β-D-arabinofuranosylcytosine as antileukemic and immunosuppressive agents. J Med Chem 15:790-795, 1972.
21. Hansch C, Deutsch EW, and Smith RN. The use of substituent constants and regression analysis in the study of enzymatic reaction mechanisms. J Am Chem Soc 87:2738-2742, 1965.
22. Hansch C, Smith N, Engle R, et al. Quantitative structure-activity relationships of antineoplastic drugs: nitrosoureas and triazenoimidazoles. Cancer Chemother Rep 56:443-456, 1972.
23. Hansch C, Steward AR, Anderson SM, et al. The parabolic dependence of drug action upon lipophilic character as revealed by a study of hypnotics. J Med Chem 11:1-11, 1968.
24. Connors TA, Cox PJ, Farmer PB, et al. Some studies of the active intermediates formed in the microsomal metabolism of cyclophosphamide and isophosphamide. Biochem Pharmacol 23:115-129, 1973.
25. Cain BF, and Atwell GJ. The experimental antitumor properties of three congeners of the acridylmethanesulfonanilides (AMSA) series. Eur J Cancer 10:539-549, 1974.

Chemical Assay for the Antitumor Agent Inosine Dialdehyde (NSC-118994) in Biologic Fluids[1,2]

Richard L. Cysyk[3,4,5]

SUMMARY

Inosine dialdehyde, an antitumor agent highly active against several murine tumors, is presently undergoing clinical trial for potential activity in man. To aid in the clinical evaluation of this drug, a chemical assay has been developed for the determination of concentrations of inosine dialdehyde in biologic fluids. The method involves reaction of inosine dialdehyde with phenylhydrazine in an acetic acid medium, followed by extraction of the product into ether and determining its absorbance at 378 nm. The reaction is specific for free inosine dialdehyde and will quantitate amounts as low as 1.0 μg.

[Cancer Chemother Rep 59:685-687, 1975]

Periodate oxidation of ribonucleosides results in the formation of the corresponding dialdehyde derivatives (1). A number of these products have been shown to be inhibitory against various transplanted tumors in mice (1). Inosine dialdehyde (IdA, fig 1), the periodate oxidation product of inosine, is highly active against murine L1210 and P388 leukemias and also against a variety of mouse tumors resistant to commonly used cancer chemotherapeutic agents.[6] Based on this activity, IdA is presently undergoing clinical trial in man. Previous pharmacologic studies of IdA in animals were performed using radioactively labelled IdA.[6] To obviate the use of radioactivity in man, a chemical assay for IdA was developed to aid in a successful clinical evaluation of this agent. This report describes the chemical assay for quantitating levels of free IdA in the urine and plasma of the dog and compares it with results obtained from radioactivity measurements using ^{14}C-IdA.

MATERIALS AND METHODS

^{14}C-[8]-IdA was synthesized by Stanford Research Institute (Calif). Phenylhydrazine was purchased from Sigma Chemical Company (St. Louis, Mo).

The assay mixture contained 1.0 ml of IdA (1.0-1000 μg), 0.1 ml of 10 M acetic acid, and 0.1 ml of an aqueous solution of phenylhydrazine (100 mg/ml). After a 60-minute incubation at 37°C with moderate shaking, the reaction was allowed to come to room temperature and was extracted with 10 ml anhydrous ether. An appropriate volume of the ether phase (usually 0.2 ml) was diluted to 1.0 ml with methanol and the 378-nm absorbancy was determined using the appropriate ether/methanol solution in the blank cuvette. For low concentrations of IdA, the ether phase was evaporated to dryness and the residue dissolved directly in methanol before determining the 378-nm absorbancy. Plasma samples (1.0 ml) were treated with 5.0 ml cold 10% TCA and the supernatant was washed three times with 10 ml ether to remove the TCA and to reduce background absorbance prior to reaction with phenylhydrazine (0.5 ml of 100 mg/ml) and acetic acid (0.5 ml of 10 M). Urine was likewise washed with ether prior to assay to reduce the background absorbance. Concentrations of IdA in urine and plasma samples were calculated from a standard curve of known concentrations of IdA dissolved in urine or plasma.

RESULTS AND DISCUSSION

Reaction of IdA with phenylhydrazine in aqueous solution under conditions described in Materials and Methods results in a product that is insoluble in aqueous media and is readily extracted into ether. When ^{14}C-[8]-IdA was used in the reaction, no radioactivity appeared in the ether phase indicating that disruption of the IdA molecule had occurred and that the ether-soluble product did not contain the hypoxanthine moiety. When the ether extract was diluted in methanol and the absorption spectrum taken on a Cary 15, the absorption spectrum was

[1]Received Oct 24, 1974; revised Mar 6, 1975; accepted Mar 19, 1975.

[2]Inosine dialdehyde: diglycolaldehyde, α-(hydroxymethyl)-α'-(6-hydroxy-9*H*-purin-9-yl)-. Supplied by Drug Research and Development, Division of Cancer Treatment (DCT), National Cancer Institute.

[3]Laboratory of Chemical Pharmacology (LCHPH), Experimental Therapeutics (EXT), DCT, NCI, Bethesda, Md.

[4]The technical assistance of Mary Ellen Ensminger is appreciated.

[5]*Reprint requests to:* Dr. Richard L. Cysyk, LCHPH, EXT, DCT, NCI, Bldg 10, Rm 6N119, National Institutes of Health, Bethesda, Md 20014.

[6]Cysyk RL, and Adamson RH. Manuscript in preparation.

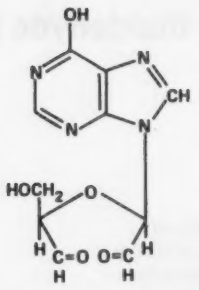

FIGURE 1.—Structure of inosine dialdehyde (IdA).

characterized by a λmax at 378 nm and compared closely to that previously reported for glyoxal bisphenylhydrazine (2), an anticipated product in the present study. Khym and Cohn (3) observed that phenylhydrazine reacted with several diglycolic aldehyde derivatives of nucleosides yielding the free base and the production of the phenylosazones of 2- and 3-carbon fragments. The data support a similar reaction of IdA with phenylhydrazine.

When the concentration of IdA was held constant (1 mg/ml) and the phenylhydrazine concentration and the length of incubation at 37°C were each varied, it was found that neither increasing the concentration of phenylhydrazine above 10 mg per reaction nor increasing the length of incubation to 4 hours increased the amount of product formed from 1 mg of IdA. Apparently, therefore, the reaction was complete by 30 minutes and product formation was not affected by a longer incubation. Also, 10 mg of phenylhydrazine was sufficient to fully convert 1 mg of IdA to the 378-nm absorbing product.

When the concentration of IdA was varied, there was a linear increase in the 378-nm absorbing product over a wide range of concentrations (figs 2A and 2B). Under the conditions employed, all of the values fell on a straight line from 1.0 to 1000 μg per reaction. Below 1 μg per reaction, determinations were somewhat more scattered and not reproducible. Above 1.0 μg, duplicate determinations were within 10%. The limit of the assay, therefore, was set at 1 μg per reaction. This should not limit its usefulness in clinical determinations since plasma values of IdA of greater than 200 μg/ml are obtained in dogs with a dose of 1.0 g/m².[7] The clinical dose in man exceeds 2 g/m². Standard curves of the same slope were obtained when known quantities of IdA were added to human urine or plasma.

Plasma and urinary levels of IdA after intravenous (iv) injections of ^{14}C-[8]-IdA (1.0 g/m²) into dogs were determined by both the chemical assay and from radioactivity determinations. Female beagles (weighing 6.7-7.2 kg) were anesthetized with iv sodium pentobarbital and anesthesia was maintained

[7] See footnote 6.

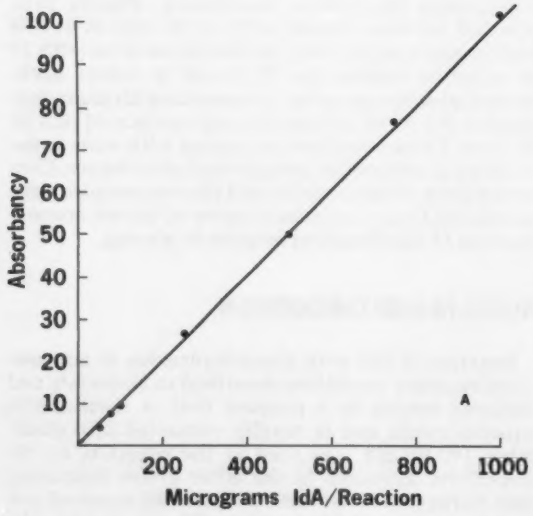

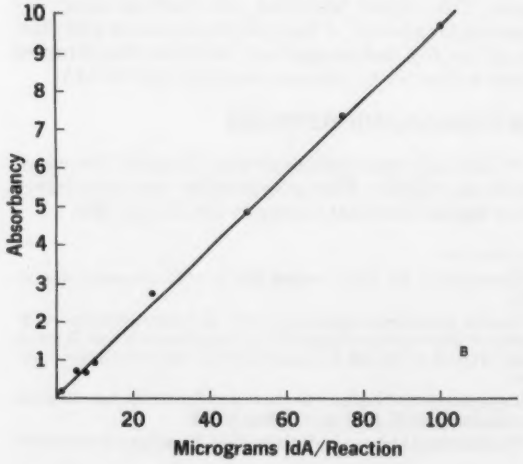

FIGURE 2 (A and B).—Standard assay curves for IdA. Varying quantities of IdA were added to H_2O and assayed according to the procedure outlined in Materials and Methods.

by intermittent injections of sodium pentobarbital throughout the experiment. ^{14}C-[8]-IdA (50 mg/kg) was injected iv into the femoral vein over a 5-minute period. Blood samples were taken periodically from a catheter in the femoral artery using a heparinized syringe. Plasma samples were treated with an equal volume of cold 20% TCA and then centrifuged, and the supernatant was used to determine radioactivity and for reaction with phenylhydrazine. Urine was collected continuously via an inserted catheter. For determination of radioactive content, urine or plasma samples (0.1 ml) were dissolved in NCS (Amersham-Searle, Arlington Heights, Ill), 18 ml scintillation fluid [6.0 g of 2,5-diphenyloxazole, 0.2 g of 1,4-bis-2-(5-phenyloxazolyl)-benzene, 1400 ml of toluene, and 600 ml of methanol] was added, and the samples were counted in a Beckman Liquid Scintillation Counter. ^{14}C-toluene was added as an internal standard to correct for quenching. A comparison of the values obtained by both techniques is presented in the data contained in figures 3 and 4. The results in figure 3 show that concentrations in urine determined by the chemical assay compare closely with those obtained from radioactivity measurements. Furthermore, it also demonstrates that the radioactivity appearing in the urine is associated with unchanged IdA. This finding agrees with a previous conclusion (*see* footnote 7) that was based on chromatographic analyses. The data in figure 4 show total plasma radioactivity levels and plasma radioactivity associated with TCA-soluble material. The curve of total plasma radioactivity is biphasic with an initial rapid component followed by a much slower decline. Treatment of each plasma sample with TCA revealed that an increasing proportion of the total radioactivity was TCA insoluble. It was reported previously (*see* footnote 7) that IdA interacts with protein forming a complex that is extremely stable under physiologic conditions. The curve (fig 4) depicting TCA-soluble radioactivity (ie, free IdA concentration) has a different kinetic pattern than the curve representing total radioactivity. When plasma samples were assayed with phenylhydrazine and compared with concentrations of IdA determined by radioactive assay, values for free IdA concentration obtained from the two techniques agreed closely (fig 4).

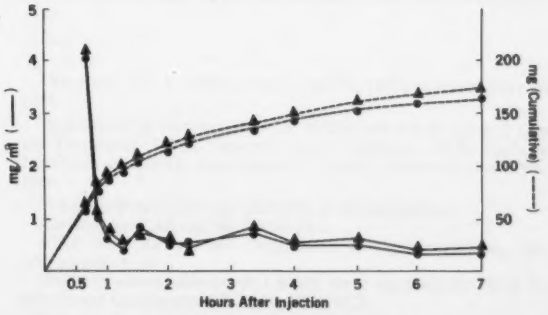

FIGURE 3.—IdA content of dog urine determined by chemical or radioactive assay. The dog was injected with a single iv dose of 1.0 g/m². Each time sample was assayed chemically (▲) and assayed for radioactivity content (●) as described in Materials and Methods: mg/ml (——); cumulative mg (------).

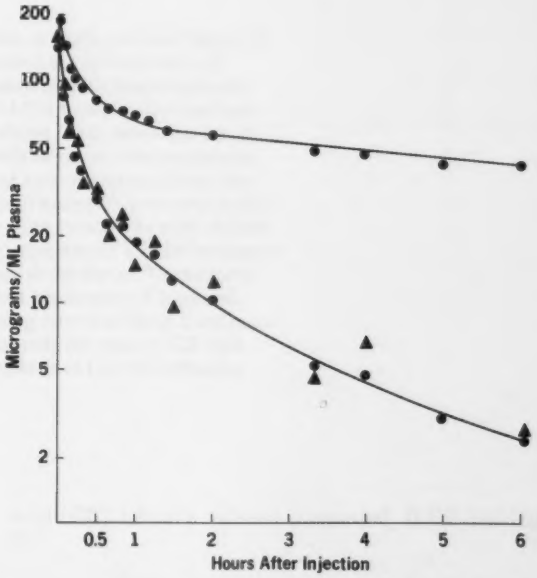

FIGURE 4.—Total and TCA-soluble concentration of IdA in dog plasma after a single iv dose of 1.0 g/m². Total concentration (●——●, top line) and TCA-soluble concentration of IdA (●——●, bottom line) calculated from radioactivity measurements. Concentration of IdA determined by chemical assay (▲).

In conclusion, the data presented demonstrate that IdA may be detected by a chemical assay that is sensitive and applicable to biologic fluids. The use of this assay in the clinical evaluation of IdA is indicated.

REFERENCES

1. DVONCH W, FLETCHER H III, GREGORY FJ, ET AL. Antitumor activity of periodate-oxidation products of carbohydrates and their derivatives. Cancer Res 26:2386-2389, 1966.
2. BARRY VC, MCCORMICK JE, and MITCHELL PWD. Properties of periodate-oxidised polysaccharides. Part V. Microdetermination of molecular weights of sugar osazones from measurements of ultra-violet-light absorption. J Chem Soc, 1955, pp 222-224.
3. KHYM JX, and COHN WE. Characterizations and some chemical reactions of periodate-oxidized nucleosides. J Am Chem Soc 82:6380-6386, 1960.

Enhancement of the Effectiveness of Daunorubicin (NSC-82151) or Adriamycin (NSC-123127) Against Early Mouse L1210 Leukemia With ICRF-159 (NSC-129943)[1,2,3]

R. J. Woodman,[4] R. L. Cysyk,[5] I. Kline,[4] M. Gang,[4] and J. M. Venditti[6,7,8]

SUMMARY

The LD50 of intraperitoneally (ip) injected daunorubicin in nonleukemic mice (1.8 mg/kg, q4d × 3) can be increased several fold by the concomitant ip injection of ICRF-159. In addition, the survival of leukemic mice treated ip with daunorubicin and ICRF-159 on Days 1, 5, and 9 after ip inoculation of L1210 tumor cells was substantially greater than after treatment with either drug alone. This potentiation of survival with combination treatment usually occurred with doses of daunorubicin greater than the LD50 of daunorubicin alone. The LD50 of subcutaneously (sc) injected daunorubicin alone (14.0 mg/kg, q4d × 3) was not increased by concomitant ip treatment with ICRF-159. However, when leukemic mice were treated sc with daunorubicin and ip with ICRF-159 on Days, 1, 5, and 9 after ip injection of L1210 leukemia cells, survival was greater than with treatment with either drug alone. The toxicity of ip injected adriamycin was not reduced by ICRF-159, but treatment of leukemic mice with this combination was more effective in prolonging survival than treatment with either drug alone. Combination treatment with daunorubicin plus ICRF-159 showed much less therapeutic enhancement against sc implanted L1210 leukemia than against the ip implanted tumor.

[Cancer Chemother Rep 59:689-695, 1975]

Clinical cardiac toxicity has been reported to result from the use of the antitumor antibiotic daunorubicin (1). During the course of animal studies designed to find ways to overcome this specific toxicity, Herman et al (2) discovered that the increased coronary perfusion pressure of an isolated dog heart system induced by daunorubicin or adriamycin could be prevented by prior addition to the perfusion fluid of the chelating agent ethylenediaminetetraacetic acid (EDTA)[9] or a related compound, ICRF-159 (fig 1).

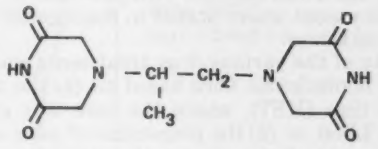

ICRF-159

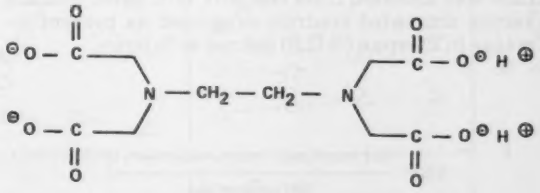

VERSENE (ETHYLENE DIAMINE TETRAACETIC ACID)

FIGURE 1.—Chemical structures of ICRF-159 and EDTA (Versene).

[1]Received Nov 6, 1973; revised Feb 17, 1975; accepted Mar 25, 1975.

[2]Supported by contract NO1-CM-33728 from the Division of Cancer Treatment (DCT), National Cancer Institute (NCI), National Institutes of Health, Department of Health, Education, and Welfare.

[3]Daunorubicin: CAS reg. No. 23541-50-6; daunomycin.
Adriamycin: CAS reg. No. 23214-92-8.
ICRF-159: CAS reg. No. 21416-87-5; 2,6-piperazinedione, 4,4'-propylenedi, (±)-.
The compounds used in this study were supplied by Drug Research and Development (DR&D), DCT, NCI.

[4]Microbiological Associates, Inc., Bethesda, Md.

[5]Laboratory of Chemical Pharmacology, Experimental Therapeutics, DCT, NCI, Bethesda, Md.

[6]Drug Evaluation Branch, DR&D, DCT, NCI, Bethesda, Md.

[7]We are grateful to Dr. R. D. Costlow for his assistance in this study, and we also acknowledge the technical assistance of E. W. Artis, D. Elam, and C. VonDerPool and their staffs in carrying out the experiments.

[8]*Reprint requests to:* Dr. Richard J. Woodman, 8627 Hempstead Ave, Bethesda, Md 20034.

[9]Ethylenediaminetetraacetic acid: NSC-2760; CAS reg. No. 6381-92-6; acetic acid, (ethylenedinitrilo)tetra-, disodium salt, dihydrate; Versene.

Since the experimental antitumor activity of ICRF-159, as well as daunorubicin and adriamycin, had already been demonstrated, Herman et al (2) suggested the therapeutic potential of combination treatment with ICRF-159 plus either of these two anthracycline antibiotics. This report describes more fully the results of experiments conducted in nonleukemic and leukemic mice designed to show whether combination chemotherapy with these agents would alleviate drug toxicity and enhance therapeutic response in L1210 leukemia. A preliminary report on some of these data was published previously (3).

MATERIALS AND METHODS

Pure dry daunorubicin and adriamycin were dissolved in water and injected immediately or stored at 4°C for not longer than 24 hours for experiments requiring more than one injection on each day of treatment. ICRF-159 was suspended in "Klucel" vehicle (0.9% NaCl in water containing 0.3% hydroxypropyl cellulose).

The drugs were injected over a wide range of doses (via routes and schedules described in the tables and figures) into BDF_1 (C57BL/6 female × DBA/2 male) mice initially weighing 18-25 g. The mice were inoculated intraperitoneally (ip) with 10^5 ascitic L1210 leukemia cells or subcutaneously (sc) with 10^6 L1210 cells. Treatment was started 24 hours later. In combination studies, ICRF-159 was injected first followed by the anthracycline antibiotic about 5 minutes later except where stated in the legends to the figures and tables.

Toxicity of the various drug treatments was evaluated in nonleukemic mice based on *(a)* the median survival time (MST), where the dose was greater than the LD50, or *(b)* the proportion of mice surviving to the end of the observation period (approximately 60 days). In this study the LD50 is defined as the maximum dose of drug in the dose-response series that results in 60-day survival for at least three of six or four of eight normal mice per group. Therapeutic effectiveness of chemotherapy in leukemic mice was assessed from the MST of treated animals versus untreated controls expressed as percent increase in lifespan (%ILS) defined as follows:

$$\%ILS = \frac{\text{MST treated mice} - \text{MST untreated mice} \times 10}{\text{MST untreated mice}}.$$

The term "therapeutic synergism" is used in this study according to the definition of Venditti and Goldin (4) and refers to situations where the %ILS of tumor-bearing animals treated with a drug combination is greater than that obtained by treatment with any single component of that drug combination.

RESULTS

Combination Therapy With ICRF-159 and Daunorubicin

Figure 2 presents the results of an initial experiment in this study where nonleukemic and leukemic mice from one randomized group were injected with ICRF-159 and daunorubicin alone or in combination on Days 1, 5, and 9. These results show that all doses of combination treatment produced longer survival times than any of the doses with either drug alone. The optimal combination dose (6.0 mg of daunorubicin plus 200 mg/kg of ICRF-159) gave survival times over twice those resulting from optimal doses of daunorubicin or ICRF-159 alone. In addition, the lower panel of figure 2 shows that treatment of nonleukemic mice with the optimal therapeutic combination doses of ICRF-159 and daunorubicin resulted in no deaths from drug toxicity by the 60th day after treatment initiation, whereas the same dose (6.0 mg/kg) of daunorubicin killed all six mice. The results of this initial experiment formed the basis for further study to determine the treatment schedule dependency and reproducibility of the apparent simultaneous therapeutic enhancement and toxicity reversal of this drug combination.

When ICRF-159 and daunorubicin were given alone or in combination on three different treatment schedules, there was a therapeutic enhancement with combination treatment given daily on Days 1-9 or daily on Days 1, 5, and 9, but not with single treatment given on Day 1 (fig 3). Treatment on Days 1, 5, and 9 was used in several confirmation experiments, the results of which are summarized in table 1. In a majority of these six experiments 3.0 mg/kg was the optimal dose of daunorubicin alone, whereas in combination with ICRF-159 the average optimal dose of daunorubicin was higher. The optimal combination dose of ICRF-159 (400 mg/kg) in five of six experiments was also higher than the optimal dose of ICRF-159 alone (200 mg/kg in four of six experiments). The %ILS values of combination treatment were higher in all six experiments than the %ILS values obtained with ICRF-159 alone, the more effective of the two drugs used singly, and the therapeutic enhancement of combination treatment was approximately three- to five-fold greater than treatment with ICRF-159 alone.

Figure 4 summarizes the results of five experiments in which ICRF-159 and daunorubicin were injected ip alone and in combination on Days 1, 5, and 9 into nonleukemic mice. The results show that daunorubicin alone is lethal to some mice even at the 1.0- and 2.0-mg/kg doses, and is 100% lethal at the 4.0- and 8.0-mg/kg doses. In combination with ICRF-159 at 200 mg/kg, however, the 1.0-, 2.0-, and 4.0-mg/kg doses resulted in no deaths, and there were 17% survivors even at the 8.0-mg/kg dose. Conversely, the 80% and 53% survival rates at the 200- and 400-mg/

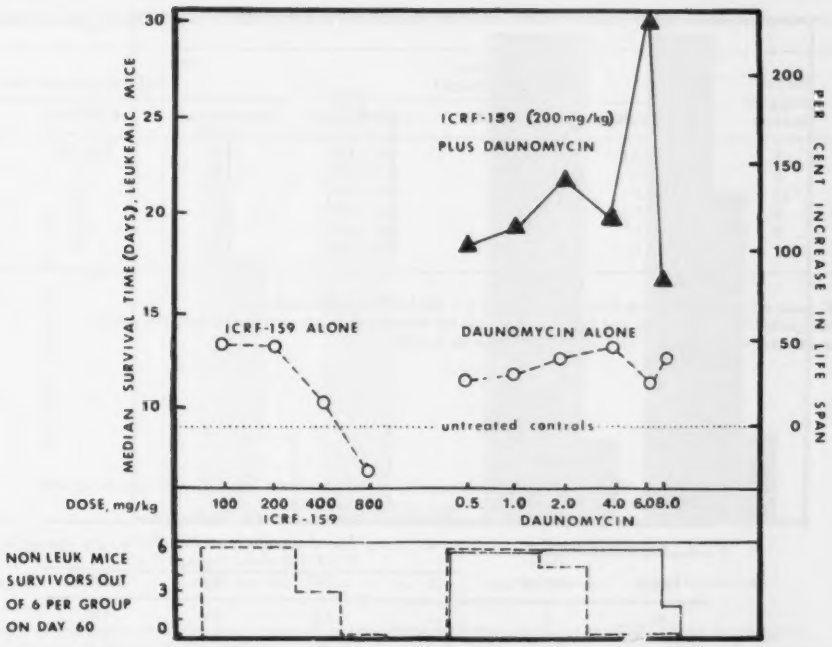

FIGURE 2.—Effect of combination treatment with ICRF-159 and daunorubicin on drug toxicity to nonleukemic mice and therapeutic effectiveness against L1210 leukemia.

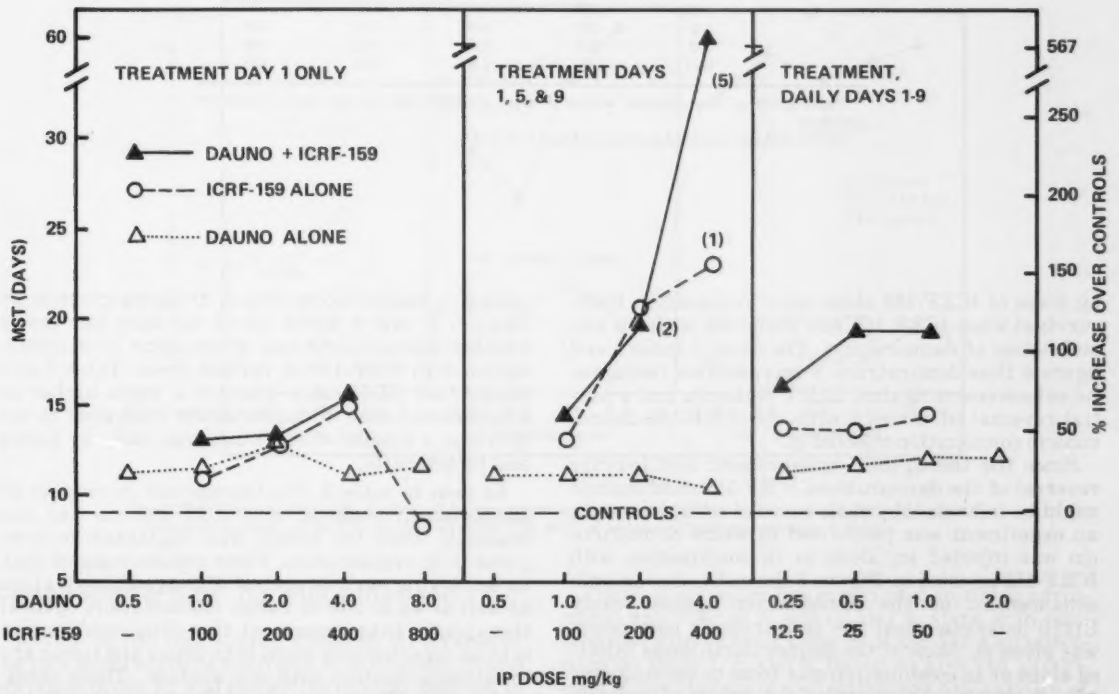

FIGURE 3.—Influence of treatment schedule on antileukemic effectiveness of combination chemotherapy with daunorubicin and ICRF-159. 10^5 L1210 leukemic cells were injected ip on Day 0. Nos. in parentheses = No. of survivors on Day 60.

TABLE 1.—Effectiveness of combination treatment with ICRF-159 plus daunorubicin in mice with L1210 leukemia: summary of six experiments*

Expt No.	MST of untreated controls	Optimal dose (mg/kg/injection)†			%ILS at optimal dose		
		Daunorubicin	ICRF-159	Combination	Daunorubicin	ICRF-159	Combination
2015	9	0.5-2.0	400	4.0 + 400	22	155 (1)‡	566 (5)
2033	9	4.0	200	6.0 + 200	44	44	233
2068	10	3.0	200	5.0 + 400	20	60	170
2082	9	3.0	200	1.8 + 400	28	78	261 (2)
2104	9	3.0	200	3.8 + 400	39	106	322 (3)
2152	9	3.0	400	5.0 + 400	44	50	150 (1)

* Eight BDF_1 male mice per test group inoculated ip with 1×10^5 L1210 ascites cells.
† Drugs were injected ip on Days 1, 5, and 9; in the combination treatment drugs were given concomitantly.
‡ Nos. in parentheses = No. of survivors out of eight mice on Day 60.

TABLE 2.—Effect of ICRF-159 on toxicity of daunorubicin injected sc or ip into normal mice (expt No. D-2162)

Daunorubicin*		No. of survivors on Day 60 at ICRF-159 doses (mg/kg) of—†			
Route	Dose (mg/kg)	0	180	300	500
Sc	0	—	6/6	5/6	1/6
	12.5	6/6	6/6	5/6	1/6
	25.0	1/6	0/6	0/6	0/6
	50.0	0/6	0/6	0/6	0/6
Ip	1.25	5/6	—	—	—
	2.5	1/6	0/6	0/6	5/6
	5.0	0/6	6/6	4/6	4/6
	10.0	0/6	6/6	6/6	0/6

*Daunorubicin was injected within 5 mins of ICRF-159 on the same treatment schedule.
†ICRF-159 was injected ip once on Days 1, 5, and 9.

kg doses of ICRF-159 alone were increased to 100% survival when ICRF-159 was combined with the 1.0- or 2.0-dose of daunorubicin. The data in table 1 and figure 4 thus demonstrate a reproducible therapeutic enhancement against L1210 leukemia and a partial reversal of toxicity with the ICRF-159-daunorubicin combination injected ip.

Since the therapeutic enhancement and toxicity reversal of the daunorubicin-ICRF-159 combination might be influenced by their route of administration, an experiment was performed in which daunorubicin was injected sc, alone or in combination with ICRF-159 injected ip. Figure 5 shows the therapeutic enhancement of the combination against early L1210 leukemia when the daunorubicin component was given sc. None of the daunorubicin doses injected alone or in combination was toxic to nonleukemic mice from the same randomized group of animals used in this test, but in the experiment described in table 2, a daunorubicin dose of 28 mg/kg given sc on Days 1, 5, and 9 killed six of six mice per group whether daunorubicin was given alone or in combination with ICRF-159 at various doses. Table 2 also shows that BDF_1 mice tolerate a much higher sc administered dose of daunorubicin compared to the ip route; a similar observation was made by Lenaz and Di Marco (5).

As seen in table 3, the therapeutic synergism of daunorubicin combined with ICRF-159 was far less dramatic when the tumor was implanted sc compared to ip implantation. These results suggest that by employing various routes of drug administration as well as an sc site of tumor implantation, optimal therapeutic enhancement of this drug combination is to be expected only when both drugs and tumor are in intimate contact with one another. These conditions are fulfilled only with ip treatment of the ip implanted leukemia.

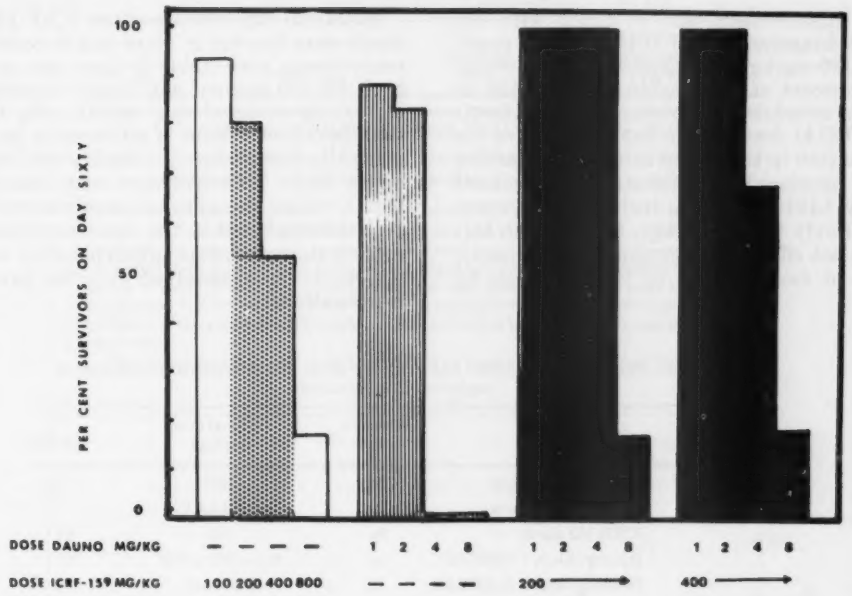

FIGURE 4.—Survival of nonleukemic mice after treatment with various doses of ICRF-159 or daunorubicin alone or in combination. Treatment ip on Days 1, 5, and 9. Pooled data of 6 mice per group from 5 separate experiments.

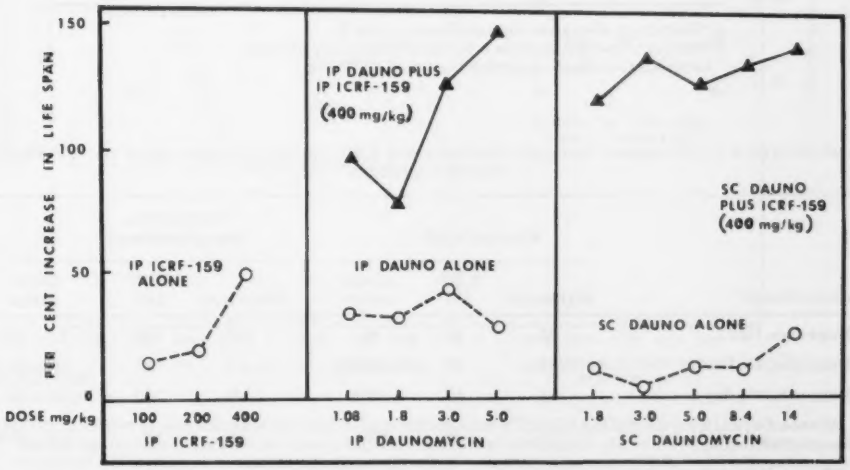

FIGURE 5.—Effect of route of injection of daunorubicin on therapeutic effectiveness against early ip L1210 leukemia in combination with ip injected ICRF-159. MST of untreated leukemic controls = 9 days.

Combination of ICRF-159 With Adriamycin

In view of the very similar chemical structures of the two anthracycline antibiotics, daunorubicin and adriamycin (fig 1), and the active clinical interest in adriamycin, further chemotherapy studies on ICRF-159 combined with adriamycin were carried out.

Figure 6 describes one experiment in which adriamycin was injected ip q3h on Day 1, alone or in combination with various doses of ICRF-159 also injected ip on Days 1, 5, and 9. Based on previous experience of the therapeutic effectiveness and toxicity of ICRF-159, more closely spaced doses of the drug were selected for combination with adriamycin.

Therapeutic enhancement was obtained with the 300-mg/kg combination dose of ICRF-159 and possibly with the 180-mg/kg dose. Confirmation of therapeutic enhancement of adriamycin by ICRF-159 on this treatment schedule was obtained in experiments D-2086 and D-2141 described in table 4. Most of the other combination ip treatment schedules described in table 4 produced therapeutic enhancement against early L1210 leukemia, including treatment once on Day 1 only for both drugs. By contrast, this schedule was not effective in producing therapeutic enhancement of daunorubicin by ICRF-159 (*see* fig 3).

In several experiments where ICRF-159 and adriamycin were injected ip alone and in combination into nonleukemic mice (table 5) there was no protection by ICRF-159 against adriamycin toxicity. This lack of toxicity reversal may explain why the combination therapeutic doses of adriamycin in table 4 were generally lower than the equivalent dose of adriamycin alone. This contrasts with daunorubicin (table 1), where the optimal combination therapeutic dose was higher than the equivalent dose of daunorubicin alone, an observation possibly related to the toxicity reversal obtained with this particular drug combination.

TABLE 3.—Effect of daunorubicin and ICRF-159 alone and in combination against sc implanted L1210 leukemia

Expt No.	Drug*	Injection route	Optimal dose (mg/kg)	%ILS†
DL-727	Daunorubicin alone	Sc	10.8	17
	Daunorubicin alone	Ip	1.8,3.0,5.0	0
	ICRF-159 alone	Ip	180	61
	Daunorubicin + ICRF-159	Sc	6.5 + 300 or 108	67
	Daunorubicin + ICRF-159	Ip	1.8 + 500	78
DL-734	Daunorubicin alone	Sc	18.0	39
	ICRF-159	Oral‡	840	88
	Daunorubicin + ICRF-159	Sc and ip	6.5 + 500	111

*Both drugs were given once on Days 1, 5, and 9.
†MST of untreated controls = 9.0 days for both experiments.
‡Animals fasted before administration of ICRF-159.

TABLE 4.—Increased lifespan of L1210 leukemic mice after treatment with ICRF-159 and adriamycin alone and in combination on various treatment schedules

Expt No.	Treatment schedule*	Maximal %ILS			Optimal dose (mg/kg/injection)†			MST of untreated controls (days)
		Adriamycin	ICRF-159	Combination	Adriamycin	ICRF-159	Combination	
D-2036	Both drugs once, Day 1	33	39	88	10.0	400	2.5 + 400	9.0
D-2059	Both drugs q3h/24h, Day 1	60	60	>560(6)‡	2.0	50	2.0 + 25	10.0
D-2118	Both drugs q3h/24h, Day 1	61	55	172(3)	1.0	14.7	0.25 + 30	9.0
D-2086	ICRF-159 once, Days 1, 5, 9 Adriamycin q3h/24h, Day 1	55	30	105	8.0	200	1.0 + 200§	10.0
D-2141	ICRF-159 once, Days 1, 5, 9 Adriamycin q3h/24h, Day 1	78	100	>200 (6/8 survivors, Day 26)	1.08	833	0.23 + 833	9.0
D-2134	ICRF-159 once, Days 1, 5, 9 Adriamycin once, Day 1	44	139	150	10.0	500	5.0 + 300	9.0
D-2134	Both drugs once, Days 1, 5, 9	61	139	228	5	500	5.0 + 108	9.0

*Both drugs were injected ip. When used in combination ICRF-159 was given first followed by adriamycin 15-20 mins later. For q3h schedules, eight injections were given 3 hrs apart. Dose ranges for both drugs contained four or five steps in 0.6 or 0.5 decrements.
† Where more than one dose of drug gave the same %ILS, only the higher dose is quoted.
‡ Nos. in parentheses = No. of survivors out of eight mice on Day 60.
§ Optimal dose may be higher than the highest one tested.

TABLE 5.—Lack of toxicity reversal of adriamycin by ICRF-159

Expt No.	Drug*	Schedule (ip)	Maximum dose of adriamycin† (mg/kg)
D-2036	Adriamycin alone	Once, Day 1	20.0
	Adriamycin + ICRF-159	Once, Day 1	20.0
D-2059	Adriamycin alone	q3h/24h, Day 1	32.0
	Adriamycin + ICRF-159	q3h/24h, Day 1	16.0
D-2384	Adriamycin alone	Days 1, 5, 9	3.0
	Adriamycin + ICRF-159	Days 1, 5, 9	3.0

*Drugs were injected into normal mice, eight per group in expt D-2036 and six per group in expts D-2059 and D-2384. ICRF-159 was injected over the range 100-800 mg/kg in expts D-2036 and D-2059, and 108-500 mg/kg in expt D-2384. Adriamycin was injected over the range 2.5-200 mg/kg (D-2036), 4.0-32.0 mg/kg (D-2059), and 3.0-14.0 mg/kg (D-2384).

†Maximum dose that was nonlethal to 50% or more of the mice by Day 60.

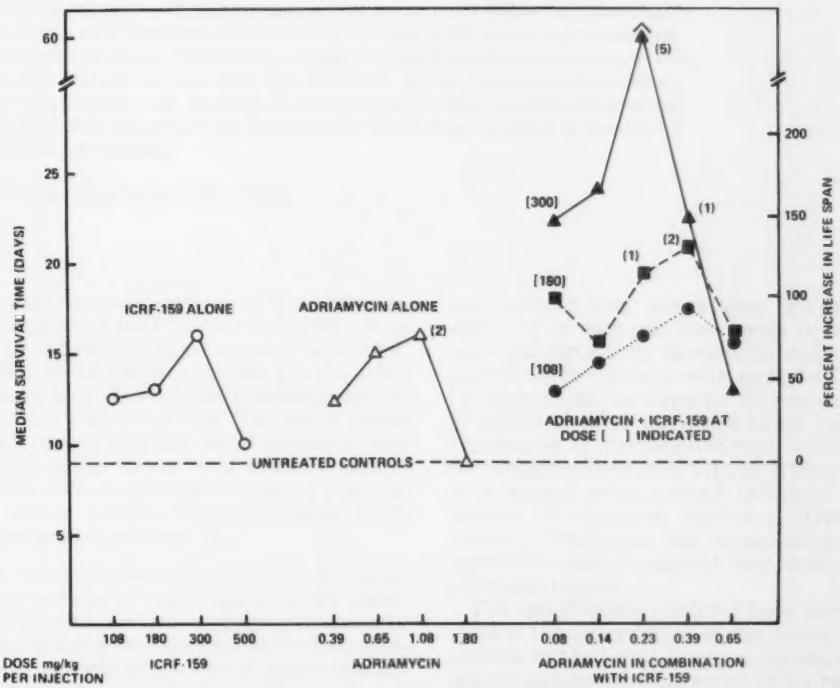

FIGURE 6.—Effect of adriamycin alone and in combination with ICRF-159 against early ip L1210 leukemia. Both drugs injected ip: ICRF-159 once on Days 1, 5, and 9 and adriamycin q3h on Day 1 only. Nos. in parentheses = No. of survivors on Day 60. Nos. in brackets = combination dose of ICRF-159 with adriamycin.

REFERENCES

1. TAN C, TASAKA H, YU K-P, ET AL. Daunomycin, an antitumor antibiotic, in the treatment of neoplastic disease. Clinical evaluation with special reference to childhood leukemia. Cancer 20:333-353, 1967.
2. HERMAN EH, MHATRE RM, LEE IP, ET AL. Prevention of the cardiotoxic effects of adriamycin and daunomycin in the isolated dog heart. Proc Soc Exp Biol Med 140:234-239, 1972.
3. WOODMAN RJ, KLINE I, and VENDITTI JM. Protection by (1,2,-bis(3,5-dioxopiperazin-1-yl)-propane) (ICRF-159) against daunomycin (DAU) toxicity and enhanced antileukemic (L1210) efficacy of the combination. Proc Am Assoc Cancer Res 13:31, 1972.
4. VENDITTI JM, and GOLDIN A. Drug synergism in antineoplastic chemotherapy. *In* Advances in Chemotherapy (Goldin A, and Hawking F, eds). New York, Academic Press, 1964, vol 1, pp 397-498.
5. LENAZ L, and DIMARCO A. Letter: On the reported lack of effectiveness of daunomycin (NSC-82151) and adriamycin (NSC-123127) on solid tumors. Cancer Chemother Rep 56:431-432, 1972.
6. CREIGHTON AM, HELLMANN K, and WHITECROSS S. Antitumour activity in a series of bisdiketopiperazines. Nature 222:384-385, 1969.

Effects of Levamisole (NSC-177023) and Tetramisole (NSC-102063) in Experimental Tumor Systems[1,2]

Randall K. Johnson, David P. Houchens, Marilyn R. Gaston, and Abraham Goldin[3,4]

SUMMARY

Levamisole and tetramisole had no antitumor effect against the following transplantable syngeneic murine tumors: L1210 leukemia, P388 leukemia, B16 melanoma, Madison 109 lung tumor, and Lewis lung carcinoma. In the Lewis lung carcinoma system there was no effect on primary tumor growth, metastasis, or survival. Tetramisole had a variable effect on the growth of rhabdomyosarcomas and the survival of BALB/c mice following intramuscular inoculation of Moloney sarcoma virus. In two experiments treatment with tetramisole either prior to or following inoculation of Moloney sarcoma virus increased the number of mice with tumor regression as opposed to progressive tumor growth, increased the number of long-term survivors, and prolonged the lifespan of mice that died of tumor. In two further tests neither levamisole nor tetramisole had an effect in this system. In mice immunosuppressed with cyclophosphamide prior to virus inoculation, there was no effect of treatment with levamisole or tetramisole.

[Cancer Chemother Rep 59:697-705, 1975]

Studies in experimental systems (1-7) and in man (8-11) have suggested that the antihelmintic drug levamisole (12) and its optical isomers act as nonspecific stimulants of the immune system. On the other hand, there have been reports that levamisole has no immunostimulatory activity (13,14). The use of immunoadjuvants in cancer therapy would appear to hold promise in light of the success with immunotherapy in some tumors with nonspecific bacterial immunostimulants, such as bacillus Calmette-Guérin (BCG) and *Corynebacterium parvum* (15).

It has been reported that levamisole has antitumor activity when used as a single agent in the treatment of Lewis lung carcinoma in syngeneic mice (16). The antitumor activity was manifested both by inhibition of tumor growth at the site of tumor implantation and by significant reduction in the number of macroscopic lung metastases. These effects were observed at nontoxic dose levels in both early disease and metastatic disease. Spreafico et al (17) reported that treatment with methyl-CCNU[5] followed by tetramisole was superior to treatment with methyl-CCNU alone in advanced Lewis lung carcinoma. Chirigos et al (18) reported that levamisole used after remission induction with BCNU[6] in a transplantable murine virus-induced leukemia increased the number of long-term survivors. However, another report (19) indicated that levamisole used as a single agent was inactive against four immunogenic transplantable tumors.

The experiments reported here were designed to confirm the observation of antitumor effects of levamisole in the Lewis lung carcinoma system and to determine whether this agent or its racemic isomer, tetramisole, had antitumor activity in other experimental tumor systems used for screening potential antineoplastic agents. Studies were also carried out in a highly immunogenic primary virus-induced tumor system to determine whether the immunostimulatory effects of levamisole or tetramisole would be manifested by enhanced tumor rejection or reversal of drug-induced immunosuppression.

---

[1]Received Dec 3, 1974; revised Feb 28, 1975; accepted Mar 19, 1975.

[2]Levamisole: CAS reg. No. 16595-80-0; imidazo[2,1-*b*]thiazole, 2,3,5,6-tetrahydro-6-phenyl-, monohydrochloride. Provided by Lederle Laboratories, Pearl River, NY.

Tetramisole: CAS reg. No. 5086-74-8; imidazo[2,1-*b*]thiazole, 2,-3,5,6-tetrahydro-*dl*-6-phenyl-, monohydrochloride. Provided by McNeil Laboratories, Inc., Port Washington, Pa.

[3]Drug Research and Development (DR&D), Division of Cancer Treatment (DCT), National Cancer Institute (NCI), Bethesda, Md.

[4]*Reprint requests to:* Dr. Randall K. Johnson, DR&D, DCT, NCI, Bldg 37, Rm 5E24, National Institutes of Health, Bethesda, Md 20014.

[5]Methyl-CCNU: NSC-95441; CAS reg. No. 33073-59-5; urea, 1-(2-chloroethyl)-3-(4-methylcyclohexyl)-1-nitroso-.

[6]BCNU: NSC-409962; CAS reg. No. 154-93-8; urea, 1,3-bis(2-chloroethyl)-1-nitroso-.

MATERIALS AND METHODS

Animals.—C57BL/6, BDF_1 (C57BL/6 × DBA/2), and BALB/c male mice, 6-8 weeks old (20-25 g), were used in these experiments. The animals were obtained from the DR&D production colonies.

Tumors.—Lewis lung carcinoma, L1210 leukemia, P388 leukemia, and B16 melanoma were maintained in syngeneic mice following the standardized protocols of the DR&D (20). The protocols were also followed for implantation of these tumors into test mice. These tumors were selected because they are widely used by the NCI in screening for potential antineoplastic agents. In addition, drug effects were evaluated in a very slow-growing solid tumor, Madison 109 lung tumor, which was maintained intramuscularly (im) in BALB/c mice by transplantation every 14 days. Viable cells were determined by trypan-blue exclusion. Two pools of virus were prepared from Moloney sarcoma virus (MSV)-infected muscle tissue of BALB/c mice by the procedure of Moloney (21). Rhabdomyosarcoma in BALB/c mice was induced by im injection into the right hind leg of 0.05 ml of virus lot MSV-A-2 diluted 100—200-fold in the experiments shown in tables 4 and 6. A similar inoculum of virus lot MSV-A-3 diluted 75-fold was used in the experiment shown in table 5.

Drugs.—Levamisole, tetramisole, and cyclophosphamide[7] were dissolved in 0.9% NaCl solution and were administered intraperitoneally (ip). The levamisole and tetramisole used in all experiments were from single samples of the drugs. Dose levels and schedules of administration of levamisole and tetramisole were based on the report of Renoux and Renoux (16) and were expanded to cover a 100-fold dose range below toxic levels. Drug solutions were prepared immediately prior to administration when a single-injection treatment schedule was employed. For multiple-treatment schedules, drug solutions were prepared at the beginning of treatment and stored at 4°C in amber bottles.

Tumor growth determination.—The growth of subcutaneously (sc) inoculated Lewis lung carcinoma was determined as indicated in the tables either directly by excising and weighing the primary tumor or indirectly by taking caliper measurements of perpendicular diameters and estimating the tumor mass by the formula (22),

$$\text{mass (in mg)} = \frac{\text{major diameter (in mm)} \times \text{minor diameter}^2 \text{ (in mm)}}{2}.$$

The number of macroscopic lung metastases was determined by the india ink insufflation technique of Wexler (23). The growth of MSV-induced rhabdomyosarcomas was monitored by palpation of the infected leg. The average thickness of a noninvolved leg was 5 mm. A progressively growing tumor was one which increased in size continually to the time of death. The criterion used for regression was a decrease of 3 mm or more from peak diameter prior to either complete disappearance or eventual regrowth and death. An animal was considered a no-take if the inoculated leg never exceeded 6 mm in diameter.

[7]Cyclophosphamide: NSC-26271; CAS reg. No. 6055-19-2; 2*H*-1,3,2-oxazaphosphorine, 2-[bis(2-chloroethyl)amino]tetrahydro-, 2-oxide, monohydrate.

RESULTS

Lewis Lung Carcinoma

Levamisole and its racemic isomer, tetramisole, had no activity against Lewis lung carcinoma in repeated experiments. Under conditions duplicating those used in the experiments of Renoux and Renoux (16), levamisole and tetramisole had no inhibitory effect on the growth of the primary tumor at the site of implantation (table 1). Furthermore, treatment with these drugs had no significant effect on the number of macroscopic lung metastases as determined at autopsy 21 days following tumor implantation. Levamisole-treated groups had, in fact, average tumor weights and numbers of macroscopic lung colonies somewhat greater than untreated controls although these differences were not statistically significant.

As shown in table 2, treatment with levamisole or tetramisole on several schedules over wide dose ranges did not inhibit tumor growth significantly or show an increased survival time (ILS) of mice injected sc with 10^6 Lewis lung carcinoma cells.

Following inoculation of 10^5 Lewis lung carcinoma cells iv, C57BL/6 or BDF_1 mice died in 3-4 weeks with massive tumor growth in the lungs. Treatment with tetramisole either prior to tumor inoculation or every other day for six injections beginning 1 day or 7 days after tumor inoculation did not increase survival (table 3).

Transplanted Murine Leukemias and Solid Tumors

The effect of treatment with levamisole or tetramisole over a range of doses was evaluated in a spectrum of murine tumors. The drugs were administered ip daily for 9 days beginning 1 day after tumor implantation. These drugs failed to significantly increase the lifespan of mice bearing ip L1210 and P388 leukemias. Similarly, there was no significant antitumor activity in two transplantable murine solid tumors, ip B16 melanoma and sc Madison 109 lung tumor.

Primary MSV-Induced Rhabdomyosarcoma

In an attempt to determine whether antitumor activity could be observed for levamisole or tetramisole in a tumor system in which the host immune system plays an important role, these drugs were tested

TABLE 1.—Effects of levamisole and tetramisole on primary and metastatic Lewis lung carcinoma*

Drugs	Dose schedule	No. of mice treated	Primary tumor weight (g, mean ± SE)	No. of macroscopic lung colonies (mean ± SE)
Untreated controls		8	1.84 ± 0.41	50±12
Levamisole	0.5 mg/kg ip, Day 1 only	8	3.04 ± 0.99	63 ± 15
Levamisole	0.5 mg/kg ip, Days 7, 9, 11, 13, 15, 17	9	2.64 ± 0.40	68 ± 12
Tetramisole	0.5 mg/kg ip, Day 1 only	9	1.59 ± 0.28	46 ± 11
Tetramisole	0.5 mg/kg ip, Days 7, 9, 11, 13, 15, 17	10†	1.73 ± 0.36	44 ± 11

*2×10^5 viable Lewis lung carcinoma cells implanted sc into C57BL/6 male mice on Day 0. Mice killed on Day 21, primary tumors excised and weighed, and No. of macroscopic lung colonies assayed by india ink insufflation (23).

†One animal had no evident sc tumor but did have lung tumor nodules suggesting that the tumor may have been inoculated ip.

TABLE 2.—Effects of levamisole and tetramisole on tumor growth and survival in mice with sc implanted Lewis lung carcinoma*

Dose (mg/kg injection)	Schedule (days of treatment)	Levamisole†			Tetramisole†		
		MST (days)	ILS (%)	Tumor size ‡ (T/C)	MST (days)	ILS (%)	Tumor size‡ (T/C)
40	1	32.5	0	127	38.0	9	108
13.33	1	37.5	7	82	38.5	10	146
4.44	1	35.5	2	107	41.5	19	64
1.48	1	37.5	7	111	36.0	3	99
20	1, 3, 5, 7, 9, 11	33.5	0	148	36.0	3	81
6.67	1, 3, 5, 7, 9, 11	34.5	0	119	38.0	9	176
2.22	1, 3, 5, 7, 9, 11	36.0	3	48	36.0	3	110
0.74	1, 3, 5, 7, 9, 11	36.0	3	107	36.5	4	102
20	7, 9, 11, 13, 15, 17	35.0	0	136	37.5	7	94
6.67	7, 9, 11, 13, 15, 17	37.0	6	133	38.0	9	80
2.22	7, 9, 11, 13, 15, 17	33.5	0	167	38.0	9	104
0.74	7, 9, 11, 13, 15, 17	38.0	9	122	34.0	0	123
Untreated controls		35.0		100			

*10^6 viable Lewis lung carcinoma cells implanted sc into groups of 10 C57BL/6 mice on Day 0. Drugs administered ip.

†MST = median survival time; ILS = increase in lifespan relative to untreated controls.

‡Mean tumor weight calculated from caliper measurements of primary tumors on Day 18. T/C = treated/control × 100. Control tumor weight on Day 18 = 1876 mg.

in the primary MSV-induced rhabdomyosarcoma in BALB/c mice.

There was some indication of activity for tetramisole in this antigenic tumor system (24) in two separate experiments. However, this positive response was not observed in two further experiments which included both levamisole and tetramisole. In experiment 1 in table 4 a single administration of tetramisole 24 hours prior to virus inoculation increased the number of survivors on Day 164 when the experiment was terminated and increased the lifespan of the mice that died. This response was inversely related to dosage level: a dose of 40 mg/kg (0.8 LD10) had little, if any, effect on survival (14% ILS, no

TABLE 3.—Effects of tetramisole on lifespan of mice with iv implanted Lewis lung carcinoma*

Tetramisole				
Dose (mg/kg/ injection)	Schedule (days of treatment)	MST (days)	ILS (%)	Survivors on Day 75/ total No. Treated
Untreated controls		26.5		0/10
40	-3	24.0	0	0/9
4	-3	25.0	0	0/10
0.4	-3	28.0	6	0/9
20	1, 3, 5, 7, 9, 11	27.0	2	1/9
8	1, 3, 5, 7, 9, 11	24.0	0	0/10
3.2	1, 3, 5, 7, 9, 11	23.5	0	0/10
20	7, 9, 11, 13, 15, 17	28.5	8	0/10
8	7, 9, 11, 13, 15, 17	23.5	0	0/10
3.2	7, 9, 11, 13, 15, 17	25.5	0	0/10

*10^5 viable Lewis lung carcinoma cells implanted iv into C57BL/6 mice on Day 0. MST = median survival time; ILS = increase in lifespan.

TABLE 4.—Effects of tetramisole on MSV-induced rhabdomyosarcoma

	Treatment*						No. of animals with—		
Experiment No.	Drugs	Dose levels (mg/kg)	Schedule (day of treatment)	Mean survival time of dying animals only (days)	T/C†	No. of long-term survivors/ total No. treated‡	Progression	Regression	No-take
1	Untreated controls			50.5	—	0/10	6/10	4/10	
	Tetramisole	40	-1	57.8	114	0/10	5/10	5/10	
	Tetramisole	4	-1	66.5	132	2/10	3/10	7/10	
	Tetramisole	0.4	-1	79.2	157	4/10	1/10	9/10	
	Cyclophosphamide	210	-1	39.9	79	0/9	9/9		
	Cyclophosphamide + Tetramisole	210 + 40	-1	34.4	68[86]	0/9	8/9	1/9	
	Cyclophosphamide + Tetramisole	210 + 4	-1	40.3	80[101]	0/10	10/10		
	Cyclophosphamide + Tetramisole	210 + 0.4	-1	35.1	70 [88]	0/9	8/9	1/9	
2	Untreated controls			53.8	—	2/10	6/10	4/10	
	Tetramisole	4	-7	49.4	92	2/10	5/10	5/10	
	Tetramisole	4	-3	60.3	112	7/10	2/10	5/10	3/10
	Tetramisole	4	-1	80.0	148	5/10	1/10	9/10	
	Tetramisole	4	0	52.8	98	4/10	4/10	6/10	
	Tetramisole	4	+1	46.6	87	3/10	3/10	7/10	
	Tetramisole	4	+3	63.7	118	2/9	4/9	4/9	1/9
	Tetramisole	4	+7	66.6	123	5/10	2/10	7/10	1/10

*Drugs administered ip. In combinations, cyclophosphamide was administered immediately prior to tetramisole.
†Mean survival time of treated mice/mean survival time of controls × 100. Nos. in brackets represent T/C when animals that received cyclophosphamide alone were used as controls.
‡No. of survivors on day experiment was terminated (experiment 1 = 164 days; experiment 2 = 138 days).

survivors among ten animals) even though there was no evident toxicity, while the lowest dose of 0.4 mg/kg was the most effective (57% ILS, four survivors among ten animals).

The characteristics of tumor growth are also listed in table 4. In the untreated group, tumors grew progressively to the time of death in six of ten mice, while in the remaining four mice the tumors regressed spontaneously, eventually recurred, and killed the animals. At 4 and 0.4 mg/kg of tetramisole, seven of ten and nine of ten mice respectively had tumor regression.

In animals immunosuppressed by the administration of cyclophosphamide 1 day prior to virus inoculation, all tumors grew progressively and mean lifespan was shorter than in untreated controls. Tetramisole administration had no effect on lifespan or survival in cyclophosphamide-treated mice (table 4).

The growth rates of virus-induced tumors in the first experiment listed in table 4 are shown in figure 1. The mean tumor diameter was less in tetramisole-treated groups (fig 1A), particularly at 4 and 0.4 mg/kg. In animals immunosuppressed with cyclophosphamide (fig 1B) the tumors grew to a larger size prior to death than in untreated controls. Tetramisole had no effect on tumor growth rate in cyclophosphamide-treated mice.

In experiment 2 (table 4) tetramisole (4 mg/kg) was administered at several time intervals prior to or after virus inoculation. Treatment 1 or 3 days prior to virus inoculation or 7 days after virus increased the mean lifespan of the animals that died and/or increased the number of survivors on Day 138. These effects on survival were paralleled by an increase in the percentage of animals with tumor regression. Also, a number of tetramisole-treated mice failed to develop palpable tumors at the site of injection at any time during the experiment.

In the experiment shown in table 5, only two of eight mice in the group that received virus alone showed progressive tumor growth and three of eight animals survived until the experiment was terminated on Day 90. Treatment with levamisole or tetramisole over a wide dose range on the day prior to virus inoculation did not markedly increase the lifespan or the number of survivors. There was also no positive effect on the number of animals with tumor regression. As in the previous experiment, tetramisole had no effect on cyclophosphamide-treated animals. Levamisole at 4 and 0.4 mg/kg resulted in an increase in the number of immunosuppressed animals with regressions, and two of eight immunosuppressed animals that received 4 mg/kg of levamisole were alive on Day 90.

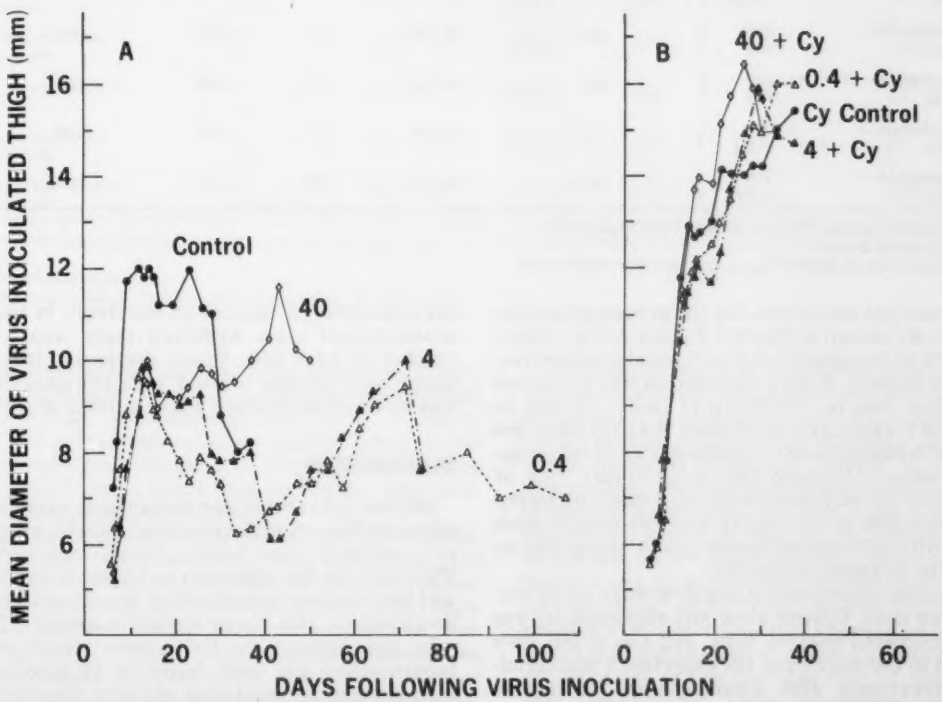

FIGURE 1.—Effects of tetramisole on growth of MSV-induced rhabdomyosarcoma im in BALB/c mice. A: Mean diameter of tumor-bearing leg after treatment with tetramisole at 40, 4, and 0.4 mg/kg, 1 day prior to virus inoculation. B: Mean diameter of tumor-bearing leg after treatment with cyclophosphamide (Cy) alone at 210 mg/kg or with tetramisole at 40, 4, and 0.4 mg/kg, 1 day prior to virus inoculation. Each group consisted of 10 mice and the curves were plotted out to median survival time.

TABLE 5.—Effect of levamisole or tetramisole given 1 day before virus inoculation in MSV-induced rhabdomyosarcoma

Treatment*		Mean survival time of dying animals only (days)	T/C†	No. of long-term survivors/ total No. treated‡	No. of animals with—		
Drugs	Dose levels (mg/kg)				Progression	Regression	No-take
Untreated controls		46.6	—	3/8	2/8	6/8	
Levamisole	40	43.6	94	1/8	4/8	4/8	
Levamisole	4	48.8	104	2/8	5/8	3/8	
Levamisole	0.4	57.0	122	2/8	4/8	4/8	
Levamisole	0.04	60.5	132	2/8	2/8	6/8	
Tetramisole	40	57.0	122	1/8	5/8	3/8	
Tetramisole	4	46.4	100	0/8	6/8	2/8	
Tetramisole	0.4	42.3	91	2/8	4/8	4/8	
Tetramisole	0.04	49.1	105	1/8	4/8	3/8	1/8
Cyclophosphamide	210	31.8	68	0/8	8/8		
Cyclophosphamide + Levamisole	210 40	37.1	80 [117]	0/8	8/8		
Cyclophosphamide + Levamisole	210 4	39.3	84 [123]	2/8	4/8	4/8	
Cyclophosphamide + Levamisole	210 0.4	35.6	76 [112]	0/8	5/8	3/8	
Cyclophosphamide + Levamisole	210 0.04	27.6	59 [87]	0/8	8/8		
Cyclophosphamide + Tetramisole	210 40	34.1	73 [107]	0/8	7/8	1/8	
Cyclophosphamide + Tetramisole	210 4	35.1	75 [110]	0/8	6/8	2/8	
Cyclophosphamide + Tetramisole	210 0.4	31.5	68 [99]	0/8	6/8	2/8	
Cyclophosphamide + Tetramisole	210 0.04	36.8	79 [115]	0/8	7/8	1/8	

*Drugs administered ip 24 hours prior to virus inoculation.
†See footnote in table 4.
‡No. of survivors on Day 90 when experiment was terminated.

The tumor growth curves for the groups presented in table 5 are shown in figure 2. Panels A and C show the effects of levamisole and tetramisole, respectively, on the growth of MSV-induced tumors in normal mice. There was no inhibition of tumor growth in any of the treated groups. Panels B and D show the effects of levamisole and tetramisole in immunosuppressed mice. Although the mean tumor size of groups treated with levamisole at 4 and 0.04 mg/kg and tetramisole at 0.04 mg/kg was less than in mice treated with cyclophosphamide alone, there was no significant increase in lifespan.

In a fourth experiment (table 6) a weak virus inoculum was used. Tumors grew and regressed in nine of ten untreated control mice, and six of ten mice survived to 100 days when the experiment was terminated. Treatment with levamisole or tetramisole (0.04-40 mg/kg) 3 days prior to virus inoculation had no effect on survival or lifespan. In immunosuppressed mice (cyclophosphamide, 210 mg/kg, Day -1) tumors grew progressively and killed nine of ten mice. Levamisole had no effect on tumor growth, survival time, or number of survivors in the immunosuppressed mice. Although there was a larger number of mice with tumor regression in immunosuppressed groups treated with tetramisole, there was no effect on lifespan or the number of survivors.

DISCUSSION

Neither levamisole nor tetramisole exerted a significant effect on primary tumor growth, metastasis, or survival of mice bearing Lewis lung carcinoma. The basis for the discrepancy between these results and the previous report (16) of curative activity for levamisole in this tumor system is unclear. Levamisole and tetramisole have been tested in other laboratories[8] and were found to be inactive when used alone in the treatment of Lewis lung carcinoma.

[8]Schabel FM, Jr. Personal communication. Southern Research Institute, Birmingham, Ala.
Garattini S. Personal communication. Istituto di Richerche Farmacologiche "Mario Negri," Milan, Italy.

TABLE 6.—Effect of levamisole or tetramisole given 3 days before virus inoculation in MSV-induced rhabdomyosarcoma

Treatment*		Mean survival time of dying animals only (days)	T/C†	No. of long-term survivors/ total No. treated‡	No. of animals with—		
Drugs	Dose levels (mg/kg)				Progression	Regression	No-take
Untreated controls		66.5	—	6/10	1/10	9/10	
Levamisole	40	55.8	84	4/10	3/10	5/10	2/10
Levamisole	4	67.3	101	7/10	1/10	8/10	1/10
Levamisole	0.4	54.5	82	4/10	5/10	5/10	
Levamisole	0.04	74.0	111	8/10		9/10	1/10
Tetramisole	40	58.4	88	0/10	6/10	4/10	
Tetramisole	4	58.0	87	4/10	5/10	3/10	2/10
Tetramisole	0.4	67.0	100	5/10	3/10	6/10	1/10
Tetramisole	0.04	49.8	75	6/10	3/10	5/10	2/10
Cyclophosphamide	210	35.7	54	1/10	9/10	1/10	
Cyclophosphamide + Levamisole	210 + 40	32.5	49 [91]	0/10	8/10	2/10	
Cyclophosphamide + Levamisole	210 + 4	38.7	58 [108]	1/10	9/10	1/10	
Cyclophosphamide + Levamisole	210 + 0.4	36.2	55[101]	1/10	8/10	1/10	1/10
Cyclophosphamide + Levamisole	210 + 0.04	33.5	50 [94]	0/9	8/9	1/9	
Cyclophosphamide + Tetramisole	210 + 40	30.5	46 [85]	0/10	6/10	4/10	
Cyclophosphamide + Tetramisole	210 + 4	36.5	55[102]	0/9	6/9	2/9	1/9
Cyclophosphamide + Tetramisole	210 + 0.4	39.9	60 [112]	0/9	6/9	3/9	
Cyclophosphamide + Tetramisole	210 + 0.04	38.4	58 [107]	0/10	8/10	1/10	1/10

*Levamisole or tetramisole administered ip 3 days prior to virus inoculation. Cyclophosphamide administered ip 1 day prior to virus inoculation.

†*See* footnote in table 4.

‡No. of survivors on Day 100 when experiment was terminated.

It is possible that pretreatment with these drugs, shown to be effective in two of the experiments with virus-induced rhabdomyosarcoma (table 4), might have had therapeutic activity against the sc Lewis lung carcinoma. Tetramisole pretreatment of mice inoculated iv with Lewis lung carcinoma was, however, totally ineffective (table 3).

The lack of effect against L1210 and P388 leukemias, Lewis lung carcinoma, B16 melanoma, and Madison 109 lung tumor suggests that levamisole and tetramisole do not have carcinostatic or carcinolytic activity in these systems, which have been used to select cytotoxic antineoplastic agents for clinical trial (25,26). Nonspecific immunostimulatory activity of levamisole and tetramisole (1-11) may not have been manifested as an antitumor effect in these systems since the tumors have low antigenicity for the syngeneic hosts. Spontaneous regressions are not observed in these tumor systems.

Following inoculation of MSV, primary rhabdomyosarcomas may grow progressively or, in many cases, grow and regress (24). Regression may be complete or temporary with eventual regrowth and death. Immunosuppression results in progressive growth in all animals (27). Various methods of immunotherapy have been evaluated in this tumor system (27-29). The effects of treatment with tetramisole or levamisole were variable. In two initial experiments (table 4 and fig 1) tetramisole treatment had a definite beneficial effect. There was an increase in the number of animals that had regressing tumors, an increase in the number of long-term survivors, and a prolongation of the survival time of those animals that died of tumor. These responders were observed in groups that received single doses of 4 or 0.4 mg/kg. Although a single dose of 40 mg/kg showed no evidence of toxicity, it was less effective than lower doses in the MSV-induced tumor system. The time of

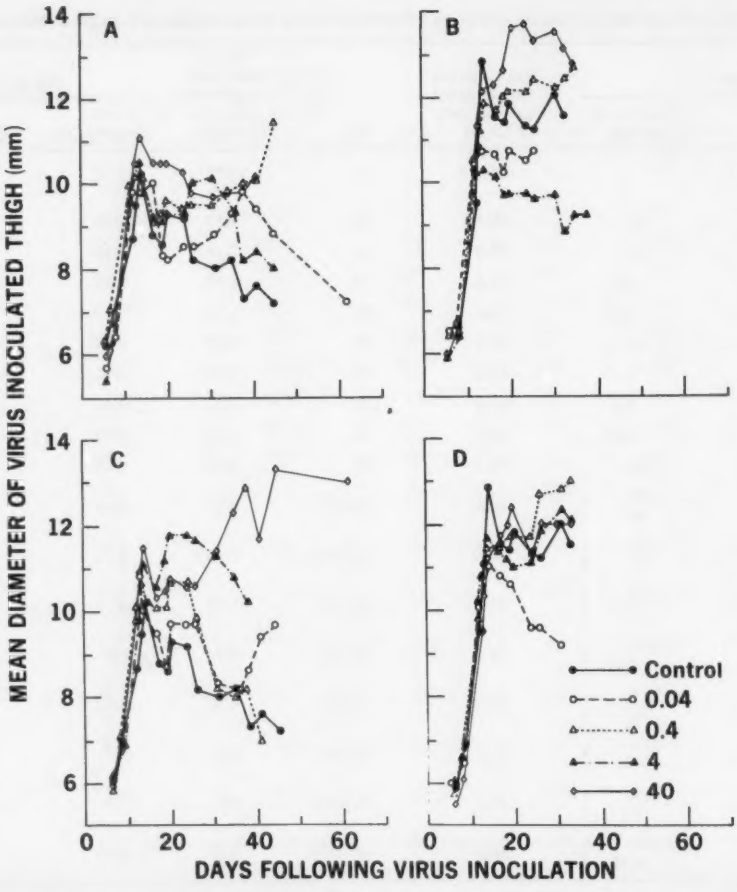

FIGURE 2.—Effects of levamisole and tetramisole on growth of MSV-induced rhabdomyosarcoma im in BALB/c mice. A: Mean diameter of tumor-bearing leg after treatment with levamisole at the indicated doses 1 day prior to virus inoculation. B: Levamisole at the indicated doses plus cyclophosphamide (210 mg/kg) 1 day prior to virus inoculation. C: Tetramisole at the indicated doses 1 day prior to virus inoculation. D: Tetramisole at the indicated doses plus cyclophosphamide (210 mg/kg) 1 day prior to virus inoculation. Each group consisted of 8 mice and the curves were plotted out to median survival time.

tetramisole administration relative to virus inoculation was an important variable in this tumor system. There was a beneficial effect when a single dose of tetramisole was given at some time points prior to or after virus but not at other time points. The number of tetramisole-treated mice that did not develop palpable tumors could suggest that the drug has antiviral activity, although this is unlikely since the greatest number of no-takes was observed when tetramisole was administered 3 days prior to virus. Furthermore, the drug had no antiviral activity in in vitro assays.[9] The no-takes, on the other hand, could be due to immune stimulation resulting in tumor rejection prior to the tumor reaching palpable size.

In two further experiments, neither tetramisole nor levamisole given 1 day (table 5) or 3 days (table 6) prior to virus inoculation had any significant antitumor effect as measured by the number of animals with tumor regression, the number of long-term survivors, or the mean survival time of the dying animals. In these experiments, a majority of the animals in the untreated control groups had tumors that regressed, and there were a number of long-term survivors. Treatment with levamisole or tetramisole at several of the dosage levels increased the number of mice with progressively growing tumors and decreased the number of long-term survivors. The variability in the response to levamisole and tetramisole of MSV-induced rhabdomyosarcoma could be related to differences in the virus challenge or the status of the immune system of the mice. The effects of these drugs on the immune system may be inconsequential when the immune response of the

[9]Kende M. Personal communication. Microbiological Associates, Inc., Bethesda, Md.

animals is strong enough to produce tumor regression and long-term survival in a majority of the untreated control mice. The detrimental effects of these drugs seen in the two experiments shown in tables 5 and 6 could be due to enhancement of humoral immune response by levamisole or tetramisole (18) resulting in interference with cell-mediated immunity (30,31).

Neither tetramisole nor levamisole had a reproducible effect on tumor growth or survival of MSV-inoculated mice that had been immunosuppressed with cyclophosphamide. In one of three experiments (table 6) tetramisole-treated immunosuppressed mice had a higher number of tumor regressions, which was not reflected in increased lifespan or survivors. Treatment with levamisole at the time of cyclophosphamide administration (table 5) affected tumor growth, lifespan, and survival. However, administration of levamisole prior to cyclophosphamide (table 6) had no effect on the tumor. These observations suggest that levamisole may be capable of altering immune status in immunosuppressed mice and that the timing of drug administration may be crucial. These results are in contrast to the effects of BCG in this experimental system. BCG pretreatment had no effect on the course of the disease in normal animals but was shown to reverse the immunosuppressive effects of cyclophosphamide (29).

In conclusion, the immunostimulatory activity of levamisole and tetramisole can influence tumor growth only under certain conditions in certain tumor systems. There is no effect on syngeneic transplantable tumors of low antigenicity. In the immunogenic virus-induced tumor system, results are dependent on such variables as dose level, time of administration of the agents relative to virus inoculation, immune status of the host, and strength of the virus challenge. Immune stimulants such as levamisole and tetramisole may be of little value as single agents in the treatment of cancer. However, the use of these agents following cytoreductive surgery or chemotherapy may be beneficial as indicated by the studies of Chirigos et al (18) and Spreafico et al (17).

REFERENCES

1. Renoux G, and Renoux M. Effet immunostimulant d'un imidothiazole dans l'immunisation des souris contre l'infection par *Brucella abortus*. C R Acad Sci 272:349-350, 1971.
2. _____. Action immunostimulante de dérives du phénylimidothiazole sur les cellules spléniques formatrices d'anticorps. C R Acad Sci 274:756-757, 1972.
3. _____. Restauration par le phénylimidothiazole de la réponse immunologique des souris âgées. C R Acad Sci 274:3034-3035, 1972.
4. _____. Action de phénylimidothiazole (tetramisole) sur la réaction de greffon contre l'hôte. Rôle des macrophages. C R Acad Sci 274:3320-3323, 1972.
5. Hoebeke J, and Franchi G. Influence of tetramisole and its optical isomers on the mononuclear phagocytic system. Effect on carbon clearance in mice. J Reticuloendothel Soc 14:317-323, 1973.
6. Lichtenfeld JL, Desner M, Mardiney MR, Jr, et al. Amplification of immunologically induced lymphocyte ^{3}H-thymidine incorporation by levamisole. Fed Proc 33:790, 1974.
7. Hokama Y, Kimura L, Perriera S, et al. Effects of levamisole and C-reactive protein on mitogen stimulated lymphocytes in vitro and on the Cx-reactive protein response in vivo. Fed Proc 33:650, 1974.
8. Tripodi D, Park L, and Brugmans J. Drug-induced restoration of cutaneous delayed hypersensitivity in anergic patients with cancer. N Engl J Med 289:354-357, 1973.
9. Verhaegen H, deBeukalaar A, and Krug F. Levamisole-induced conversion of tuberculin-negative patients. St Bartholomeus Tijdingen 2:79, 1973.
10. Hirshaut Y, Pinsky C, Marguardt H, et al. Effects of levamisole on delayed hypersensitivity reactions in cancer patients. Proc Am Assoc Cancer Res 14:109, 1973.
11. Verhaegen H, DeCree J, DeCock W, et al. Levamisole and the immune response. N Engl J Med 289:1148, 1973.
12. Raeymakers AHM, Roevens LFC, and Janssen PAJ. The absolute configurations of the optical isomers of the broad spectrum antihelmintic, tetramisole. Tetrahedron Lett 16:1467-1470, 1967.
13. Hirshaut Y, Pinsky C, Fried J, et al. Trial of levamisole as immunopotentiator in cancer patients. Proc Am Assoc Cancer Res and ASCO 15:126, 1974.
14. Copeland D, Stewart T, and Harris J. Effect of levamisole (NSC-177023) on in vitro human lymphocyte transformation. Cancer Chemother Rep 58:167-170, 1974.
15. Bast RC, Jr, Zbar B, Borsos T, et al. BCG and cancer. II. Clinical studies. N Engl J Med 290:1458-1469, 1974.
16. Renoux G, and Renoux M. Levamisole inhibits and cures a solid malignant tumour and its pulmonary metastases in mice. Nature [New Biol] 240:217-218, 1972.
17. Spreafico F, Vecchi A, Montavani A, et al. Characteristics of the immunostimulants levamisole and tetramisole. Eur J Cancer. In press.
18. Chirigos MA, Pearson JW, and Pryor J. Augmentation of chemotherapeutically induced remission of a murine leukemia by a chemical immunoadjuvant. Cancer Res 33:2615-2618, 1973.
19. Potter CW, Carr I, Jennings R, et al. Levamisole inactive in treatment of four animal tumours. Nature 249:567-569, 1974.
20. Geran RI, Greenberg NH, Macdonald MM, et al. Protocols for screening chemical agents and natural products against animal tumors and other biological systems (third edition). Cancer Chemother Rep Part 3, vol 3(2):1-103, 1972.
21. Moloney JB. Biological studies on a lymphoid-leukemia virus extracted from Sarcoma 37. I. Origin and introductory investigations. J Natl Cancer Inst 24:933-951, 1960.
22. Simpson-Herren L, and Lloyd HH. Kinetic parameters and growth curves for experimental tumor systems. Cancer Chemother Rep 54:143-174, 1970.
23. Wexler H. Accurate identification of experimental pulmonary metastases. J Natl Cancer Inst 36:641-645, 1966.
24. Fefer A, McCoy JL, Perk K, et al. Immunologic, virologic and pathologic studies of regression of autochthonous Moloney sarcoma virus-induced tumors in mice. Cancer Res 28:1577-1585, 1968.
25. Carter SK. Some thoughts on experimental models and their clinical correlations. Eur J Cancer 9:833-841, 1973.
26. Johnson RK, and Goldin A. The clinical impact of screening and other experimental tumor studies. Cancer Treat Rev 2:1-31, 1975.
27. Fefer A. Immunotherapy and chemotherapy of Moloney sarcoma virus-induced tumors in mice. Cancer Res 29:2177-2183, 1969.
28. _____. Immunotherapy of primary Moloney sarcoma virus-induced tumors in mice. Int J Cancer 5:327-337, 1970.
29. Houchens DP, Goldberg AI, Gaston MR, et al. Studies of the effects of bacillus Calmette-Guérin on Moloney sarcoma virus-induced tumors in normal and immunosuppressed mice. Cancer Res 33:685-690, 1973.
30. Hellström I, and Hellström KE. Studies on cellular immunity and its serum-mediated inhibition of Moloney-virus-induced mouse sarcomas. Int J Cancer 4:587-600, 1969.
31. Hellström I, Sjögren HO, Warner G, et al. Blocking of cell-mediated tumor immunity by sera from patients with growing neoplasms. Int J Cancer 7:226-237, 1971.

Toxicologic Screening of Daunorubicin (NSC-82151), Adriamycin (NSC-123127), and Their Derivatives in Rats[1,2,3]

Gerhard Zbinden and Elisabeth Brändle[4,5,6]

SUMMARY

The cardiotoxicity of seven anthracycline antibiotics was evaluated in small groups of rats treated with repeated intraperitoneal injections. The electrocardiogram showed a widening of the QRS complex often with the appearance of a distinct S-wave trough and occasionally with an increase or flattening of the T wave. Ventricular extrasystoles, intraventricular block, bradycardia, and heart failure developed either during treatment or after discontinuation of therapy. Based on the cumulative dose required to induce significant electrocardiographic changes, the compounds were ranked in the following order of decreasing cardiotoxicity: adriamycin, daunorubicin, NSC-149584, rubidazone, NSC-143496, daunomycin-semicarbazone, and NSC-118714. For three of these compounds used in humans (adriamycin, daunorubicin, and rubidazone) the rat screening results are in good agreement with the clinically observed cardiotoxicity.

[Cancer Chemother Rep 59:707-715, 1975]

The anthracycline antibiotics daunorubicin and adriamycin have gained a prominent place in the treatment of leukemias, lymphomas, and some solid tumors. However, their therapeutic usefulness is limited by adverse effects, particularly bone marrow suppression and cardiac toxicity (1-10). In order to find compounds with a more favorable therapeutic index derivatives have been synthesized, many of which show appreciable antileukemic and antitumor activities in animal models (11-13). A preliminary toxicologic evaluation of the active substances is now required to permit a rational selection of the most promising candidate drugs for further development and clinical trials.

Useful information on general toxic and bone marrow suppressant effects is often obtained from routine antitumor screening in mice. The cardiotoxic qualities of the anthracycline antibiotics are much more difficult to demonstrate. In a first attempt to solve this problem Herman et al (14,15) investigated the acute cardiovascular effects of selected compounds during intravenous (iv) infusion into various animal species. In golden hamsters and rhesus monkeys daunorubicin and adriamycin induced ventricular arrhythmias. It was found, however, that these changes were reversible and apparently caused by the stimulation of the sympathetic nervous system (16). Thus, the acute pharmacologic experiment is not an appropriate model for cardiomyopathy that occurs in man after prolonged administration of anthracycline antibiotics.

Early toxicologic studies have shown that multiple iv injections of daunorubicin in rabbits caused serofibrinous pericarditis, myofiber degeneration, and interstitial fibrosis of the heart muscle (17). Based on these observations, Jaenke (18) has developed a toxicologic assay which evaluates this lesion by a semiquantitative rating of degenerative changes observed by light and electron microscopy. With daunorubicin and adriamycin, cardiomyopathy developed after 2-4 months of treatment with maximally tolerated doses. The similarity of the structural changes of the rabbit heart to those described in cancer patients dying of congestive heart failure after treatment with anthracycline antibiotics was striking. The cardiomyopathy observed in rabbits, therefore, offers a promising approach for a relevant toxicologic screening.

Due to the scarcity of starting material and the difficulty of chemical synthesis, many of the new anthracycline derivatives are in short supply. A toxicologic screening method using small amounts of

---

[1]Received Dec 17, 1974; revised Mar 26, 1975; accepted Apr 23, 1975.

[2]Supported in part by a grant from the Swiss National Sciences Foundation.

[3]Chemical nomenclature, NSC numbers, and CAS registry numbers for all compounds mentioned in this paper are included in the List of Compounds at the end of the text. The drugs used in this study were received through the courtesy of Dr. H. B. Wood, Jr., Drug Development Branch, Drug Research and Development, Division of Cancer Treatment (DCT), National Cancer Institute (NCI), Bethesda, Md.

[4]Institute of Toxicology, Federal Institute of Technology and University of Zurich, Switzerland.

[5]We thank Prof. W. Rutishauser, Zurich, for his help in evaluating the ECGs, and Mrs. A. Häkkinen and Messrs. C. Häberlin and H. Nef for their technical assistance.

[6]*Reprint requests to:* G. Zbinden, MD, Institute of Toxicology, Federal Institute of Technology and University of Zurich, Schorenstrasse 16, 8603 Schwerzenbach, Switzerland.

test compounds is therefore desirable. The procedure described in this paper permits a rapid preliminary assessment of the toxic properties of anthracycline antibiotics, usually with less than 200 mg of the test compounds. The method makes use of a recent observation (19) that repeated injections of daunorubicin caused changes in the electrocardiogram (ECG) of unanesthetized rats. General toxic and hematotoxic effects were also evaluated in the same animals.

MATERIALS AND METHODS

Experimental Animals

Female rats of the Siv 50 strain weighing approximately 160 g were housed in pairs in Macrolone cages and received Nafag-890 rat cubes and water ad libitum. They were divided into groups of six and received the drugs (fig 1) or 0.2 ml/100 g body weight of 0.9% saline or dimethylsulfoxide (DMSO) five times weekly by intraperitoneal (ip) injection. The drugs were dissolved in water, with the exception of NSC-143496 which was prepared in DMSO. Adriamycin was provided in 10-mg vials containing 50 mg of lactose. The daily doses were 1 and 4 mg/kg for the more toxic compounds and 4 and 8 mg/kg for well-tolerated derivatives. With NSC-118714 the 4-mg/kg dose was doubled after ten injections. All solutions were made fresh daily and adjusted to give an injected volume of 0.2 ml/100 g body weight. The number of injections is listed in tables 1-3.

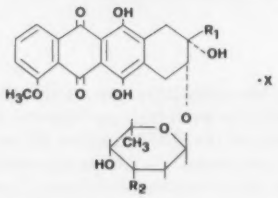

Daunomycin	R_1 = $-\overset{O}{\overset{\|}{C}}-CH_3$	R_2 = NH_2	X = HCl
NSC 118 714	id	$NH-\overset{O}{\overset{\|}{C}}-CH_3$	$CH_3-\overset{CH_3}{\overset{\|}{C}}HOH$
NSC 143 496	id	$HN-\overset{O}{\overset{\|}{C}}-NH-(CH_2)_3CH_3$	-
Adriamycin	$-\overset{O}{\overset{\|}{C}}-CH_2OH$	NH_2	HCl
NSC 143 114	$-\overset{CH_3}{\overset{\|}{C}}=N-NH-\overset{O}{\overset{\|}{C}}-NH_2$	NH_2	HCl
NSC 149 584	$-\overset{O}{\overset{\|}{C}}-CH_2-O-\overset{O}{\overset{\|}{C}}-(CH_2)_6-CH_3$	NH_2	HCl
NSC 164 011	$-\overset{CH_3}{\overset{\|}{C}}=N-NH-\overset{O}{\overset{\|}{C}}-C_6H_5$	NH_2	HCl

FIGURE 1.—Structural formulas of the compounds tested. Daunomycin = daunorubicin; NSC-143114 = daunomycin-semicarbazone; NSC-164011 = rubidazone.

TABLE 1.—General toxicity of anthracycline antibiotics

Drug	Dose (mg/kg)	No. of injections	No. of deaths/ total No. of animals*	Mean change in body weight† (g ± SD)	Ascites‡
Daunorubicin	1	20	0	12.2 ± 6	0
Daunorubicin	4	7	5/6	1.7 ± 7	++
Adriamycin	1	20	0	10.8 ± 3	0
Adriamycin	4	5	5/6	−32.3 ± 9	+
NSC-118714	1	20	0	12.1 ± 6	0
NSC-118714	4→8	10→10	0	14.7 ± 8 12.3 ± 5	— 0
Daunomycin-semicarbazone	4	10	0	25.5 ± 8	0
Daunomycin-semicarbazone	8	10	0	11.3 ± 2	0
NSC-143496	4	10	0	13.2 ± 8	0
NSC-143496	8	10	0	14.0 ± 3	0
NSC-149584	1	25	0	12.8 ± 4	+
NSC-149584	4	7	1/6	−22.2 ± 10	++
Rubidazone	4	10	0	19.2 ± 5	0
Rubidazone	8	10	1/6	2.3 ± 5	++
DMSO	0.2§	30	0	17.8 ± 8	0
0.9%NaCl	0.2§	30	0	25.7 ± 10	0

*During treatment and up to 10 days after treatment.
†During first wk of treatment.
‡ + = Moderate, + + = marked.
§ Ml/kg.

TABLE 2.—Hematotoxicity of anthracycline antibiotics

Drug	Dose (mg/kg)	No. of injections	Minimal mean values (± SD) reached during or immediately after treatment		
			Hemoglobin (g/100 ml)	Hematocrit (%)	Wbc (10^3 cells/mm^3)
Daunorubicin	1	20	14.2 ± 2.1	47 ± 6	9.3 ± 1.6
Daunorubicin	4	7	11.3 ± 1.7*	43 ± 6*	4.4 ± 1.3*
Adriamycin	1	20	12.5 ± 15*	43.0 ± 5.5*	5.7 ± 1.9*
Adriamycin	4	5	14.5 ± 0.6†	56 ± 2†	2.8 ± 0.8*
NSC-118714	1	20	14.5 ± 0,8	51 ± 3	11.3 ± 2.1
NSC-118714	4→8	10→10	14.8 ± 0.4	53 ± 1	12.9 ± 3.1
			14.4 ± 1.0	52 ± 3	11.2 ± 0.9
Daunomycin-semi-carbazone	4	10	14.4 ± 0.6	52 ± 2	11.4 ± 1.8
Daunomycin-semi-carbazone	8	10	15.0 ± 0.5	53 ± 2	9.3 ± 1.6
NSC-143496	4	10	14.4 ± 0.4	52 ± 3	12.2 ± 0.8
NSC-143496	8	10	15.4 ± 0.9	55 ± 1	10.1 ± 1.3
NSC-149584	1	25	12.9 ± 0.8*	47 ± 3*	8.5 ± 1.4*
NSC-149584	4	7	8.7 ± 4.0*	34 ± 13*	5.7 ± 1.5*
Rubidazone	4	10	13.7 ± 0.4	51 ± 3	8.0 ± 2.0*
Rubidazone	8	10	11.1 ± 2.3*	40 ± 9*	5.2 ± 2.3*
DMSO	0.2‡	30	15.4 ± 0.2	52 ± 1	11.5 ± 2.1
0.9% NaCl	0.2‡	30	15.2 ± 0.5	5 ± 1	11.7 ± 2.7

*Statistically significant difference in comparison with NaCl- or DMSO-treated controls ($P < 0.05$, U-test of Mann and Whitney).
†Severe hemoconcentration.
‡Ml/kg.

Animals were inspected and weighed five times weekly. ECGs were recorded 2 days before treatment, and from one to four times weekly thereafter. After treatment, rats were kept alive for up to 59 days. ECGs were recorded in the morning before drug injection with a Narco Physiograph DMP 4B (Narco Bio Systems Inc., Houston, Tex). Unanesthetized rats were confined to a small animal holder. Twenty-six-gauge needle electrodes were inserted under the skin over the right scapula and the lumbar vertebrae (lead D) (20). Paper speed was 10 cm/second (sec). ECGs were coded for blind evaluation. All measurements were made on tracings of ten consecutive cardiac cycles. The heart rate was calculated from R-R intervals.

Hemoglobin (cyanohemoglobin "Roche" Diagnostica), hematocrit (standard procedure), and white blood cell (wbc) counts (Coulter Counter Model B) were determined once before and at least once weekly during and after treatment.

After completion of the experiments, surviving animals were sacrificed. At autopsy, the presence of ascites was recorded. Hearts were excised, rinsed in physiologic saline, and fixed in 4% buffered formaline. Frozen sections were stained with oil red O for fat. Paraffine-embedded atrial and ventricular myocardium was sectioned and stained with hematoxylin and eosin.

RESULTS

General Toxicity

The number of animals dying up to the tenth day after the last injection, mean body weight changes during the first treatment week, and development of ascites were used as indicators of general toxicity (table 1). The experiments with the high dose showed that adriamycin was the most toxic compound, followed by daunorubicin, NSC-149584, and rubidazone. At the low dose level these four compounds were well tolerated although ascites was noted with 1 mg/kg of NSC-149584. The other three substances had no effect on survival and body weight and did not induce ascites even at the high dose of 8 mg/kg.

TABLE 3.—ECG effects of anthracycline antibiotics

Drug	Dose (mg/kg)	No. of injections	No. of injections required to induce widening of QRS (≥22 msec)	No. of injections required to induce significant ($P<0.05$) widening of QRS*	Maximum mean QRS duration plus S-wave trough (msec ± SD)	No. of animals developing late ventricular extrasystoles
Daunorubicin	1	20	13	8	23.2 ± 2.1	0
Daunorubicin	4	7	5	4	26.0 ± 2.8	0
Adriamycin	1	20	11	6	24.2 ± 2.5	1
Adriamycin	4	5	3	3	27.8 ± 1.2	0
NSC-118714	1	20	—	—	19.0 ± 1.3	0
NSC-118714	4→8	10→10	—	—	18.3 ± 0.8 19.3 ± 1.0	0
Daunomycin-semicarbazone	4	10	—	—	20.0 ± 1.5	0
Daunomycin-semicarbazone	8	10	10	5	22.0 ± 1.8	4
NSC-143496	4	10	—	—	20.7 ± 1.0	0
NSC-143496	8	10	4	4	22.0 ± 1.0	1
NSC-149584	1	25	18	6	23.7 ± 2.0	0
NSC-149584	4	7	5	5	25.0 ± 2.2	0
Rubidazone	4	10	—	—	21.2 ± 2.6	0
Rubidazone	8	10	3	3	27.0 ± 5.9	0
DMSO	0.2†	30	—	—	19.0 ± 1.6	0
0.9% NaCl	0.2†	30	—	—	18.7 ± 0.5	0

*U-test of Mann and Whitney.
† Ml/kg.

Hematotoxicity

The decreases in hemoglobin and hematocrit values and wbc count were used as screening parameters for bone marrow suppression. Table 2 contains the lowest mean value reached by each group either during or immediately after treatment. Adriamycin and NSC-149584 depressed hemoglobin and hematocrit values significantly at 1 mg/kg. Similar changes were induced with 4 mg/kg of daunorubicin and 8 mg/kg of rubidazone. The other substances had no effect on hemoglobin and hematocrit values.

Significant leukopenia was present in rats treated with 4 and 1 mg/kg of adriamycin and NSC-149584. Daunorubicin caused a marked drop in the wbc count at 4 mg/kg and a borderline decrease at 1 mg/kg. The same effect was seen with rubidazone at 8 and 4 mg/kg. The other substances had no significant effect on the wbc count. All hematologic changes became normal within 2 weeks after treatment.

Cardiotoxicity

An evaluation of the ECGs showed that early changes of the QRS complex provided the most sensitive indicator of cardiotoxicity. The mean duration of the QRS complex determined in 192 ECGs from 96 rats prior to treatment was 18.1 msec (SD ± 1.33 msec). The extreme values found were 15 and 21 msec. No ST segment was present in the control ECGs. During drug treatment there was progressive widening of the QRS complex often associated with the appearance of a distinct S-wave trough and, occasionally, an ST segment. With some of the compounds these were the only ECG changes observed. With the other compounds, QRS became extremely wide (> 25 msec), often deteriorating into an intraventricular block. In some animals, marked bradycardia (<400 beats/minute) was observed a few hours before death. The development of these ECG changes is illustrated in an example shown in figure 2. Increase or flattening of the T wave as described for daunorubicin (19) was also observed. These changes occurred irregularly and could not be used as screening parameters.

The mean duration of the QRS complex including the S-wave trough was calculated from the measurements of all animals of each group. In order to compare the various treatments the number of injections necessary to produce a mean QRS duration of 22 msec (= mean QRS duration of 192 normal ECGs ± 3 SD) or more was determined. These figures are

shown in table 3. This table also indicates the number of injections required to cause a significant ($P<0.05$) widening of the QRS in comparison with control groups treated with NaCl or DMSO. Adriamycin and daunorubicin caused a rapid widening at the 4-mg/kg level of the QRS complex with the appearance of an S-wave trough. Intraventricular block developed in most animals. Repeat experiments not reported confirmed the finding that adriamycin was slightly but consistently more cardiotoxic than daunorubicin. Both drugs also induced moderate ECG changes at 1 mg/kg.

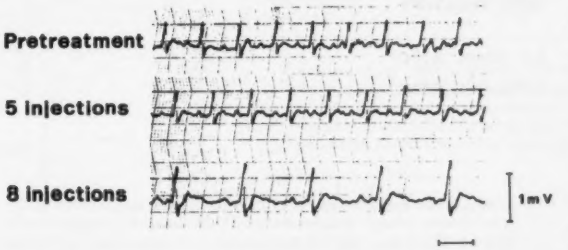

FIGURE 2.—Development of QRS widening after 5 injections and bradycardia and intraventricular block after 8 injections of 8 mg/kg of rubidazone. ⊢—⊣ = 0.1 Sec.

The only other compound causing QRS widening at 1 and 4 mg/kg was NSC-149584. The effect was moderate, and an intraventricular block did not develop. Rubidazone, NSC-143496, and daunomycin-semicarbazone caused widening of the QRS at 8 mg/kg. With rubidazone, the effect developed most rapidly and was most pronounced. The ECGs of rats treated with NSC-118714 remained unchanged.

The development of the QRS change during treatment with adriamycin is demonstrated in figure 3. With both doses, a widening of the QRS complex and an appearance of an S-wave trough were seen rapidly. At 1 mg/kg, the QRS complex reached a duration

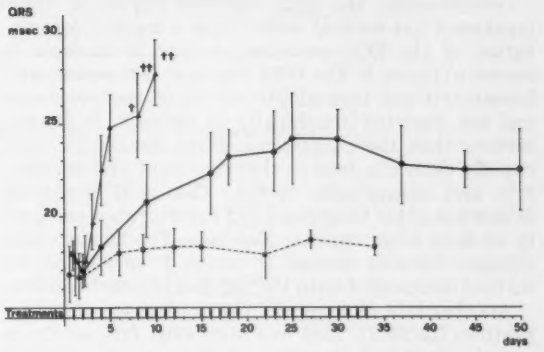

FIGURE 3.—Graphic representation of the QRS widening (including S-wave trough) in groups of 6 rats treated with adriamycin (▲), 5 × 4 mg/kg ip; adriamycin (●), 20 × 1 mg/kg ip; and 0.9% NaCl (■), 30 × 0.2 ml/kg (mean of the group + SD).
† = Time of death of 1 animal.

of 22 msec 24 hours after the eleventh injection. In two repeat experiments nine and ten injections were needed to obtain the same effect. Thus, the reproducibility of the test result is satisfactory, despite the small size of the groups.

After treatment was discontinued, a followup of the animals provided information on the reversibility of the cardiotoxic effects and on late degenerative changes. In most of the animals the duration of the QRS decreased and the S-wave trough became less prominent, but only in rare instances did the ECG tracings revert to normal. In some animals who showed rapid development of the QRS changes, deterioration of the ECG continued after cessation of treatment. A typical series of ECG tracings demonstrating the development of an intraventricular block, bradycardia, and heart failure 3 days after the last injection of 4 mg/kg of daunorubicin is shown in figure 4.

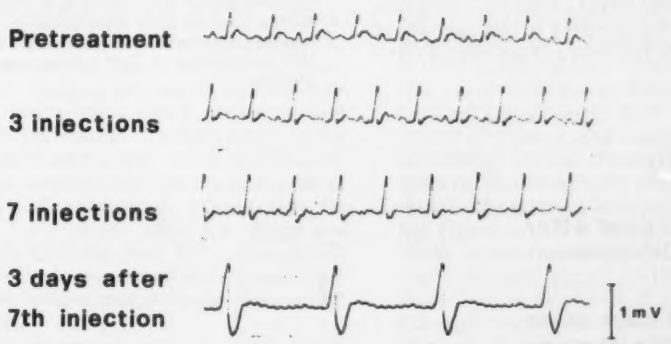

FIGURE 4.—Widening of QRS complex with appearance of distinct S-wave trough after 3 and 7 injections of 4 mg/kg of daunorubicin. Heart failure, bradycardia, and intraventricular block developed 3 days after the last injection. ⊢—⊣ = 0.1 Sec.

Occasionally, the QRS changes improved after treatment but several weeks later a marked deterioration of the ECG occurred. A typical example is shown in figure 5. The QRS changes, wbc count, and hematocrit and hemoglobin values of the same animal are depicted graphically in figure 6. It demonstrates that the cardiotoxic effect developed more rapidly than the drop in the wbc count and hematocrit and hemoglobin values. The ECG improved somewhat after treatment but deteriorated markedly 40 days after the last injection. The hematologic changes became normal in about 2 weeks and remained unchanged until the rat died of heart failure.

Another late change was the occurrence of extrasystoles (table 3). This was seen most frequently in rats treated with 8 mg/kg of daunomycin-semicarbazone. At this dose the compound had only a marginal effect on QRS but four of the six rats developed ventricular extrasystoles 11-47 (mean 24) days after the last injection (fig 7).

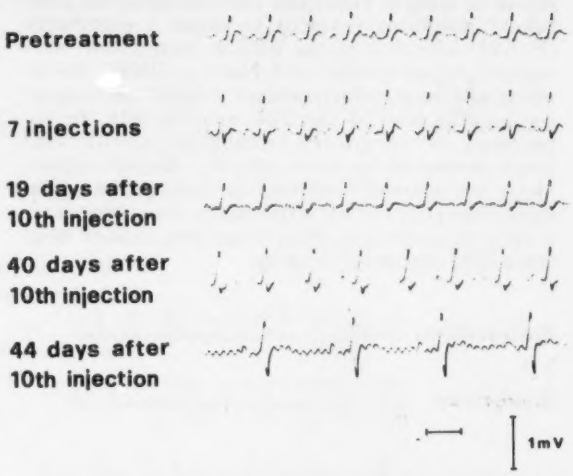

FIGURE 5.—Marked widening of QRS complex and appearance of distinct S-wave trough observed after 7 injections of 8 mg/kg of rubidazone. There was partial improvement 19 days after last (10th) injection and rapid deterioration 40 days after last injection; death was 4 days later. |—| = 0.1 Sec.

Histopathologic Examinations

Light microscopic examination of the animal hearts disclosed no fatty change and in most instances no significant structural alterations of the myocardial tissues. Slight focal fiber degeneration or atrophy with modest proliferation of interstitial connective tissue was seen in rats treated with adriamycin and daunorubicin. A correlation of these findings with ECG determinations was not possible, since animals were kept alive after treatment for up to 59 days.

DISCUSSION

The toxicologic screening differs in many respects from the conventional procedures of the safety testing of new drugs. Screening tests must be rapid and inexpensive and use small quantities of the test substances. The measurements are usually restricted to a few characteristic effects amenable to quantitative assessment. This permits a comparison of the test compounds with reference drugs whose clinical toxicity is known.

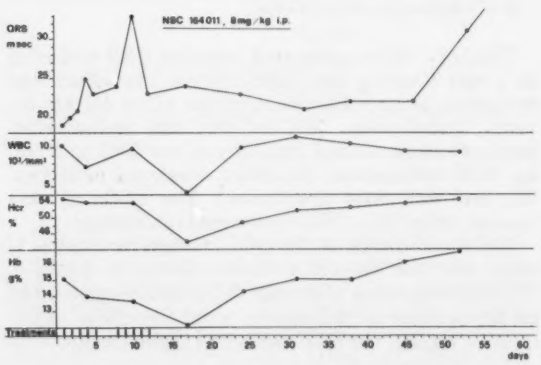

FIGURE 6.—Graphic representation of the ECG and blood changes of the same animal as shown in fig 5. Rapid widening of QRS with partial recovery after discontinuation of therapy; late development of intraventricular block. Slow decrease in wbc, hemoglobin (Hb), and hematocrit (Hcr) with recovery after discontinuation of treatment.

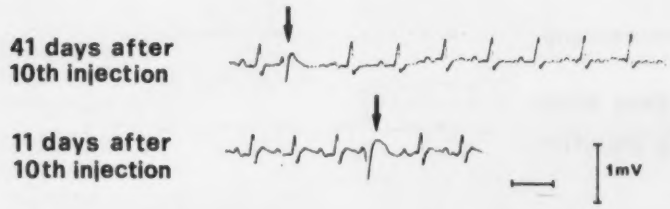

FIGURE 7.—Examples of ventricular extrasystoles occurring after discontinuation of treatment with 8 mg/kg of daunomycin-semicarbazone.

TABLE 4.—Toxicity ranking of anthracycline antibiotics

Drug	Toxicity ranking*			
	General toxicity	Hematotoxicity		Cardiotoxicity†
		Hgb and Hct	Wbc	
Adriamycin	1	1	1	1 (68)
Daunorubicin	2	3	3	2 (80)
NSC-149584	3	2	2	3 (110)
Rubidazone	4	4	4	4 (148)
Daunomycin-semicarbazone	5 ‡	5 ‡	5 ‡	6 (490)
NSC-143496	6	6	6	5 (195)
NSC-118714	7	7	7	7 (>800)

*Ranking of 1-7 indicates most to least toxic.

†Nos. in parentheses represent approximate minimal cumulative cardiotoxic dose (mg/m²) calculated for a rat with total body surface of 325 m² (taking from table 2 the minimal cardiotoxic dose causing QRS widening of 22+ msec).

‡There were no differences in ranking between drugs in brackets.

The evaluation of anthracycline antibiotics in rats described in this paper fulfills many of these requirements. The experiments are conducted with small numbers of animals and the duration of treatment is short. Only small quantities of the test drugs are therefore required. The toxic effects are assessed quantitatively. This permits a ranking of the test compounds with regard to general toxicity, hematologic effects, and cardiotoxic effects in comparison with the standards, daunorubicin and adriamycin. Table 4 shows that a very good correlation exists between general toxicity and cardiotoxicity induced by the seven analogs tested. In the ranking order of the hematotoxic effects, however, daunorubicin and NSC-149584 have exchanged their positions.

An important step in the development of a relevant toxicologic assay system is the selection of a sensitive animal species. Up to now the rat has not been considered a suitable laboratory animal for the evaluation of cardiomyopathy induced by anthracycline antibiotics. This judgement was based on the pharmacologic observation that iv infusion of daunorubicin in doses as high as 300 mg/kg caused only minor changes in heart rate, blood pressure, and ECG (14). Moreover, myocardial damage could not be demonstrated by light microscopy after a large single iv dose (21). The present experiments prove, however, that evidence of cardiotoxic effects may be observed at much lower doses when the drugs are given repeatedly. In fact, the first ECG changes occurred at considerably lower cumulative doses than those necessary to induce morphologic damage of the rabbit heart (18).

The experiments disclosed certain similarities between the cardiotoxic effects observed in rats and in man; in both, myocardial damage develops gradually and is usually dependent on total dose. Heart failure in rats occurred suddenly, often weeks after discontinuation of therapy. This is in good agreement with clinical experience showing that the occurrence of heart failure in patients is unpredictable. The ECG changes described in man, although by no means specific for anthracycline antibiotics, were similar to those seen in rats (19). In addition, the ultrastructural lesions of the heart muscle observed in rats after repeated ip or iv injection of daunorubicin resembled those described in patients treated with daunorubicin and adriamycin (8, 10, 21, 22). These changes, however, are not specific for anthracycline antibiotics but occur also in other forms of cardiomyopathy (10,18).

The final evaluation of a toxicologic test system requires a comparison of its results with clinical experience in man. Since three of the drugs have been used in cancer and leukemia patients, a preliminary appraisal of the predictive value of the animal test can be made. From the screening experiments in rats it was concluded that, on a milligram for milligram basis, adriamycin was slightly more cardiotoxic than daunorubicin. Published information on clinical cardiotoxicity is difficult to evaluate since patients differed widely with regard to age, nature and extent of disease, and treatment schedule. Moreover, knowledge gained through extensive use of daunorubicin was available when adriamycin was introduced into clinical therapy. From data published in the literature it is apparent that both drugs may cause severe cardiomyopathy if the total dose exceeds 500-550 mg/m² (1-10). Thus, there is no evidence for the existence of a major difference between the cardiotoxic qualities of the two antibiotics. The clinical experience, therefore, is in good agreement with the rat screening results.

Only limited clinical information on the cardiotoxicity of rubidazone is available: fifty-seven leukemic children and adults were treated with total doses

which ranged from 20 to 30 mg/kg for most patients and were over 30 mg/kg in six. Only one case of sinus tachycardia was observed (11).

From these preliminary data it is probable that rubidazone is less cardiotoxic than adriamycin and daunorubicin when given at clinically effective doses. This is in good agreement with the screening results obtained in rats. Further clinical studies are needed to confirm these results and to assess the practical value of the rat screening test as a tool for a preliminary toxicologic evaluation of new anthracycline antibiotics.

From the present study some information on structure-activity relationships may be gained. The screening results indicate that substitution at the C-9 position of the tetracycline structure had a profound effect on the cardiotoxic properties: the hydroxyacetyl (adriamycin) and acetyl (daunorubicin) derivatives were the most toxic compounds, followed by the 14-octanoate of adriamycin (NSC-149584). In order to induce comparable ECG changes, higher doses of the benzylhydrazone derivative of daunorubicin, rubidazone, were necessary. The semicarbazone derivative of daunorubicin, daunomycin-semicarbazone, had only weak cardiotoxic properties.

In this group of derivatives the chemotherapeutic activity in various animal tumor models roughly parallels the cardiac toxicity demonstrated in the rat screening. Adriamycin and daunorubicin are outstandingly effective against many experimental tumors. NSC-149584 is also highly active in several tumor model systems but its effectiveness against L1210 leukemia is not as good as that of the two standard drugs, adriamycin and daunorubicin. Rubidazone, although active against various experimental tumors (L1210 and P388 leukemias and B16 melanoma) appears to be somewhat less effective than the three more toxic compounds. Daunomycin-semicarbazone was tested against L1210 leukemia and found to be slightly active at relatively high doses (12).[7]

Two additional compounds tested were daunorubicin analogs with substitution at the sugar moiety. Substitution with butylcarbamoyl (NSC-143496) markedly reduced but did not abolish cardiotoxicity and eliminated all chemotherapeutic activity against L1210 leukemia (12).[7] The *N*-acetyl derivative NSC-118714 was not cardiotoxic at the dose levels tested. In the antitumor screening the drug was quite effective against P388 leukemia but had only marginal activity against L1210 leukemia (12).[7] Adamson (23) has suggested that the daunosamine portion of the anthracycline antibiotics was responsible for the uptake of the molecules by the cardiac muscle and might thus determine the cardiotoxic properties. The lack of cardiotoxicity of the *N*-acetyl derivative supports this speculation. The *N*-butylcarbamoyl derivative is probably less stable. Some daunorubicin may be formed in the body which would explain the slight ECG effect observed with this drug.

From these comparisons it appears that the reduction in toxicity of the newer anthracycline antibiotics is, to a certain extent, offset by a loss in chemotherapeutic activity. The compound which combines the strong and broad-spectrum antitumor activity of adriamycin with very low cardiac toxicity has not yet been identified. Improved toxicologic methods are now available for the assessment of cardiotoxicity in rabbits (18) and in rats and will facilitate the search for better compounds.

[7]Schepartz SA. Personal communication. Data are on file at the DCT, NCI, National Institutes of Health, Bethesda, Md, 1974.

LIST OF COMPOUNDS

Adriamycin: NSC-123127; CAS reg. No. 23214-92-8

Daunomycin-semicarbazone: NSC-143114; daunomycin, 3-semicarbazone, monohydrochloride, dihydrate

Daunorubicin: NSC-82151; CAS reg. No. 23541-50-6; daunomycin

NSC-118714: L-lyxo-hexopyranoside, 3-β-acetyl-1,2,3,4,6,11-hexahydro-3,5,12-trihydroxy-10-methoxy-6,11-dioxo-1α-naphthacenyl-3-acetamido-2,3,6-trideoxy-, α-, compd. with isopropyl alcohol (1:1)

NSC-143496: CAS reg. No. 38942-75-5; daunomycin, *N*-(butylcarbamoyl)-

NSC-149584: adriamycin, 14-octanoate, hydrochloride

Rubidazone: NSC-164011; CAS reg. No. 36508-71-1; daunorubicin, benzoylhydrazone, monohydrochloride

REFERENCES

1. Macrez C, Marneffe-Lebrequier H, Ripault J, et al. Accidents cardiaques observés au cours des traitements par la rubidomycine. Pathol Biol 15:949-953, 1967.
2. Ripault J, Weil M, and Jacquillat C. Etude nécropsique de quatre malades traites par la rubidomycine. Pathol Biol 15:955-957, 1967.
3. Serpick AA, and Henderson ES. Observations on toxicity and clinical trials with daunomycin. Pathol Biol 15:909-912, 1967.
4. Tan C, Tasaka H, Yu KP, et al. Daunomycin, an antitumor antibiotic, in the treatment of neoplastic disease. Clinical evaluation with special reference to childhood leukemia. Cancer 20:333-353, 1967.
5. Malpas JS, and Scott RB. Rubidomycin in acute leukaemia in adults. Br Med J 3:227-229, 1968.
6. Bonadonna G, and Monfardini S. Cardiac toxicity of daunorubicin. Lancet 1:837, 1969.
7. Malpas JS, and Scott RB. Daunorubicin in acute myelocytic leukaemia. Lancet 1:469-470, 1969.
8. Ainger LE, Bushore J, Johnson WW, et al. Daunomycin: a cardiotoxic agent. J Natl Med Assoc 63:261-267, 1971.
9. Gottlieb JA, Baker LH, Quagliana JM, et al. Chemotherapy of sarcomas with a combination of adriamycin and dimethyl triazeno imidazole carboxamide. Cancer 30:1632-1638, 1972.
10. Lefrak EA, Pitha J, Rosenheim S, et al. A clinicopathologic analysis of adriamycin cardiotoxicity. Cancer 32:302-314, 1973.
11. Bernard J, Jacquillat C, Boiron M, et al. Cinquante-sept observations de leucemies aigües. Essai de traitement par un dérivé semi-synthetique de la daunorubicine: le 22 050 R.P. Nouv Presse Med 33:2149-2152, 1972.
12. Driscoll JS, Hazard GF, Jr, Wood HB, Jr, et al. Structure-antitumor activity relationships among quinone derivatives. Cancer Chemother Rep Part 2, vol 4(2):1-362, 1974.
13. Maral R, Ponsinet G, and Jollès G. Étude de l'activité antitumorale expérimentale d'un nouvel antibiotique semi-synthétique: la rubidazone (22 050 R.P.). C R Acad Sci 275:301-304, 1972.

14. Herman EH, Schein P, and Farmar RM. Comparative cardiac toxicity of daunomycin in three rodent species. Proc Soc Exp Biol Med 130:1098-1102, 1969.

15. Herman E, Mhatre R, Lee IP, et al. A comparison of the cardiovascular actions of daunomycin, adriamycin, and *N*-acetyldaunomycin in hamsters and monkeys. Pharmacology 6:230-241, 1971.

16. Herman EH, Schein P, and Farmar RM. Influence of pharmacologic or physiologic pretreatment on acute daunomycin cardiac toxicity in the hamster. Toxicol Appl Pharmacol 16:335-344, 1970.

17. Maral R, Bourat G, Ducrot R, et al. Etude toxicologique et activite antitumorale expérimentale de la rubidomycine (13.057 R.P.). Pathol Biol 15:903-908, 1967.

18. Jaenke RS. An anthracycline antibiotic-induced cardiomyopathy in rabbits. Lab Invest 30:292-304, 1974.

19. Cargill C, Bachmann E, and Zbinden G. Effects of daunomycin and anthramycin on electrocardiogram and mitochondrial metabolism of the rat heart. J Natl Cancer Inst 53:481-486, 1974.

20. Grauwiler J. Herz und Kreislauf der Säugetiere. Basel, Birkhäuser Verlag, 1965.

21. Chalcroft SCW, Gavin JB, and Herdson PB. Fine structural changes in rat myocardium induced by daunorubicin. Pathology 5:99-105, 1973.

22. Buja LM, Ferrans VJ, Mayer RJ, et al. Cardiac ultrastructural changes induced by daunorubicin therapy. Cancer 32:771-788, 1973.

23. Adamson RH. Letter: Daunomycin (NSC-82151) and adriamycin (NSC-123127): a hypothesis concerning antitumor activity and cardiotoxicity. Cancer Chemother Rep 58:293-294, 1974.

Inhibition of Deamination of ^{14}C-Cytosine Arabinoside (NSC-63878): A Useful Biologic Assay for Tetrahydrouridine (NSC-112907)[1,2,3]

R. L. Furner and L. B. Mellett[4,5,6]

SUMMARY

Inhibition of the deamination of ^{14}C-cytosine arabinoside by two lots of tetrahydrouridine was studied in monkey serum. The average inhibition of deaminase activity was 78% for tetrahydrouridine lot AJ39 (1.0 μM) when the concentration of cytosine arabinoside ranged from 44.2 to 170.7 μM; under the same conditions tetrahydrouridine lot AJ22 inhibited deamination by an average of 68%. Apparent K_i values were 0.26 μM for AJ39 and 0.43 μM for AJ22. The assay may be used to check the relative biologic activity of various lots of tetrahydrouridine.

[Cancer Chemother Rep 59:717-720, 1975]

Tetrahydrouridine is synthesized by the catalytic reduction of cytidine in water (1). It is a potent inhibitor of cytosine arabinoside deamination (2-4) and, as such, may be used to prolong the biologic half-life of cytosine arabinoside during the treatment of acute leukemia.

Camiener (5) described an enzymatic "competitive efficiency test" based on isotope dilution. The inhibition of deamination of labeled substrate by the test material was compared to the apparent decrease in deamination upon the addition of unlabeled substrate. In a later report the K_i of the enzyme inhibitor complex for tetrahydrouridine was approximately 10-4-10-5 M. This report confirms the deaminase inhibition previously reported for tetrahydrouridine and suggests that the assay of deaminase activity as affected by this agent may be useful as a tool in determining the relative biologic activity of different lots of tetrahydrouridine.

MATERIALS AND METHODS

Tetrahydrouridine was supplied in two separate lots labeled AJ39 (95% pure) and AJ22 (purity unknown). Stock solutions of each lot were prepared in H_2O. Predetermined amounts of these solutions were added to conical centrifuge tubes and evaporated to dryness. Final concentrations of tetrahydrouridine in monkey serum ranged from 0.08 to 77.7 μM. The final substrate concentrations (^{14}C-cytosine arabinoside; 3.24 microcuries/mg) ranged from 11.2 to 170.7 μM. Control samples of serum were assayed for deaminase activity in the absence of tetrahydrouridine.

Reactions were initiated by addition of substrate to the serum-tetrahydrouridine mixture. Incubations were carried out at 37°C for 10 minutes and the reactions were terminated by direct spotting of the incubation mixture on Gelman SA-20 instant thin-layer chromatography media. Previous experiments indicated that the reaction did not continue after spotting, and there was no protein interference.

Chromatograms were developed in $CHCl_3$:CH_3OH:concentrated HCl (60:40:0.02) (6). Each chromatogram was cut into a vertical column 2.54 cm wide; the column was subdivided into 0.5-cm segments. Each segment was placed into a scintillation vial and eluted with 1 ml of H_2O. Ten ml of Aquasol was added as the scintillator. Values were recovered as observed counts per minute and corrected to reflect nmols of uracil arabinoside (1-β-D-arabinofuranosyluridine) formed per ml of serum per 10 minutes of incubation. The number of each strip divided by the strip number of the solvent front provided an estimate of the R_f values for cytosine arabinoside and uracil arabinoside.

RESULTS

Five of six experiments (fig 1) show greater inhibition of deaminase activity by tetrahydrouridine lot AJ39 than by lot AJ22. Differences in the inhibitory capacities were greater at 1 μM than at 0.1 μM of the inhibitor. Compared with the control series in which no inhibitor was present, AJ39 inhibited the

[1]Received Jan 13, 1975; revised Mar 24, 1975; accepted Apr 23, 1975.

[2]Supported by contracts NO1-CM-50654 and NO1-CM-43780 from the Division of Cancer Treatment (DCT), National Cancer Institute (NCI), National Institutes of Health, Department of Health, Education, and Welfare.

[3]Cytosine arabinoside: CAS reg. No. 69-74-9; cytosine, 1- β -D-arabinofuranosyl-, monohydrochloride; ara-C.

Tetrahydrouridine: CAS reg. No. 5627-05-4; 2(*1H*)-pyrimidinone, tetrahydro-4-hydroxy-1- β-D-ribofuranosyl-; H_4U. Supplied by Dr. Harry B. Wood, Drug Research and Development, DCT, NCI.

[4]Southern Research Institute, Birmingham, Ala.

[5]We acknowledge the expert technical assistance provided by Mrs. Barbara Garrett and Mr. Thomas Herren.

[6]*Reprint requests to:* Dr. R. L. Furner, Southern Research Institute, 2000 9th Ave S, Birmingham, Ala 35205.

formation of uracil arabinoside 77% at a substrate concentration of 170.7 μM (table 1), while AJ22 inhibited this formation only 65% at the same substrate concentration.

At high concentrations of inhibitor the kinetics are nonlinear as indicated earlier by Camiener (2). Therefore, only three inhibitor concentrations were used in fitting the data to a Dixon plot (7). Even though the plot is not strictly linear, it is useful for comparison when two inhibitors are used over the same concentration range. As shown in figure 2, the apparent K_i values are 0.26 μM for lot AJ39 and 0.43 μM for lot AJ22.

DISCUSSION

These experiments confirm the nonlinearity of deaminase inhibition by tetrahydrouridine as reported by Camiener (2). However, the apparent K_i values are in the range of 10^{-7}-10^{-6} in contrast to a 10^{-5}-10^{-4} range found by Camiener for human liver deaminase. These differences may be due to several different factors such as methods used in estimating the K_i, source of the deaminase enzyme, and purity of the tetrahydrouridine. Indeed, Camiener reported that tetrahydrouridine concentrations of 10^{-6}-10^{-5} M inhibited by 95% the deaminase preparations from mouse kidney, rhesus monkey liver, and *Actinomycete mycelium*.

The use of the kinetics described here is limited for interpretation by their nonlinear nature. However, since the plot does indicate a K_i value within the range expected (in view of fig 1), it is considered valid.

The biologic activity of the lots tested here is not readily comparable with the activity of the lots used by Camiener, but it is possible that purer material may be available now than could be prepared several years ago.

The assay described is sensitive enough to detect 10%-20% differences in inhibitory potency. For practical purposes the inhibition of the deamination of ^{14}C-cytosine arabinoside can be monitored as described in figure 1C, using serum containing 1.0 μM tetrahydrouridine and 170 μM ^{14}C-cytosine arabinoside. In the event that tetrahydrouridine is accepted for clinical use, knowledge of the biologic activity of each lot will become critical to proper therapy.

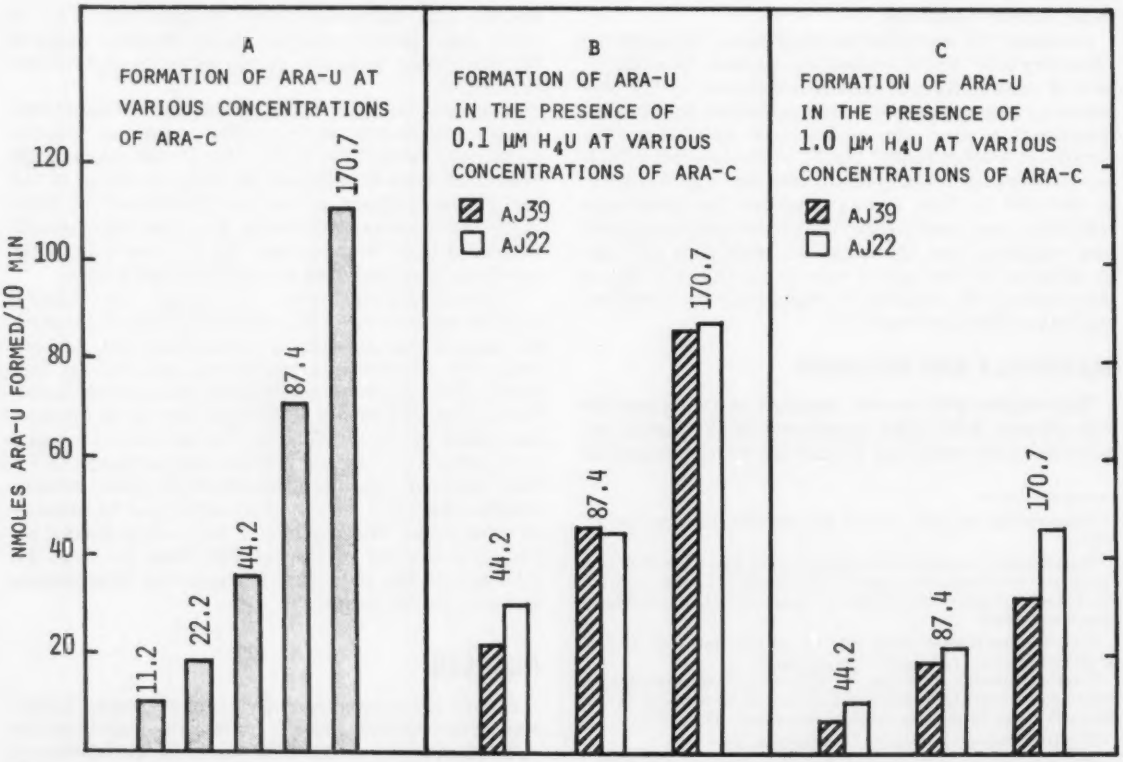

FIGURE 1.—A: ^{14}C-cytosine arabinoside (ara-C) added to monkey serum at concentrations (μM) indicated above each bar. Incubations were for 10 mins at 37°C. Values are expressed as nmols of ^{14}C-uracil arabinoside (ara-U) formed per incubation. B: Monkey serum contained 0.1 μM tetrahydrouridine (H_4U) lot AJ39, or 0.1 μM H_4U lot AJ22 and ^{14}C-ara-C as indicated. C: Monkey serum contained 1.0 μM H_4U lot AJ39, or 1.0 μM H_4U lot AJ22 and ^{14}C-ara-C as indicated.

TABLE 1.—Percent inhibition of uracil arabinoside formation by tetrahydrouridine

^{14}C-cytosine arabinoside	Percent inhibition by—* Tetrahydrouridine lot— AJ39 (0.1 μM)	AJ22 (0.1 μM)	AJ39 (1.0 μM)	AJ22 (1.0 μM)
170.7	22.7	21.0	77.4	64.6
87.4	35.3	37.5	74.0	70.2
44.2	39.5	17.0	83.1	71.5
Average†	32.5	25.1	78.1	68.7

*Inhibition = $1 - \frac{\text{nmols experimental}}{\text{nmols control}} \times 100$.

†Average inhibition of deaminase activity covering 3 different substrate concentrations.

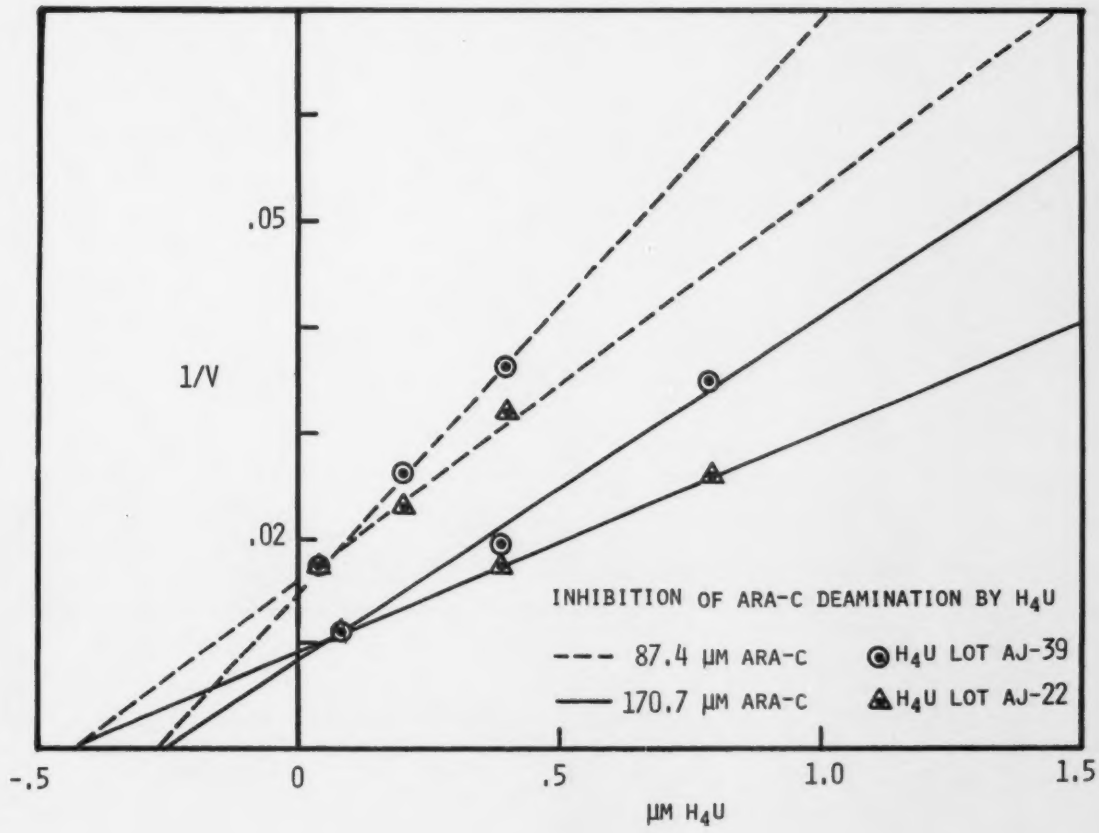

FIGURE 2.—Money serum containing tetrahydrouridine (H_4U) lots AJ39 or AJ22 as indicated and 87.4 or 170.7 μM ^{14}C-cytosine arabinoside (ara-C) was incubated for 10 mins at 37°C. Velocity was measured as ^{14}C-uracil arabinoside formed per 10-min incubation.

REFERENCES

1. Hanze AR. Nucleic acids. 4. The catalytic reduction of pyrimidine nucleosides (human liver deaminase inhibitors). J Am Chem Soc 89:6720-6725, 1967.
2. Camienier GW. Studies of the enzymatic deamination of ara-cytidine. V. Inhibition in vitro and in vivo by tetrahydrouridine and other reduced pyrimidine nucleosides. Biochem Pharmacol 17:1981-1991, 1968.
3. Ho DHW. Inhibition of 1-β -d-arabinofuranosyl cytosine phosphorylation in human livers by tetrahydrouridine. Biochem Pharmacol 21:2936-2940, 1972.
4. Mellett LB, El Dareer SM, White V, et al. Inhibition of deamination of ^{3}H-arabinosylcytosine (ara-C) by tetrahydrouridine (H_4U) in BDF_1 mice. Pharmacologist 16:210, 1974.
5. Camienier GW. Studies of the enzymatic deamination of cytosine arabinoside. 3. Substrate requirements and inhibitors of the deaminase of human livers. Biochem Pharmacol 16:1691-1702, 1967.
6. Furner RL, Strobel JD, El Dareer SM, et al. Factors influencing the chromatographic analysis of 2,2'-*O*-cyclocytidine. J Chromatogr 92:105-111, 1974.
7. Ayling JE. Enzyme kinetic approach to the analysis of structure function relationship in the evaluation of drug action. In A Guide to Molecular Pharmacology-Toxicology, Part I (Featherstone RM, ed). New York, Marcel Dekker, Inc., 1973.

Potential Biologic Markers in Burkitt's Lymphoma[1]

T. Phillip Waalkes,[2] Charles W. Gehrke,[3] Werner A. Bleyer,[2,4] Robert W. Zumwalt,[3] Charles L. M. Olweny,[5] Kenneth C. Kuo,[3] Duane B. Lakings,[2] and Samuel A. Jacobs[2,6,7]

SUMMARY

Specific biochemical molecules used as potential biologic markers, including modified nucleosides, polyamines, and pyrimidine catabolic end-products, were quantitatively measured in the urine of seven patients with Burkitt's lymphoma before, during, and after one or more courses of therapy. The results of this preliminary study demonstrated that patients with this disease frequently excrete significantly increased amounts of modified nucleosides (considered to be derived primarily from transfer ribonucleic acid), polyamines, and β-aminoisobutyric acid during the course of their disease. With successful treatment and rapid destruction of tumor cells, a concomitant rise in these molecules occurs. Elevations were observed prior to chemotherapy and changes in levels associated with treatment or tumor progression appeared to correlate with disease status and to aid in assessing antitumor response. Periodic follow-up analysis of these molecules may be helpful in appraising relapse or recurrence of the malignancy prior to overt evidence of tumor by existing clinical means.

[Cancer Chemother Rep 59:721-727, 1975]

Determining elevated levels of biologic markers for cancer in the body fluids of patients can aid in the diagnosis of malignancy and in the assessment of response to antitumor treatment. A rise in the level of a marker induced by therapeutic measures should reflect tumor cell destruction. When monitored at the time of treatment, the degree of change in the level of a marker would depend upon the rate and number of tumor cells destroyed and the catabolism of the marker under study.

Burkitt's lymphoma is a rapidly growing malignant tumor, characterized by its high proliferative cell rate, its short doubling time (1,2), and, for the majority of patients, its prompt dramatic response to antitumor chemotherapeutic agents (3). Associated with such rapid tumor cell lysis due to treatment, toxic effects secondary to the rise in blood levels of normal cellular constituents (4) have been reported. A marker for Burkitt's lymphoma cells would undergo similar changes in level, the degree of which should be related to the number of malignant cells destroyed.

The objectives of this preliminary investigation were to determine if specific biochemical molecules, as potential markers, are elevated in the pretreatment urine samples of patients with Burkitt's lymphoma and to assess whether variations in their levels may correspond to the changes in tumor mass associated with therapy. These studies were carried out as part of a program to find, develop, and evaluate the usefulness of biologic markers during the treatment of malignant diseases.

In this investigation, selected compounds (urinary excretion end-products) were quantitatively measured in aliquot samples of 24-hour urine collections from seven patients with Burkitt's lymphoma, and the results were compared to normal control values. Included in this initial evaluation were (*a*) three minor nucleosides found predominantly as constituents of transfer ribonucleic acid (tRNA), (*b*) polyamines, and (*c*) β-aminoisobutyric acid (β-AIBA) and β-alanine, pyrimidine degradation products.

The nucleosides studied were two methylated derivatives, N^2,N^2-dimethylguanosine (m^2_2G) and 1-methylinosine (m^1I), and pseudouridine. Increased tRNA methylase activity has been a consistent finding in malignant cells when compared to their normal tissue counterparts (5), and elevated levels of

[1]Received Jan 17, 1975; revised Apr 4, 1975; accepted Apr 23, 1975.

[2]Laboratory of Chemical Pharmacology (LCHPH), Experimental Therapeutics (EXT), Division of Cancer Treatment (DCT), National Cancer Institute (NCI), Bethesda, Md.

[3]Department of Biochemistry and Experimental Station Chemical Laboratories, University of Missouri, Columbia.

[4]*Present address:* Division of Hematology/Oncology, Children's Orthopedic Hospital and Medical Center, Seattle, Wash.

[5]Uganda Cancer Institute, Kampala.

[6]We wish to acknowledge the kind assistance of Dr. John L. Ziegler, Chief, Pediatric Oncology Branch, Medical Oncology, DCT, NCI, in obtaining urine samples from patients with Burkitt's lymphoma.

[7]*Reprint requests to:* T. Phillip Waalkes, MD, PhD, LCHPH, EXT, DCT, NCI, Bldg 10, Rm 6B18, National Institutes of Health, Bethesda, Md 20014.

methylated nucleic acid bases have been reported in the tRNAs of animal and human tumors (5). Pseudouridine, which is neither metabolically re-utilized or destroyed but is excreted intact (6,7), is considered a measure of tRNA turnover (7,8). Preliminary investigations had indicated that methylated nucleic acid bases are elevated in the urine of patients with leukemia (9-11), and that pseudouridine is elevated in the urine of patients with leukemia (8,9,11,12) and Hodgkin's disease (8,13). More recently, we have found that these molecules are increased in the urine of patients with advanced solid tumors including a variety of different tumor types (14).

Increased synthesis of polyamines has been reported to be associated with rapid cellular growth (15), and elevated levels for putrescine, spermidine, and spermine have been found in the urine of patients with cancer (16,17).

β-AIBA, derived from the catabolism of thymine (18,19), and β-alanine, derived from uracil, were studied because of the increased proliferative rate for Burkitt's lymphoma cells. β-AIBA levels have been reported to be elevated in the urine of some patients with malignant disease (20) and in the urine of patients with lymphomas after therapy with mechlorethamine (21).[8]

MATERIALS AND METHODS

Patients and Collection of Urine Samples

Seven patients between the ages of 3 and 16 years with Burkitt's lymphoma were studied, five at the time of their initial chemotherapy and two following relapse or recurrence after prior treatment. Five of the patients were hospitalized in the Pediatric Oncology Branch, DCT, NCI. Two of the patients were seen and treated at the Lymphoma Treatment Center, Uganda Cancer Institute, Kampala. Twenty-four-hour urine samples were obtained from all patients before, during, and after at least one or more courses of antitumor therapy. Two patients (A and B) were studied at length during multiple courses of drug treatment. As estimated by clinical measures, patient A had a large amount of tumor present with abdominal disease, ascites, and central nervous system involvement, whereas patient B had the least amount of tumor burden, localized to the abdomen, of all the seven patients evaluated. For control purposes, similar urine collections were obtained from normal subjects within the same age range, including two children from Uganda. The urine was refrigerated without preservative during the collection period. After measurement of the total volume, aliquot samples were frozen at -70°C or lower for storage until analysis.

Nucleosides

The three nucleosides were quantitatively determined by means of gas-liquid chromatography utilizing the method of Chang et al (22). This procedure involves a preliminary charcoal adsorption cleanup step followed by elution with pyridine-ethanol solution and eventual determination of the nucleosides by gas-liquid chromatography as their trimethylsilyl derivatives. Details of the chromatographic method, the reagents and apparatus, the peak identifications, the internal standards, and the calculations employed are given in the prior publication (22); also, we have applied the method to a large number of urine samples from patients with advanced malignancy (14).

Polyamines

Polyamines, including putrescine, spermidine, spermine, and, in addition, cadaverine, were determined by an automated cation-exchange procedure utilizing an amino acid analyzer. The method, including details as to urine sample preparation, apparatus, buffer, and analysis sequence, was developed by Gehrke et al (23).

β-AIBA and β-Alanine

Details of the gas-liquid chromatography method and the apparatus and reagents needed to determine amino acids in physiologic fluids have been published (24). This procedure was modified specifically for β-AIBA and β-alanine utilizing a chromatographic packing of 5.5% diethylene glycol succinate on 80/100 mesh gas chromatograph Q, 1.5 m × 4 mm ID glass column.[9]

Ribonuclease Assay

The procedure of Zimmerman and Sandeen (25) was used to determine ribonuclease in aliquot urine samples. This assay (run in tris-HCl buffer at pH 8.2) measures the release of perchloric acid-soluble, ultraviolet-absorbing products from polycytidylic acid (Sigma Chemical Co., St. Louis, Mo). A standard curve using pancreatic ribonuclease-A (type 1-S, Sigma Chemical Co.) was employed and the amount of urine ribonuclease was extrapolated from this curve and expressed and calculated as μg of pancreatic ribonuclease/kg of body weight/24-hour urine. The volume of urine for each individual assay, run in triplicate, was 0.1 ml and the reaction mixture was incubated at 37°C for 30 minutes.

[8]Mechlorethamine: NSC-762; CAS reg. No. 55-86-7; diethylamine, 2,2'-dichloro-*N*-methyl-, hydrochloride; nitrogen mustard.

[9]Gehrke CW, Zumwalt RW, Kuo KC, et al. Unpublished observations.

RESULTS

Nucleosides

Figure 1 presents the individual determinations for pseudouridine, m_2^2G, and m^1I in the pretreatment urine samples for the seven patients with Burkitt's lymphoma compared to values obtained from normal control subjects. The normal average and 2 SDs above this average indicating the extent of the normal range are shown for each nucleoside. As indicated, four of seven patients for pseudouridine, six of seven for m_2^2 G, and five of seven for m^1I were excreting amounts greater than the 2 SDs of the normal range.

Polyamines

Figure 2 shows the amounts of polyamines found in the same pretreatment individual urines from Burkitt's lymphoma patients compared to the normal control subjects. The normal average and 2 SDs above this average are indicated. For putrescine and cadaverine, six of seven patients had levels above the normal range. For spermidine and spermine all seven of the patients excreted amounts greater than 2 SDs above the normal average.

In figure 3, total urinary polyamines, expressed as μmols/kg/24-hour urine, are plotted at intervals during the course of treatment for patients A and B.

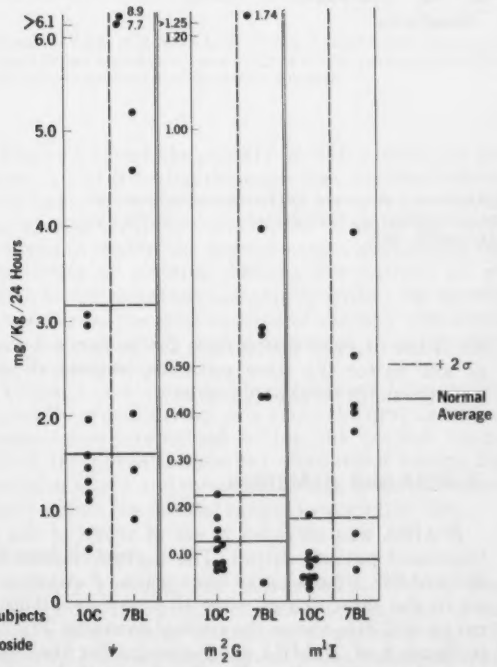

FIGURE 1.—Comparison of pretreatment urinary excretion levels for pseudouridine (ψ), m_2^2G, and m^1I expressed as mg/kg/24 hrs for patients with Burkitt's lymphoma (BL) and normal control subjects (C). ———— Indicates normal average; — — — — is 2 SDs above this average.

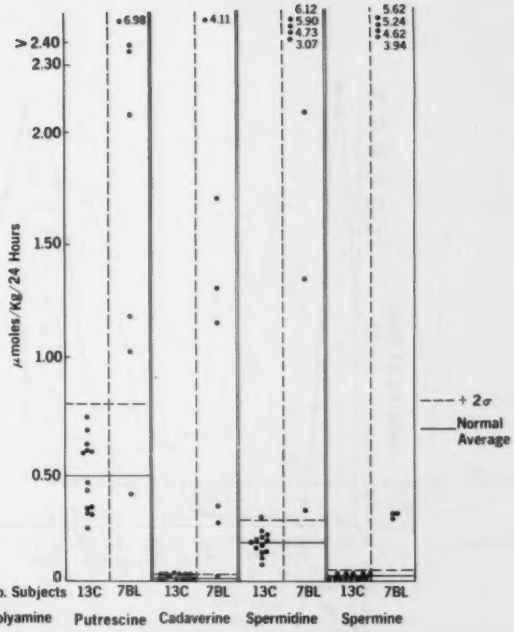

FIGURE 2.—Comparison of pretreatment urinary polyamine levels for putrescine, cadaverine, spermidine, and spermine expressed as μmols/kg/24 hrs for patients with Burkitt's lymphoma (BL) and normal control subjects (C). ———— Indicates normal average; — — — — is 2 SDs above this average.

Patient A was treated on Days 1, 23, and 33 with courses of the combination of cyclophosphamide, vincristine, and methotrexate, followed by intrathecal methotrexate and cytosine arabinoside.[10] By Day 23 the patient was considered clinically free of tumor. Polyamine levels, after the rise with drug therapy on Day 1, decreased to normal levels but by Day 22 were again above normal range and rising. Within a few days after receiving the third course of drug therapy on Day 33, an abdominal tumor mass was once again palpable and there was a reappearance of cells in the cerebrospinal fluid. Adriamycin[11] was given on Day 45, plus further intrathecal chemotherapy and cranial irradiation with clearing of the abnormal cells in the cerebrospinal fluid. This treatment was associated with decreased polyamine levels. Thereafter, however, the patient's course was intermittently downhill despite vigorous treatment

[10]Cyclophosphamide: NSC-26271; CAS reg. No. 6055-19-2; 2*H*-1,3,2-oxazaphosphorine, 2-[bis(2-chloroethyl)amino]tetrahydro-, 2-oxide, monohydrate.

Vincristine: NSC-67574; CAS reg. No. 2068-78-2; leurocristine, sulfate (1:1).

Methotrexate: NSC-740; CAS reg. No. 59-05-2; glutamic acid, *N*-[*p*-[[(2,4-diamino-6-pteridinyl)methyl]methylamino]benzoyl]-.

Cytosine arabinoside: NSC-63878; CAS reg. No. 69-74-9; cytosine, 1-β-D-arabinofuranosyl-, monohydrochloride.

[11]Adriamycin: NSC-123127; CAS reg. No. 23214-92-8.

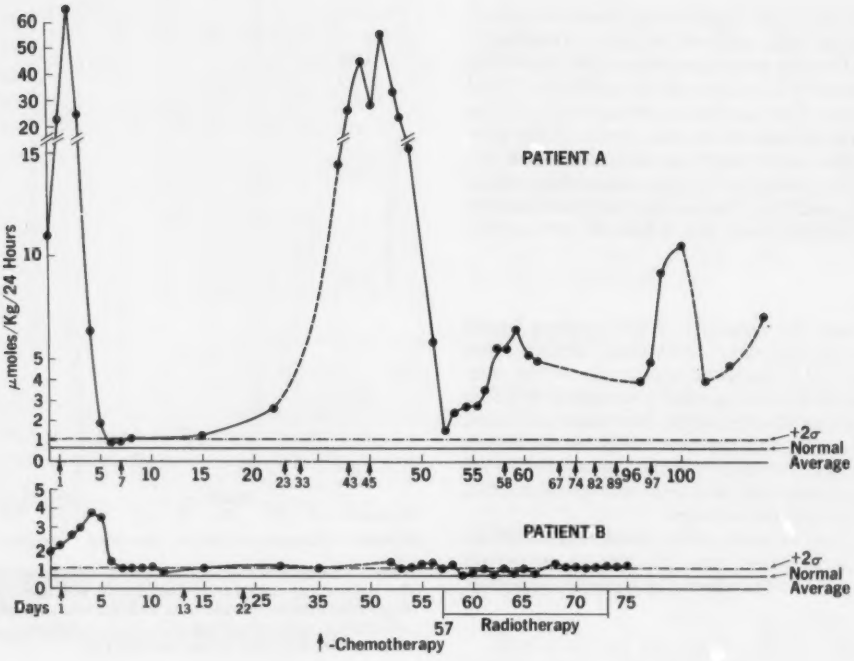

FIGURE 3.—Total 24-hr urinary polyamines in μmols/kg/24 hrs vs time in days before and during treatment for patients A and B. Arrows indicate the days courses of drug therapy were started.——— Shows condensed time scale. Urines and time interval the same as shown in fig 5.

with high-dose methotrexate followed by citrovorum factor rescue. Partial response was noted with each course of therapy but complete clearance of tumor was never observed. Total polyamine levels during this interval were elevated and the patient died.

Three days following the initial course of the same drug combination (cyclophosphamide, vincristine, and methotrexate) the abdominal tumor mass of patient B was no longer palpable. The total polyamine level, somewhat elevated prior to treatment, rose over the ensuing 5 days with a return to normal level thereafter. The patient subsequently received further courses of chemotherapy plus left upper-quadrant abdominal radiation, and for almost a year has been free of any evidence of disease.

The change in levels for total polyamines for all the individual patients during and after therapy followed a similar pattern. The similar changes in levels of the urinary nucleosides for patients A and B, as well as for the other patients, in general paralleled those for total polyamines.

β-AIBA and β-Alanine

β-AIBA was elevated in six of seven of the pretreatment patient urines. The highest values were 360 and 648 μmols/kg/24-hour urine. β-Alanine levels in the same urines were all below or within the range of 2 SDs above the normal average. The ratio in figure 4 of β-AIBA to β-alanine for the normal controls was 1 or less. For the Burkitt's lymphoma patients this ratio was calculated to be 20 or greater as demonstrated in figure 4, thus significantly elevated with respect to the normal values.

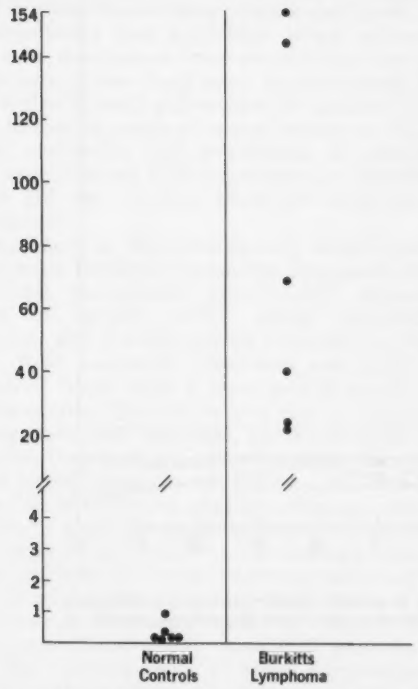

FIGURE 4.—Ratio of β-AIBA to β-alanine concentration in pretreatment urines expressed as μmols/kg/24 hrs for patients with Burkitt's lymphoma and normal control subjects.

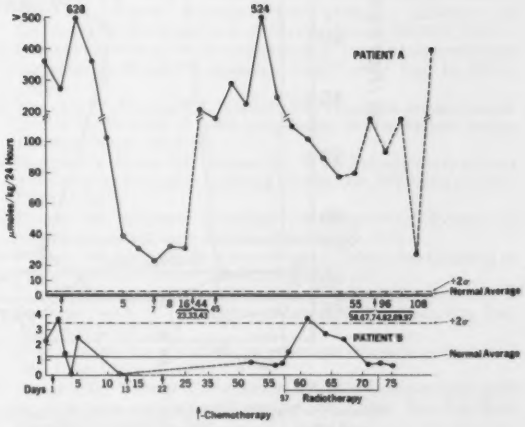

FIGURE 5.—Twenty-four-hr urinary β-AIBA levels in μmols/kg/24 hrs vs time in days before and during treatment for patients A and B. Arrows indicate the days courses of drug therapy were started.— — — — Shows condensed time scale. Urines and time interval the same as shown in fig 3.

Figure 5 shows the urinary β-AIBA levels for patients A and B during the same time periods indicated in figure 3. As shown, β-AIBA levels for patient A varied with treatment and initial response but never dropped to within the normal range, suggesting the possibility of residual disease. For patient B, β-AIBA levels remained essentially within the normal range during the entire period of therapy with small variations in levels which appeared to accompany specific treatment.

Urinary creatinine levels determined for patients A and B before, during, and after the first course of chemotherapy remained within the normal range. All of the patients received allopurinol during the period of study and serum uric acids remained essentially within the normal range through this time.

Ribonuclease

Urinary ribonuclease was measured in the pretreatment urine samples and at intervals during the 11 days after initial treatment for patients A and B. The levels were compared to those obtained from normal age-matched control subjects. As presented in figure 6, pretreatment levels were within the normal range. A rise in level with drug therapy was noted for patient A, but only a small variation in ribonuclease level within the normal range was found for patient B.

DISCUSSION

The characteristic behavior of Burkitt's lymphoma, its high tumor growth rate, and its prompt dramatic response to chemotherapy make this disease ideal for measuring changes in specific molecules in body fluids which may be associated with rapid cellular changes or may be found as the result of destruction of cells secondary to therapy. The urinary pretreatment levels for the three nucleosides (fig 1), the polyamines (fig 2), and β-AIBA (fig 4) were increased for the majority of the patients with Burkitt's lymphoma when compared to normal control subjects in the same age range. Because of the difficulty in estimating the amount of tumor mass, no attempt was made to compare the urine levels for these compounds with total tumor cell burden in the individual patients. However, patient B, who had recent onset of recurrent disease with minimal involvement, had the least apparent total tumor mass of the patients studied and the lowest levels for all the various biologic markers analyzed.

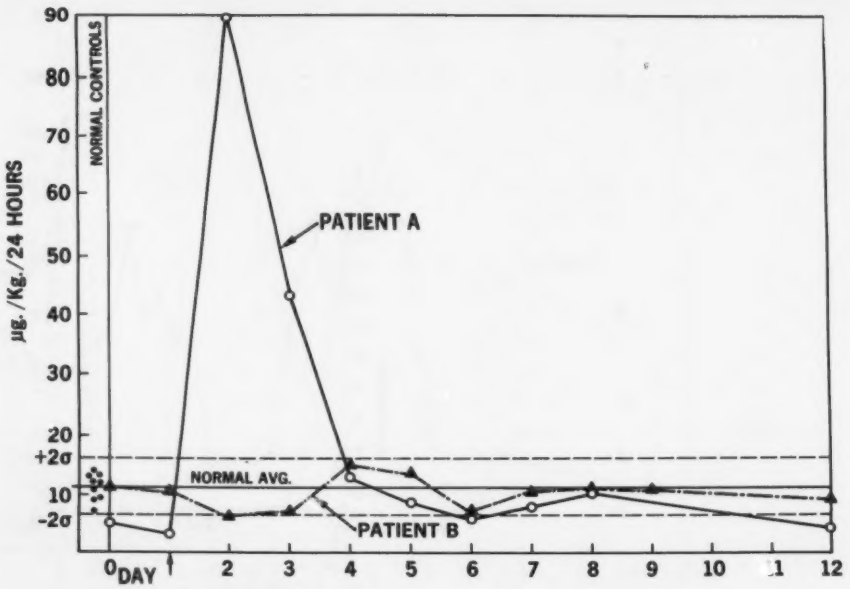

FIGURE 6.—Twenty-four-hr urine ribonuclease levels expressed as μg/kg/24 hrs for patients A and B before and after 1 course of drug treatment. Values determined based on pancreatic ribonuclease activity as given under Materials and Methods.

When antitumor chemotherapy was given, the urine levels for the nucleosides, the polyamines, and β-AIBA increased sharply and then exhibited a subsequent fall to lower levels. The latter drop appeared to parallel the rapid antitumor response as determined by clinical assessment. These changes are demonstrated in figures 3 and 5 for patients A and B. Curves similar to those for patient A were found for the other patients with regard to elevated pretreatment nucleosides, polyamines, and β-AIBA.

After the initial peak and fall in total polyamine level associated with chemotherapy for patient A (fig 3), the subsequent rise above the normal range occurred prior to an indication of tumor reappearance by clinical measurements. Meanwhile, β-AIBA levels (fig 5), although fluctuating with therapy, remained elevated above the normal range throughout the entire same period of treatment, suggesting that residual tumor cells persisted despite the lack of direct evidence by clinical examination.

The finding that β-AIBA urine levels for Burkitt's lymphoma patients may be greatly elevated and associated with normal levels of β-alanine is of distinct interest. β-AIBA in urine has been shown to be the catabolic end-product of thymine (18,19) and is considered present in urine secondary to degradation of deoxyribonucleic acid (DNA). A dual origin for urinary β-AIBA, however, has been demonstrated (26). In addition to thymine in DNA, β-AIBA can be derived from uridine in tRNA after conversion of thymidine by the action of tRNA methylase. Although the possible amounts of β-AIBA from this source are unknown, the fact that increased levels of the methylated nucleosides were also found in the urines from the Burkitt's lymphoma patients further suggests that a portion of this β-AIBA may be the end-product from tRNA thymine. The relatively low levels of β-alanine in these urines tend to support this suggestion. For a few normal individuals, urinary β-AIBA has been found to be elevated. This increased excretion is considered to be secondary to genetic factors (27). Since urine samples prior to the disease onset were not available, it is unknown if any of the patients with Burkitt's lymphoma should be considered in this category.

Increased serum and urine ribonuclease activity has been reported for some patients with neoplastic disease (28,29) and was indicated as a useful marker for following patients with multiple myeloma (30). It was suggested that elevated urine levels for tRNA nucleosides as well as for the other biologic markers under investigation might be secondary to increased ribonuclease activity. As presented in figure 6, the urine ribonuclease level, under the experimental conditions described, was within the normal range for patients A and B in their pretreatment urine samples. In view of this result, it appears doubtful that increased circulating ribonuclease is a factor in the elevated pretreatment urine levels for the nucleosides. With chemotherapy and presumably the

rapid lysis of tumor cells for patient A, a sharp rise and fall in urine ribonuclease content was found.

The possibility that antitumor drugs, acting on normal cells, could cause urine elevations of the various markers under study must be considered. The lack of a rise in total polyamines for patient B following the second course of chemotherapy on Day 13 tends to contradict this possibility. In addition, normal mice injected with vincristine or cyclophosphamide did not excrete increased amounts of polyamines.[12]

On the basis of this preliminary investigation, patients with Burkitt's lymphoma frequently have been found to excrete significantly increased amounts of specific tRNA minor nucleosides, polyamines, and β-AIBA during the course of their disease. With successful treatment and rapid destruction of tumor cells a concomitant rise in the molecules occurs. This rise in level may be helpful in assessing antitumor response, particularly for patients with tumors not readily accessible to measurement by the usual clinical means. Lack of a rise in these levels following adequate therapy may be indicative of prior complete response to treatment or may suggest resistance to the therapy used. In addition, periodic followup determinations may be helpful in appraising relapse or recurrence of disease before any evidence of tumor by current methods. Because of the small number of patients involved, the relative merit of these compounds as potential markers could not be determined adequately.

REFERENCES

1. Iversen C, Iversen OH, Bluming AZ, et al. Cell kinetics of African cases of Burkitt's lymphoma. Eur J Cancer 8:305-308, 1972.
2. Ziegler JL, Bluming AZ, Fass L, et al. Burkitt's lymphoma cell kinetics treatment and immunology. Bibl Haematol 39:1046-1052, 1973.
3. Ziegler JL. Chemotherapy of Burkitt's lymphoma. Cancer 30:1534-1540, 1972.
4. Arseneau JC, Bagley CM, Anderson T, et al. Hyperkalemia, a sequel to chemotherapy of Burkitt's lymphoma. Lancet 1: 10-14, 1973.
5. Borek E. Introduction to symposium: transfer RNA and transfer RNA modification in differentiation and neoplasia. Cancer Res 31:596-597, 1971.
6. Dlugajczyk A, and Eiler JJ. Lack of catabolism of 5-ribosyluracil in man. Nature 212: 611-612, 1966.
7. Weissman SM, Eisen AZ, Lewis M, et al. Pseudouridine metabolism. III. Studies with isotopically labeled pseudouridine. J Lab Clin Med 60: 40-47, 1962.
8. Dlugajczyk A, and Eiler JJ. Studies on 5-ribosyluracil in man. Proc Soc Exp Biol Med 123:453-457, 1966.
9. Adams WS, Davis F, and Nakatani M. Purine and pyrimidine excretion in normal and leukemic subjects. Am J Med 28:726-734, 1960.
10. Fink K, and Adams WS. Urinary purines and pyrimidines in normal and leukemic subjects. Arch Biochem Biophys 126:27-33, 1968.
11. Park RW, Holland JF, and Jenkins A. Urinary purines in leukemia. Cancer Res 22:469-477, 1962.
12. Weissman SM, Eisen AZ, and Karon M. Pseudouridine metabolism. II. Urinary excretion in gout, psoriasis, leukemia and heterozygous oroticaciduria. J Lab Clin Med 59:852-858, 1962.
13. Pinkard KJ, Cooper IA, Motteram R, et al. Purine and pyrimidine excretion in Hodgkin's disease. J Natl Cancer Inst 49: 27-37, 1972.
14. Waalkes TP, Gehrke CW, Zumwalt RW, et al. The urinary excretion of nucleosides of RNA by patients with advanced malignancies. Cancer. In press.
15. Snyder SH, Kreuz DS, Medina UJ, et al. Polyamine synthesis and turnover in rapidly growing tissues. Ann NY Acad Sci 171: 749-771, 1970.
16. Russell DH. Increased polyamine concentrations in the urine of human cancer patients. Nature 223: 144-145, 1971.
17. Russell DH, Levy CC, Schimpff SC, et al. Urinary polyamines in cancer patients. Cancer Res 31:1555-1558, 1971.
18. Fink K, Henderson RB, and Fink RM. β-Aminoisobutyric acid, a possible factor in pyrimidine metabolism. Proc Soc Exp Biol Med 78:135-142, 1951.
19. Fink K. Excretion of pyrimidine reduction products by the rat. J Biol Chem 218:9-13, 1956.
20. Nielsen HR, Nyholm K, and Sjolin KE. β-Aminoisobutyric acid in urine from patients with urothelial tumours. Rev Eur Etud Clin Biol 16:444-450, 1971.
21. Awapara J, and Schullenberger CC. Urinary excretion of β-aminoisobutyric acid after administration of thymine and nitrogen mustard. Clin Chim Acta 2:199-204, 1957.
22. Chang SY, Lakings DR, Zumwalt RW, et al. Quantitative determination of methylated nucleosides and pseudouridine in urine by gas-liquid chromatography. J Lab Clin Med 83:816-830, 1974.
23. Gehrke CW, Kuo KC, Zumwalt RW, et al. Determination of polyamines in human urine by an automated ion-exchange method. J Chromatogr 89: 231-238, 1974.
24. Kaiser FE, Gehrke CW, Zumwalt RW, et al. Amino acid analysis. Hydrolysis, ion-exchange cleanup, derivatization, and quantitation by gas-liquid chromatography. J Chromatogr 94:113-133, 1974.
25. Zimmerman SB, and Sandeen SB. A sensitive assay for pancreatic ribonuclease. Anal Biochem 10:444-449, 1965.
26. Nielsen HR, Borek E, Sjolin KE, et al. Dual origin of β-aminoisobutyric acid, a thymine catabolite. Acta Pathol Microbiol Scand 80:687-688, 1972.
27. Berry HK. Individual metabolic patterns. II. Excretion of β-aminoisobutyric acid. Metabolism 9:373-376, 1960.
28. Zytko J, and Cantero A. Serum ribonuclease in patients with malignant disease. Can Med Assoc J 86:482-485, 1962.
29. Levy AL, and Rottino A. Effect of disease states on the ribonuclease concentration of body fluids. Clin Chem 6:43-51, 1960.
30. Fink K, Adams WS, and Skoog WA. Serum ribonuclease in multiple myeloma. Am J Med 50:450-457, 1971.

[12]Waalkes TP, Gehrke CW, and Adamson RH. Unpublished observations.

Review of Selected Experimental Brain Tumor Models Used in Chemotherapy Experiments[1,2,3]

Philip C. Merker,[4] Isidore Wodinsky,[4] and Ruth I. Geran[5,6]

Five drugs were described by Walker (1) as causing "distinct clinical improvement" in the treatment of malignant brain tumors in man. These drugs are methotrexate, BCNU, CCNU, triethylenemelamine, and hydroxyurea. Of these five, the nitrosourea derivatives, BCNU and CCNU, are considered to possess pharmacophysiologic characteristics most favorable for the treatment of malignant brain tumors (2). The nitrosoureas were first described by Skipper et al (3) as agents which slightly to moderately increased the lifespan of mice bearing intracerebral (ic) implants of an ascites line of L1210 leukemia, and subsequently, Schabel et al (4) demonstrated that BCNU was markedly active against ic L1210 leukemia. Research continues on compounds of this class. Recently, suitable formulations have been developed for lipid-soluble nitrosoureas which can be used parenterally in the treatment of cancer in man (5).

The responsiveness of the ic L1210 brain tumor model system to the inhibitory activity of BCNU, coupled with the clinical effectiveness of this drug in the treatment of malignant brain tumors, encouraged the further development and continued use of animal models in experimental brain tumor chemotherapy studies. Accordingly, it is appropriate to periodically review the use of brain tumor models in experimental chemotherapy studies as was done by Shapiro and Ausman (6).

Transplantable brain tumor models used in chemotherapy experiments have been divided into two broad classifications (nonneurogenic and neurogenic) based on the tumor used in the model. In a strict sense, the transplantable glial tumors are not neurogenic in origin because they are derived from nonmesenchymal stromal tissue, but the term neurogenic has been commonly extended to include glial tumors, and thus, this terminology is retained for purposes of convenience.

Examples of nonneurogenic tumors which have been used in ic brain tumor models for chemotherapy experiments are: L1210 mouse leukemia (3,4); Dunning leukemia (7); B16 melanoma (8); and Ehrlich carcinoma and Sarcoma 180 (9). An advantage of these tumors is that they have been routinely used as extracerebral tumor model systems in chemotherapy programs, and thus they can serve dual roles. A recent illustration of this is the report of Fox et al (10) in which they showed that anhydro-ara-5-fluorocytidine was an effective chemotherapeutic agent against intraperitoneally (ip) injected L1210, and in a comparative study data showed that the drug was as effective as BCNU against the ic L1210 model.

The pathologic properties of the ic L1210 model have been extensively studied by a number of investigators (3,4,11-14). Chirigos et al (11) first demonstrated that ic L1210 infiltrates diffusely in the arachnoid space and becomes systemic within 2-3 days after ic inoculation. Thomas et al (12) described the distribution of ic L1210 cells in the meninges as being similar to leukemic cell infiltrates in the meninges of patients with acute leukemia. In a discussion of the effect of treatment with cyclophosphamide against the ic L1210 system it was pointed out that the drug completely destroyed leukemic cells which had spread from the ic site to the liver, spleen, bone marrow, and dura, whereas the leukemic cells in the subarachnoid space and brain continued to proliferate.

Based on additional studies of Thomas et al (13), a potentially useful brain tumor model for chemotherapy was described by Chirigos and Humphreys (14). In that model, CDBA mice were inoculated subcutaneously (sc) with L1210 leukemia, and animals were then treated with methotrexate 7 days after tumor inoculation. The therapy extended the survival time of mice so that all animals developed metastatic growth of leukemic cells in the subarachnoid and perivascular spaces of the brain as reported by Thomas et al (13). Using this model, Chirigos and Humphreys (14) demonstrated that BCNU was highly effective in suppressing the leukemic infiltration in the brain. This potentially useful brain tumor model has not been utilized extensively.

A number of investigators concerned with the chemotherapy of malignant brain tumors have questioned the use of nonneurogenic tumors in model systems. In a few instances, neurogenic tumors have been implanted in extracerebral sites to study the antitumor activity of chemicals (15-19); however, the work of Torack (20) on the ultrastructure of capillary reaction to brain tumor growth has shown distinct differences between extracerebrally and ic implanted neurogenic tumors, and it is his contention that the ic implanted tumor model bears a closer resemblance to the human malignant brain tumor

[1]Received Feb 3, 1975; revised Apr 10, 1975; accepted Apr 23, 1975.

[2]Supported by contract NO1-CM-33727 from the Division of Cancer Treatment (DCT), National Cancer Institute (NCI), National Institutes of Health, Department of Health, Education, and Welfare.

[3]Drugs used in this study were supplied by Drug Research and Development (DR&D), DCT, NCI. Chemical nomenclature, NSC numbers, and CAS registry numbers for all compounds mentioned in this paper are included in the List of Compounds at the end of the text.

[4]Arthur D. Little, Inc., Cambridge, Mass.

[5]DR&D, DCT, NCI, Bethesda, Md.

[6]*Reprint requests to:* Dr. Philip C. Merker, Arthur D. Little, Inc., Acorn Park, Cambridge, Mass 02140.

than, for example, an sc implanted tumor. In addition, Shapiro (18) suggested, on the basis of a direct comparison between results obtained for mithramycin in a controlled clinical study of brain tumor chemotherapy and ic and sc brain tumor models, that the ic brain tumor model which uses survival time as an index of response is more predictive for man than the sc model which uses tumor growth inhibition as the index of response.

In recent years, ic brain tumor models using neurogenic tumors have been extensively studied for use in chemotherapy experiments. The results of Ausman et al (21), and more recently those of Wassenaar et al (22), suggest that ic neurogenic brain tumor models are suitable for routine use in chemotherapy test programs. With the exception of the work of Tansley and Wilson (23), Wilson et al (24), and Edelman et al (25), the investigations using ic neurogenic tumors shown in table 1 were done in the 1970s (19, 26-37). The majority of these studies used one or several antitumor agents, but Geran et al (34) used an ic murine ependymoblastoma model described by Ausman et al (21) to test 177 experimental drugs. The ready availability of this large body of test data, as well as data for compounds tested against two nonneurogenic brain tumor test systems (ic L1210 and ic B16 melanoma), makes it possible to compare these three systems for compounds of special current interest as antineoplastic agents against solid tumors in man (table 2).

The drugs listed in table 2 have been classified as S++ because they have "definite activity against at least two major solid tumors in man."[7] Maximum response data, designated in terms of the percentage of increase in lifespan (%ILS), are shown for each of the model systems. In general, drugs were administered ip with the initial dose given 24 hours after tumor implantation; for simplicity, the details of dose, route of administration, and schedule have not been included in the data shown in table 2, although these tended to differ among the test systems. In addition, sufficient details of statistical variation for each brain tumor model system were not readily available; therefore, "weighting" of response data for purposes of comparison could not be done.

It is apparent from the data shown in table 2 that relatively strong responses are associated with CCNU, BCNU, methyl-CCNU, cyclophosphamide, and thioTEPA, and very negligible or weak responses are associated with methotrexate, adriamycin, hexamethylmelamine, melphalan, mechlorethamine, 5-FUDR, and 5-FU. The differences in cell kinetics of each tumor system may partially explain the differences in response to chemotherapeutic agents; Shapiro and Ausman (6) and Wilson et al (38) have reviewed the tumor kinetics of brain tumors, and these authors have stressed that the kinetic parameters of tumor cell growth should be seriously considered in the design of brain tumor chemotherapy. Broder and Rall (39), in their review of brain tumor chemotherapy, have indicated that the S-phase specificity of antimetabolites renders them less effective against relatively slow growing brain tumors.

Table 3 shows that the transplantable ependymoblastoma tumor used by Geran et al (34) was tentatively found to have a doubling time of 2-4 days by Shapiro and Ausman (6), and the B16 melanoma was found by Wodinsky et al (8) to have a doubling time of 1.26 days when it was grown as a solid tumor ic. In contrast to these two tumors, L1210 leukemia was shown to have a doubling time of 0.5 days (8,40). In spite of these time differences, the chemotherapeutic responses of the three ic brain tumor models to BCNU, CCNU, and methyl-CCNU were essentially similar. This finding is to be expected because the nitrosoureas are cycle-specific drugs. The ic L1210 tumor showed a greater sensitivity than the other two tumors to the antimetabolites; this may primarily be because these drugs are phase-specific and, therefore, they are more effective against those tumors that have a rapid cell cycle and a large proliferative fraction (8). In addition, the antimetabolites may also prevent the ic L1210 tumor from becoming systemic.

A number of investigators using survival time as an index of response have shown that ic nonneurogenic tumor model systems are less sensitive to chemotherapy than extracerebral tumor model systems (3,4,41,42). Survival-time data for two nonneurogenic tumors, L1210 leukemia and B16 melanoma, implanted ic and extracerebrally, show a similar tendency, eg, with the possible exception of thioTEPA, drugs were more efficacious against extracerebral than ic tumors (table 4).

Shapiro et al (19) observed essentially the same phenomenon in studies which used a neurogenic ic and sc tumor model; in those studies, mithramycin significantly inhibited the growth of an sc implanted ependymoblastoma, but the survival time of ic implanted animals was not significantly prolonged. Shapiro (18) recently studied the effect of an epipodophyllotoxin (NSC-122819) against the growth of ic and sc implanted Glioma 26. Data showed that the drug significantly inhibited tumor growth in both sites of implantation, but the survival time of treated animals with ic implantations was only negligibly increased by 20% relative to control animals. The data from these two studies (18,19) show that it is more difficult to prolong with chemotherapy the survival time of mice implanted ic with solid neurogenic tumors than it is to inhibit tumor growth as measured by actual tumor weight.

Kotsilimbas et al (41) and Chirigos et al (42) ascribed the lack of responsiveness of ic nonneurogenic tumor systems to a reduced efficiency of penetration of drug into the brain because of the selectivity of the blood-brain barrier. Among factors affecting the permeability of brain tumors to pharmacologic

[7]Venditti JM. Plan for antitumor screening in animals and selection of new agents as candidates for clinical trial. *In* Report of the DCT, NCI, 1973 (Program Logic and Scientific Reports). Bethesda, NCI, Sept 1973, vol 2, pp 2.27-2.75.

TABLE 1.—Ic neurogenic tumor model systems used in chemotherapy experiments

Model systems	Investigators	Year	Ref No.
Chemically induced systems			
1. Transplantable mouse tumors			
a. Glioma (Tansley and Wilson): methylcholanthrene-induced; host animal, Ni strain	Tansley and Wilson	1947	23
b. Ependymoblastoma (Zimmerman): methylcholanthrene-induced; host animal, C57BL/6	Edelman et al	1964	25
	Shapiro et al	1970	19
	Levin et al	1970	26
	Shapiro	1971	27
	Thomson et al	1971	31
c. Glioma 261 (Shear): methylcholanthrene-induced; host animal, C57BL/6	Shapiro et al	1970	19
	Shapiro	1971, 1972	27-29
	Levin et al	1970	26
d. Glioma 26 (Sugiura): host animal, C57BL/6	Shapiro et al	1970	19
	Levin et al	1970	26
	Shapiro	1971	27
	Madigan et al	1974	32
	Levin	1974	33
e. Ependymoblastoma A: methylcholanthrene-induced; host animal, C57BL/6	Shapiro et al	1970	19
	Shapiro	1971	27
	Geran et al	1974	34
f. Ependymoblastoma: host animal, C3H	Papadakis et al	1972	35
2. Transplantable rat tumor			
Rat glioma (Sweet): 1-methyl-1-nitrosourea-induced; host animal, CD Fisher rat	Gurcay et al	1970	36
	Gurcay et al	1971	37
	Barker et al	1973	30
Animal origin systems: virally induced			
1. Autochthonous: B-77 avian sarcoma virus; host animal, Sprague-Dawley rat	Swenberg et al	1974	53
2. Transplantable (homologous): Schmidt-Ruppin strain, Rous sarcoma virus; host animal, neonatal beagles	Jacobs et al	1970, 1971	58, 59
Human origin system	Wilson et al	1967	24
Oligodendroglioma hetero-transplanted to adult Sprague-Dawley rats			

TABLE 2.—ILS of ic tumor-bearing mice from treatment with drugs having definite activity against human solid cancer (S++)

Drug	%ILS in—*		
	Ic L1210 leukemia	Ic B16 melanoma	Ic ependymo-blastoma
CCNU	234	120	165
BCNU	107	41	111
Methyl-CCNU	221	NT	192
ThioTEPA	128	48	58
Methotrexate	59	<25	<25
Cyclophosphamide	132	<25	75
Mechlorethamine	<25	<25	<25
Melphalan	62	<25	<25
5-FU	27	<25	<25
5-FUDR	60	NT	<25
Hexamethylmelamine	<25	NT	<25
Adriamycin	<25	<25	<25

*NT = not tested.

TABLE 3.—Relationship between doubling time of tumor and survival time of ic tumor-bearing mice

Tumor	Doubling time (days)	Survival time of ic tumor-bearing mice (days)
L1210 leukemia	0.5*	9†
B16 melanoma	1.26‡	12‡
Ependymoblastoma (Zimmerman)	2-4§	20-30§
Ependymoblastoma A	—	20¶

*Data from Wodinsky et al (8) and Skipper et al (40) for ip transplants of L1210 leukemia.

†Ic inoculum = 10^4 cells.

‡Data from Wodinsky et al (8) for ic transplanted tumor. Inoculum = 10^5 cells.

§Data from Shapiro and Ausman (6).

¶Data from Geran et al (34).

agents are the physicochemical properties of the compound administered and the nature of the blood-brain tumor and tumor-cell membrane (43). It has been suggested that effective drugs should have high tumor:normal brain and high tumor:plasma distribution ratios (44). To study the question of the relative importance of drug transport to brain and tumor, experiments have been designed with neurogenic tumors transplanted ic (26,45-50).

Shapiro and Ausman (6) credited Rall and Zubrod with having first pointed out in 1962 that lipid-soluble nonionized molecules more easily enter normal brain tissue than water-soluble ionized species, and Shapiro and Ausman also reported that subsequent studies raised doubts that lipid solubility was a necessary requirement for drug entry into solid brain tumors. The details of these solubility-penetration relationships have been studied by many investigators during the past decade and are still a subject of intense interest. The work of Levin et al (26) has indicated that the antitumor activity of the highly lipid-soluble drug, CCNU, is probably independent of preferential uptake and distribution between the ic tumor and other tissues; uptake and distribution data for ^{14}C-CCNU in ic and sc tumors (brain adjacent to tumor) and distant (normal) brain indicated that the parent drug had relatively constant tissue:plasma ratio levels. In studies with 5-FU, Levin and Chadwick (47) showed that the drug was taken up by an ic tumor to a considerably greater extent than normal brain; these data suggest that 5-FU can penetrate into an ic tumor, and thus the failure of the drug to markedly increase the survival time of mice bearing ic implanted tumors shown in table 2 and also reported by Kotsilimbas et al (42) may not necessarily be ascribed to lack of drug penetration into the tumor. However, failure of chemotherapy may be due to lack of significant penetration of the drug into the tumor cells per se. The data of Levin et al (26) and Levin and Chadwick (47) showed that intravenously administered drugs passed from the blood to the tumorous side of the blood-brain barrier, but the procedures used in these studies did not provide data which clearly demonstrated that drug penetrated into the tumor cell. To partially answer this question, Shapiro (29) used a biochemical experimental design to study drug penetration into brain tumors and tumor cells; data from his experiments, which were planned to study the effect of chemotherapeutic agents on the incorporation of tracer DNA-precursors into brain tumors, indicated that methotrexate crossed the blood-brain barrier and entered tumor cells. Studies of this type are of importance because they supply data that can be used to differentiate between those drugs and chemicals which primarily are retained in the interstitial space of the tumor and those which are absorbed into the tumor cell per se.

In addition to the use of transplantable ic tumor models in chemotherapy and biochemical pharmacology experiments sited above, alternate and potentially more useful experimental brain tumor models are now available. A number of these have been reviewed and discussed by Wilson and Bates (51), and Druckrey et al (52) have described a potentially useful chemically induced tumor in the rat. Swenberg et

TABLE 4.—ILS comparison between ip and ic inoculated nonneurogenic tumors

Drug	%ILS in—*			
	L1210 leukemia		B16 melanoma	
	Ip tumor, ip treatment	Ic tumor, ip treatment	Ip and sc tumor, ip treatment	Ic tumor, ip treatment
CCNU	>200	>200	200	120
BCNU	>200	107	109	41
Methyl-CCNU	>200	>200	134	NT
ThioTEPA	80	128	<25	48
Methotrexate	105	59	<25	<25
Cyclophosphamide	>200	132	62	<25
Mechlorethamine	60	<25	85	<25
Melphalan	120	62	105	<25
5-FU	80	27	40	<25
5-FUDR	52	60	38	NT
Hexamethylmelamine	<25	<25	<25	NT
Adriamycin	64	NT	187	<25

*NT = not tested.

al (53) recently reported on the use of an autochthonous virally induced brain tumor in rats, and Wilson et al (24) have even explored the use in chemotherapy experiments of a human brain tumor heterotransplanted in adult rats. Wilson and Bates (51), however, pointed out the shortcomings of small animal models and suggested that a larger animal model would offer significant advantages to the surgeon-investigator and brain oncologist. Walker (1) has also emphasized that an adequate experimental brain tumor model in large animals, which can be used for toxicity and pharmacologic studies, is required for effective research on the chemotherapy of malignant brain disease.

One approach would be to use dogs bearing either autochthonous or transplanted brain tumors. Gliomas and meningeal sarcomas have been induced in dogs by ic inoculation of oncogenic doses of the Rous sarcoma virus as described by Rabotti et al (54,55), Bigner et al (56), and Wodinsky et al (57). The autochthonous virally induced dog-brain tumor model system has not been explored for its utility in chemotherapeutic and pharmacologic experiments, but this does not deny the potential usefulness of such a brain tumor model in the dog.

An alternate approach is to use a transplantable dog-brain tumor. Jacobs et al (58,59) reported on the use of a transplanted virally induced dog-brain tumor in chemotherapeutic and toxicologic studies. The tumor (DGW/4) from which the transplantable line was established was induced as originally described by Rabotti et al (54) using beagle puppies less than 24 hours old. The tumor produced by this procedure was a mixed tumor, ie, it was composed of neoplastic cells of neuroepithelial (gliomata) and mesodermal (sarcomata) origin as described by Rabotti et al (54). Histopathologic examination of representative blocks of tissue selected from each of 18 transplant generations from our laboratories showed that the tumor is of mixed type, consisting of glial and sarcomatous portions; consequently, the term "gliosarcoma" can be appropriately used to describe this neoplasm. The histologic appearance of this mixed tumor has been found to be consistent throughout the 18 transplant generations.

A full description of the dog-brain transplantation procedure and other technical considerations will be published elsewhere. For the purpose of this review suffice it to state that the dog gliosarcoma is prepared as a 50% tumor brei in suitable suspending media and implanted in a volume of 0.1-0.2 ml into the dorsomedial portion of the right frontal lobe of the brain of beagle puppies less than 24 hours old. Donor tissue is derived from ic grown tumors which are stored under liquid nitrogen for no longer than 90 days. For chemotherapy experiments, treatment is started 6 days after tumor implantation, when the puppies are 7 days old.

For purposes of evaluating the "effectiveness" of chemotherapy response data, a grading system was developed using the mean survival time of 13.1 days obtained from 101 control animals and an estimate of the standard error of the mean of 3.25 days for a minimum sample of six animals. Based on these statistics, a threshold value for minimal effectiveness (+) was set at 32% ILS of treated animals relative to controls ($P = 0.09$), and the maximum effectiveness (+++) was set at $\geq$ 106% ILS ($P = 0.0001$). Treated or control animals that lived 22 days or longer were designated "long-term survivors."

Data in table 5 show the response to chemotherapy of the ic dog-brain tumor model when long-term survivors are used as an index of responsiveness: streptozotocin, BCNU, dibromodulcitol, and procarbazine caused 50%-67% of the treated animals to survive for 22 days or longer. Methyl-CCNU and ^{60}Co-radiation (200 rads × 5) were somewhat less effective, and adriamycin did not prolong the survival of ic tumor-implanted animals.

Comparative data for the ic dog-brain tumor, murine ependymoblastoma, B16 melanoma, and L1210 leukemia tumors are shown in table 6. Of considerable interest is the marked effect of procarbazine against the ic dog-brain tumor because Geran et al

TABLE 5.—Long-term survivors resulting from treatment of beagle neonates inoculated ic with tumor

Treatment	Dose (mg/kg)	Treatment route	Schedule of treatment	No. of puppies	Long-term survivors * (%)
Streptozotocin	16	Ip	1 × Days 7-12	6	67
BCNU	5	Ip	1 × Day 7	9	67
Dibromodulcitol	8	Ip	1 × Days 7-12	5	60
Procarbazine	40	Ip	1 × Days 7-12	8	50
Methyl-CCNU	5	Iv	1 × Days 7-9	6	33
Adriamycin	2	Iv	1 × Days 7-9	6	0
^{60}Co gamma radiation	200 rads		1 × Days 7-11	13	23
Control†	0			61	5

*Tumor-inoculated puppies living ≥ 22 days; see text for a description of the statistics describing long-term survivors.

†Combining all non-drug-treated puppies used as controls in chemotherapy experiments shown in this table.

TABLE 6.—ILS of animals bearing ic tumor implants

Drug	%ILS in—*			
	Dog-brain tumor (DGW/4)	Ependymo-blastoma	B16 melanoma	L1210 leukemia
Procarbazine	>200	134	75	55
Streptozotocin	147	<50	NT	NT
Methyl-CCNU	38	192	NT	>200
Dibromodulcitol	>200	50	35	28
BCNU	140	111	41	107
CCNU	100	165	120	234
Mithramycin	<25	<25	NT	NT
Adriamycin	<25	<25	<25	<25

*NT = not tested.

(34) have indicated that this drug was one of the most active of 177 agents tested against the murine ic ependymoblastoma. Two of the drugs, dibromodulcitol and streptozotocin, especially affected the dog-brain tumor system. Data for adriamycin show the lack of responsiveness of the four ic tumor models to this drug. At present, cell-cycle kinetics do not explain the differential responsiveness of the ic dog-brain tumor because preliminary kinetic data obtained in experiments with ^{3}H-thymidine show that the cell cycle of the dog-brain tumor is about 0.5 days with a proliferating cell fraction of 38%.

In summary, a number of small animal nonneurogenic and neurogenic transplantable brain tumor models were reviewed primarily in terms of response to chemotherapy. Comparative chemotherapeutic data suggest that ic neurogenic brain tumor models can respond differently than ic nonneurogenic tumor models. The final choice of optimal brain tumor model systems for use in chemotherapy experiments must wait until more definitive clinical data are available with which to compare results from animal models. In the future, chemotherapy data that are derived from animal models which use specific brain tumors should be compared with results obtained from treating specific human brain neoplasia. A comparison of this type would then allow an evaluation to be made of the relative merits of various animal brain tumor models for selecting agents which will be useful in treating brain cancer in man. It may be that different neurogenic ic animal tumors will be required to select drugs for treating the various types of human primary brain tumors, and it may also be that nonneurogenic ic brain tumor models will be helpful in selecting drugs for treating various human tumors which have metastasized to the brain.

LIST OF COMPOUNDS

Adriamycin: NSC-123127; CAS reg. No. 23214-92-8

Anhydro-ara-5-fluorocytidine: NSC-166641; CAS reg. No. 40505-45-1; O^2, 2′-cyclocytidine, 5-fluoro-, monohydrochloride

BCNU: NSC-409962; CAS reg. No. 154-93-8; urea, 1,3-bis(2-chloroethyl)-1-nitroso-

CCNU: NSC-79037; CAS reg. No. 13010-47-4; urea, 1-(2-chloroethyl)-3-cyclohexyl-1-nitroso-

Cyclophosphamide: NSC-26271; CAS reg. No. 6055-19-2; 2*H*-1,3,2-oxazaphosphorine, 2-[bis(2-chloroethyl)amino]tetrahydro-, 2-oxide, monohydrate

Dibromodulcitol: NSC-104800; CAS reg. No. 10318-26-0; galactitol, 1,6-dibromo-1,6-dideoxy-

5-FU: NSC-19893; CAS reg. No. 51-21-8; 5-fluorouracil

5-FUDR: NSC-27640; 5-fluoro-2′-deoxyuridine

Hexamethylmelamine: NSC-13875; CAS reg. No. 645-05-6

Hydroxyurea: NSC-32065; CAS reg. No. 127-07-1

Mechlorethamine: NSC-762; CAS reg. No. 55-86-7; diethylamine, 2,2′-dichloro-*N*-methyl-, hydrochloride; HN_2; nitrogen mustard

Melphalan: NSC-8806; CAS reg. No. 3223-07-2; alanine, 3-[*p*-[bis(2-chloroethyl)amino]phenyl]-, monohydrochloride, L-

Methotrexate: NSC-740; CAS reg. No. 59-05-2; glutamic acid, *N*-[*p*-[[(2,4-diamino-6-pteridinyl)methyl]methylamino]benzoyl]-

Methyl-CCNU: NSC-95441; CAS reg. No. 33073-59-5; urea, 1-(2-chloroethyl)-3-(4-methylcyclohexyl)-1-nitroso-

Mithramycin: NSC-24559; CAS reg. No. 18378-89-7

NSC-122819: 4′-demethylepipodophyllotoxin 9-(4,6-*O*-2-thenylidene-β-D-glucopyranoside); VM-26

Procarbazine: NSC-77213; CAS reg. No. 491-88-3; *p*-toluamide, *N*-isopropyl- α -(2-methylhydrazino)-, monohydrochloride

Streptozotocin: NSC-85998

ThioTEPA: NSC-6396; CAS reg. No. 52-24-4; phosphine sulfide, tris(1-aziridinyl)-

Triethylenemelamine: NSC-9706; CAS reg. No. 51-18-3; *s*-triazine, 2,4,6-tris(1-aziridinyl)-

REFERENCES

1. WALKER MD. Brain and peripheral nervous system tumors. *In* Cancer Medicine (Holland JF, and Frei E III, eds). Philadelphia, Lea and Febiger, 1973, p 1385.
2. ——. Nitrosoureas in central nervous system tumors. Cancer Chemother Rep Part 3, vol 4(3):21-26, 1973.
3. SKIPPER HE, SCHABEL FM, JR, TRADER MW, ET AL. Experimental evaluation of potential anticancer agents. VI. Anatomical distribution of leukemic cells and failure of chemotherapy. Cancer Res 21:1154-1164, 1961.
4. SCHABEL FM, JR, JOHNSTON TP, MCCALEB GS, ET AL. Experimental evaluation of potential anticancer agents. VIII. Effects of certain nitrosoureas on intracerebral L1210 leukemia. Cancer Res 23:725-733, 1963.
5. DAVIGNON JP, YANG KW, WOOD HB, JR, ET AL. Formulation of three nitrosoureas for intravenous use. Cancer Chemother Rep Part 3, vol 4(3):7-11, 1973.
6. SHAPIRO WR, and AUSMAN JI. The chemotherapy of brain tumors: a clinical and experimental review. *In* Recent Advances in Neurology (Plum F, ed). Philadelphia, F. A. Davis Co., 1969, pp 150-235.
7. WODINSKY I, and KENSLER CJ. Effectiveness of antitumor agents against intraperitoneally and intracerebrally inoculated Dunning leukemia in the Fischer rat. *In* Proceedings of the 9th International Cancer Congress, Tokyo, Oct 23-29, 1966, p 380.

8. Wodinsky I, Kensler CJ, and Venditti JM. Comparative kinetics and chemotherapy of the slow growing B16 melanoma and the fast growing L1210 leukemia. Proc Am Assoc Cancer Res 13:8, 1972.
9. Rosso R, Donelli MG, Innocenti IR, et al. Chemotherapy of tumors transplanted intracerebrally. Eur J Cancer 3:125-137, 1967.
10. Fox JJ, Falco EA, Wempen I, et al. Oral and parenteral activity of 2,2'-anhydro-1-β-D arabinofuranosyl-5-fluorocytosine against both intraperitoneally and intracerebrally inoculated mouse leukemia. Cancer Res 32:2269-2272, 1972.
11. Chirigos MA, Thomas LB, Humphreys SR, et al. Intracerebral growth and treatment of leukemia L1210. Proc Soc Exp Biol Med 104:643-645, 1960.
12. Thomas LB, Chirigos MA, Humphreys SR, et al. Pathology of the spread of L1210 leukemia in the central nervous system of mice and effect of treatment with Cytoxan. J Natl Cancer Inst 28:1355-1389, 1962.
13. ———. Development of meningeal leukemia (L1210) during treatment of subcutaneously inoculated mice with methotrexate. Cancer 17:352-360, 1964.
14. Chirigos MA, and Humphreys SR. Effect of alkylating agents on meningeal leukemia L1210 arising in methotrexate-treated mice. Cancer Res 26:1673-1677, 1966.
15. Soloway AH, Mark VH, Dukat EG, et al. Chemotherapy of brain tumors 1. Transplanted murine ependymoblastomas. Cancer Chemother Rep 36:1-4, 1964.
16. Sugiura K. Effect of 1,3-bis(2-chloroethyl)-1-nitrosourea (NSC-409962) and two related compounds on a spectrum of tumors. Cancer Res (suppl) 27 (No. 3, part 2):179-189, 1967.
17. Wollheim-Sandberg M. Effect of mithramycin on a mouse glioma. Cancer Res 28:91-97, 1968.
18. Shapiro WR. The chemotherapy of intracerebral vs subcutaneous murine gliomas. A comparative study of the effect of VM26. Arch Neurol 30:222-226, 1974.
19. Shapiro WR, Ausman JI, and Rall DP. Studies on the chemotherapy of experimental brain tumors: evaluation of 1,3-bis(2-chloroethyl)-1-nitrosourea, cyclophosphamide, mithramycin, and methotrexate. Cancer Res 30:2401-2413, 1970.
20. Torack RM. Ultrastructure of capillary reaction to brain tumors. Arch Neurol 5:416-428, 1961.
21. Ausman JI, Shapiro WR, and Rall DP. Studies on the chemotherapy of experimental brain tumors: development of an experimental model. Cancer Res 30:2394-2400, 1970.
22. Wassenaar W, Tator CH, and So WS. The development of an intracerebral glioma model for brain tumor chemotherapy. J Neurosurg 39:293-301, 1973.
23. Tansley K, and Wilson CW. Irradiation of experimental cerebral tumors. I. Experimental production of brain tumors in mice. Radiology 49:62-71, 1947.
24. Wilson CB, Norrell H, Jr, and Barker M. Intrathecal injection of methotrexate (NSC-740) in transplanted brain tumors. Cancer Chemother Rep 51:1-6, 1967.
25. Edelman FL, Alen F, Scheinberg LC, et al. Effect of irradiation on the growth of intracerebral gliomas in mice. J Neuropathol Exp Neurol 23:1-17, 1964.
26. Levin VA, Shapiro WR, Clancy TP, et al. The uptake, distribution and antitumor activity of 1-(2-chloroethyl)-3-cyclohexyl-1-nitrosourea in murine glioma. Cancer Res 30:2451-2455, 1970.
27. Shapiro WR. Studies on the chemotherapy of experimental brain tumors: evaluation of 1-(2-chloroethyl)-3-cyclohexyl-1-nitrosoureа, vincristine and 5-fluorouracil. J Natl Cancer Inst 46:359-368, 1971.
28. ———. Effect of 1-(2-chloroethyl)-3-cyclohexyl-1-nitrosourea (CCNU; NSC-79037) in sesame oil administered intramuscularly in the treatment of experimental brain tumors. Cancer Chemother Rep 56:457-463, 1972.
29. ———. The effect of chemotherapeutic agents on the incorporation of DNA precursors by experimental brain tumors. Cancer Res 32:2178-2185, 1972.
30. Barker M, Hoshino T, Gurcay O, et al. Development of an animal brain tumor model and its response to therapy with 1,3-bis(2-chloroethyl)-1-nitrosourea. Cancer Res 33:976-986, 1973.
31. Thomson JM, Maruyama Y, Schwartz S, et al. Effect of chemotherapy and/or head irradiation on survival of mice with intracranial glioma. Radiology 101:187-194, 1971.
32. Madigan J, Albright L, and Houchens D. Therapy studies in an intracerebral murine glioma model. Proc Am Assoc Cancer Res and ASCO 15:13, 1974.
33. Levin VA. Relationship of late treatment with nitrosoureas and lipid solubility in intracerebral rodent tumors. Proc Am Assoc Cancer Res and ASCO 15:32, 1974.
34. Geran RI, Congleton GF, Dudeck LE, et al. A mouse ependymoblastoma as an experimental model for screening potential antineoplastic drugs. Cancer Chemother Rep Part 2, vol 4(4):53-87, 1974.
35. Papadakis N, Mark VH, and Burke JF. Effect of treatment with L-phenylalanine mustard and antibody on survival time of mice with intracerebral ependymoblastomas. Surg Forum 23:432-434, 1972.
36. Gurcay O, Wilson CB, and Eliason J. The effect of methylprednisolone acetate on transplantable rat glioma. Surg Forum 21:437-439, 1970.
37. Gurcay O, Wilson CB, Barker M, et al. Corticosteroid effect on transplantable rat glioma. Arch Neurol 24:266-269, 1971.
38. Wilson CB, Hoshino T, Barker M, et al. Kinetics of gliomas in rat and man. Prog Exp Tumor Res 17:363-372, 1972.
39. Broder LE, and Rall DP. Chemotherapy of brain tumors. Prog Exp Tumor Res 17:373-399, 1972.
40. Skipper HE, Schabel FM, Jr, and Wilcox WS. Experimental evaluation of potential anticancer agents. XXI. Scheduling of arabinosylcytosine to take advantage of its S-phase specificity against leukemic cells. Cancer Chemother Rep 51:125-141, 1967
41. Kotsilimbas DG, Karpp R, Meredith S, et al. Evaluation of parenteral 5-FU on experimental brain tumors. Neurology 16:916-918, 1966.
42. Chirigos MA, Humphreys SR, and Goldin A. Effectiveness of Cytoxan against intracerebrally and subcutaneously inoculated mouse lymphoid leukemia L1210. Cancer Res 22:187-195, 1962.
43. Soloway AH. Factors affecting the permeability of brain tumors to pharmacologic agents. *In* The Experimental Biology of Brain Tumors (Kirsch WM, Grossi-Paoletti E, and Paoletti P, eds). Springfield, Charles C. Thomas, 1972, pp 407-428.
44. Bourke RS. Brain tumors and the permeability of adjacent brain. *In* The Experimental Biology of Brain Tumors (Kirsch WM, Grossi-Paoletti E, and Paoletti P, eds). Springfield, Charles C. Thomas, 1972, pp 533-548.
45. Levin VA, Clancy TP, and Ausman JI. Methotrexate permeability and steady-state distribution in the murine ependymoblastoma. Trans Am Neurol Assoc 94:294-296, 1969.
46. Levin VA, Clancy TP, Ausman JI, et al. Uptake and distribution of ^{3}H-methotrexate by the murine ependymoblastoma. J Natl Cancer Inst 48:875-883, 1972.
47. Levin VA, and Chadwick M. Distribution of 5-fluorouracil-2-^{14}C and its metabolites in a murine glioma. J Natl Cancer Inst 49:1577-1584, 1972.
48. Tator CH. The uptake of tritiated methotrexate by an experimental glioma. Cancer Res 31:1600-1605, 1971.
49. ———. Chemotherapy of brain tumors. Uptake of tritiated methotrexate by a transplantable intracerebral ependymoblastoma in mice. J Neurosurg 37:1-8, 1972.
50. Ushio Y, Hayakawa T, and Modami H. Chemotherapy of brain tumor. The uptake of ^{3}H-methotrexate and ^{14}C-bleomycin in mouse glioma. Neurol Med Chir (Tokyo) 11:261-262, 1971.
51. Wilson CB, and Bates EA. Transplantable brain tumors. *In* The Experimental Biology of Brain Tumors (Kirsch WM, Grossi-Paoletti E, and Paoletti P, eds). Springfield, Charles C. Thomas, 1972, pp 19-56.
52. Druckrey H, Ivankovic S, Preussmann R, et al. Selective induction of malignant tumors of the nervous system by resorptive carcinogens. *In* The Experimental Biology of Brain Tumors (Kirsch WM, Grossi-Paoletti E, and Paoletti P, eds). Springfield, Charles C. Thomas, 1972, pp 85-147.
53. Swenberg JA, Bigner D, and Hall TL. Experimental chemotherapy of viral-induced brain tumors. Proc Am Assoc Cancer Res and ASCO 15:43, 1974.
54. Rabotti GF, Grove AS, Jr, Sellers RL, et al. Induction of multiple brain tumors (gliomata and leptomeningeal sarcomata) in dogs by Rous sarcoma virus. Nature 209:884-886, 1966.
55. Rabotti GF. Experimental intracranial tumors of viral etiology. *In* The Experimental Biology of Brain Tumors (Kirsch WM, Grossi-Paoletti E, and Paoletti P, eds). Springfield, Charles C. Thomas, 1972, pp 148-180.

56. Bigner DD, Fritz RB, and Day ED. Cerebral physiology in dogs after brain-tumor induction with Schmidt-Ruppin Rous sarcoma virus: experiences with radioiodinated normal and antiviral immunoglobulin G. J Natl Cancer Inst 43:565-573, 1969.
57. Wodinsky I, Kensler CJ, and Rall DP. The induction and transplantation of brain tumors in neonatal beagles. Proc Am Assoc Cancer Res 10:99, 1969.
58. Jacobs SP, Wodinsky I, Kensler CJ, et al. Chemotherapy of transplanted glioblastoma in beagles. Pharmacologist 12:282, 1970.
59. ————. The induction and chemotherapy of a transplantable glioma in beagles. (Abstr B-2/4) *In* Proceedings of the 6th International Congress of Chemotherapy, Aug 1971.

Clinical Study of the New Podophyllotoxin Derivative, 4′-Demethylepipodophyllotoxin 9-(4,6-*O*-ethylidene-β-D-glucopyranoside) (NSC-141540; VP-16-213), in Solid Tumors in Man[1,2]

Walter Felix Jungi and Hans Joerg Senn[3,4]

SUMMARY

The new semisynthetic epipodophyllotoxin, 4′-demethylepipodophyllotoxin 9-(4,6-*O*-ethylidene-β-D-glucopyranoside) (NSC-141540), was tested for antitumor activity against solid tumors and for clinical toxicity in 30 patients. The first two courses were given intravenously (60 mg/m²/day × 5, every 21 days), and subsequent courses were given orally (60-120 mg/m²/day × 5, every 21 days). The drug was subjectively well tolerated but induced considerable leukothrombocytopenia and alopecia. It demonstrated significant activity in oat cell carcinoma of the lung (eight responses out of 11 patients) and ovarian cancer (four responses out of six patients). NSC-141540 has valuable cytostatic activity against these two tumors and warrants further clinical trials, especially in combination chemotherapy.

[Cancer Chemother Rep 59:737-742, 1975]

The cytostatic activity of the podophyllotoxins, derivatives of the plants *Podophyllum peltatum* and *Podophyllum emodi*, has been known for many years (1). However, none of the substances entering clinical trials has found a place among the standard chemotherapeutic agents. In the search for more active congeners of podophyllotoxins, two new semisynthetic compounds have been recently developed: 4′-demethylepipodophyllotoxin 9-(4,6-*O*-2-thenylidene-β-D-glucopyranoside) (NSC-122819) and 4′-demethylepipodophyllotoxin 9-(4,6-*O*-ethylidene-β-D-glucopyranoside) (NSC-141540). Neither agent is a spindle poison as are the older podophyllotoxins, but they do inhibit the entry of cells into mitosis (2,3). The chemical structures of these two new semisynthetic epipodophyllotoxins are shown in figure 1.

NSC-122819 and NSC-141540 have shown definite antitumor activity in a variety of animal and human tumors (2,4-15).[5] NSC-141540 is the most effective plant product against L1210 leukemia. Both agents have a similar spectrum of tumor inhibition. NSC-141540 seems to be the more interesting and promising of the two substances due to its larger therapeutic index and its applicability by the oral route. On a dose-to-dose basis, NSC-141540 is less active in vitro and in vivo than NSC-122819.

NSC-141540 was tested as a single drug in a nonrandomized phase II trial in patients with solid tumors, predominantly lung and ovarian cancers. The purpose of this study was to assess the antitumor activity and toxicity of NSC-141540 in a given schedule which was based on animal experiments and pilot studies in man.

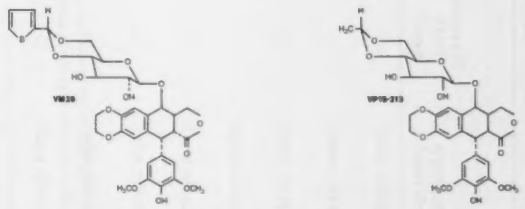

FIGURE 1.—Chemical structures of the two new semisynthetic epipodophyllotoxins, NSC-122819 (VM26) and NSC-141540 (VP16-213).

MATERIALS AND METHODS

Patients

Of 33 patients treated, 30 were evaluable. The three inevaluable patients either received only one or two doses of the drug or died within 7 days from the start of treatment due to causes not related to therapy. There were 21 men and nine women. The mean age of the group was 58 years (range, 18-72 years). All patients had histologically and/or cytologically proven malignant neoplasms and in all cases they had advanced widespread metastatic disease or leukemia in relapse after standard treatment.

[1]Received Oct 31, 1974; revised Mar 3, 1975; accepted Apr 2, 1975.

[2]Chemical nomenclature, NSC numbers, and CAS registry numbers for all compounds mentioned in this paper are included in the List of Compounds at the end of the text. NSC-141540 was supplied by Drs. Neff and Radielovic, Sandoz AG Ltd., Basel, Switzerland.

[3]Division of Oncology and Hematology, Medizinische Klinik C Kantonsspital, St. Gallen, Switzerland.

[4]*Reprint requests to:* Dr. Walter Felix Jungi, Division of Oncology and Hematology, Medizinische Klinik C Kantonsspital, CH-9006 St. Gallen, Switzerland.

[5]Brunner KW. Privileged communication through Sandoz AG.

TABLE 1.—Clinical data, drug doses, and responses in 30 patients treated with NSC-141540

Patient No.	Sex/age (yrs)	Tumor site	Diagnosis (cell type)	Previous treatment*	NSC-141540 treatment		Response		Degree of toxicity†			
					Total dose (mg/m²)	Duration (days)	Extent (%)	Duration (days)	Wbc	Platelets	Gastro-intestinal	Hair loss
1	M/40	Lung	Anaplastic, small cell	—	5937	145	PR(60)	139	1	0	0	3
2	M/72	Lung	Anaplastic, small cell	—	3027	166	IMP(40)	150	4	3	2	4
3	M/66	Lung	Anaplastic, small cell	—	3319	192	PR(75)	160	2	0	0	2
4	M/72	Lung	Anaplastic, small cell	—	313	10	PR(50)	‡	1	2	0	1
5	M/56	Lung	Anaplastic, small cell	—	8017	215	NC	126	2	1	2	3
6	M/57	Lung	Anaplastic, small cell	R	1350	50	NC	46	2	0	0	2
7	M/50	Lung	Anaplastic, small cell	—	819	58	P		3	2	2	3
8	M/57	Lung	Anaplastic, small cell	R	8300	260+	PR(50)	207+	0	2	1	2
9	M/66	Lung	Anaplastic, small cell	—	480	41	IMP(10)	41	1	0	0	1
10	M/65	Lung	Anaplastic, small cell	—	1450	55	P		1	1	0	3
11	M/56	Lung	Anaplastic, small cell	—	'294	17	IMP(15)	17	4	0	§	§
12	M/71	Lung	Anaplastic, small cell	S,R	6200	329	PR(70)	320	2	3	0	3
13	M/53	Lung	Anaplastic, medium cell	R	1212	50	IMP(10)	50	2	0	3	2
14	M/52	Lung	Anaplastic, large cell	—	558	27	P		3	0	3	2
15	M/56	Lung	Anaplastic, large cell	S	550	39	P		1	2	2	§
16	M/63	Lung	Anaplastic, large cell	—	552	25	P		0	0	0	0
17	M/65	Lung	Adenocarcinoma	R,C	1200	56	P		2	1	0	3
18	M/52	Lung	Adenocarcinoma	R	1787	75	IMP(15)	68	1	1	2	3
19	F/61	Lung	Epidermoid	R	3716	107	NC	72	2	0	0	1
20	M/64	Lung	Epidermoid	R	1970	118	NC	118	4	0	0	3

21	M/68	Lung	Epidermoid	—	608	34	P		0	0	1	0
22	F/43	Ovary	Adenopapillary	S, C	535	50	NC	50	4	0	§	4
23	F/51	Ovary	Adenopapillary	S,R,C	533	24	P		3	3	§	3
24	F/69	Ovary	Papillary, solid	S,R,C	767	71	IMP(30)	30	2	1	2	3
25	F/69	Ovary	Adenopapillary	S,R,C	200	41	IMP(20)	25	3	1	§	§
26	F/60	Ovary	Papillary, solid	C	441	43+¶	PR(50)	45+¶	3	3	0	3
27	F/37	Ovary	Adenopapillary	S,C,R	590	33+	IMP(40)	33+	2	1.	0	1
28	M/61	Prostate	Adenocarcinoma	—	910	60	IMP(25)	45	4	4	3	4
29	F/18	Acute myelomonocytic leukemia	—	C	625	29	NC/P**		§	§	0	4
30	F/58	Acute myelomonocytic leukemia	—	C	588	26	NC/P**		§	§	0	3

* S = surgery, R = radiation therapy, C = chemotherapy, H = hormone therapy.
† See text for definitions of toxicity scores.
‡ Patient died on Day 10 (respiratory failure).
§ Not recorded or not evaluable due to pre-existing toxic signs (from previous treatment or disease).
¶ Patient was switched to followup study (NSC-141540 given continuously for 21 days); total remission duration, 196+ days.
** No distinction possible between NC and P.

Fifteen patients had received prior therapy (ie, radiation, chemotherapy, and/or hormone therapy), and 15 of the patients were previously untreated. Treatment was always started on an inpatient basis and was continued in the outpatient clinic if possible.

Drug Administration

NSC-141540 was supplied in 5-ml vials containing 100 mg of active drug for intravenous (iv) use, and in 100-mg capsules for oral use. The drug was administered in 5-day courses which were repeated every 21 days. The usual therapeutic schedule for courses 1 and 2 was: 60 mg/m^2/day × 5 given in 250 cc of normal saline or 5% dextrose in water iv over 30 minutes. Subsequent courses consisted of 60-120 mg/m^2/day × 5 (according to the hematologic tolerance in previous courses) given orally in two fractionated doses daily.

Patients showing clearcut progression of their disease after the initial two courses were taken off the study. Iv treatment with NSC-141540 was continued in subsequent courses when anorexia, nausea, or vomiting occurred.

Control Tests

Complete blood counts were done twice weekly during the first two courses and then once weekly. Blood urea nitrogen, creatinine, uric acid, electrolytes, alkaline phosphatase, transaminases, blood glucose, and coagulation profile were determined weekly during the initial two drug courses, and thereafter they were determined at the beginning of each subsequent course. Clinical examination, chest roentgenograms, and other roentgenograms pertinent for tumor measurement were repeated before each drug course.

Dosage Modification

Doses of NSC-141540 were reduced by 50% if the white blood cell count (wbc) dropped below 3000 cells/mm^3 or the platelet count dropped below 100,000 cells/mm^3. Treatment was stopped when the wbc was below 2000 cells/mm^3 or the platelet count was below 75,000 cells/mm^3. Subsequent drug courses were delayed until complete hematologic recovery occurred. Doses were also reduced if there was undue subjective toxicity in previous courses. Oral doses were increased by 50%-100% of the initial dose in the absence of objective mainly hematologic toxicity.

Assessment of Toxicity

Subjective and objective adverse side effects were rated according to the evaluation criteria commonly used by cooperative chemotherapy groups: 0 = none, negative, or normal; 1 = mild; 2 = moderate; 3 = severe; 4 = life-threatening or fatal. Toxicity scores for hematologic values were as follows:

Wbc (cells/mm^3).—0 = > 4000; 1 = 3000-4000; 2 = 2000-3000; 3 = 1000-2000; 4 = < 1000.

Platelet count (platelets/mm^3):—0 = > 150,000; 1 = 100,000-150,000; 2 = 75,000-100,000; 3 = 50,000-75,000; 4 = < 50,000.

Mean toxicity scores were calculated for each category of side effects.

Evaluation of Response

Tumor response was rated as follows: *partial remission* (PR) = reduction in tumor size of more than 50%; *improvement* (IMP) = documented but less than 50% reduction of original tumor size; *no change* (NC) = no change in tumor size or increase of less than 25%; and *progressive disease* (P) = tumor increasing at least 25% in one diameter.

RESULTS

Antitumor Activity

Remission rate.—Of 30 evaluable patients, 16 (53%) responded objectively to NSC-141540 using this schedule. Five had a good PR and 11 demonstrated objective tumor reduction of lesser extent. Patient data, total drug doses, and duration of NSC-141540 treatment are shown in table 1.

Quality of remission.—No complete remissions (CR) were observed in this study. The best remissions were seen in patients with oat cell carcinoma of the lung (mean reduction of tumor size, approximately 50%; range, 20%-75%). The quality of responses in lung cancers of other histologic types was poor. The only patient with huge hilar and mediastinal masses metastatic to a prostatic cancer showed a poor PR. Of six patients with metastatic ovarian cancer (stages III and IV), four responded with one good and three poor PRs. There was no detectable improvement in the two patients with acute myelomonocytic leukemia in relapse. Four of the five patients in the NC category had remarkably benign clinical courses while receiving NSC-141540, some of them for more than 6 months. Survival data cannot be calculated at the present time for the whole group because two patients are still alive and many patients received alternative chemotherapy or radiotherapy after having failed to respond to NSC-141540.

Duration of remission.—The overall remission duration (PR + IMP) was 3 months (mean, 92 days; range, 17-320 days). The longest remission was observed in a patient with oat cell carcinoma. The quality of remission correlated well with its duration.

Onset of and maximum remission.—Measurable shrinking of tumor could be documented after only 1

week of treatment, especially in patients with oat cell carcinoma. The maximal response usually was obtained by Day 42-45 after the start of treatment, ie, after two drug courses. Symptomatic subjective improvement was prompt and often quite striking in patients with small cell carcinoma of the lung.

Toxicity

In the schedule used in this trial NSC-141540 was generally well tolerated by either iv or oral administration. The therapy never had to be stopped because patients refused further drug administration. There were no abnormal sensations during NSC-141540 infusion with the exception of chills in one patient (No. 2). The etiology of these chills could not be elucidated despite detailed investigations. They did not recur with continuing treatment. Burning sensation and thrombophlebitis at the infusion site, as have been described with NSC-122819 (12), were never seen with NSC-141540. Gastrointestinal side effects were observed in ten patients (33%). They consisted of anorexia, flatulence, nausea, and occasional vomiting. In most cases they could have been related to the tumor itself (abdominal masses, liver metastases, or malignant ascites) as well as to the drug. One patient felt abnormal palpitations while taking NSC-141540 orally without concomitant EKG changes, a phenomenon already described by Falkson et al (8) in 18 of 65 patients.

Hematologic toxicity: leukocytes.—The mean toxicity score for leukopenia was 2.1 and the mean nadir of wbc was 2700 cells/mm^3, usually seen on Day 8. This signifies a moderate to severe depression of the leukocytes (predominantly granulocytes). Severe granulocytopenia (grade 4) was seen in five patients, occurring early after completion of the first iv course. The lowest wbc reported was 160 cells/mm^3 on Day 8. Bone marrow recovery in every case occurred in less than 10 days. There was no documented infection during the granulocytopenic episodes. Granulocytopenia never reached the same extent in subsequent courses due to dosage adjustments. Subsequent oral administration of NSC-141540 in the maintenance phase of the study resulted in only mild to moderate leukopenia.

Hematologic toxicity: platelets.—The mean toxicity score for this effect was 1.6, equaling a mild to moderate thrombocytopenia. Only one grade 4 thrombocytopenia was observed in a patient with diffuse neoplastic bone marrow infiltration (patient No. 21). The nadir of platelet depression was usually seen around Day 11, ie, 3-4 days later than for leukocytes. Platelet counts came back to normal more slowly than leukocytes. No episode of major hemorrhage was observed.

Hypercalcemia.—Elevated serum calcium was reported in five cases, but only two patients had clinical symptoms of hypercalcemia. Hypercalcemia in all five cases was certainly not related to therapy with NSC-141540; it was probably a result of the neoplastic (bone metastases) or para-neoplastic (ectopic hormone production) activity.

Hyperuricemia.—Eight patients had elevated serum uric acid levels while being treated with NSC-141540. With one exception these reactions were seen only in responders, usually immediately after completing the first drug course. They are explained by rapid tumor lysis and could be easily controlled by hydration and allopurinol medication. No relevant deviation from pretreatment levels was recorded for any other laboratory parameters.

Alopecia.—Twenty-seven of the 30 patients (90%) exhibited marked hair loss (mean toxicity score, 2.3), sometimes resulting in complete baldness. In the patients surviving for a sufficiently long period, the hair grew back despite continuing NSC-141540 therapy.

Cardiovascular side effects.—Careful and frequent monitoring of heart and blood pressure was done during and after iv courses with NSC-141540. No relevant alternations could be observed, including hypotension, as had been seen with NSC-122819 therapy (9).

Neurotoxicity.—No peripheral neurotoxicity (paresthesias, etc) was noted. One patient with anaplastic lung cancer (No. 15) experienced prolonged coma after two courses of NSC-141540. No satisfactory explanation could be found for this condition. He died 21 days later, and no brain metastases were found at autopsy. It is unlikely, although possible that this coma was induced by NSC-141540. Most possibly the episode was due to undetected metabolic or vascular alterations.

Mortality.—Among the 30 evaluable patients, no deaths could be directly related to drug application. Autopsies were performed on 20 patients, ten of whom died while receiving therapy. Causes for death could be found in all cases except patient No. 4 who had small cell carcinoma with massive upper venous obstruction rapidly decreasing while receiving NSC-141540 (it is possible that he died from acute right heart failure).

NSC-141540 toxicity is summarized in table 2.

TABLE 2.—Toxicity of NSC-141540 in 30 patients

Toxic effects	No. of patients
Subjective	
Gastrointestinal	
Nausea, vomiting	5
Meteorism	1
Diarrhea	1
Anorexia	4
Chills during infusion	1
Palpitation (oral drug)	1
Objective	
Leukopenia (nadir, 2700 cells/mm^3)	25*
Thrombocytopenia (nadir, 146,000 cells/mm^3)	16*
Alopecia	27
Coma of unknown etiology	(1)

*Evaluated in 28 patients only; the 2 patients with leukemia were not evaluable in this respect.

DISCUSSION

The semisynthetic epipodophyllotoxin NSC-141540 has been given only limited clinical trials in man. A cooperative study by the European Organization for Research and Treatment of Cancer has found antitumor activity against myelomonocytic leukemia (four CRs among eight cases), against malignant lymphomas, especially of the histiocytic type (one CR and six PRs among 21 patients), and to a lesser extent against various solid tumors in man (7). The longest and most useful remissions have been seen in acute monocytic leukemia and reticulosarcoma. Similar results have been obtained by Brunner[6] and Nissen et al (11). Falkson et al (8) obtained PRs in small cell carcinoma of the lung and histiocytic lymphoma. Newman et al (10) did not see any useful objective responses in 38 patients. A large cooperative study with two dose levels of NSC-141540 is now in progress by the Acute Leukemia Group B. No results of combination chemotherapy with NSC-141540 have been presented so far.

The toxicity of NSC-141540 was mainly reversible leukopenia/thrombocytopenia, alopecia, and nausea. The drug was generally well tolerated, and iv therapy was tolerated better than oral therapy.

The most important result of our study was the activity of NSC-141540 against small cell carcinoma of the lung, with a PR rate of 42%.

Encouraging responses were obtained in our small patient group with far-advanced ovarian cancer in relapse after standard chemotherapy including cyclophosphamide and 5-fluorouracil.[7] No response could be seen in the two patients with acute leukemia. It became evident even after the first drug course if a patient would respond to NSC-141540. Two courses were necessary to achieve the maximal response.

The drug was subjectively well tolerated by the oral as well as the iv route. It regularly induced moderate to marked but never life-threatening leukopenia and thrombocytopenia. It almost always produced total alopecia, and in one third of the patients tolerable gastrointestinal side effects were noted. No drug-related deaths were observed. There was no correlation between hematologic toxicity and antitumor response.

Our results with NSC-141540 are in good agreement with those of other investigators with respect to antitumor activity and toxicity. Considering the far-advanced stage of the disease in all our patients, our therapeutic results are quite encouraging.

A subsequent, and still ongoing, phase II trial at our institution is showing even more complete and longer remissions in oat cell carcinomas of the lung and ovarian cancers when NSC-141540 is initially given over a longer period (up to 21 days). This study should also give more information about the still controversial enteral resorption of the drug.

This new compound has definite and valuable activity against solid tumors in man, predominantly small cell carcinoma of the lung and ovarian cancer. It induces acceptable toxicity. NSC-141540 warrants further controlled clinical trials to establish optimal dosage regimens, and should be tested in combination chemotherapy in the near future.

[6] See footnote 4.

[7] Cyclophosphamide: NSC-26271; CAS reg. No. 6055-19-2; 2*H*-1,3,-2-oxazaphosphorine, 2-[bis(2-chloroethyl)amino]tetrahydro-, 2-oxide, monohydrate.

5-Fluorouracil: NSC-19893; CAS reg. No. 51-21-8.

REFERENCES

1. Stähelin H. Chemie und Wirkungsmechanismus von Podophyllin-Derivaten. Planta Med 22:336, 1972.
2. ———. Activity of a new glycosidic lignan derivative (VP 16-213) related to podophyllotoxin in experimental tumors. Eur J Cancer 9:215-221, 1973.
3. ———. Wirkungsdauer, in vitro und in vivo, einmaliger Gaben des Podophyllum-Cytostaticums VP 16-213. Krebsinformation 8:79, 1973.
4. Dombernowsky P, Nissen NI, and Larsen V. Clinical investigation of a new podophyllum derivative, epipodophyllotoxin, 4'-(demethyl-9-(4,6-0-2-thenylidene-β-D-glucopyranoside) (NSC-122819), in patients with malignant lymphomas and solid tumors. Cancer Chemother Rep 56:71-82, 1972.
5. Dombernowsky P, and Nissen NI. Schedule dependency of the antileukemic activity of the podophyllotoxin-derivative VP 16-213 (NSC-141540) in L1210 leukemia. Acta Pathol Microbiol Scand [A] 81:715-724, 1973.
6. European Organization for Research and Treatment of Cancer. Clinical screening of epipodophyllotoxin VM 26 in malignant lymphomas and solid tumors. Br Med J 2:744, 1972.
7. ———. Epipodophyllotoxin VP 16-213 in treatment of acute leukaemias, haematosarcomas and solid tumors. Br Med J 2:199, 1973.
8. Falkson G, and Falkson H. Clinical trial of the oral form 4'-demethyl-epipodophyllotoxin-β-D ethylidene glucoside (NSC-141540) VP 16-213. Proc Am Assoc Cancer Res and ASCO 15:160, 1974.
9. Muggia FM, Selawry OS, and Hansen HH. Clinical studies with a new podophyllotoxin derivative, epipodophyllotoxin, 4'-demethyl-9(4,6-0-2-thenylidene-β-D-glucopyranoside) (NSC-122819). Cancer Chemother Rep 55:575-581, 1971.
10. Newman SJ, Creaven PJ, and Selawry OS. Phase I clinical trial of 4'-demethylepipodophyllotoxin 9-(4,6-0-ethylidene β-D-glucopyranoside) (NSC 141540, VP 16-213). Proc Am Assoc Cancer Res and ASCO 15:132, 1974.
11. Nissen NI, Larsen V, Pedersen H, et al. Phase I clinical trial of a new antitumor agent 4'-demethylepipodophyllotoxin 9-(4,6-0-ethylidene-β-D-glucopyranoside) (NSC-141540; VP-16-213). Cancer Chemother Rep 56:769-777, 1972.
12. Sonntag RW, Senn HJ, Nagel G, et al. Experience with 4'-demethylepipodophyllotoxin 9-(4,6-0-2-thenylidene-beta-D-glucopyranoside); VM-26; NSC-122819 in the treatment of malignant lymphosis. Eur J Cancer 10:93-98, 1974.
13. Stähelin H. 4'-Demethyl-epipodophyllotoxin thenylidene glucoside (VM 26) a podophyllum compound with a new mechanism of action. Eur J Cancer 6:303-311, 1970.
14. Trempe G, Sykes M, Young C, et al. Phase 1 trial of the podophyllotoxin derivative VM-26. Proc Am Assoc Cancer Res 11:79, 1970.
15. Wang JJ, and Chervinsky DS. Effect of a podophyllotoxin derivative (VP-16) on nucleic acid and protein biosynthesis in L1210 leukemic cells. Proc Am Assoc Cancer Res 14:110, 1973.

4′-Demethylepipodophyllotoxin 9-(4,6-*O*-2-thenylidene-β-D-glucopyranoside) (NSC-122819; VM-26) and 4′-Demethylepipodophyllotoxin 9-(4,6-*O*-ethylidene-β-D-glucopyranoside) (NSC-141540; VP-16-213) in Childhood Cancer: Preliminary Observations[1,2,3]

Gaston Rivera, Thomas Avery, and Charles Pratt[4,5]

SUMMARY

We evaluated the responses of 39 children with cancer who, after failure to respond to conventional chemotherapeutic agents, received either or both of two epipodophyllotoxins: 4′-demethylepipodophyllotoxin 9-(4,6-*O*-2-thenylidene-β-D-glucopyranoside) (NSC-122819) and 4′-demethylepipodophyllotoxin 9-(4,6-*O*-ethylidene-β-D-glucopyranoside) (NSC-141540). Seventeen patients had acute lymphocytic leukemia (ALL), 12 had acute nonlymphocytic leukemia (ANLL), and ten had solid tumors. Initially, the patients in each disease category were randomized to receive 50 mg/m^2/dose of NSC-122819 intravenously (iv) twice weekly or 75 mg/m^2/dose iv of NSC-141540 twice weekly for 4 weeks. Drug dosages and schedules of administration were adjusted during the course of the study. Although objective responses were not detected in the heterogeneous group of solid tumor patients, definite clinical responses were obtained in nine of the 29 patients with acute leukemia. The responses to the two epipodophyllotoxins were noted in patients with ALL as well as in patients with ANLL. Toxic side effects included nausea, vomiting, diarrhea, fever, alopecia, leukopenia, and thrombocytopenia. These results, the first reported with both NSC-122819 and NSC-141540 in childhood cancer, indicate that the epipodophyllotoxins are well tolerated and may be effective against acute leukemia.

[Cancer Chemother Rep 59:743-749, 1975]

The epipodophyllotoxins, 4′-demethylepipodophyllotoxin 9-(4,6-*O*-2-thenylidene-β-D-glucopyranoside) (NSC-122819) and 4′-demethylepipodophyllotoxin 9-(4,6-*O*-ethylidene-β-D-glucopyranoside) (NSC-141540), are relatively new chemotherapeutic agents with antitumor properties in experimental animal systems and in man. Excellent oncolytic activity by these agents has been reported in the treatment of transplantable murine tumors (1-4), and NSC-122819, in contrast to NSC-141540, has also produced significant prolongation of survival time in animals inoculated intracerebrally with L1210 cells (1,5). NSC-122819 has a high degree of lipid solubility and a low molecular weight, characteristics required to cross the blood-brain barrier (5,6). With both drugs, promising results have been obtained in patients with advanced neoplasms, especially malignant lymphoma, acute monocytic leukemia, brain tumors, and bladder carcinoma (6-17). Most of the patients in these series were adults and, except for one case in which the leukocyte count was reduced after drug administration (7), objective responses to the epipodophyllotoxins have not been reported for patients with acute lymphocytic leukemia (ALL). The present study was limited to children with various malignancies, and its objectives were to determine the therapeutic effectiveness and toxicity of the epipodophyllotoxins for childhood cancer patients.

MATERIALS AND METHODS

Children with acute leukemia and solid tumors were studied. The acute leukemia group was partitioned into ALL and acute nonlymphocytic leukemia (ANLL), while the solid tumor group was subdivided into patients with neuroblastoma, rhabdomyosarcoma, osteosarcoma, and other tumors.

Forty-one patients were admitted to the study, of whom 39 were evaluable. Twenty-four were white

[1]Received Nov 15, 1974; revised Mar 26, 1975; accepted Apr 23, 1975.

[2]Supported by Public Health Service grant CA-08480 from the National Cancer Institute (NCI), National Institutes of Health, Department of Health, Education, and Welfare, and by the American-Lebanese-Syrian Associated Charities.

[3]NSC-122819 and NSC-141540 were supplied by Cancer Therapy Evaluation, Division of Cancer Treatment, NCI.

[4]St. Jude Children's Research Hospital, Memphis, Tenn.

[5]*Reprint requests to:* Dr. G. Rivera, St. Jude Children's Research Hospital, PO Box 318, Memphis, Tenn 38101.

TABLE 1.—Oncolytic responses of leukemia patients to the epipodophyllotoxins

Patient No.	Age (yrs)	Diagnosis*	Duration and status of disease when admitted to study	No. of previously administered chemotherapeutic agents	Study drug and dosage	Complications	Days on study	Oncolytic responses and outcome†
1	5	ALL	28 mos, 4th hematologic relapse, previous CNS leukemia	9	NSC-141540, 8 doses, 75 mg/m²/dose twice weekly	Bacterial septicemia	28	Reduction in wbc from 138,000 (blasts, 98%) to 5900 (blasts, 19%); died 5 days after completion of trial (septicemia); leukemia present at autopsy
2	3	ALL	14 mos, 4th hematologic relapse, CNS leukemia	8	NSC-122819, 3 doses, 75 mg/m²/dose daily × 3 (no response to previous NSC-122819 and NSC-141540 in original doses)	Systemic candidiasis	36	Reduction in wbc from 332,000 (blasts, 96%) to 1000 (no blasts); disappearance of lymphadenopathy and hepatosplenomegaly; no marrow or spinal fluid examinations available; died 13 days after 3-day course (systemic candidiasis); no leukemia identified at autopsy
3	10	ALL	51 mos, 3rd hematologic relapse	10	NSC-141540, 5 doses, 75 mg/m²/dose twice weekly	Bacterial septicemia	20	Disappearance of bone pains; reduction in wbc from 62,200 (blasts, 90%) to 12,300 (blasts, 90%); incomplete trial; discharge required despite no significant acute toxicity
4	2	ALL	13 mos, 3rd hematologic relapse, previous CNS leukemia	10	NSC-122819, 8 doses, 100 mg/m²/dose twice weekly	Bacterial septicemia	45	Reduction in wbc from 38,800 (blasts, 97%) to 1100 (blasts, 58%); followed with 6 doses of NSC-141540 (no marrow response); died 8 days after completion of chemotherapy (septicemia); minimal leukemia at autopsy
5	8	ALL	56 mos, 2nd hematologic relapse, CNS leukemia, previous testicular relapse	8	NSC-122819, 8 doses, 100 mg/m²/dose over 20-day period (no response to previous NSC-141540, 5 doses, 150 mg/m²/dose)	Bacterial septicemia	60	No initial leukocytosis or organomegaly; last available bone marrow test showed reduction in blasts from 95% to 25%; spinal fluid cleared of blasts; later had normal hemograms (wbc 4000, 70% neutrophils, normal platelets); unmaintained response lasted 60 days; patient did not return for follow-up and died at home on Day 95 after completion of trial
6	10	AML	10 mos, 1st hematologic relapse, CNS leukemia	9	NSC-141540, 10 doses, 150 mg/m²/dose over a 15-day period	Bacterial septicemia	20	Reduction in wbc from 600,000 (blasts, 100%) to 600 (blasts, 4%); disappearance of lymphadenopathy; reduction of hepatomegaly; no bone marrow test available; died 6 days after completion of trial (septicemia); leukemia present at autopsy
7	5	AMML	8 mos, 2nd hematologic relapse, previous CNS leukemia	9	NSC-141540, 9 doses, 150 mg/m²/dose over 15-day period	Probable septicemia (not confirmed bacteriologically)	28	Reduction in wbc from 101,000 (blasts, 58%) to 12,100 (blasts, 78%); reduction in hepatomegaly; died 7 days after completion of chemotherapy (probable septicemia); no autopsy

8	15	CML	33 mos, 3rd blastic crisis, CNS leukemia	6	NSC-122819, 3 doses, 100 mg/m²/dose over 4-day period	Bacterial septicemia	10	Reduction of wbc from 13,800 (blasts, 84%) to 800 (no blasts); disappearance of lymphadenopathy and hepatosplenomegaly of 10.0 cm; no marrow or spinal fluid available; died 6 days after last dose of chemotherapy (septicemia); no autopsy
9	3	AHL	5 mos, 1st hematologic release, CNS leukemia, mediastinal and abdominal tumor masses	5	NSC-141540, 4 doses, 150 mg/m²/dose over 20-day period	Severe malnutrition	40	Disappearance of lymphadenopathy; reduction of mediastinal mass and pleural effusion; reduction of abdominal masses and hepatomegaly; reduction in bone marrow blasts from 90% to 2% and reappearance of normal hematopoiesis; duration of response 25 days; patient was still on chemotherapy but did not return for followup; died at home on Day 60 after admission to study

*AHL = acute histiocytic leukemia; AMML = acute myelomonocytic leukemia; AML = acute myelocytic leukemia; CML = chronic myelocytic leukemia; ALL = acute lymphocytic leukemia; CNS = central nervous system.

† Autopsy results were available for 4 of the 9 patients. Wbc counts given in cells/mm³.

boys, ten were white girls, four were black boys, and one was a black girl. Their median age was 8 years, with a range of 2-20 years. Seventeen patients had ALL, 12 had ANLL, and ten had solid tumors. Two patients were not evaluable because they died with septicemia within 24 hours after receiving only one dose of epipodophyllotoxin.

Patient Selection and Assignment to Treatment

Informed consent of the parents was requisite for admission of patients to the study. Adequate liver and kidney function as defined by sulfobromophthalein (BSP) retention not exceeding 20% in 45 minutes, serum glutamic oxaloacetic transaminase (SGOT) not exceeding 200 units, bilirubin levels not exceeding 3 mg/100 ml, blood urea nitrogen (BUN) not exceeding 20 mg/100 ml, and creatinine levels not exceeding 2 mg/100 ml were also required before admission into the study. All patients had advanced disease, they had previously received extensive drug and radiation therapy, and their neoplasms were clearly resistant to currently available chemotherapeutic agents of established effectiveness. Some had also received other experimental drugs. In addition, 25 of the 29 patients with leukemia had bacterial septicemia and/or systemic candidiasis when admitted to or during the study.

Patients in each disease category were randomized by the card-envelope method to receive either NSC-122819 or NSC-141540. If after 2-4 weeks no response or progressive disease was observed with the first agent, patients were given the alternate analog. Other antitumor therapy was not given during the administration of the epipodophyllotoxins.

Drug Preparation and Administration

The epipodophyllotoxins are only slightly soluble in water and hence require special formulation before they can remain in aqueous solution. NSC-122819 was supplied in 5-ml vials containing 50 mg of drug, 0.15 g of benzyl alcohol, 0.30 g of N_1, N-dimethylacetamide, 2.50 g of polyethoxylated castor oil (purified), qs of maleic acid to pH 5.1, and qs of absolute alcohol to 5 ml. NSC-141540 was supplied in vials containing 100 mg of drug, 400 mg of Tween 80, 3.25 g of polyethylene glycol 300, 150 mg of benzyl alcohol, and 10 mg of citric acid and absolute alcohol added qs to 5 ml. Since hypotension had been reported with intravenous (iv) push administration (8), both drugs were given as 30-45-minute iv infusion (5% glucose/⅓ N saline) at a concentration of 1 mg/ml.

Initial dosages and schedules of administration were 50 mg/m^2/dose iv twice weekly for 4 weeks for NSC-122819 and 75 mg/m^2/dose iv twice weekly for 4 weeks for NSC-141540. Drug dosages were adjusted after five consecutive patients in each drug group showed no evidence of significant toxic response. Dosage was increased 50%-100% for each drug and the timing of administration was varied according to tolerance and response.

Criteria of Response

Because of the stage of disease and the amount of previous therapy given to patients admitted to the study, remissions were not anticipated. Antitumor responses were therefore defined as (*a*) reductions greater than 80% in the white blood cell (wbc) count of leukemia patients with peripheral blast cells, (*b*) reductions greater than 50% in the percentage of leukemic or tumor cells in the bone marrow, or (*c*) decreases greater than 50% in the size of lymphadenopathy, organomegaly, and tumor masses. Anticipated toxic responses were gastrointestinal symptoms and bone marrow depression.

To assist in monitoring toxicity the following laboratory tests were performed before the study started and twice weekly during the study: BUN, creatinine, uric acid, bilirubin, SGOT, serum glutamic pyruvic transaminase, lactic dehydrogenase, alkaline phosphatase, serum albumin and globulin, amylase, lipase, and determinations of coagulation factors. BSP, chest roentgenograms, bone marrow examinations, and, for leukemic patients, lumbar punctures obtained prior to the study and at 2-4-week intervals. Confirmatory postmortem examinations were performed as permitted.

RESULTS

Response to Epipodophyllotoxins by Leukemia Patients

As evaluated by the previously stated criteria, nine of the 29 patients with acute leukemia responded to treatment with NSC-122819, NSC-141540, or both agents given sequentially (table 1). Five patients responded to NSC-141540 and four responded to NSC-122819. Two patients responded while receiving NSC-122819 after initial lack of response with NSC-141540. The most pronounced response was achieved in a child with acute histiocytic leukemia. In this patient (No. 9 in table 1), peripheral lymphadenopathy disappeared, tumor masses were reduced, and, most significantly, leukemic blast cells in the bone marrow decreased from 90% to 2% with concomitant reappearance of normal hematopoiesis. Another child (No. 5 in table 1) had a reduction in the percentage of bone marrow blast cells from 95% to 25% and, later, had a disappearance of blast cells in the spinal fluid and peripheral blood, as well as normal leukocyte counts with 70% neutrophils and normal platelet counts. Ten of the 20 patients who did not have objective clinical responses showed no evidence of progressive leukemia while in the study for 2-4 weeks. Postmortem examinations were performed on 20 patients. Three showed no evidence of leukemia and four others had only minimal evidence

of disease. Only two of these seven patients had been classified as having clinical response. The cause of death in these seven children was gram-negative rod septicemia and/or disseminated candidiasis.

Response by Disease Category: ALL and ANLL

Of the nine patients who showed clinical oncolytic responses, five had ALL and four had ANLL (one with acute myelocytic leukemia, one with acute myelomonocytic leukemia, one with acute histiocytic leukemia, and one with chronic myelocytic leukemia in blastic crisis). The frequency of clinical oncolytic responses did not differ significantly between ALL and ANLL patients.

Administration of Epipodophyllotoxins to Solid Tumor Patients

Ten children were studied in this group: four with rhabdomyosarcoma, three with neurobla· toma, one with osteosarcoma, one with Ewing's sarcoma, and one with hepatoblastoma. Five of the patients had extension of their neoplasms to the bone marrow. Seven patients received both drugs, two rhabdomyosarcoma patients were given NSC-122819 only, and the Ewing's sarcoma patient received NSC-141540 only. None of the patients had responses, and tumor was found in the five patients who had postmortem examinations.

Toxicity

In this study a total of 181 doses of NSC-122819 and 160 doses of NSC-141540 were administered. Of 31 children receiving NSC-122819, three had nausea, 16 had vomiting, ten had diarrhea, and one had fever directly related to drug administration. Seven of the 28 evaluable patients had alopecia. Of 28 children receiving NSC-141540, two had nausea, 13 had vomiting, eight had diarrhea, and two had fever directly related to drug administration. Hair loss was noted in four of the 29 patients evaluable for alopecia.

Hematologic toxicity could be evaluated only in solid tumor patients. Five of nine children who received NSC-122819 had leukopenia (<2500 cells/mm^3); two of these had counts below 1000 cells/mm^3. Recovery was noted within 1week. Of seven patients evaluable for the development of thrombocytopenia, four had a reduction in platelet counts to less than 100,000 cells/mm^3 (lowest count, 57,000 cells) with recovery to normal levels in 10-15 days. Six of eight patients who received NSC-141540 had leukopenia but none had wbc counts below 1000 cells/mm^3. Of five patients evaluable for the development of thrombocytopenia, one had a decrease in the platelet count to 75,000 cells/mm^3 for 3 days (table 2).

DISCUSSION

The results of this study indicate that the recently introduced epipodophyllotoxins, NSC-122819 and NSC-141540, are potentially effective agents for the treatment of childhood leukemia. Because of the heterogeneity of the solid tumors, no conclusions can be drawn from that group of patients. However, definite clinical responses were noted in nine of the 29 patients with acute leukemia. The disappearance of large tumor masses as well as the reductions in the concentration of leukemic cells in the peripheral blood were especially encouraging. More important, one child (patient No. 9, table 1) achieved a hematologic remission and another (patient No. 5, table 1) may have achieved a complete remission, hematologic and meningeal. This patient's hematologic remission status could not be confirmed because he did not return for followup bone marrow examinations.

It was interesting to note that postmortem examinations in seven of 20 leukemia patients showed little or no evidence of disease. Five of these seven patients did not have a clinical response. A review of the autopsy reports of other leukemia patients with advanced disease who died after receiving different chemotherapeutic agents other than the epipodophyllotoxins confirmed the uncommon nature of these findings. The meaning is still not clear; however, it could indicate antileukemic effectiveness of NSC-122819 and NSC-141540.

The responses in this study were observed in both ANLL and ALL patient groups. This unexpected result was encouraging because ANLL patients are usually less responsive to chemotherapy. On the basis of clinical responses, the two podophyllum analogs appeared equally effective. Of the two patients with the most pronounced responses, one responded to NSC-141540 and the other, who had not responded to this agent, showed evidence of response during the administration of NSC-122819.

Evaluation of the relative oncolytic effectiveness of the two epipodophyllotoxins was complicated by the administration of both drugs to approximately half of our leukemia patients. The rationale for performing a crossover study was based on the main objective of the study: to test the activity of both drugs in childhood cancer. Since our total test population was small, we wished to enlarge our base of evaluation. Ideally, in performing this crossover, we would have preferred to allow a reasonable time interval between the administration of the agents. However, for this poor-risk population with short life expectancies, this was impractical. In addition, at the outset of the study, knowledge of the mechanisms of action of NSC-122819 and NSC-141540 was limited, and whether one of these agents would produce an effect not elicited by the other was unknown. The two analogs now appear to have similar modes of action; they apparently act during the last S and G_2 phases of the cell cycle (17-19).

Initial drug dosages and schedules of administration were based on a limited number of available reports (7-10). Drug dosages were increased when they did not elicit significant acute toxicity (only moderate leukopenia and thrombocytopenia in solid tumor patients with bone marrow involvement).

TABLE 2.—Solid tumor patients admitted to the study

Patient No.	Diagnosis	Age (yrs)	First treatment: Agent and dosage (administered twice weekly)	First treatment: Toxicity*	First treatment: Response†	Second treatment: Agent and dosage (administered twice weekly)	Second treatment: Toxicity*	Second treatment: Response†
1	Rhabdomyosarcoma, bone marrow involvement	20	NSC-141540, 75 mg/m²/dose, 7 doses	None	NR	NSC-122819, 50 mg/m²/dose, 3 doses	Thrombocytopenia, 69,000 (Day 7)	NR
2	Rhabdomyosarcoma, pulmonary metastases	17	NSC-122819, 50 mg/m²/dose, 4 doses	Leukopenia, 2400 (Day 11)	NR	—	—	
3	Rhabdomyosarcoma, pulmonary and bony metastases	15	NSC-141540, 150 mg/m²/dose, 6 doses	Leukopenia, 2300 (Day 3); thrombocytopenia, 75,000 (Day 15)	NR	NSC-122819,100 mg/m²/dose, 5 doses	Thrombocytopenia, 87,000 (Day 8)	NR
4	Rhabdomyosarcoma, pulmonary metastases	17	NSC-122819, 100 mg/m²/dose, 4 doses	Leukopenia, 800 (Day 11); thrombocytopenia, 57,000 (Day 14)	NR	—	—	—
5	Neuroblastoma, bone marrow involvement	2	NSC-122819, 50 mg/m²/dose, 4 doses	Leukopenia, 1800 (Day 7); thrombocytopenia, 72,000 (Day 10)	NR	NSC-141540, 37.5 mg/m²/dose, 4 doses	Leukopenia, 1900 (Day 3)	NR
6	Neuroblastoma, bone marrow involvement	2	NSC-141540, 150 mg/m²/dose, 4 doses	Leukopenia, 2000 (Day 11)	NR	NSC-122819, 100 mg/m²/dose, 4 doses	Nausea and vomiting; leukopenia, 1400 (Day 6)	NR
7	Neuroblastoma, bone marrow involvement	7	NSC-122819, 100 mg/m²/dose, 4 doses	Leukopenia, 900 (Day 7)	NR	NSC-141540, 150 mg/m²/dose, 6 doses	Leukopenia, 1400 (Day 7)	NR
8	Osteosarcoma, pulmonary metastases	19	NSC-122819, 100 mg/m²/dose, 4 doses	Vomiting	NR	NSC-141540, 150 mg/m²/dose, 3 doses	Nausea and vomiting; diarrhea; leukopenia, 2300 (Day 4)	NR
9	Ewing's sarcoma, bone marrow involvement	16	NSC-141540, 150 mg/m²/dose, 4 doses	Leukopenia, 1400 (Day 7)	NR	—	—	—
10	Hepatoblastoma, pulmonary metastases	2	NSC-122819, 50 mg/m²/dose, 4 doses	None	NR	NSC-141540, 150 mg/m²/dose, 3 doses	None	NR

*Wbc and platelet counts given in cells/mm³.
† NR = no response.

Some children who had not responded previously showed objective responses to these increased dosages and acute toxicity was observed. As responses began to be obtained, schedules of drug administration were adjusted mainly on the basis of variations in leukocyte counts. When the drugs were given in 30-45-minute iv infusions, no episodes of hypotension or other evidences of cardiovascular symptomatology were encountered. Variations in renal and hepatic functions could not be associated with drug administration, nor could hematologic toxicity be evaluated in the group of patients with leukemia, since pancytopenia could be disease related rather than drug induced.

The results of this study strongly suggest that NSC-122819 and NSC-141540 are effective for some patients with advanced acute leukemia refractory to many of the currently available chemotherapeutic agents. The advanced disease status of the patients in this study was complicated in many instances by severe bacterial and/or fungal infections, making it difficult to identify the full chemotherapeutic potential of the epipodophyllotoxins. These agents may therefore be used to better advantage in patients with less advanced disease. At the present time superiority of either epipodophyllotoxin has not been determined.

In view of the generally established superiority of combination drug therapy for acute leukemia (21-24), studies with the epipodophyllotoxins in combination with other oncolytic agents appear indicated. Cytosine arabinoside,[6] for example, an agent with proven effectiveness against human leukemia (23),

[6]Cytosine arabinoside: NSC-63878; CAS reg. No. 69-74-9; cytosine, 1-β-D-arabinofuranosyl-, monohydrochloride; ara-C.

has been recommended for combination chemotherapy with NSC-141540 in the treatment of acute myelomonocytic leukemia (25). In preclinical studies at this institution, the combination of cytosine arabinoside with either of the podophyllum compounds has produced complementary action against murine L1210 leukemia.[7]

REFERENCES

1. Stähelin H. 4'-Demethylepipodophyllotoxin thenylidine glucoside (VM-26), a podophyllum compound with a new mechanism of action. Eur J Cancer 6:303-311, 1970.
2. Venditti JM. Treatment schedule dependency of experimentally active antileukemic (L1210) drugs. Cancer Chemother Rep Part 3, vol 2:35-59, 1971.
3. Stähelin H. Activity of a new glycosidic lignan derivative (VP16-213) related to podophyllotoxin in experimental tumors. Eur J Cancer 9:215-221, 1973.
4. Avery T, Roberts D, and Price R. Delayed toxicity of 4'-demethylepipodophyllotoxin 9-(4,6-0-2-thenylidine-β-D-glucopyranoside) (NSC-122819; VM-26) in mice. Cancer Chemother Rep 57:165-173, 1973.
5. Preclinical brochure: Sandoz compound VM-26. Hanover, NJ, Sandoz Pharmaceuticals, 1967.
6. Slansky BD, Mann-Kaplan RS, Reynolds AF, et al. 4'-Demethylepipodophyllotoxin-β-D-thenylidene-glucoside (PTG) in the treatment of malignant intracranial neoplasms. Cancer 33:460-467, 1974.
7. Trempe G, Sykes M, Young C, et al. Phase I trial of the podophyllotoxin derivative VM-26. Proc Am Assoc Cancer Res 11:79, 1970.
8. Muggia FM, Selawry OS, and Hansen HH. Clinical studies with a new podophyllotoxin derivative, epipodophyllotoxin 4'-demethyl-9(4,6-0-2-thenylidene-β-D-glucopyranoside) (NSC-122819). Cancer Chemother Rep 55:575-581, 1971.
9. Dombernowsky P, Nissen NI, and Larsen V. Clinical investigation of a new podophyllum derivative, epipodophyllotoxin, 4'-demethyl-9-(4,6-0-2-thenylidene-β-D-glucopyranoside) (NSC-122819), in patients with malignant lymphomas and solid tumors. Cancer Chemother Rep 56:71-82, 1972.
10. Nissen NI, Larsen V, Pedersen H, et al. Phase I clinical trial of a new antitumor agent, 4'-demethylepipodophyllotoxin 9-(4,6-0-ethylidene-β-D-glucopyranoside) (NSC-141540; VP-16-213). Cancer Chemother Rep 56:769-777, 1972.
11. European Organization for Research of the Treatment of Cancer. Clinical screening of epipodophyllotoxin VM-26 in malignant lymphomas and solid tumours. Br Med J 2:744-748, 1972.
12. ———. Epipodophyllotoxin VP16-213 in treatment of acute leukemias, haematosarcomas, and solid tumours. Br Med J 3:199-202, 1973.
13. Goldsmith M, and Carter SK. 4'-Demethylepipodophyllotoxin-β-D-thenylidene glucoside (VM-26). A brief review. Eur J Cancer 9:477-482, 1973.
14. Mathé G, Schwarzenberg L, Pouillart P, et al. Essai de traitement de divers hématosarcomes par le 4-déméthylépipodophyllotoxine-β-D-thénylidine glucoside (VM-26 ou EPT). Nouv Presse Med 3:447-451, 1974.
15. Sonntag RW, Senn HJ, Nagel G, et al. Experience with 4'-demethylepipodophyllotoxin 9(4,6-0-2-thenylidene-β-D-glucopyranoside); VM-26; NSC-122819 in the treatment of malignant lymphosis. Eur J Cancer 10:93-98, 1974.
16. Mathé G, Schwarzenberg L, Pouillart P, et al. Leucémies aigües et hématosarcomes divers. Essai de traitement par un second dérive de la podophyllotoxine (le 4-demethylpipodophyllotoxin-β-D-ethylidene glucoside VP 16-213 ou EPT). Nouv Presse Med 3:521-524, 1974.
17. Rivera G, Avery T, and Pratt C. Epipodophyllotoxins in childhood cancer. (Abstr) *In* Proceedings of the 11th International Cancer Congress, Oct 20-26, 1974.
18. Huang CC, Hou Y, and Wang JJ. Effects of a new antitumor agent, epipodophyllotoxin, on growth and chromosomes in human hematopoietic cell lines. Cancer Res 33:3123-3129, 1973.
19. Grieder A, Maurer R, and Stähelin H. Effect of an epipodophyllotoxin derivative (VP 16-213) on macromolecular synthesis and mitosis in mastocytoma cells in vitro. Cancer Res 34:1788-1793, 1974.
20. Misra N, and Roberts D. Inhibition by 4'-demethylepipodophyllotoxin 9(4,6-0-2-thenylidene-β-glucoside) of human lymphoblast cultures in G_2 phase of the cell cycle. Cancer Res 35:99-105, 1975.
21. Henderson ES, and Samaha RJ. Evidence that drugs in multiple combinations have materially advanced the treatment of human malignancies. Cancer Res 29:2272-2280, 1969.
22. Aur RJ, Simone J, Hustu HO, et al. Central nervous system therapy and combination chemotherapy of childhood lymphocytic leukemia. Blood 37:272-281, 1971.
23. Goldin A, Sandberg JS, Henderson ES, et al. The chemotherapy of human and animal acute leukemia. Cancer Chemother Rep 55:309-507, 1971.
24. DeVita VT, and Schein PS. The use of drugs in combination for the treatment of cancer: rationale and results. N Engl J Med 288:998-1006, 1973.
25. Mathé G, Schwarzenberg L, Pouillart P, et al. Two epipodophyllotoxin derivatives, VM-26 and VP16-213, in the treatment of leukemias, hematosarcomas, and lymphomas. Cancer 34:985-992, 1974.

[7]Rivera G, Avery T, and Roberts D. Response of L1210 to combination of cytosine arabinoside and VM-26 or VP16-213. Eur J Cancer. In press.

Phase I Clinical Trial of Isophosphamide (NSC-109724)[1,2]

M. H. Cohen,[3] P. J. Creaven,[3] F. Tejada,[3] H. H. Hansen,[3] F. Muggia,[3] A. Mittelman,[4] and O. S. Selawry[3,5]

SUMMARY

An initial clinical phase I trial of isophosphamide has been carried out at dose levels of 200-10,000 mg/m^2 of body surface area using a single-dose, every-3-week schedule. Significant toxicity was not seen at isophosphamide dose levels less than 2900 mg/m^2. At higher doses, nausea and vomiting was nearly universal. Hematologic toxicity manifested by leukopenia occurred in 12 of 20 patients treated with doses of 3800-7000 mg/m^2. Thrombocytopenia to 100,000 platelets/mm^3 was not seen in any patient. Urinary bladder toxicity manifested by hemorrhagic cystitis was seen in 15 of 23 patients treated with doses of 3800-10,000 mg/m^2. Hemorrhagic cystitis could be completely prevented by bladder irrigation with *N*-acetyl-L-cysteine (1% solution, 2000 ml/day). With careful attention to hydration, renal toxicity was largely prevented with blood urea nitrogen elevations to 30 mg/dl in only two of 14 patients receiving isophosphamide doses of 5000-7000 mg/m^2. Another side effect was central nervous system toxicity in seven of 17 patients at doses of 5000-10,000 mg/m^2. For phase II trials a dose of 5000 mg/m^2 is recommended, with careful attention to the state of hydration in the patient and with the knowledge that bladder irrigation may be necessary for the prevention and/or amelioration of bladder toxicity.

[Cancer Chemother Rep 59:751-755, 1975]

Isophosphamide, a cyclophosphamide[6] analog differing from the parent compound by the transposition of a chloroethyl group from the side chain to the ring nitrogen, is more active than the parent compound against certain experimental tumor systems (1) and has documented clinical activity in man (2-4). In addition, the toxicity of isophosphamide appears to be quantitatively different from that of cyclophosphamide, with the former drug having greater renal and urinary bladder toxicity and somewhat less hematologic toxicity (5,6).

The present report is the result of a phase I trial of isophosphamide using a single dose every 3 weeks. Because of the expected renal and bladder toxicity, studies of renal glomerular and tubular function were done before and after drug treatment, and the role of bladder irrigation with the sulfhydryl compound *N*-acetyl-L-cysteine in the prevention and/or amelioration of hemorrhagic cystitis was also investigated.

METHODS

Patients

Patients with histologically confirmed cancer not amenable to conventional treatment were eligible for inclusion in the study provided their renal function was adequate as determined by a blood urea nitrogen (BUN) level of less than 25 mg/100 ml and a serum creatinine level of less than 1.5 mg/100 ml. Other requirements included a serum bilirubin of < 1.5 mg/100 ml, as serum glutamic oxaloacetic transaminase (SGOT) of < 100 IU, pretreatment white blood cell (wbc) and platelet counts in excess of 5000 and 100,000 cells/mm^3 respectively, and a sufficient interval after previous chemotherapy to avoid possible additive toxicity (2-8 weeks depending on preceding treatment).

Laboratory and Clinical Studies

The following tests were performed twice weekly during treatment and for at least 3 weeks after the completion of each treatment course: determination of wbc, differential, platelet, and reticulocyte counts, BUN, and creatinine. Urinalyses were done daily for 2-4 days after isophosphamide injection

[1]Received Dec 16, 1974; revised Mar 14, 1975; accepted Mar 20, 1975.

[2]Isophosphamide: CAS reg. No. 3778-73-2; 1,3,2-oxazaphosphorine, 3-(2-chloroethyl)-2-[(2-chloroethyl)amino]tetrahydro-, 2-oxide. Supplied by Drug Research and Development, Division of Cancer Treatment, National Cancer Institute (NCI).

[3]NCI-VA Medical Oncology Section and Medical Service, Veterans Administration Hospital, Washington, DC.

[4]Roswell Park Memorial Institute, Buffalo, NY.

[5]*Reprint requests to:* Martin H. Cohen, MD, NCI-VA Medical Oncology Section, Veterans Administration Hospital, 50 Irving St, NW, Washington, DC 20422.

[6]Cyclophosphamide: NSC-26271; CAS reg. No. 6055-19-2; 2*H*-1, 3,-2-oxazaphosphorine, 2-[bis(2-chloroethyl)amino]tetrahydro-, 2-oxide, monohydrate.

and then at weekly intervals. SGOT, alkaline phosphatase, bilirubin, total serum proteins and albumin, and serum calcium were performed once weekly. Tumor measurements using the product of the greatest horizontal and the greatest vertical diameter were obtained weekly or biweekly. Additional examinations such as skeletal and chest roentgenograms were obtained before the study and as clinically indicated except when measurable lesions were present on chest roentgenograms.

STUDY PLAN

The starting dose for the present study, based on preclinical toxicology studies, was 200 mg/m^2 of body surface area given as an intravenous (iv) infusion over 30 minutes. Doses were escalated in accordance with a modified Fibonacci search. Three patients were treated at nontoxic dose levels and six or more patients were treated at each moderately toxic dose. Patients were to receive at least two doses of isophosphamide at 3-week intervals. Those patients with no toxicity after a single dose were eligible to receive the next higher dose of isophosphamide on their second course. Patients with documented antitumor effect continued to receive treatment as long as response persisted. All patients were to receive oral or iv fluids (2000 ml/m^2) starting 24 hours before drug administration and continuing for 1-2 days after treatment. At an isophosphamide dose of 5000 mg/m^2 patients were randomized to receive iv hydration either alone or with *N*-acetyl-L-cysteine bladder irrigation (1% in saline, 2000 ml/day) during their first treatment course. Patients then received the opposite regimen during their second treatment course, ie, patients treated initially with hydration plus bladder irrigation received only hydration alone while the alternate group received the combination.

STUDIES OF RENAL TUBULAR FUNCTION

Renal concentrating ability.—This was measured by the method of Miles et al (7). Patients were fasted for a period of 12-14 hours prior to determination of urinary osmolality. Tests were performed in patients before isophosphamide administration and were repeated 4 days after drug administration.

Renal tubular acidification capacity.—After completion of the concentration test, ammonium chloride (0.1 g/kg in gelatin capsules) was given orally along with as much oral fluid as the patient would tolerate. At the same time, iv hydration was started. Urinary pH was determined on specimens taken over the next 8 hours. Tests were done before isophosphamide administration and were repeated 4 days after drug administration.

RESULTS

The characteristics of the patients studied are summarized in table 1. Of the 42 patients entered in the study, 11 received two different doses of isophosphamide. Two patients were declared inevaluable, one because of the development of congestive heart failure during the phase of intensive iv hydration, and the other because of early death due to pulmonary emboli as proved at postmortem examination. The median age of the patients entered was 58 years with a range of from 36 to 76 years. Eleven of the 42 patients entered in this study had received no prior therapy. The histologic diagnoses of the patients are also shown in table 1.

TABLE 1.—Patient characteristics

	No. of patients
Entered into study	42
Total patient trials	53
Evaluable patient trials	51
Patient age (yrs)	
Mean, 58	
Range, 36-76	
Patients with no prior therapy	11
Patients with prior therapy	
Chemotherapy	15
Radiotherapy	8
Chemotherapy + radiotherapy	8
	31
Histologic type	
Epidermoid carcinomas	
Lung	4
Esophagus	3
Head and neck	6
	13
Adenocarcinomas	
Gastrointestinal tract	5
Lung	3
Bladder	3
Renal	4
Other	3
	18
Sarcomas	3
Others	8

The major toxic effects seen with isophosphamide administration are listed in table 2. Nausea and vomiting were not seen at single doses of less than 2200 mg/m^2. Beginning at that dose and at all subsequent doses nausea and vomiting was a nearly universal finding that increased in severity and duration with increased dose. Nausea usually began within 2-4 hours after the dose and usually lasted 1-3 days. The nausea and vomiting at higher isophosphamide doses appeared to be somewhat more severe than that seen with comparable single-dose cyclophosphamide administration (dose levels of 1100 mg/m^2).

With the exception of one patient whose wbc count fell to 4600 cells/mm^3 on Day 9 at an isophosphamide dose of 1000 mg/m^2, no leukopenia was seen until the

TABLE 2.—Isophosphamide toxicity

Dose (mg/m²)	No. of patient trials	No. of episodes of— Nausea and vomiting	Leukopenia (<5000 cells/mm³)	Thrombocytopenia (<100,000 cells/mm³)	Bladder and renal toxicity	Central nervous system toxicity
200	3	0	0	0	0	0
330	3	0	0	0	0	0
500	3	0	0	0	0	0
700	3	0	0	0	0	0
1000	3	0	1 (4600 on Day 9)	0	0	0
1300	3	0	0	0	0	0
1700	3	0	0	0	1*	0
2200	3	2	0	0	1	0
2900	4	3	1 (2900 on Day 8)	0	1	0
3800	6	6	3	0	4	0
5000	10	10	6	0	7	4
7000	4	4	3	0	2	1
10,000	3	3	1†	0	2	2

*Probably disease related.
†Does not include two patients who died early in the course of treatment.

dose was increased to 2900 mg/m². At this dose level, one of the four patients treated (a patient having received prior chemotherapy and radiotherapy) had a wbc nadir of 2900 cells/mm³ on Day 8 after treatment, with recovery by Day 14. Leukopenia at subsequent isophosphamide doses is recorded in figure 1. Of the six patients treated with doses of 3800 mg/m², three had no wbc depression below 5000 cells/mm³. The other three patients had wbc nadirs of 2900, 3100, and 3600 cells/mm³ respectively, the nadirs occurring on Days 7-9 with recovery by Day 12. At a dose of 5000 mg/m² relatively mild leukopenia was seen in six of the ten patients treated. Four of the six patients with leukopenia had wbc nadirs greater than 3000 cells/mm³, while the other two patients had wbc nadirs of 2800 and 2100 cells/mm³ respectively. The nadir of leukopenia at this dose level occurred between Days 6 and 9 with recovery between Days 10 and 15. A somewhat greater degree of leukopenia was seen at an isophosphamide dose of 7000 mg/m². Three of the four patients treated at this level had leukopenia which persisted for longer durations than at lower dose levels. At an isophosphamide dose of 10,000 mg/m² only one patient was evaluable for hematologic toxicity and this patient had a wbc nadir of 4300 cells/mm³ on Day 9 of treatment.

No thrombocytopenia below 100,000 platelets/mm³ was seen in any patient at any isophosphamide dose level.

Urinary bladder and renal toxicity were major concerns in patients receiving isophosphamide. As indicated in table 2, no bladder toxicity was seen in patients receiving doses less than 1700 mg/m². At that dose, a patient with bladder cancer had microscopic hematuria which did not represent a significant change from his pretreatment pattern of intermittent hematuria. Mild microscopic hematuria of 1-2 days' duration developed in one patient each at doses of 2200 and 2900 mg/m². At dose levels of 3800 mg/m² and above hematuria occurred more frequently as indicated in figure 2. Patients receiving isophosphamide at a dose of 5000 mg/m² were randomized to receive either their first or second treatment with *N*-acetyl-L-cysteine bladder irrigation. The results shown in figure 2 indicate hematuria that developed after the isophosphamide dose in which no bladder irrigation was given. *N*-acetyl-L-cysteine bladder irrigation completely prevented the development of hematuria in all patients. Nearly all patients with hemorrhagic cystitis had symptoms of dysuria and frequency. The duration and severity of these symptoms closely paralleled the duration of hematuria.

There were no elevations in the BUN or creatinine levels for isophosphamide doses of 3800 mg/m² or less. Of the ten patients receiving isophosphamide at a dose of 5000 mg/m², only two had BUN elevations to 30 mg/100 ml, the BUN reaching its maximal value 2-3 days after drug administration and returning

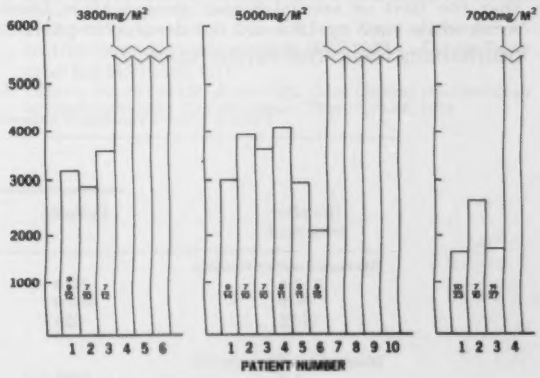

FIGURE 1.—Leukopenia after various isophosphamide doses.

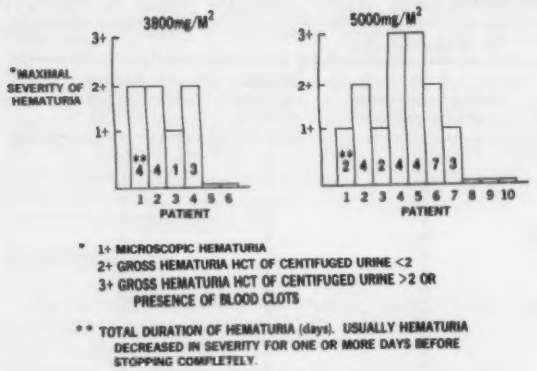

FIGURE 2.—Hematuria after isophosphamide at two dose levels.

to normal within 1 week. Two other patients had BUN values reaching 25 mg/100 ml with the remaining six patients having maximal values less than 20 mg/100 ml. There were no consistent rises of serum creatinine in the four patients having mildly elevated BUN levels. No elevation of BUN or creatinine was seen in the four patients receiving isophosphamide at a dose of 7000, mg/m², while one of the three patients receiving 10,000 mg/m² went into renal failure 1 day after receiving treatment and died 3 days later of septicemia with an accompanying BUN of 87 mg/100 ml.

Renal tubular function was studied in five patients receiving 5000 mg/m² of isophosphamide. None of the five patients had changes in either renal concentrating ability or in tubular acidification capacity after drug administration when compared to pretreatment results.

Urine output in seven patients receiving isophosphamide at a dose of 5000 mg/m² correlated with bladder toxicity in that hemorrhagic cystitis developed in patients having a fall in urine output in either the first or second 8-hour period after treatment while such cystitis did not develop in patients maintaining their urine output (table 3).

Central nervous system toxicity manifested most frequently by lethargy, somnolence, confusion, and disorientation was seen at isophosphamide doses of 5000 mg/m² and higher as indicated in table 2. Such symptoms usually began a few hours after completion of the iv infusion and persisted from 1 to 5 days. Other possible central nervous system toxic effects not directly attributable to drug treatment were focal seizures in a patient with documented brain metastases during isophosphamide administration and paresthesias of the extremities developing in a patient with leiomyosarcoma during treatment.

The only other toxic effect noted with isophosphamide treatment was mild to moderate alopecia in 50% of the patients receiving the higher dose levels.

Transient partial responses to therapy were noted in only two patients, one with squamous cell carcinoma of the head and neck and one with papillary adenocarcinoma of the fallopian tube. It should be pointed out however, that many patients had nonmeasurable disease and had received extensive prior therapy. No patients with small cell bronchogenic carcinoma or ovarian carcinoma were included in this trial.

DISCUSSION

The toxic effects associated with single-dose iv administration of isophosphamide every 3 weeks have been documented. As indicated in previous studies, the toxic effects of isophosphamide, although qualitatively similar, differ quantitatively from those of cyclophosphamide, with lesser degrees of bone marrow toxicity and increased renal and urinary bladder toxicity. Since the latter effects appear to be dose limiting, attempts were made to define the nature of the toxicity and to consider methods for ameliorating the toxicity.

Renal toxicity of isophosphamide, as manifested by azotemia, was seen by van Dyk et al (5) in 66% of 24 patients treated with isophosphamide doses of 150 mg/kg. Six of the 24 patients died within 15 days of isophosphamide administration and four of the patients had acute tubular necrosis. No studies of tubular function were done by these authors although granular casts were observed in the urine of

TABLE 3.—Urine volumes of patients with marked and minimal bladder toxicity

Hrs after treatment	Urine volume (ml) Patient 1	Patient 2	Patient 3	Patient 4
Marked bladder toxicity				
1-8	1115	700	1160	1900
8-16	None	1200	660	350
16-24	600	2450	450	450
Minimal bladder toxicity				
1-8	1190	2300	1215	
8-16	1925	1400	1375	
16-24	600	1180	1170	

subsequent patients treated on a daily schedule (5). More recently, DeFronzo et al (8) reported glomerular dysfunction and numerous tubular abnormalities consistent with the Fanconi syndrome in a patient treated with isophosphamide. As compared to these reports we have seen considerably less renal toxicity in our study. Thus, using a dose of 5000 mg/m^2 (approximately equivalent to 135 mg/kg) we saw only mild BUN elevations in four of ten patients, all abnormal BUN values returning to normal in 1 week with two of the four patients showing no concomitant elevation in serum creatinine. Similarly, at drug doses of 7000 mg/m^2 (equivalent to 190 mg/kg) no BUN elevation was seen in four patients. In the entire study, only one case of renal failure was seen at a dose of 10,000 mg/m^2. A possible reason for the difference in results between this study and that of van Dyk et al is the intensive hydration given to all patients prior to receiving isophosphamide. Two factors related to isophosphamide administration may play a role in renal toxicity: the antidiuresis that accompanies both this drug and cyclophosphamide, and the associated nausea and vomiting within a few hours of treatment. Evidence for these assumptions comes from our results showing that bladder toxicity correlated with urine output during the first 8-16 hours after drug administration. Neither van Dyk nor DeFronzo give data on the fluid intake of their patients.

With regard to bladder toxicity we were able to completely prevent hemorrhagic cystitis by bladder irrigation with volumes of 2000 ml/day. This is in contrast to the study of van Dyk et al who were unable to prevent cystitis by irrigating with sulfhydryl compounds on a schedule of 20 ml every 2 hours. This difference in results appears to relate to the fact that the volume of irrigation may be more important than the concentration or composition of reducing substances infused, since Creaven et al (9) showed no neutralization of alkylating activity, as measured by NBP[4-(4-nitrobenzyl)pyridine] reactivity, by *N*-acetyl-L-cysteine. Because of the antidiuresis associated with isophosphamide administration, one must consider the possibility of using diuretics along with intensive hydration to avoid the renal and bladder toxicity.

The second major dose-limiting effect related to isophosphamide administration is the central nervous system toxicity. While patients recover completely, symptoms may be severe enough to require hospitalization for each course of therapy. Although the pathophysiology of this complication is unknown, there is the possibility that it might relate to central nervous system water intoxication since it was noted predominantly in patients whose urine outputs decreased after drug administration.

The hematologic toxicity noted in this study was quantitatively less than that reported by van Dyk et al (5) or Ahmann et al (3), for single-dose administration, or by Bremner et al (4), for a daily schedule for 2-3 days. The reasons for these differences are uncertain but might be attributable to various combinations of more advanced patients, greater degrees of bone marrow involvement by tumor, or higher cumulative drug doses on a daily schedule.

On the basis of the above considerations, a starting dose of 4000-5000 mg/m^2, depending on prior therapy and the presence of bone marrow involvement, given every 3 weeks is a clinically tolerable schedule suitable for phase II trials.

REFERENCES

1. Brock N. Pharmacologische untersuchungen mit neun *N*-chloroathyl-phosphoraureester-diamiden. *In* Proceedings of the 5th International Congress of Chemotherapy (Spitzy KH, and Haskek H, eds). Vienna, Verlag der Wiener Medizinischen Akademie, 1967, vol 2, p 1155.
2. Scheef W. Problems, experience, and results of clinical investigations with ifosfamide. *In* Proceedings of the 7th International Congress of Chemotherapy, Prague, 1971 (Hejzlar M, Semonsky M, Masak S, eds). Munich, Urban and Schwarzenberg, 1972.
3. Ahmann DL, Bisel HF, and Hahn RG. Phase II clinical trial of isophosphamide (NSC-109724) in patients with advanced breast cancer. Cancer Chemother Rep 58:861-865, 1974.
4. Bremner DN, McCormick JStC, and Thomson JWW. Clinical trial of isophosphamide (NSC-109724)—results and side effects. Cancer Chemother Rep 58:889-893, 1974.
5. van Dyk JJ, Falkson HC, van der Merwe AM, et al. Unexpected toxicity in patients treated with iphosphamide. Cancer Res 32:921-924, 1972.
6. Cohen MH, and Mittelman A. Initial clinical trials of isofosfamide. Proc Am Assoc Cancer Res 14:64, 1973.
7. Miles BE, Paton A, and de Wardener HE. Maximum urine concentration. Br Med J 2:901-905, 1954.
8. DeFronzo RA, Abeloff M, Braine H, et al. Renal dysfunction after treatment with isophosphamide (NSC-109724). Cancer Chemother Rep 58:375-382, 1974.
9. Creaven PJ, Allen LM, Alford DA, et al. Clinical pharmacology of isophosphamide. Clin Pharmacol Ther 16:77-86, 1974.

Daunorubicin (NSC-82151), Vincristine (NSC-67574), Cytosine Arabinoside (NSC-63878), and Prednisone (NSC-10023) Combination Therapy for Advanced Adult Acute Leukemia[1,2,3]

C. Patrick Burns[4,5]

Daunorubicin and various daunorubicin combinations have been shown to be effective in inducing remissions when used as initial therapy for adult acute leukemia (1-8). The drug is less effective for previously treated adult patients whether used alone (9) or in combination with cytosine arabinoside (7), prednisone (6,10), or L-asparaginase (11). A previous, promising study of daunorubicin combined with vincristine, cytosine arabinoside, and prednisone has been reported in abstract form (5). The present study was undertaken to assess the response of advanced acute leukemia to that latter combination which includes the two most effective single agents for acute leukemia in adults combined with two drugs having minimal myelosuppressive effects.

METHODS

All previously treated adults admitted to the University of Iowa Hospitals with acute leukemia in relapse, and who had received no prior daunorubicin, were eligible. All patients had failed to respond to therapy with other drug combinations before being placed on this protocol. They received an induction program consisting of daunorubicin (40 mg/m^2) by intravenous (iv) push on Days 1-3, vincristine (1.5 mg) by iv push on Day 1, cytosine arabinoside (80 mg/m^2) by iv push on Days 1-3, and prednisone (40 mg/m^2) orally on Days 1-3. The response was assessed and the combination repeated up to three times according to the protocol of Wiernik and Serpick (3). If the patient had received combinations which included vincristine, cytosine arabinoside, and prednisone on more than two occasions in the past, or if the patient had progressive disease after two courses of the study combination, daunorubicin (60 mg/m^2 via iv push on Days 1-3) was given as a single agent. The criteria for evaluation of response were those of Acute Leukemia Group B, December 1969 (12), except that low hemoglobin levels were not considered sufficient to exclude a remission.

Hemoglobin level and white blood cell, differential, and platelet counts were obtained at least four times a week. Patients were monitored for signs of cardiac, renal, and hepatic toxicity at least once a week. Bone marrow examinations were performed prior to and on Day 8 of each course and at least weekly thereafter. Broad spectrum antibiotics were utilized for fever or other signs of infection. Most patients were hospitalized in private rooms with standard reverse isolation; none were in laminar air flow rooms at the time of the daunorubicin therapy.

RESULTS

Twenty-two patients with acute leukemia were entered into the study between October 1972 and November 1974. The clinical characteristics of these patients are listed in table 1. In all of the patients, the previous induction therapy had failed primarily or after relapse. Fifteen patients were eligible for the daunorubicin combination (12 nonlymphoblastic and three lymphoblastic; median age 47). Seven patients received daunorubicin alone (five nonlymphoblastic and two lymphoblastic; median age 24). The median duration of disease from diagnosis to start of daunorubicin therapy was 25 weeks for the patients receiving the combination and 38 weeks for all patients. The median dose of daunorubicin given to those patients treated with the combination was 330 mg/m^2 compared with 360 mg/m^2 for those treated with daunorubicin alone. There was one partial remission after the daunorubicin combination, and there were two complete remissions and one partial remission after daunorubicin alone. Two patients had a short trial due to early death, but all patients were evaluated. These early deaths occurred on Days 4 and 12, respectively; an autopsy was performed on the latter case only and there was evidence of widespread residual leukemia. Four patients had a remission of some type and the clinical data for these patients are shown in table 2. Those patients attaining a complete remission have had long durations of response, and both are alive (one remains in remission) at the time of this report. The combination was no more successful in the induction of remission in patients with lymphoblastic as com-

[1]Received Dec 23, 1974; revised Mar 14, 1975; accepted Mar 19, 1975.

[2]Supported in part by Public Health Service grant FR-05372 from the General Research Support Branch, Division of Research Resources, National Institutes of Health, Department of Health, Education, and Welfare.

[3]Daunorubicin was supplied by Cancer Therapy Evaluation, Division of Cancer Treatment, National Cancer Institute. Chemical nomenclature, NSC numbers, and CAS registry numbers for all compounds mentioned in this paper are included in the List of Compounds at the end of the text.

[4]Department of Medicine, University of Iowa College of Medicine, Iowa City.

[5]*Reprint requests to:* C. Patrick Burns, MD, Department of Medicine, University Hospitals, Iowa City, Iowa 52242.

TABLE 1.—Summary of clinical characteristics of patients with acute leukemia

Patient No.	Age/sex	Type of leukemia*	Prior therapy† and response	Time from diagnosis to daunorubicin treatment (wks)	Response
Daunorubicin combination					
1	42/M	AML	COAP; cytosine arabinoside + 6-thioguanine	25	PR
2	22/M	AML	Cytosine arabinoside + 6-thioguanine	8	NR§
3	26/F	AML	Cytosine arabinoside + 6-thioguanine	9	NR
4	49/M	AML	Cytosine arabinoside + 6-thioguanine; COAP (CR)	41	NR
5	64/F	AMML	Cytosine arabinoside + 6-thioguanine	9	NR§
6	32/M	AMML	COAP; cytosine arabinoside + 6-thioguanine	14	NR
7	65/F	AMML	Cytosine arabinoside + 6-thioguanine (CR)	25	NR
8	53/F	AMML	Cytosine arabinoside + 6-thioguanine	11	NR
9	54/M	AMML	Cytosine arabinoside + 6-thioguanine (CR); COAP; 6-mercaptopurine + methotrexate	48	NR
10	33/F	AMML	COAP (CR); cytosine arabinoside + 6-thioguanine (CR)	68	NR
11	30/F	AMML	Cytosine arabinoside + 6-thioguanine	18	NR
12	47/F	AMML	Busulfan; cytosine arabinoside + 6-thioguanine; hydroxyurea; COAP	177	NR
13	58/F	ALL	COAP; OAP; cytosine arabinoside + 6-thioguanine	10	NR
14	26/M	ALL	OAP (CR); CNS prophylaxis‡; methotrexate‡; COAP (CR); cytosine arabinoside + 6-thioguanine	58	NR
15	47/F	ALL	Chlorambucil + prednisone; 6-mercaptopurine + prednisone; OAP (CR × 2); methotrexate‡; cytosine arabinoside + 6-thioguanine; COAP	65	NR
Daunorubicin alone					
16	24/M	AML	Methotrexate + vincristine + prednisone (CR); bacillus Calmette-Guérin‡; cytosine arabinoside + 6-thioguanine (CR); COAP (CR)	265	CR
17	20/F	AML	COAP (CR); methotrexate‡	129	PR
18	64/F	AML	COAP (CR); cytosine arabinoside + 6-thioguanine	49	NR
19	20/F	AML	OAP	8	NR
20	46/M	AMoL	COAP (CR); cytosine arabinoside + 6-thioguanine (CR)	36	NR
21	17/M	ALL	Vincristine + prednisone (CR); COAP	67	CR
22	50/M	ALL	OAP (CR × 2); CNS prophylaxis‡; COAP; VAMP	53	NR

*AML = acute myeloblastic leukemia; AMML = acute myelomonoblastic leukemia; ALL = acute lymphoblastic leukemia; AMoL = acute monoblastic leukemia.

†In chronologic order. Induction therapies that resulted in complete remission (CR) are indicated; other entries were partial remissions (PR) or no response (NR).

‡Indicates drugs used only for maintenance; maintenance drugs which were also included in induction combinations are not listed separately.

§Early death.

pared to nonlymphoblastic forms of the disease. The median survival of all nonresponders from the time of initiation of daunorubicin was 10.3 weeks (range 0.3-27), and there was little difference between those nonresponders receiving the daunorubicin combination (median survival 9.6 weeks, range 0.3-27) and those receiving the single agent (median survival 12.9 weeks, range 10-19.1).

The toxicity of the combination was considerable. Myelosuppression was uniform and the frequency of life-threatening infections was high. The median nadir of the leukocyte count was 600 cells/mm^3 and it occurred on median Day 10 for both those receiving the combination and for those treated with daunorubicin alone. There were nine instances of infection including gram-negative septicemia, pneumonia, enterocolitis, dental abscess, folliculitis, labial abscess, and perirectal abscess. Most patients required prophylactic platelet transfusions. The median nadir of the platelet count for those patients receiving the combination was 4000 platelets/mm^3 on median Day 10. This compares with 12,000 platelets/mm^3 on Day 13 for those receiving the single agent. Other toxic effects from the combination included

TABLE 2.—Clinical characteristics of responding patients

Patient No.	Time to response* (days)	Daunorubicin dose to response (mg/m²)	Maintenance therapy	Remission duration† (wks)	Survival time‡ (wks)
1	52	240	Cytosine arabinoside + 6-thioguanine, q12h × 10 doses monthly	33	40+
16	26	360	Adriamycin + bacillus Calmette-Guerin, q6wks	30	76+
17	45	180	Daunorubicin × 3 days; 1 course only	7	62
21	20	180	6-Mercaptopurine daily, methotrexate + cyclophosphamide weekly§	69+	72+

*Start of daunorubicin to 1st day of remission.
†From day of remission to relapse. Patient No. 21 remains in remission at time of report.
‡From initiation of daunorubicin. Patient Nos. 1 and 16 are alive in relapse at time of report.
§Remission consolidated with two courses of daunorubicin, 30 mg/m²/ day × 3 days.

nausea, vomiting, phlebitis at injection site, alopecia, oral ulcers, transient elevation of serum glutamic pyruvic transaminase, diarrhea, and a full sensation of tongue and jaw. Disseminated intravascular coagulation developed in one patient on two separate occasions after receiving the combination. No symptomatic cardiac toxicity occurred, but nonspecific ST-T wave changes (three patients), QT segment lengthening (two patients), bigeminy (one patient), and P wave changes of biatrial disease (one patient) not present prior to daunorubicin were noted on serial ECGs.

DISCUSSION

The daunorubicin combination was ineffective for remission induction in most of these adult patients with refractory acute leukemia. There are several possible explanations for this low response. All 15 patients had received cytosine arabinoside as part of a combination regimen which had failed prior to initiating the study combination. Cytosine arabinoside is converted to the inactive arabinosyl uridine by the enzyme cytidine deaminase. It has been demonstrated that sequential courses of cytosine arabinoside result in an increase in blast cell cytidine deaminase activity and a concomitant decrease in therapeutic response to the drug (13). Furthermore, nine of the 15 patients treated with the daunorubicin combination had received prior treatment with vincristine. Reciprocal cross resistance of vincristine and daunorubicin has been demonstrated in Ehrlich ascites tumor cells (14) and Chinese hamster cells (15). Danø (14) has shown that there is a decreased accumulation of daunorubicin by Ehrlich cells that are resistant to vincristine. This may be due to an active outward transport of the drug by the resistant cells (16).

Patients were not randomized between the daunorubicin combination and daunorubicin alone. Those who did not qualify for the combination received the alternative therapy. As a result, one cannot strictly compare the two therapies for patients with resistant disease. However, it is noteworthy that a higher response rate was achieved using daunorubicin alone. This may have been in part related to the higher doses of daunorubicin these patients received. Although daunorubicin probably has a role in the treatment of refractory disease, it appears that its combination with vincristine, cytosine arabinoside, and prednisone has limited induction potential when given to patients with advanced adult acute leukemia.

LIST OF COMPOUNDS

Adriamycin: NSC-123127; CAS reg. No. 23214-92-8
L-Asparaginase: NSC-109229; CAS reg. No. 9015-68-3
Busulfan: NSC-750; CAS reg. No. 55-98-1; 1,4-butanediol, dimethanesulfonate
Chlorambucil: NSC-3088; CAS reg. No. 305-03-3; butyric acid, 4-[p-[bis(2-chloroethyl)amino]phenyl]-
COAP: cyclophosphamide, vincristine, cytosine arabinoside, and prednisone
Cyclophosphamide: NSC-26271; CAS reg. No. 6055-19-2; 2*H*-1,3,2-oxazaphosphorine, 2-[bis(2-chloroethyl)amino]tetrahydro-, 2-oxide, monohydrate
Cytosine arabinoside: NSC-63878; CAS reg. No. 69-74-9; cytosine, 1-β-D- arabinofuranosyl-, monohydrochloride; ara-C
Daunorubicin: NSC-82151; CAS reg. No. 23541-50-6
Hydroxyurea: NSC-32065; CAS reg. No. 127-07-1
6-Mercaptopurine: NSC-755; CAS reg. No. 6112-76-1; purine-6-thiol, monohydrate; 6-MP
Methotrexate: NSC-740; CAS reg. No. 59-05-2; glutamic acid, *N*-[p-[[(2,4-diamino-6-pteridinyl)methyl]methylamino]benzoyl]-
OAP: vincristine, cytosine arabinoside, and prednisone
POMP: 6-mercaptopurine, vincristine, methotrexate, and prednisone
Prednisone: NSC-10023; CAS reg. No. 53-03-2; pregna-1,4-diene-3,-11,20-trione, 17,21-dihydroxy-
6-Thioguanine: NSC-752; CAS reg. No. 1832-72-0; purine-6-thiol, 2-amino-; 6-TG

VAMP: vincristine, methotrexate, 6-mercaptopurine, and prednisone

Vincristine: NSC-67574; CAS reg. No. 2068-78-2; leurocristine, sulfate (1:1); Oncovin

REFERENCES

1. Weil M, Glidewell OJ, Jacquillat C, et al. Daunorubicin in the therapy of acute granulocytic leukemia. Cancer Res 33:921-928, 1973.
2. Medical Research Council's Working Party in Leukaemia in Adults. Treatment of acute myeloid leukaemia with daunorubicin, cytosine arabinoside, mercaptopurine, L-asparaginase, prednisone and thioguanine: results of treatment with five multiple-drug schedules. Br J Haematol 27:373-389, 1974.
3. Wiernik PH, and Serpick AA. A randomized clinical trial of daunorubicin and a combination of prednisone, vincristine, 6-mercaptopurine, and methotrexate in adult acute nonlymphocytic leukemia. Cancer Res 32:2023-2026, 1972.
4. Crowther D, Powles RL, Bateman CJT, et al. Management of adult acute myelogenous leukaemia. Br Med J 1:131-137, 1973.
5. Bodey GP, Coltman CA, Jr, and Freireich EJ. Combination chemotherapy with arabinosyl cytosine (ara-C) in adult acute leukemia. (Abstr) Cancer Chemother Rep 57:112, 1973.
6. Bloomfield CD, Brunning RD, Theologides A, et al. Daunorubicin-prednisone remission induction with hydroxyurea maintenance in acute non-lymphocytic leukemia. Cancer 31:931-938, 1973.
7. Yates JW, Wallace HJ, Jr, Ellison RR, et al. Cytosine arabinoside (NSC-63878) and daunorubicin (NSC-83142) therapy in acute nonlymphocytic leukemia. Cancer Chemother Rep 57:485-488, 1973.
8. Rosenthal DS, and Moloney WC. The treatment of acute granulocytic leukemia in adults. N Engl J Med 286:1176-1178, 1972.
9. Lippman M, Zager R, and Henderson ES. High dose daunorubicin (NSC-83142) in the treatment of advanced acute myelogenous leukemia. Cancer Chemother Rep 56:755-760, 1972.
10. Bloomfield CD, Brunning RD, and Kennedy BJ. Daunorubicin therapy in adult acute lymphatic leukemia. Cancer 30:47-55, 1972.
11. Bodey GP, Hewlett JS, Coltman CA, Jr, et al. Therapy of adult acute leukemia with daunorubicin and L-asparaginase. Cancer 33:626-630, 1974.
12. Cortes EP, Ellison RR, and Yates JW. Adriamycin (NSC-123127) in the treatment of acute myelocytic leukemia. Cancer Chemother Rep 56:237-243, 1972.
13. Steuart CD, and Burke PJ. Cytidine deaminase and the development of resistance to arabinosyl cytosine. Nature [New Biol] 233:109-110, 1971.
14. Danø K. Cross resistance between vinca alkaloids and anthracyclines in Ehrlich ascites tumor in vivo. Cancer Chemother Rep 56:701-708, 1972.
15. Biedler JL, and Riehm H. Cellular resistance to actinomycin D in Chinese hamster cells in vitro: cross-resistance, radioautographic, and cytogenetic studies. Cancer Res 30:1174-1184, 1970.
16. Danø K. Active outward transport of daunomycin in resistant Ehrlich ascites tumor cells. Biochim Biophys Acta 323:466-483, 1973.

Phase II Study of ICRF-159 (NSC-129943) in Advanced Colorectal Carcinoma[1,2,3]

T. A. Marciniak, C. G. Moertel, A. J. Schutt, R. G. Hahn, and R. J. Reitemeier[4,5]

ICRF-159 was developed at the Imperial Cancer Research Fund facilities in London, England, and was selected for clinical trial on the basis of its antitumor activity in L1210, Lewis lung, and other model tumor systems (1,2). It has been studied quite extensively overseas as well as in phase I investigations in the United States (3-5). The principal toxicity has been leukopenia and thrombocytopenia. Gastrointestinal and mucocutaneous side effects have been uncommon. In a phase I study conducted by Bellet and associates in this country (4), an objective response was observed in one of four patients with measurable advanced colon cancer. The maximum tolerated dose in that study was 1.0 g/m^2/day for 3 days.

The purpose of this study was to determine the therapeutic activity in advanced colorectal carcinoma of ICRF-159 administered in a 3-day intensive course at a maximum clinically tolerable dosage.

MATERIALS AND METHODS

Patients

Twenty-five patients were chosen for this study. All had histologically confirmed adenocarcinomas that originated in the colon or rectum and all had measurable areas of known malignant disease which served as objective indicators of response to therapy. Each patient had been ambulatory and maintaining a reasonable state of nutrition before the initiation of treatment. Treatment had been deferred for at least 1 month after any previous chemotherapy, radiation therapy, or abdominal surgery which involved a resection or anastomosis and for at least 3 weeks after abdominal surgery which involved exploration and biopsy only. To insure optimal conditions for demonstrating therapeutic activity, particular emphasis was placed on the selection of patients who had been in good general condition and who had not had previous exposure to cytotoxic drugs.

[1]Received Jan 20, 1975; revised Mar 31, 1975; accepted Apr 23, 1975.

[2]Supported by contract N01-CM-02066 from the Division of Cancer Treatment (DCT), National Cancer Institute (NCI), National Institutes of Health, Department of Health, Education, and Welfare.

[3]ICRF-159: CAS reg. No. 21416-87-5; 2,6-piperazinedione, 4,4'-propylenedi-,(±)-; 1,2-di(3,5-dioxopiperazin-1-yl) propane. Supplied by Drug Development Branch, Drug Research and Development, DCT, NCI.

[4]Mayo Clinic and Mayo Foundation, Rochester, Minn.

[5]*Reprint requests to:* Thomas A. Marciniak, MD, Gastrointestinal Oncology, Mayo Clinic, Rochester, Minn 55901.

Drug Administration

ICRF-159 was supplied in scored tablets in dosages of 50, 250, and 500 mg. The planned course of therapy was 1.0 g/m^2/day orally for 3 consecutive days. Each day's dose was divided into three approximately equal parts which were administered every 8 hours.

Evaluation

Prior to therapy, each patient had a general medical evaluation including the following laboratory studies: urinalysis, hemoglobin level, leukocyte and platelet counts, serum creatinine, calcium, bilirubin, alkaline phosphatase, glutamic oxaloacetic transaminase, sodium, potassium, uric acid, and glucose, as well as a chest roentgenogram. Leukocyte and platelet counts were repeated on Day 3. After treatment, leukocyte counts were obtained twice weekly and platelet counts once weekly.

Patients were reevaluated at 4 weeks with repetition of all pretreatment laboratory studies. Objective improvement was claimed if there was a decrease by at least 50% in the product of the largest perpendicular diameters of the most clearly measurable area of cancer chosen prior to therapy. If hepatomegaly was chosen, there must have been a reduction of at least 30% in the sum of the measurements below the xiphoid process and each costal margin at the midclavicular lines. In addition, there must have been no increase in any other indicator lesions, no new areas of malignant disease, and no significant deterioration in weight, symptoms, or performance status. If regression of the indicator lesion was insufficient to meet the criteria for objective response and yet the increase in any indicator lesion was less than 25%, objective stability was claimed. If the increase in any indicator lesion was more than 25%, objective progression was claimed. Patients who remained in good clinical condition and showed no evidence of objective progression were re-treated every 4 weeks until progression was evident.

RESULTS

The characteristics of the patients chosen for study are given in table 1. All were ambulatory, most were capable of working full- or part-time, and 12 of the 25 had received previous chemotherapy. These 12 patients had completed a total of 15 regimens: eight involved 5-fluorouracil (5-FU) only, four involved 5-FU and other agents, one involved 5-FU

TABLE 1.—Patient characteristics

Characteristics	No. of patients
Sex (male/female)	14/11
Age (yrs)	
Mean, 59	
Range, 38-72	
ECOG performance score *	
0-1	16
2-3	9
Previous treatment	
Chemotherapy	8
Radiation therapy	1
Chemotherapy and radiation therapy	4

*Based on Eastern Cooperative Oncology Group (ECOG) scale of 0 (fully active) to 4 (totally disabled).

TABLE 2.—Toxic reactions in 25 patients

Toxic reactions	No. of patients
Nausea	5
Vomiting	3
Leukopenia (cells/mm³)	
≤4000>3000	1
≤3000>2000	9
≤2000>1000	10
≤1000	5
Thrombocytopenia (cells/mm³)	
≤150,000> 100,000	3
≤100,000>48,000	6
Alopecia	19
Dermatitis	1
Stomatitis	1
Diarrhea	1

and radiation therapy, and one each involved adriamycin and cyclophosphamide.[6] Objective improvement was observed in two patients, both during treatment with 5-FU, methyl-CCNU, and vincristine.[7]

Twenty-two patients had the full planned initial course of therapy. Two patients did not receive the dose on Day 3 because a significant decrease in the leukocyte count was observed on that day. One patient erred and missed taking a tablet which amounted to 10% of the full planned dosage.

Toxic Effects

The toxic reactions experienced by our patients are shown in table 2. Leukopenia was the dose-limiting toxic effect, with a mean leukocyte count nadir of 1800 cells/mm³ occurring on an average of Day 12 (range 6-18) of the first course. The duration of leukopenia (defined as the estimated number of days the leukocyte count was less than 4000 cells/mm³) was an average of 8 days and ranged from 1 to 14 days with the longer durations corresponding to the lower nadirs. Leukopenia was reproducible and dose-related on subsequent courses, necessitating a reduction in dosage for nine of the 17 patients treated a second time to a mean dosage of 850 mg/m²/day for all patients. The two patients whose first courses were terminated after the second treatment day had leukocyte count nadirs which were less than 2000 cells/mm³. In fact, a decrease in the leukocyte count from Day 1 to 3 of greater than 2000 cells/mm³ was associated with a nadir of less than 2000 cells/mm³ in five of six applicable cases. Thrombocytopenia was mild and not clinically important.

Nausea and vomiting were infrequent and in only one patient was the absorption of the drug questioned because of vomiting shortly after administration. Stomatitis and diarrhea occurred in one patient each and in both instances were minimal. However, alopecia was universal: hair loss was evident in 19 of 23 patients who returned for the first followup and was moderate to severe in all patients who had been treated with two or more courses.

One patient exhibited an unusual acneiform papular dermatitis involving the trunk, face, and proximal extremities after each of four courses. The dermatitis developed approximately 1 week after each treatment and was persistent, although resolving, at the time of the next treatment. The patient, a physician, treated himself with a corticosteroid cream with claimed benefit. A second patient reported a few similarly described lesions which appeared during one course, but they were not evident at the followup examination.

One patient died shortly after initiation of therapy. That patient was hospitalized because of fever and a leukocyte count of 300 cells/mm³ on Day 8 of therapy. She died suddenly the next day and although a postmortem examination was not done, it was assumed that this was a drug-related death. Her pretreatment clinical and laboratory parameters did not differ from those of patients with fewer toxic reactions except that she had received prior radiation therapy. The other four patients with leukocyte count nadirs less than 1000 cells/mm³ had been treated previously: two with chemotherapy and radiation therapy and the other two with chemotherapy alone.

[6] 5-FU: NSC-19893; CAS reg. No. 51-21-8.
Adriamycin: NSC-123127; CAS reg. No. 23214-92-8.
Cyclophosphamide: NSC-26271; CAS reg. No. 6055-19-2; 2H-1,3,2-oxazaphosphorine, 2-[bis(2-chloroethyl)amino]tetrahydro-, 2-oxide, monohydrate.

[7] Methyl-CCNU: NSC-95441; CAS reg. No. 33073-59-5; urea, 1-(2-chloroethyl)-3-(4-methylcyclohexyl)-1-nitroso-.
Vincristine: NSC-67574; CAS reg. No. 2068-78-2; leurocristine, sulfate (1:1).

Therapeutic Results

Objective improvement was observed in three patients. All of these patients had had a performance status of 0 or 1 before therapy and none had received prior chemotherapy (as shown in table 3) or prior radiation therapy. The primary indicator lesions were malignant hepatomegaly in two patients and an abdominal mass in the third; all three were biopsy proved. One of the responders had as secondary indicator lesions pulmonary metastases which remained stable until the time of objective progression. Improvement was evident in each patient at the time of the first followup visit but did not meet the criteria for objective response until the second or third visit. The duration of improvement was brief: objective progression occurred after 28 weeks (six courses) in one patient, 21 weeks (five courses) in the second patient, and 25 weeks (six courses) in the third patient. Symptomatic relief was impressive only in the third patient. A fourth patient experienced pain relief for 16 weeks associated with a 28% reduction (at best) in the sum of his liver measurements.

Objective progression in the nonresponders occurred after one course in eight patients, two courses in another eight, three courses in four, and four courses in two.

TABLE 3.—Response rate and prior chemotherapy

	No. of patients treated	No. of objective responses
Prior chemotherapy	12	0
No prior chemotherapy	13	3 (23%)
Totals	25	3 (12%)

DISCUSSION

In this phase II study of ICRF-159 administered in a 3-day intensive course for advanced colorectal carcinoma, the principal side effect was leukopenia. This was moderately severe and associated with one drug-related death. We feel that for further exploration of this schedule of administration, a somewhat lower dosage would be preferable. Based on results with our dosage adjustments, 850 mg/m^2/day for 3 consecutive days would seem appropriate.

Objective improvement of relatively brief duration was observed in three of the 25 patients we treated. If one considers only those patients who had not been previously exposed to cytotoxic drugs, a reasonable response rate of 23% (three of 13 patients) was observed.

Although the therapeutic potential of ICRF-159 for advanced large bowel cancer would seem to be limited, there is, nevertheless, a paucity of active drugs for this neoplasm. Further evaluation of ICRF-159 in more extensive phase II and phase III studies and its possible role in combination drug regimens would seem warranted.

REFERENCES

1. CREIGHTON AM, HELLMANN K, and WHITECROSS S. Antitumour activity in a series of bisdiketopiperazines. Nature 222:384-385, 1969.
2. HELLMANN K, and BURRAGE K. Control of malignant metastases by ICRF 159. Nature 224:273-275, 1969.
3. HELLMANN K, NEWTON K, WHITMORE D, ET AL. Preliminary clinical assessment of I.C.R.F. 159 in acute leukemia and lymphosarcoma. Br Med J 1:822-824, 1969.
4. BELLET RE, MASTRANGELO MJ, DIXON LM, ET AL. Phase I study of ICRF-159 (NSC-129943) in human solid tumors. Cancer Chemother Rep 57:185-189, 1973.
5. CREAVEN PJ, COHEN MH, HANSEN HH, ET AL. Phase I clinical trial of a single-dose and two weekly schedules of ICRF-159 (NSC-129943). Cancer Chemother Rep 58:393-400, 1974.

Cardiac Uptake of Adriamycin (NSC-123127) Not Affected by Strophanthin G (NSC-25485)[1,2]

Brief Reports and Preliminary Communications

Nicholas R. Bachur,[3] William Reiter,[3] and Emanuela Arena[4,5]

Several proposals have been proffered to decrease the clinical cardiotoxicity of the anthracycline antibiotics, adriamycin and daunorubicin.[6] Among these proposals is pretreatment with cardiac glycosides, such as strophanthin G, prior to anthracycline antibiotic therapy (1) to reduce anthracycline accumulation by the heart. However, this technique remains unsubstantiated. Recently, clinical groups have been accepting pretreatment with strophanthin G as a proven technique for reduction of cardiac adriamycin uptake (2). Therefore, we feel obliged to present additional data on strophanthin G pretreatment of adriamycin-dosed laboratory animals. Since we utilized adriamycin extraction and quantification techniques having a high degree of specificity and reproducibility (3), these data may contribute to the clarification of this problem.

Laboratory mice (15-25 g) were pretreated with 50 or 100 μg/kg of strophanthin G by intramuscular (im) injection. One hour later, the animals were given an intravenous (iv) dose of 1 or 15 mg/kg of adriamycin. The equivalent human adriamycin doses for these two doses based on surface area conversion factors are 0.08 and 1.25 mg/kg respectively. One currently utilized therapeutic dose of 60 mg/m^2 approximates 1.4-1.7 mg/kg. One hour after the adriamycin was given, the animals were killed and their entire hearts were removed, quickly cleansed of blood in ice-cold saline, and homogenized in 0.3 N HCl/50% ethanol for adriamycin extraction as previously described (3). Total adriamycin and metabolite fluorescence of the tissue extracts was quantified by comparison to standard adriamycin. Hearts from control animals that had received strophanthin G followed by saline injections were used for control fluorescence.

Strophanthin G pretreatment did not decrease the adriamycin accumulation by the heart in mice receiving single doses of strophanthin G (50 or 100 μg/kg) and adriamycin (table 1).

TABLE 1.—Strophanthin G pretreatment and cardiac adriamycin concentration

Expt No.	Pretreatment agent	Dose	Adriamycin treatment (mg/kg)	Cardiac adriamycin* (μg/g ± SD)
1	Saline		15, iv	17.6 ± 2.8
	Strophanthin G	50 μg/kg, im	15, iv	19.9 ± 4.1
2	Saline		15, iv	14.3 ± 3.4
	Strophanthin G	100 μg/kg, im	15, iv	15.4 ± 5.6
3	Saline		2.5 × 3, sc	6.3 ± 1.0
	Strophanthin G	10 μg/kg × 3, im	2.5 × 3, sc	9.1 ± 2.2
4	Saline		1.0, iv	1.1 ± 0.08
	Strophanthin G	100 μg/kg, im	1.0, iv	1.2 ± 0.07

*Mean values for 3-5 animals.

To simulate previous experiments more closely, mice were treated with a multiple-dose scheme (1). They received strophanthin G (10 μg/kg im) followed in 1 hour by adriamycin (2.5 mg/kg subcutaneously [sc] on each of 3 consecutive days.) Eight hours after the third treatment, the animals' hearts were analyzed. Strophanthin G treatment did not reduce the total adriamycin concentration in the heart and may have increased the antibiotic concentration (table 1). Finally, we isolated and measured adriamycin metabolites in the mice pretreated with the saline and strophanthin G (100 μg/kg) that also received adriamycin (15 mg/kg iv). The mouse hearts

[1]Received Apr 7, 1975; accepted Apr 23, 1975.

[2]Adriamycin: CAS reg. No. 23214-92-8. Supplied by Farmitalia, Milan, Italy. Strophanthin G: CAS reg. No. 630-60-4; ouabain, octahydrate. Supplied by Sigma Chemical Corp., St. Louis, Mo.

[3]Biochemistry Section, Laboratory of Pharmacology, Baltimore Cancer Research Center, Division of Cancer Treatment (DCT), National Cancer Institute (NCI), Md.

[4]NATO Scholar. Istituto di Farmacologia, Policlinico-Filliciuzza, Palermo, Italy.

[5]*Reprint requests to:* Nicholas R. Bachur, MD, Baltimore Cancer Research Center, DCT, NCI, 3100 Wyman Park Dr, Baltimore, Md 21211.

[6]Daunorubicin: NSC-82151; CAS reg. No. 23541-50-6.

were homogenized and extracted by the chloroform:methanol technique and the drug components were separated by thin-layer chromatography as previously described (4). These were quantified by comparison to adriamycin standards. No differences in adriamycin, adriamycinol, or adriamycin total aglycone concentrations were seen in strophanthin G- or saline-pretreated animals.

From these data we feel that strophanthin G pretreatment does not reduce the cardiac uptake of adriamycin in the mouse, and we strongly recommend that further experimentation be done before this treatment is considered to be of value in man. Species differences in this problem must be considered, especially in view of the apparent species specificity of toxicity. It is possible that the in vivo protective effects of strophanthin G treatment previously reported (1) may have other explanations.

In addition, we also suggest that a retrospective appraisal be done of concomitant cardiac glycoside therapy in cases of adriamycin cardiotoxicity. From those patients with cardiotoxicity it should be easy to determine how many were receiving cardiac glycoside therapy for cardiac disease when they were treated with adriamycin. These two groups could be compared for incidence of cardiotoxicity and intercurrent problems. From such a retrospective study enough data could be obtained to determine if a prospective study is merited.

REFERENCES

1. Arena E, D 'Alessandro N, Dusonchet L, et al. Influence of pharmacokinetic variations on the pharmacological properties of adriamycin. *In* International Symposium on Adriamycin (Carter SK, et al, eds). New York, Springer-Verlag, 1972, pp 96-116.
2. Fiorentino M, Grigoletto R, Fosser V, et al. Preventing cardiac toxicity from adriamycin. *In* Proceedings of the International Society of Hematology, 1974, vol 1, p 222.
3. Bachur NR, Moore AL, Bernstein JG, et al. Tissue distribution and disposition of daunomycin (NSC-82151) in mice: fluorometric and isotopic methods. Cancer Chemother Rep 54:89-94, 1970.
4. Bachur NR, Hildebrand RC, and Jaenke RS. Adriamycin and daunorubicin disposition in the rabbit. J Pharmacol Exp Ther 191:331-340, 1974.

Treatment of Malignant Melanoma With Vinblastine (NSC-49842), Procarbazine (NSC-77213), and Actinomycin D (NSC-3053)[1,2,3]

Brief Reports and Preliminary Communications

Elliott Perlin,[4] James Engeler,[4] James W. Reid,[5] Julian L. Lokey,[4] and John Kostinas[5,6,7]

Chemotherapy for patients with advanced malignant melanoma has been far from satisfactory. Treatment with 5-(3,3-dimethyl-1-triazeno)imidazole-4-carboxamide (NSC-45388) has been associated with approximately a 25% response rate (1). The addition of vincristine (2), actinomycin D (3), or BCNU (4) to NSC-45388 has not significantly improved these results.

In a review of the chemotherapy for malignant melanoma by Luce (5), it was noted from collective data that as single agents, vinblastine, actinomycin D, and procarbazine produced objective response rates of 20%, 17.5%, and 28% respectively. In a more recent review by Comis and Carter (6), respective response rates of 15%, 35%, and 16% were reported. We report here the results of a pilot study which tested the therapeutic efficacy in malignant melanoma of these three agents in combination.

PATIENTS AND METHODS

Our original study population was a group of 16 patients with advanced melanoma.

The basic treatment protocol consisted of a 28-day cycle as follows: vinblastine, 5.0 mg/m^2 intravenously (iv) on Days 1 and 8; actinomycin D, 0.5 mg/m^2 iv on Days 1 and 8; and procarbazine, 100 mg/m^2 orally on Days 1-10.

Later in the study, two patients (Nos. 9 and 10) received the same regimen every 21 days. Another patient (No. 7) received one of his courses at a 21-day interval. In a dosage exploration, two patients received one fourth to one half the dose of procarbazine early in the study. One patient (No. 1) was treated with one half the dosage of vinblastine and procarbazine and then continued to receive this lower dosage when her disease responded completely.

To be considered evaluable a patient must have had histologically proven malignant melanoma, have received at least two courses of therapy, have had measurable disease, and have not received other concomitant therapy (such as steroid compounds).

Response criteria were as follows: *complete response*—disappearance of all measurable or apparent tumor masses; *partial response*—>50% decrease in the sum of the products of the diameters of measured lesions; and *no response*—<50% decrease in the sum of the products of diameters of measured lesions or no change in the size of any lesion.

RESULTS

Of our 16 patients, 13 were evaluable and of these 13 there was one complete response and four partial responses for an overall response rate of 38%. The mean time to complete response was 4 months and the mean time to partial response was 2.2 months. It is notable that one of the partial responses was observed in a patient (No. 2) whose disease had failed to respond to a combination of NSC-45388 and BCNU as well as a combination of cyclophosphamide, methotrexate, and 5-fluorouracil. Responses were not seen in the two patients who received therapy every 21 days. A response was observed in one patient (No. 2) who received a reduced dose of procarbazine.

Responders who eventually died survived an average of 9.0 months and nonresponders 6.3 months from the start of therapy. Of nine patients receiving further therapy after failing the initial combination, none responded. Six patients received NSC-45388, two methyl-CCNU, and one BCNU.

Other pertinent data are summarized in table 1.

TOXICITY

There were no serious side effects. Most patients had mild to moderate nausea and vomiting on Days 1 and 8. One patient (No. 8) had persistent nausea and vomiting for several days; she required hospitalization and iv fluids and her dosage of actinomycin D was subsequently reduced by one half.

Hematologic toxicity was mild and well tolerated. Of 18 full-dosage 28-day courses, 11 (61%) were associated with mild leukopenia (white blood cell [wbc] count >2000 but <4000 cells/mm^3); of the latter, the median time to nadir was 14 days (range 7-21 days).

[1]Received Nov 18, 1974; revised Apr 3, 1975; accepted Apr 23, 1975.

[2]Supported in part by Bureau of Medicine and Surgery, Clinical Investigation Program, CI 2-06-348.

[3]Chemical nomenclature, NSC numbers, and CAS registry numbers for all compounds mentioned in this paper are listed in the List of Compounds at the end of the text.

[4]Internal Medicine Department, National Naval Medical Center, Bethesda, Md.

[5]Hematology/Oncology Division, Naval Hospital, Naval Regional Medical Center, Portsmouth, Va.

[6]The opinions or assertions contained in this paper are those of the authors and do not necessarily represent the views of the Department of the Navy, Bureau of Medicine and Surgery, or any other government department or agency thereof.

[7]*Reprint requests to:* Elliott Perlin, CDR MC USN, Head, Hematology/Oncology Branch, Internal Medicine Department, National Naval Medical Center, Bethesda, Md 20014.

TABLE 1.—Patients with melanoma treated with vinblastine, actinomycin D, and procarbazine

Patient No.	Age (yrs)/ sex	Disease sites	Prior chemotherapy	Responses*	No. of courses	Duration of response† (mos)	Survival‡ (mos)
1	46/F	Nodes	Yes§	CR	18	19+	Alive
2	52/M	Skin, nodes	No	PR	3	2	3.5
3	38/M	Liver, lung, nodes	Yes	PR	4	4	7.5
4	43/F	Skin, nodes	No	PR	6	6	16
5	77/M	Soft tissue, lung	No	PR	5	4+	Alive
6	60/M	Liver, lung	No	NR	5	—	7.5
7	52/M	Skin, nodes	No	NR	6	—	8
8	22/F	Nodes, lung, scalp, brain	No	NR	2	—	4
9	58/F	Liver	No	NR	3	—	Alive
10	51/M	Skin, liver, bone	No	NR	3	—	3
11	44/M	Lung, pleura	No	NR	4	—	9
12	36/M	Multiple skin	No	NR	2.5	—	Alive
13	50/M	Soft tissue, lung	No	NR	5	—	Alive

*CR = complete response; PR = partial response; NR = no response.
† + = Continuing response.
‡ From initiation of treatment.
§ Regional.

Three of the 18 courses were associated with moderate leukopenia (wbc >1500 but <2000 cells/mm^3) with the nadirs occurring on Days 14, 21, and 21 respectively. One of the latter courses was associated with a neutropenia of 450 cells/mm^3 which recovered in 14 days; no infectious complications resulted. Only three of the 18 courses were associated with mild transient thrombocytopenia (>50,000 but <100,000 cells/mm^3) occurring on Days 7, 14, and 14 respectively. Fifteen of the 18 courses were associated with a reduction in the hematocrit value. Of these 15, the mean decrease in the hematocrit reading was 4.6% (range 2%-9%); the median time to nadir was 21 days (range 8-28 days).

Of seven courses given every 21 days, three were associated with mild leukopenia, the nadirs occurring on Days 14, 21, and 21 respectively; in all seven there was a decrease in the hematocrit value (mean 3.7%, range 1%-9%); the median time to nadir was 21 days (range 8-28 days). There was no thrombocytopenia.

DISCUSSION

The results of this pilot study indicate that the combination of vinblastine, actinomycin D, and procarbazine is therapeutically active toward malignant melanoma and suggest that additional clinical investigation of this combination is warranted. Soft tissue, nodal, and lung disease responded best. While preliminary data suggest that courses given every 21 days may not be associated with prohibitive toxicity, the 28-day schedule appears to allow for more adequate bone marrow recovery and thus is currently being used for further clinical trials.

LIST OF COMPOUNDS

Actinomycin D: NSC-3053
BCNU: NSC-409962; CAS reg. No. 154-93-8; urea, 1,3-bis(2-chloroethyl)-1-nitroso-
Cyclophosphamide: NSC-26271; CAS reg. No. 6055-19-2; 2*H*-1,3,2,-oxazaphosphorine, 2-[bis(2-chloroethyl)amino]tetrahydro-, 2-oxide, monohydrate
5-Fluorouracil: NSC-19893; CAS reg. No. 51-21-8
Methotrexate: NSC-740; CAS reg. No. 59-05-2; glutamic acid, *N*-[*p*-[[(2,4-diamino-6-pteridinyl)methyl]methylamino]benzoyl]-
Methyl-CCNU: NSC-95441; CAS reg. No. 33073-59-5; urea, 1-(2-chloroethyl)-3-(4-methylcyclohexyl)-1-nitroso-
NSC-45388: CAS reg. No. 4342-03-4; DTIC
Procarbazine: NSC-77213; CAS reg. No. 491-88-3; *p*-toluamide, *N*-isopropyl-α-(2-methylhydrazino)-, monohydrochloride
Vinblastine: NSC-49842; CAS reg. No. 6449-03-2; vincaleukoblastine, sulfate (1:1), monohydrate
Vincristine: NSC-67574; CAS reg. No. 2068-78-2; leurocristine, sulfate (1:1)

REFERENCES

1. NATHANSON L, WOLTER J, HORTON J, ET AL. Characteristics of prognosis and response to an imidazole carboxamide in malignant melanoma. Clin Pharmacol Ther 12:955-962, 1971.
2. AHMANN DL, HAHN RG, and BISEL HF. A comparative study of 1-(2-chloroethyl)-3-cyclohexyl-1-nitrosourea (NSC-79037) and imidazole carboxamide (NSC-45388) with vincristine (NSC-67574) in the palliation of disseminated malignant melanoma. Cancer Res 32:2432-2434, 1972.
3. GERNER RE, MOORE GE, and DIDOLKAR MS. Chemotherapy of disseminated malignant melanoma with dimethyl triazeno imidazole carboxamide and dactinomycin. Cancer 32:756-760, 1973.
4. COSTANZA ME, NATHANSON L, LENHARD R, ET AL. Therapy of malignant melanoma with an imidazole carboxamide and bis-chloroethyl nitrosourea. Cancer 30:1457-1461, 1972.
5. LUCE JK. Chemotherapy of malignant melanoma. Cancer 30:1604-1615, 1972.
6. COMIS RL, and CARTER SK. Integration of chemotherapy into combined modality therapy of solid tumors. IV. Malignant melanoma. Cancer Treat Rev 1:285-304, 1974.

Combination Chemotherapy With CCNU (NSC-79037) and 5-[3, 3-Bis(2-chloroethyl)-1-triazeno]-imidazole-4-carboxamide (NSC-82196)[1,2,3]

Brief Reports and Preliminary Communications

Hui-Yen Chang,[4] Emil J Freireich,[4] Abdul Khaliq,[5] Lawrence Einhorn,[4,6] and Jeffrey A. Gottlieb[4,7]

CCNU, one of the new oral nitrosoureas, has been shown to cross the blood-brain barrier and has been found effective against previously untreated murine central nervous system leukemia. It has also shown activity in human neoplasms including carcinoma of the lung, malignant lymphoma, and to a lesser degree adenocarcinoma of the gastrointestinal tract (1). 5-[3,3-Bis(2-chloroethyl)-1-triazeno]imidazole-4-carboxamide (NSC-82196) is one of a variety of substituted triazeno imidazole carboxamides initially designed to produce inhibition of purine nucleoside synthesis. Their exact mechanism of action remains unknown. NSC-82196 has been found active against a number of animal tumor systems and has produced complete inhibition of murine L1210 leukemia, Walker 256 carcinosarcoma, Sarcoma 180, and Adenocarcinoma 755 (2).

Schabel et al at the Southern Research Institute, Birmingham, Alabama, have shown that the combination of CCNU and NSC-82196 is clearly synergistic against murine L1210 leukemia even when given at the LD10 of each drug (3). Based on this observation, we designed a study to determine the efficacy and toxicity of combination treatment with CCNU and NSC-82196 in patients with advanced (predominantly refractory) solid tumors, especially adenocarcinomas.

METHODS AND MATERIALS

Twenty-three patients, 12 men and 11 women ranging in age from 17 to 76 years with a median age of 52, with a variety of disseminated solid tumors were treated with a combination of CCNU and NSC-82196 from September 1972 through April 1974. All of the patients except two had been previously treated with antineoplastic chemotherapy or radiotherapy, but no patient had previously received either of the two agents (or their congeners) used in this study.

Drug Regimen

CCNU was supplied in 10-, 40-, and 100-mg capsules which were kept refrigerated in amber bottles until administration, at which time the capsules were given orally to patients with an empty stomach. NSC-82196 was supplied in vials containing 300 or 1000 mg of drug which was first dissolved in 0.01 N hydrochloric acid (provided as a special diluent by the NCI) and then further diluted in 100-250 cc of 5% dextrose and water and administered as a rapid intravenous (iv) infusion over 15-30 minutes. The initial starting dose for CCNU was 65 mg/m^2 on Day 1 (which is approximately 50% of the usual dose when the drug is given alone [1]). For NSC-82196, the dose was 450 mg/m^2/day iv for 5 days also starting on Day 1 (again, approximately 50% of the single drug dose [4]); both drugs were repeated every 6 weeks.

After initial observations had indicated that this dose was well tolerated with minimal myelosuppression, the subsequent doses of both drugs were escalated by approximately 25%. For patients who experienced adequate myelosuppression during a course, no escalation was used for subsequent courses. Patients with severe myelosuppression (lowest absolute granulocyte count <500 cells/mm^3 and/or platelet count <50,000 platelets/mm^3) had the dose of both drugs reduced by 25%. If a patient's blood cell and platelet counts had not returned to normal at the end of 6 weeks, additional time off therapy was allowed for recovery. The number of patients treated at each dose level is indicated in table 1. Patients had weekly complete blood and platelet counts taken which were repeated more frequently if necessary. Tests of hepatic and renal function were performed at 1 – 2-week intervals and before each treatment cycle. Tumor response was assessed by serial physical examinations and roentgenographic studies, if appropriate. A partial response indicated a greater than 50% decrease in the sum of the area of all measurable lesions. A patient's disease was considered stable if there was no change in tumor size for at least one complete 6-week cycle.

[1]Received Jan 25, 1975; revised Apr 7, 1975; accepted Apr 23, 1975.

[2]Supported in part by Public Health Service grants CA-10379, CA-14528, CA-11520, and CA-05831 from the National Cancer Institute (NCI), National Institutes of Health, Department of Health, Education, and Welfare.

[3]CCNU: CAS reg. No. 13010-47-4; urea, 1-(2-chloroethyl)-3-cyclohexyl-1-nitroso-.

NSC-82196: CAS reg. No. 5034-77-5; BIC.

Both drugs were supplied by Cancer Therapy Evaluation, Division of Cancer Treatment, NCI.

[4]Department of Developmental Therapeutics, The University of Texas System Cancer Center, M. D. Anderson Hospital and Tumor Institute, Houston.

[5]W. W. Cross Cancer Institute, Edmonton, Alberta, Canada.

[6]*Present address:* Indiana University School of Medicine, Indianapolis.

[7]*Reprint requests to:* Jeffrey A. Gottlieb, MD, Head, Section of Chemotherapy, Department of Developmental Therapeutics, University of Texas System Cancer Center, M.D. Anderson Hospital and Tumor Institute, Houston, Tex 77025.

TABLE 1.—Doses of NSC-82196 and CCNU administered

No. of patients	No. of courses	Drug	
		NSC-82196 (mg/m²/day × 5)	CCNU (mg/m²/day ×1)
2	7	300	50
11	13	450	65
15	20	560	80
7	9	670	100

RESULTS

Twenty-three patients received the combination of CCNU and NSC-82196. Two patients with adenocarcinoma of the colon and stomach, respectively, were considered inevaluable due to death from rapidly advancing disease within 2 weeks of therapy. Of the 21 evaluable patients, nine patients had stabilization of previously progressive disease, but no partial responses were observed. Stabilization occurred in four of ten patients with adenocarcinoma of the colon, in three of six patients with renal cell carcinoma, in one patient with adenocarcinoma of the stomach, and in one patient with neurofibrosarcoma. The median duration of stable disease was 3.5 months (range 2-8 months). The remaining 12 patients (including one patient with an adenocarcinoma from an unknown primary, one with an osteogenic sarcoma, and one with a mixed salivary gland tumor) who progressed despite treatment all died with disseminated tumor within 6 months from the initiation of therapy. By comparison, seven of the nine patients who were stabilized were still alive at 6 months. Because of the advanced state of their disease, most of the patients received only one to two courses of this combination regimen except for one patient with renal cell carcinoma who received six courses of treatment. This patient's lung lesions were held in check for 1 year, having been advancing rapidly before starting treatment with NSC-82196 and CCNU, but no shrinkage was observed in any of her metastases.

Toxicity

Myelosuppression, particularly granulocytopenia, was the most consistent dose-related side effect of this combination. The hematologic toxic effects observed in 19 patients (two of the 21 evaluable patients had inadequate data) are summarized in table 2. Thrombocytopenia was not severe. All patients recovered from their thrombocytopenia within a 2-week period; recovery from the dose-limiting granulocytopenia was also prompt. No patient had an infection associated with granulocytopenia or hemorrhage associated with thrombocytopenia. A starting dose of 80 mg/m² of CCNU on Day 1 with 560 mg/m²/day of NSC-82196 on Days 1-5 seemed the most tolerable with regard to granulocytopenia. Nausea and vomiting, which were often severe with higher doses, were observed in 15 of the 23 patients (particularly on the first day when both drugs were given) and caused two patients to withdraw from the program. No renal or hepatic abnormality could be ascribed to this combination regimen.

DISCUSSION

Using CCNU alone at its maximum tolerable dose, the Southwest Oncology Group (Hoogstraten et al) reported five improvements or stabilization of disease in 16 patients with adenocarcinoma of the colon but no responses were seen in their six patients with renal cell carcinoma (5). Mittelman et al observed four regressions in 20 evaluable patients with renal cell carcinoma receiving CCNU alone (6). Using oral and parenteral NSC-82196, response has been noted in lymphoma (4,7) and melanoma (8). Moertel et al, using NSC-82196 at a dosage of 900-1200 mg/m²/day for 5 days in the treatment of 31 patients with advanced gastrointestinal cancer, did not see any evidence of improvement (9).

Although we did not observe any major response in our treated patients, nine patients did have stabilization of previously progressive disease and possibly, as a result, had a modest prolongation in their survival. This combination was well-tolerated with reasonable safety from a hematologic standpoint. The synergism noted in the rapidly progressive murine leukemia L1210 tumor system was not seen in this study. Nevertheless, it would seem reasonable to conclude that this combination may offer some palliation in the treatment of the refractory advanced malignant diseases recorded herein. It is also possible that other schedules of these agents used in less advanced patients with rapidly dividing tumors (and thus more analogous to the animal tumor model) might be more effective.

REFERENCES

1. HANSEN HH, SELAWRY OS, MUGGIA FM, ET AL. Clinical studies with 1-(2-chloroethyl)-3-cyclohexyl-1-nitrosourea (NSC-79037). Cancer Res 31:223-227, 1971.
2. SHEALY YF, and KRAUTH CA. Complete inhibition of mouse leukaemia L1210 by 5 (or 4)-[3,3-bis(2-chloroethyl)-1-triazeno]imidazole-4(or 5)-carboxamide (NSC-82196). Nature 210: 208-209, 1966.
3. SCHABEL FM, JR, WHEELER GP, LASTER WR, JR, ET AL. Therapeutic potentiation of CCNU by BIC against leukemia L1210. Proc Am Assoc Cancer Res 14:24, 1973.
4. BAGLEY CM, JR, CANELLOS GP, YOUNG RC, ET AL. Clinical trials with 5-[3,3-bis(2-chloroethyl)-1-triazeno]imidazole-4-carboxamide (NSC-82196) given intravenously. Cancer Chemother Rep 56:387-391, 1972.
5. HOOGSTRATEN B, GOTTLIEB JA, CAOILI E, ET AL. CCNU (1-(2-chloroethyl)-3-cyclohexyl-1-nitrosourea, NSC-79037) in the treatment of cancer. Phase II study. Cancer 32:38-43, 1973.
6. MITTELMAN A, ALBERT DJ, and MURPHY GP. Lomustine treatment of metastatic renal cell carcinoma. JAMA 225:32-35, 1973.
7. VOGEL CL, DEVITA VT, DENHAM C, ET AL. Preliminary clinical trials and clinical pharmacologic studies with 5-[3,3-bis(2-chloroethyl)-1-triazeno]imidazole-4-carboxamide (NSC-82196) given orally. Cancer Chemother Rep 55:159-165, 1971.
8. FALKSON G, VAN DER MERWE AM, and FALKSON HC. Clinical experience with 5-[3,3-bis(2-chloroethyl)-1-triazeno]imidazole-4-carboxamide (NSC-82196) in the treatment of metastatic malignant melanoma. Cancer Chemother Rep 56:671-677, 1972.
9. MOERTEL CG, SCHUTT AJ, REITEMEIER RJ, ET AL. Phase II study of 5-[3,3-bis(2-chloroethyl)-1-triazeno]imidazole-4-carboxamide (NSC-82196) in advanced gastrointestinal cancer. Cancer Chemother Rep 56:267-269, 1972.

TABLE 2.—Myelosuppression observed with combination CCNU and NSC-82196

Drug		Platelet count*				Wbc count*				
				Day of—			Leukopenia nadir ($\times 10^3$ cells/mm^3)		Day of—	
CCNU (mg/m^2/day × 1)	NSC-82196 (mg/m^2/day × 5)	Day of first observation of <100,000 platelets/mm^3	Thrombocytopenia nadir ($\times 10^3$ platelets/mm^3)	Nadir	Recovery to >100,000	Day of first observation of <4000 cells/mm^3	Wbc	Granulocytes	Nadir	Recovery to >4000
50	300	34 (29-38)	87 (85-120)	38 (26-42)	44 (43-45)	46.5 (46-47)	3.4 (3.0-4.3)	2.3 (1.7-2.8)	50 (44-52)	55 (46-64)
65	450	23 (6-34)	89 (12-29)	30 (9-48)	34 (12-56)	31 (5-47)	3.2 (1.4-5.9)	1.5 (0.9-3.2)	37 (18-53)	41 (29-67)
80	560	22 (12-36)	66 (19-255)	28 (5-41)	36 (25-42)	15 (5-33)	3.3 (0.7-8.8)	1.7 (0.1-4.2)	22.5 (7-45)	33 (22-57)
100	670	21 (10-31)	88 (32-230)	27 (17-37)	35 (28-40)	22 (20-24)	3.3 (2.4-7.3)	1.0 (0.3-1.6)	27 (19-48)	41 (24-59)

*All values are medians with ranges in parentheses.

Proceedings of the 17th National Meeting of the APhA Academy of Pharmaceutical Sciences

Pharmacokinetic Modeling of Anticancer Drugs

New Orleans, Louisiana
November 10-14, 1974

Contents

Opening Remarks
Ti Li Loo

Some Fundamental Considerations of the Applications of Pharmacokinetics to Cancer Chemotherapy
Kenneth B. Bischoff

Pharmacokinetic Considerations on Resistance to Anticancer Drugs
Robert L. Dedrick, Daniel S. Zaharko, Richard A. Bender, W. Archie Bleyer, and Robert J. Lutz

Cytokinetic Aspects of Clinical Drug Resistance
Richard A. Bender and Robert L. Dedrick

Kinetic Model for the Disposition and Metabolism of Moderate and High-Dose Methotrexate (NSC-740) in Man
Paulo R. Leme, Patrick J. Creaven, Larry M. Allen, and Mones Berman

Preliminary Pharmacokinetic Model for Adriamycin (NSC-123127)
Phillip A. Harris and Joseph F. Gross

Mathematic Models for Cancer Chemotherapy: Pharmacokinetic and Cell Kinetic Considerations
Shui-Nan Chuang

Stochastic Compartmental Modeling of the Disposition of 5-(3,3-Dimethyl-1-triazeno)imidazole-4-carboxamide (NSC-45388)
Bayliss McInnis, Asha Kapadia, Souhail El-Asfouri, and Ti Li Loo

Analysis of the Effects of Antitumor Drugs on Cell Cycle Kinetics
Kwang B. Woo, Larry B. Brenkus, and Karl M. Wiig

Disposition of Cytosine Arabinoside (NSC-63878) and Its Metabolites: A Pharmacokinetic Simulation
P. F. Morrison, T. L. Lincoln, and J. Aroesty

Human Pharmacokinetic Model for Isophosphamide (NSC-109724)
Larry M. Allen and Patrick J. Creaven

Opening Remarks

Biochemically and pharmacologically, normal and malignant cells are qualitatively similar, and there are few differences that can be exploited to the advantage of the cancer chemotherapist. Although tumors responsive to current anticancer drugs generally have a short doubling time and a large growth fraction, these features are not unique to neoplastic cells but are shared with many cells of normal tissues. As a result, this lack of selectivity imposes a serious limitation on cancer chemotherapy. However, by the judicious manipulation of drug dose, route, and schedule of administration, it is possible to achieve an effective drug level in the target tumor cell and maintain it sufficiently long for the drug to exert its maximal lethality on the malignant cell at the least risk to the normal cell. To this end, knowledge of the pharmacokinetics of anticancer drugs as well as the cytokinetics of normal and tumor cells is essential. Since in pharmacologic experiments the plasma is usually the only body compartment in which drug concentrations can be assayed with certainty, great efforts must be made to develop pharmacokinetic models that reliably estimate drug levels in other compartments, particularly the tumor.

Even though it was only recently that Bischoff, Dedrick, and Zaharko described for the first time an elegant pharmacokinetic model for the important antitumor agent methotrexate, considerable progress has since been made in this critical field to warrant the present symposium.

It is singularly appropriate that the first presentation in this proceedings is by Dr. Kenneth Bischoff, who has pioneered in the field of pharmacokinetic modeling of anticancer drugs. The succeeding papers deal with recent advances in aspects of pharmacokinetic modeling of antitumor agents that are of particular interest to the chemotherapist. These include the extension of the Bischoff-Dedrick model to new agents like adriamycin and isophosphamide. The Bischoff-Dedrick model works well with methotrexate because the pharmacologic disposition and metabolism of this agent have been previously thoroughly investigated and the results are well documented. Further, when administered intravenously at conventional dosages, methotrexate is not metabolized in man. However, in view of the fact that the patterns of metabolism and disposition of anticancer drugs are as varied as their chemical structures, the straightforward application of the Bischoff-Dedrick model to other drugs would be difficult unless they closely resemble methotrexate pharmacokinetically. Since this usually is not the case, the solution of this problem severely taxes the imagination and ingenuity of the investigator.

A second area in which a noticeable beginning has been made concerns the incorporation of cytokinetic parameters in pharmacokinetic modeling. From a chemotherapeutic point of view cytokinetic dissimilarities between normal and malignant cells should be exploitable therapeutically. The dosing and scheduling of an anticancer agent must be strategically timed in relation to the phases of the cell cycle so as to deliver an effective dose of the agent to the target cancer cells when the majority of them are most susceptible to cytotoxic action. At the same time considerations must be made of the cytokinetics of the sensitive normal cells in order to expose them to the least risk. The realization of these goals depends heavily upon the potential contributions of pharmacokineticists well versed in comparative cytokinetics.

Finally, random biologic variations and uncertainties inherent in pharmacologic experimentation suggest that stochastic models should be preferable to deterministic models in which scatter is not considered. This approach permits the probabilistic prediction of drug levels in peripheral compartments, especially the tumor cell. At the present time, stochastic compartmental analysis has not been extensively applied to the pharmacokinetics of anticancer drugs; nevertheless, a worthy beginning has already been made.

We thank the American Pharmaceutical Association Academy of Pharmaceutical Sciences and the Program Committee of the Pharmacology and Toxicology Section of the same Academy for sponsoring this symposium. We also gratefully acknowledge financial support from the Division of Cancer Treatment, National Cancer Institute, National Institutes of Health (grant CA-17440).

Ti Li Loo

Section of Pharmacology
Department of Developmental Therapeutics
University of Texas System Cancer Center
Houston, Texas

Some Fundamental Considerations of the Applications of Pharmacokinetics to Cancer Chemotherapy

Kenneth B. Bischoff[1,2]

SUMMARY

The purpose of this paper is to document the procedures needed to construct pharmacokinetic models based on physiologic, physicochemical, and pharmacologic principles. Extensive descriptions of the basic ideas are provided, along with the corresponding equations. The notions of scaling between various animal species will be described and examples will be given. The important factors determining the choice and number of compartments are based on the properties of the drug and the desired purposes of the pharmacokinetic model. The important concept of flow-limiting conditions with regard to local uptake will be described. The quantitative description of plasma and tissue binding is discussed, along with the notion of effective protein concentrations for the latter. Using these basic ideas, the fundamental mass balances describing the flow, diffusion, and reactions of the drug are presented. An example of the prediction of the pharmacokinetics of a strongly bound drug is used as an illustration of the methods, and this example also indicates the types of useful simplifications that can be made. The special, but important, case of linear binding is next derived, and an example involving the drug methotrexate will illustrate the principles involved. Finally, cytosine arabinoside will be used to indicate methods that can be used for rapidly metabolized drugs. Since existing examples are primarily utilized, this paper brings together a comprehensive collection of the several sets of physiologic data and modeling techhiques that have been used for the past several years. It is hoped that this documentation will provide a useful basis for those wishing to use this approach to pharmacokinetics.

[Cancer Chemother Rep 59:777-793, 1975]

Pharmacokinetic models are used to permit rational prediction, as much as possible, of the events occurring during the processes of drug disposition throughout the body. As we will see, it appears feasible to do this with certain parts of the overall problem, although other aspects are more elusive.

There are several specific reasons for pursuing this approach. One is the scientific intellectual satisfaction of having quantitative predictive models based on underlying knowledge, rather than the more empirical, curve-fitting approaches often used. The latter are always needed to some extent, of course, but should hopefully be minimized. Another important purpose is to aid in the constant problems of interpreting animal experiments in drug screening, dosage regimen formulation, and similar matters. In quantitative terms this can be called "scaling" the results from one species to another, and ultimately to man (1,2). It would seem clear that having pharmacokinetic models specifically incorporating known animal physiology and pharmacology would be of benefit in these endeavors. Yet another use of quantitative predictive models is in the development of optimal dosage regimens for clinical applications.

This paper is primarily intended to document our work, which, as usual, is in several scattered publications. It is hoped that other investigators will find it useful to have these ideas, methods, formulations, and basic data gathered in one place. In addition to using these by-and-large published results, estimates of the current state-of-the-art will be given as well as some thoughts for further extensions, especially for applications in cancer chemotherapy.

CHOICE OF COMPARTMENTS

The natural basis for the choice of compartments is the anatomy and physiology of the body, from the cellular level to the whole body. It is clear that the main question is how much detail need be used in order to provide an adequate description of the events. Even though consideration of these events in individual cells throughout the whole body is not feasible, special collections of cells (eg, tumors) may have to be modeled in this much detail. However, the main features of drug distribution can often be described with models having surprisingly little detail

[1]School of Chemical Engineering, Cornell University, Ithaca, NY.

[2]*Reprint requests to:* Dr. Kenneth B. Bischoff, School of Chemical Engineering, Cornell University, Ithaca, NY 14850.

(this seems to be a case where "nature is kind to us" in our scientific work).[3] Thus, certain parts of the body can be lumped together (eg, an organ) and described by "a" (one) concentration level. We will often term these parts "body regions," with a definite anatomic/physiologic basis, in order to avoid confusion with the term "compartment," which is often used in a more abstract sense.

This still does not resolve the question of exactly how many body regions, or compartments, are needed. In fact, there is no simple way to decide this, since judgment is required as to the important aspects of the drug distribution events. We base the initial choice(s) upon whatever is known about the physicochemical (binding, lipid solubility, ionization) and pharmacologic (mechanisms of transport, site[s] of action) properties of the drug. For example, if the drug is not lipid soluble, the details of the adipose tissues of the body are not particularly important.

The third basis for the initial determination of the number of required body regions is the speed or the time scale of events. Perhaps the simplest example of this is to consider the necessity of including the finite time of passage around the circulatory system (in man this is about 1 minute). Thus, if one is attempting to describe tracer concentrations in an indicator-dilution experiment, the observations of interest are obviously occurring with a time scale the same as the mean circulation time, and the details of the transit times in the arteries and veins must be accounted for. (It should be mentioned here that if only an overall property [such as total cardiac output] of the tracer concentration curves is of interest, then the detail may not be required.) Pharmacokinetic models containing this amount of "anatomic geography" are rather complicated, as will be discussed in more detail below, and they should not be considered unless they are truly required.

The time scale of interesting events for most drugs is usually many minutes, hours, days, or even longer. After an hour, about sixty circulations have elapsed, and this is more than adequate to have "mixed" the drug such that the blood in the circulatory system has an essentially uniform concentration of drug. For a bolus injection, in fact, this is a good approximation after about three transit times. Thus, most pharmacokinetic models for drugs ignore the very early time events and lump the entire circulatory system into one "blood pool." If the local (physiologic) behavior *is* of interest, this approximation is probably not suitable. Also, to model very fast-acting drugs, such as anesthetic agents, more detailed pharmacokinetic models than those normally used may be required. However, for most of our discussion, only relatively long time scales will be considered. A pioneering (1937) consideration of these questions, that still provides unique insights, was by Teorell (3).

[3]De Rocco AG. Personal communication, 1973.

If one carries this lumping to the extreme, the entire body can be assumed to have uniform (water) concentrations of the drug, with no detailed distinction between body regions. We will see later what is actually being assumed here, but pharmacologists know from experience that this approach often leads to reasonably accurate descriptions of the drug distribution. From the above discussion, one can reason that it is likely to be most useful for a drug that is rather slow acting, is primarily water soluble, has no complicated transport mechanisms, etc. Empirical evidence of this is that a plot of log concentration versus time gives a single straight line for a bolus injection. The mathematical equations resulting from this simple model are easy to manipulate and are the basis for most of the current detailed calculations of optimal dosage regimens by, for example Krüger-Thiemer (4). An example of drugs that seem to reasonably satisfy the above requirements are the sulfa-compounds, as described by Krüger-Thiemer (5).

However, it is probably more common to find that a semilog plot of blood (or plasma) concentration versus time has two rather pronounced phases with different slopes. The first, or earliest time phase (sometimes denoted by α) is dominated by the distribution of drug between the central and peripheral parts of the body, and the second phase (or β) is dominated by the ultimate drug removal process(es). Riegelman and co-workers (6,7) have extensively explored the use of this two-compartment model for many specific drugs, and they have discussed the proper evaluation of the various model parameters. A detailed analysis of this model was given by Bischoff and Dedrick (8), and Wagner (9) provides a compendium of the detailed mathematical features of a collection of these and similar models.

Even though the biphasic model can often give a reasonable fit to pharmacokinetic data, the specific interpretation of the model parameters, such as "central compartment," is often ambiguous. Thus, one of our original goals of having a predictive model incorporating physiologic and pharmacologic data may not be entirely met by this approach. It should be emphasized, though, that for semi-empirical projections of clinical data, these models are often most convenient. For our purposes, however, we still wish to construct the pharmacokinetic models from (close to) first principles.

The above matters are the most intellectually difficult on the theoretical side, since no one set of specific rules can enable us to automatically choose the appropriate compartments. The writing of the mathematical equations, and their use with experimental data, is more straightforward, although the actual doing of this may be equally difficult and certainly more time-consuming. I will now outline the modeling details in order to illustrate the concepts in a concrete manner. I will often refer to, or imply, the above general discussion in constructing the models, and hopefully thereby clarify the philosophy of the approach.

Let us first consider a body region consisting of cells randomly distributed in the interstitial fluid and supplied by a "typical" capillary, as shown in figure 1. Even this may not be truly applicable to organs with a specific structure, such as the liver, but more appropriate models have not yet been developed. Mass balances for the drug in each of the three components could be written, including three-dimensional diffusion, any flows of the fluids, membrane transport, etc, but we normally have nowhere near the amount of information to justify this. Therefore, some approximate form of these balances is used for a capillary, and these are then combined according to the architecture of the capillary bed, eg, the "Krogh cylinder" (*see* ref 10 for a recent review of many of these approaches and a rather complete citation of the literature.

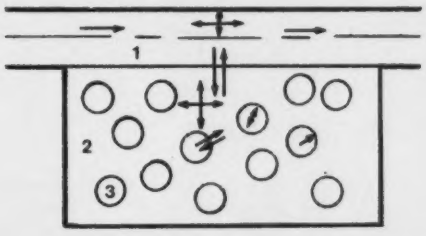

FIGURE 1.—Schematic diagram of tissue region. 1 = Blood (capillary); 2 = interstitial; 3 = cells. The arrows signify various flow, diffusion, and transport steps. [*From* ref 33.]

For drug pharmacokinetic models, this model of a body region is even further lumped as shown in figure 2a. If the region contains more than one type of cell, the sketch in figure 2b might be more appropriate. Often, an even more pragmatic lumping, based on what is normally done in an experimental biopsy, is used (fig 3). Examples of the use of these conceptual diagrams will be given below.

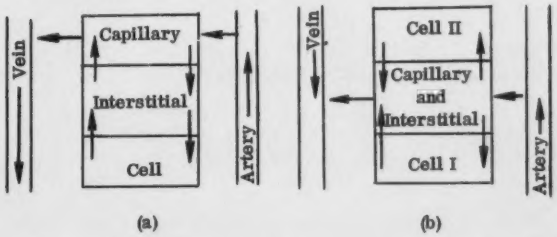

FIGURE 2.—Models for local tissue regions. [*From* ref 12.]

Let us for the moment ignore several complications such as binding, complicated transport steps, etc, ie, a water-soluble drug. We can then focus on the physiologic or anatomic basis for the mass balances appropriate to figure 2a. If intracapillary diffusion is ignored, but the interstitial and cellular regions are each considered spatially homogeneous

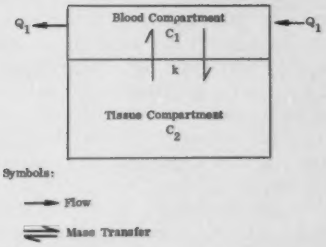

FIGURE 3.—Body region containing blood and tissue compartments. [*From* ref 17.]

in composition, relatively simple mass balances result. These are probably reasonable approximations for drug transport, but not for such solutes as oxygen where the transverse tissue gradients can be important (this might also be true for certain tumors).

The actual mass balances are as follows:

capillary

$$\frac{\partial C_B}{\partial t} + \frac{1Q}{V_B}\frac{\partial C_B}{\partial z} = \frac{P_b A_b}{V_B}(C_I - C_B) \qquad (2.1)$$

interstitial

$$\frac{dC_I}{dt} = \frac{P_b A_b}{V_I} \cdot \frac{1}{l}\int_0^l (C_B(z,t) - C_I(t))dz + \frac{P_c A_c}{V_I}(C_c - C_I) \qquad (2.2)$$

cellular

$$\frac{dC_c}{dt} = \frac{P_c A_c}{V_c}(C_I - C_c) + r(C_c) \qquad (2.3)$$

The third of these is perhaps the most familiar, since it is the usual form of a lumped mass balance, with a term to represent any biochemical reactions occurring in the cells. Normally the product of the permeability and transfer area is left combined, since it is difficult to measure each separately. In fact, the quantity usually actually measured is the complete coefficient of the concentration driving force: permeability × area/volume. The first balance not only contains the time change of blood concentration, but also a term representing concentration gradients along the capillary. The interstitial fluid balance looks complicated because the capillary membrane term must be averaged over the length of the region.

These types of balances were formulated by Bellman, Kalaba, and Jacquez (11), but the mathematical solution of them is rather formidable even if done numerically. Therefore, Bellman et al and Bischoff and Brown (12) made the approximation that the continuous capillary gradients can be represented by a few compartments-in-series (*see* eg, ref 13).

These modified balances can be written for the various body regions around a mammalian circulatory system. As a brief example of a model appropriate for a fast-acting tracer, figure 4 shows an anatomically detailed set of body regions, for each of which the above balances are used. The large set of differential equations is actually simple to solve numerically with a computer, and figure 5 illustrates the type of concentration waves that would move down the circulatory system after a sharp bolus injection. To test the time of mixing no clearance of the tracer was allowed, so that it would ultimately have a unit concentration everywhere. With typical human values for the model parameters, it is seen that the waves are dissipated within a few minutes, as was qualitatively reasoned earlier. Also note the rather large overshoot during the first pass of the drug. The implications of this for toxic drugs aren't clear, but such models could be of use in investigating proper injection techniques, which some investigators are beginning to consider in a quantitative way.

I will not consider these anatomically complicated models for tracers any further here, but instead will turn to the more common cases of relatively slowly acting drugs which can be modeled with far fewer compartments. However, other aspects of the processes important in drug distribution must also first be quantitatively discussed.

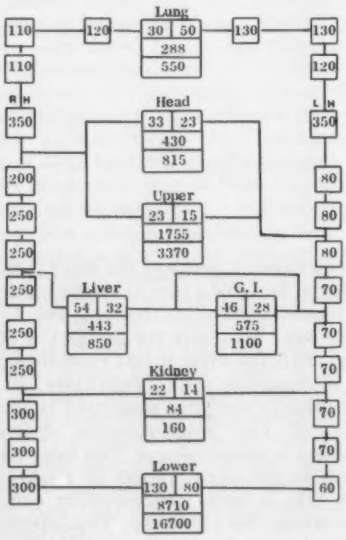

FIGURE 4.—Mammalian flow diagram; volumes given in ml. [*From* ref 12.]

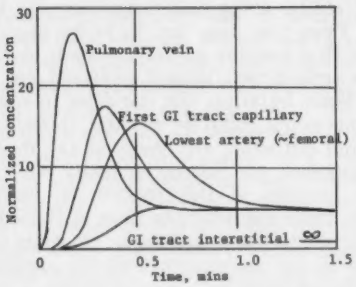

FIGURE 5.—Drug transport. [*From* ref 12.]

DRUG-PROTEIN BINDING

Only the basic ideas of this area will be presented here, for completeness, since whole treatises are available on the subject. Certain aspects, such as tissue binding, are rather interconnected with the pharmacokinetic models, and these will be deferred until later.

Most basic pharmacology books discuss the concept of binding according to the fundamental law of mass action (15, 16), both for nonspecific binding and for interactions with specific sites of action. For a drug molecule, A, and a vacant site, 1,

$$A + 1 \rightleftharpoons A1 \tag{3.1}$$

where A1 is the bound moiety. The equilibrium *association* constant for this reaction is

$$K_A = C_{A1}/C_A C_1 \tag{3.2}$$

Thus, if the total number of available uniform binding sites is C_t,

$$C_t = C_1 + C_{A1} = C_1 (1 + K_A C_A) \tag{3.3}$$

and

$$C_{A1} = K_A C_A C_1 = \frac{C_t K_A C_A}{1 + K_A C_A} \tag{3.4}$$

This expression is usually called a Langmuir isotherm in physical chemistry, and often provides an adequate representation of binding and/or adsorption phenomena. Not all data can be handled this way, and sometimes the Freundlich isotherm provides a better fit:

$$C_{Al} = AC_A^m \tag{3.5}$$

This can be derived from the Langmuir isotherm by using a certain distribution of non-uniform sites, but it is often just used empirically.

The Langmuir isotherm is usually most convenient mathematically, and is sometimes written in terms of the dissociation constant $\equiv 1/K_A$. However, we believe the original formulation is often preferable, especially since it can be extended in a rational way to multiple solutes binding on the same sites:

$$A + l \rightleftharpoons Al \qquad K_A = C_{Al}/C_A C_l \tag{3.6}$$

$$B + l \rightleftharpoons Bl \qquad K_B = C_{Bl}/C_B C_l \tag{3.7}$$

$$C_t = C_l + C_{Al} + C_{Bl} = C_l(1 + K_A C_A + K_B C_B) \tag{3.8}$$

and

$$C_{jl} = \frac{C_t K_j C_j}{1 + K_A C_A + K_B C_B} \tag{3.9}$$

Expressions such as equation (3.9) might be useful in describing drug interactions caused by competitive binding displacement, although this degree of sophistication remains for the future.

Finally, it is often found that more than one type of discrete site is important in the binding, and this is usually handled by simply adding Langmuir isotherms for each type of site:

$$C_{Al} = \sum_l \frac{C_t^{(l)} K_A^{(l)} C_A}{1 + K_A^{(l)} C_A} \tag{3.10}$$

Extensions to solute interactions and other complications are possible for small molecule binding to specific proteins, but this would bring us too far afield from the major purpose; books on biophysical chemistry should be consulted. The results developed above will be adequate for our purposes.

BASIC MASS BALANCES

All of the above discussions and developments will now be incorporated into mass balance equations of various degrees of completeness that can be used in actual pharmacokinetic models. Only the fully lumped models for body regions will be considered, but the physicochemical complications will now be retained. A complete set of anatomically and physicochemically complicated mass balances could be formulated, but these are probably much too involved for any practical use at this time.

The balances will explicitly account for free unionized, ionized, and bound forms of the drug, assuming that both of the latter are in instantaneous dynamic equilibrium with the free concentration. This seems to be a reasonable approximation right from the start, since the ionization and binding processes are normally very rapid. Sketches of the types of overall models that the balances would apply to are seen in figures 6 or 7.

Mass Balance: Blood Pool

$$\underbrace{w_B V_B \frac{dC_B}{dt}}_{\text{unbound drug}} + \underbrace{w_B V_B \frac{dC_B^*}{dt}}_{\text{ionized drug}} + \underbrace{p_B V_B \frac{dx_B}{dt}}_{\text{bound drug}} =$$

$$= -Q_B(w_B C_B + w_B C_B^* + p_B x_B)$$

$$+ \sum_l Q_l(w_{Bl} C_{Bl} + w_{Bl} C_{Bl}^* + p_{Bl} x_{Bl})$$

$$+ (\text{Injections}) \tag{4.1}$$

Each of the terms in equation (4.1) should be clear. In order to use the balance, the relationships between ionized and free drug concentrations, C^* (C, pH, $\cdots$), must be known from the ionization equilibrium constant, and likewise the bound drug concentration, x (C, $\cdots$), from equation (3.10) with $x \equiv C_{Al}$. Equation (4.1)is valid for whole blood for a solute that instantaneously equilibrates with erythrocytes or for plasma when the solute is excluded from the erythrocytes. Cases with an intermediate degree of cell uptake are usually handled semi-empirically.

The tissue regions will be described as in the section on Choice of Compartments. Only two of the three subregion balances will be written, although the third could be easily added. The trans-membrane transport will be written as simple passive diffusion of the *free drug*; again, more complicated expressions could be added for specific cases.

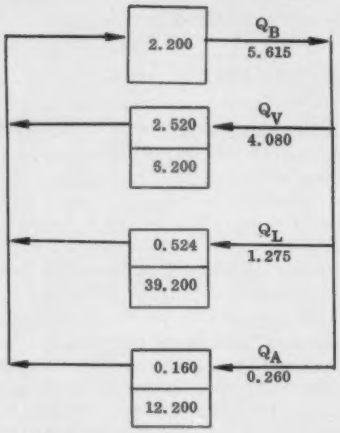

FIGURE 6.—Body regions and flows. B = blood pool not in equilibrium with tissues; V = viscera; L = lean tissue; A = adipose tissue. [*From* ref 21.]

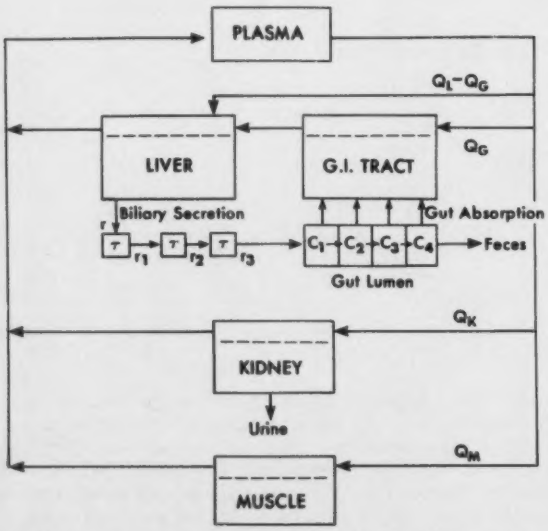

FIGURE 7.—Compartmental model for methotrexate distribution. [From ref 31. Reproduced with permission of the copyright owner.]

Mass Balance: Tissue Region

Equilibrium blood

$$w_{Bl}V_{Bl}\frac{dC_{Bl}}{dt} + w_{Bl}V_{Bl}\frac{dC_{Bl}^{*}}{dt} + p_{Bl}V_{Bl}\frac{dx_{Bl}}{dt} =$$

$$= Q_i\,(w_B C_B + w_B C_B^{*} + p_B x_B - w_{Bl}C_{Bl} - w_{Bl}C_{Bl}^{*} - p_{Bl}x_{Bl}) \qquad (4.2)$$

$$+ \underbrace{k_i(C_{Ti} - C_{Bl})}_{\text{Membrane transfer of free drug}}$$

Tissue

$$w_{Ti}V_{Ti}\frac{dC_{Ti}}{dt} + w_{Ti}V_{Ti}\frac{dC_{Ti}^{*}}{dt} + p_{Ti}V_{Ti}\frac{dx_{Ti}}{dt} =$$

$$= k_i\,(C_{Bl} - C_{Ti})$$

$$+ \underbrace{r_i\,(C_{Ti};\, C_{Ti}^{*};\, x_{Ti})}_{\text{Removal by secretion, metabolism, etc}} \qquad (4.3)$$

The rate, r_i, in equation (4.3) could be a function of only the free concentration, or sometimes the bound concentration also plays a role, eg, hepatic secretion.

The combination of equation (4.1) and equations (4.2) and (4.3) for each of the appropriate body regions, together with equation (3.10) and the ionization equilibrium, would permit solving for all of the various concentration levels. In order to actually do this, of course, numerical values of all the parameters must also be known. As we will see shortly, rather good estimates are possible for the various organ volumes and flows, and plasma protein binding can be measured in in vitro experiments as can ionization. The most difficult to obtain are tissue binding and the specific membrane permeabilities. An approximate method for the former will be described, but the latter just have to be measured and not very much information is yet available.

SIMPLIFICATIONS OF MASS BALANCES

In order to get around this last problem of membrane permeabilities, the concept of *flow-limited conditions* is most often introduced. Physically, this means that the membrane permeability is so large that any molecules that flow into the region have an easy time moving throughout the space. Thus, the part of the process that determines the drug concentration level is how much drug was able to flow in from the blood pool. A corollary is that the free concentration is essentially identical throughout the region, since this is the driving force for mass transfer across the membrane.

Mathematically, a very large permeability in equations (4.2) and (4.3) is $k_i \longrightarrow \infty$, and $C_i = C_{Bi} = C_{Ti}$ (equal free concentrations). Adding equations (4.2) and (4.3)then eliminates the mass transfer term, and the result is:

$$(w_{Bl}V_{Bl} + w_{Ti}V_{Ti})\frac{dC_i}{dt} + p_{Bl}V_{Bl}\frac{dx_{Bl}}{dt} + p_{Ti}V_{Ti}\frac{dx_{Ti}}{dt} =$$

$$= Q_i\,(w_B C_B + p_B x_B - w_{Bl}C_i - p_{Bl}x_{Bl}) + r_i(C_i) \qquad (5.1)$$

(The ionized moiety terms have been dropped for simplicity.) Thus, one equation results, but, more

importantly, the exact value of k_i need not be known, just that it is very large.

Some reflection indicates that we still don't know how large k_i must be in order to assume the very convenient flow-limiting conditions. One way would be to compare the solutions of the full equations (4.2) and (4.3) with that of equation (5.1) and see when there is a negligible difference. This was done by Dedrick and Bischoff (17) for a simple water-soluble drug with no binding; the result was that the difference between the two solutions could be expressed as a multiplying factor:

$$\left[1 - \frac{Q_i}{k_i}\left(1 + \frac{V_{Bl}}{V_{Ti}}\right)^{-2}\right] + \text{higher order terms in } \left(\frac{Q_i}{k_i}\right) \tag{5.2}$$

For realistic values of the volumes, this is essentially equivalent to the statement that the assumption of flow-limiting conditions is permissible if

$$\frac{Q_i}{k_i}\left(1 + \frac{V_{Bl}}{V_{Ti}}\right)^{-2} << 1$$

or

$$\frac{k_i}{Q_i} >> 1 \tag{5.3}$$

with the actual error approximately given by the multiplying factor, equation (5.2). Equation (5.3) is about what one would expect; that is, if the rate of mass transfer is much greater than the regional perfusion, one can assume the former to be relatively very rapid and the only important resistance to transport is the flow limitation.

Some knowledge of the permeability is still required in order to use the criterion, equation (5.3), and such data are scarce. Dedrick and Bischoff (17) provided some information on how these may be estimated, and Dedrick et al (18) have given specific values for some tumor systems and normal tissues. Data from biologic handbooks could also be recast into an appropriate form for using the criterion. Despite this, there is definitely still a paucity of information and more studies are needed. Flow-limited conditions will usually be assumed, but the true validity of this cannot often be assessed.

The opposite extreme of membrane permeability being the dominant mass transfer resistance has the implication that the blood concentration in the region is constant; there is essentially no concentration gradient across the region since more than enough drug is supplied by the blood flow. Mathematically, equation (4.2) basically gives

$$C_{Bl} = C_B$$

and then equation (4.3) reduces to

$$w_{Ti}V_{Ti}\frac{dC_{Ti}}{dt} + p_{Ti}V_{Ti}\frac{dx_{Ti}}{dt} = k_i(C_B - C_{Ti}) + r_i(C_{Ti}) \tag{5.4}$$

For no binding (or linear binding, see below), equations (5.1) and (5.4) have essentially the same form as a function of C_B, and so the mathematical solutions would also be the same. With strong (nonlinear) binding, there could be some differences between the equations representing the two extreme limiting cases, but it is not clear how easily these differences might be observed. Thus, it is of interest that both limits have the same form of mathematical equation, except that the parameters have a quite different physical meaning.

Dedrick and Bischoff (17) showed that constant infusion experiments (without nonlinear binding) would yield linear semilog plots for both extremes, and the intermediate case would primarily have a curvature for short times on such a plot. Therefore, an overall conclusion is that it would be expected to be quite difficult to differentiate between various controlling resistances only on the basis of empirical straight-line plots, and independent data verification, using a criterion such as equation (5.3), is needed to make a confident decision. Further aspects of this will also be discussed below.

It is useful at this point to list values for the volumes and flows for various important body regions. The Appendix contains a table from Mapleson (19), and this seems to be a very useful, consistent set of values for a sufficient number of organs so that reasonable estimates of these parameters can be found to use in most pharmacokinetic models of interest. Most often, a model this detailed would not be used, and various parts of the body would need to be grouped together based on their similar properties.

For flow-limited models, the most important property is the perfusion rate of a tissue. This then leads to four main compartments: the blood pool, highly perfused viscera, low-perfusion lean tissue, and low-perfusion adipose tissue. The last two would be kept separate for lipid-soluble drugs because of the greatly different physicochemical nature of the two types of regions. For primarily water-soluble drugs, the two low-perfusion regions could be combined. Table 1 (adapted from Dedrick and Bischoff [17]) lists the volumes for these regions. The last part of the table indicates the values of parameters that could be used in a two-compartment model, such as discussed in the section on Choice of Compartments, where the central compartment represents all the highly perfused regions and the peripheral compartment represents the poorly perfused regions. It should be noted that several other combinations are also possible, including those based on plasma rath-

er than blood volume. Again, the properties of the drug can be used to help decide on the most appropriate values, as will be illustrated in the examples presented later.

Table 2 (*from* Krüger-Thiemer [20]) is an alternate breakdown of the body. These values are important for drugs that are membrane limited, the opposite extreme from flow limited, ie, equation (5.4) rather than equation (5.1). It is very interesting to compare tables 1 and 2 and to note that the magnitudes of the sizes of the regions that are either readily or poorly accessible to the drug are rather similar in either extreme of controlling resistance. This is especially apparent in the final groupings for a two-compartment model; the volume ratios are 8.1/30.4=0.27 and 10.7/32.3=0.33. Even though this does not guarantee that the same would be true for situations intermediate between the two extremes, it is likely that there would not be gross changes.

If this conclusion is combined with the observation made earlier about the similarity of mathematical forms between the flow-limited, equation (5.1), and membrane-limited, equation (5.4), mass balance equations, it would seem that the predictions from either type of assumed rate-controlling aspect would be similar. Also, even if the drug actually had properties intermediate between the two extremes, a fairly good prediction might still be possible. In general terms, this may be the reason for successful predictions from rather simple pharmacokinetic models attempting to simulate very complicated events. It is probably fortunate from the pragmatic point of view of using pharmacokinetic models in various applications; however, from the reverse point of drugs. This is an important topic, but seems to have had very little comprehensive study. The binding view of determining true mechanisms from observations, it is not so good. The latter goal can probably only be achieved by adding other independent types of biologic observations to the overall drug distribution measurements.

To obtain values for organ weights in other animals, the Appendix contains several relations as a function of body weight. Also, graphs are given to estimate plasma/blood flows. This then summarizes data for many of the parameters needed for the above models.

The last unresolved complication in the use of the rigorous models is the matter of tissue binding of

TABLE 1.—Physiologic volumes for a 70-kg man based on the anatomic breakdown of Mapleson (19)

Compartment	Symbol	Volume (liters)
Blood not in equilibrium with tissues	V_B	2.2
Blood in equilibrium with viscera	V_{BV}	2.52
Blood in equilibrium with lean tissue	V_{BL}	0.52
Blood in equilibrium with adipose tissue	V_{BA}	0.16
Blood, total	ΣV_{Bi}	5.4
Visceral tissue	V_{TV}	6.2
Lean tissue	V_{TL}	39.2
Adipose tissue	V_{TA}	12.2
Water contents ($w_B \simeq 0.8$, $w_{TV} \simeq 0.7 \simeq w_{TL}$, $w_{TA} \simeq 0.2$)		
$0.8\,(\Sigma V_{Bi})$		4.3
$0.8\,(V_B + V_{BV}) + 0.7\,V_{TV}$		8.1
$0.8\,(V_{BL} + V_{BA}) + 0.7\,V_{TL} + 0.2\,V_{TA}$		30.4
Total (last 2 entries)		38.5

TABLE 2.—Physiologic volumes for a 70-kg man based on the functional spaces of Krüger-Thiemer (20)

Compartment	Symbol	Volume (liters)	Volume (ml/kg)
Plasma water (Evans blue dye)	V_1	3.0	43
Rapidly equilibrating interstitial water (inulin space—V_1)	V_2	7.7	109
Slowly equilibrating interstitial water (chloride space—V_1—V_2)	V_4	8.3	118
Intracellular water (D_2O space—V_1—V_2—V_4)	V_5	24.0	340
Plasma + rapidly equilibrating interstitial water (inulin space)	V_{13}	10.7	152
Intracellular + slowly equilibrating interstitial water (D_2O space—V_1—V_3)	V_{45}	32.3	458
Total body water (D_2O space)	V_{1345}	43.0	610

would be presumed to be similar to plasma protein binding, and would be some combination of nonspecific binding plus whatever specific role the particular tissue plays with regard to the drug. The only sure way to measure tissue binding is by in vivo experiments utilizing tissue samples. This is difficult and time consuming, and some way is still needed to correlate the data, especially for nonlinear binding.

Due partly to lack of much rigorous data, Bischoff and Dedrick (17,21) introduced the concept of *effective protein binding* in the tissues. This was based on the assumption that the nonspecific binding might be similar to plasma protein binding, and the important consideration is how much tissue "protein" can effectively bind the drug. It would be expected that this effective protein amount would *not* be the total tissue protein because of poor conformations, etc; also, direct use of total tissue protein greatly overestimated the binding actually observed. A recent paper by Shen and Gibaldi (22) shows this in detail and also discusses other possible complications. The real test of the concept will be how well it can be used in diverse pharmacokinetic models, but there just isn't sufficient data to come to a definite conclusion.

The use of the concept in a semi-empirical way is not difficult. The plasma protein binding isotherm is assumed to be known (eg, equation [3.4]), and this seems to be rather commonly done. Then, at least one tissue binding experiment must be performed. The basic assumption is made that the binding isotherm is the same for all tissues and plasma, so that in the context of equation (4.3)

$$\begin{aligned} &\text{if } x_B = \psi(C_B) \\ &\text{then } x_{Ti} = \psi(C_{Ti}), \text{ same } \psi \end{aligned} \tag{5.5}$$

The differences in various types of tissue binding are entirely accounted for by the various effective protein amounts, p_{Ti}. These are determined from the one (or more) tissue-binding experiment, and can then be used for further predictions. It is found that these effective protein amounts often do not bear any simple relation to the actual proteins present, and so they definitely must be considered as semi-empirical parameters, eg, Shen and Gibaldi (22), and Dedrick and Bischoff (17).

This postulate not only greatly reduces the number of tissue-binding studies required, but it also considerably reduces the complexity of the mass balance equations. Thus, equation (5.1) becomes

$$\begin{aligned} &\left\{ w_{Bl} V_{Bl} + w_{Ti} V_{Ti} + \left[p_{Bl} V_{Bl} + p_{Ti} V_{Ti} \right] \frac{d\psi}{dC_{Cl}} \right\} \frac{dC_i}{dt} = \\ &= Q_i \left[w_B C_B + p_B \psi \left(C_B \right) - w_{Bl} C_i - p_B \psi \left(C_i \right) \right] \\ &\qquad + r_i \left(C_i \right) \end{aligned} \tag{5.6}$$

Once the parameters are evaluated, the value in the braces ({}) is essentially the *predicted* tissue volume of distribution, which, of course, need not be a constant for nonlinear binding.

It is useful at this point to briefly consider an example of the actual use of the above developments. Figure 6 shows the minimum detail estimated to be adequate to represent the distribution of highly lipid-soluble drugs, such as barbiturates, by Price et al (23), Rackow et al (24), and Bischoff and Dedrick (17, 21). The latter authors specifically used mass balances, equations (4.1) and (5.6), with the binding isotherm given by a two-term form of equation (3.10) (and equation [5.5]):

Blood pool

$$\begin{aligned} &\left\{ w_B V_B + p_B V_B \frac{d\psi}{dC_B} \right\} \frac{dC_B}{dt} = Mg(t) - Q_B \left[w_B C_B + p_B \psi \left(C_B \right) \right] \\ &\quad + Q_V \left[w_B C_V + p_B \psi \left(C_V \right) \right] \\ &\quad + Q_L \left[w_B C_L + p_B \psi \left(C_L \right) \right] \\ &\quad + Q_A \left[w_B C_A + p_B \psi \left(C_A \right) \right] \end{aligned} \tag{5.7}$$

(The first term on the right side represents injection of "M" amount of drug in a time course, g (t)).

Viscera

$$\begin{aligned} &\left\{ w_B V_{BV} + w_{TV} V_{TV} + \left[p_B V_{BV} + p_{TV} V_{TV} \right] \frac{d\psi}{dC_V} \right\} \frac{dC_V}{dt} = \\ &= Q_V \left[w_B C_B + p_B \psi \left(C_B \right) - w_B C_V - p_B \psi \left(C_V \right) \right] \\ &\qquad - \frac{k_V C_V}{K_{MV} + C_V} \end{aligned} \tag{5.8}$$

The last term represents hepatic metabolism and is a simple Michaelis-Menten form based on the *free* concentration of drug.

Similar balances were also written for the lean and adipose tissue regions, with the tissue binding term in the latter replaced by the lipid solubility, $x_{TA} = B_A C_A$. The flow and volume parameter values were those described above, and both the plasma binding function, Ψ, and the effective protein amount, p_{TV}, were determined from the data of Goldbaum and Smith (25). This left only the metabolism term in equation (5.8), which had to be empirically fit due to lack of more extensive data. Figure 8 shows the agreement between the model predictions and some relatively short time data for the blood and adipose regions for thiopental. Figure 9 gives longer time predictions of the free concentrations, where it is seen that the highly perfused visceral values are virtually identical to those in blood; this observation can be the basis for further reductions in model complexity, as will be seen below. The lean water (vs

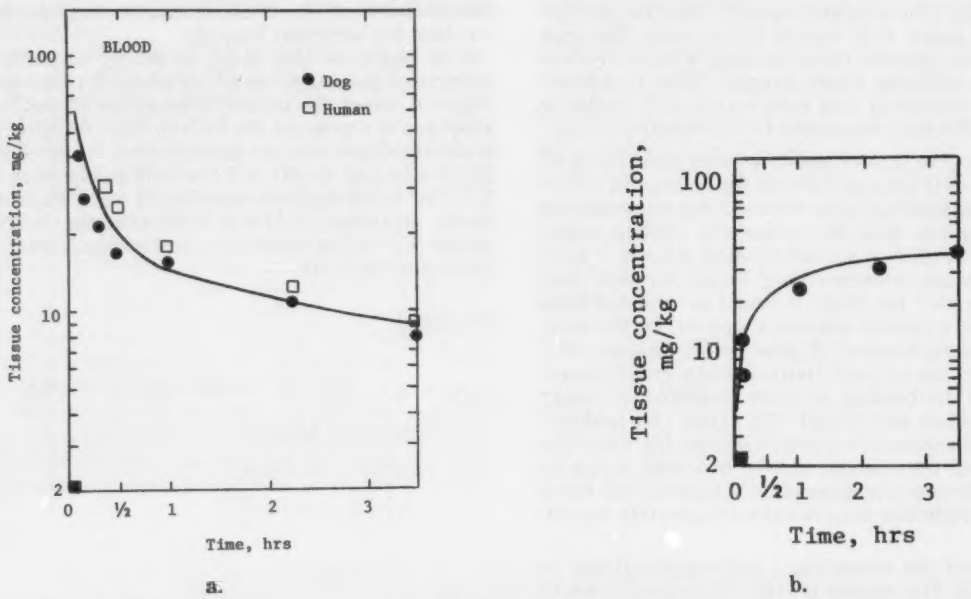

FIGURE 8.—a. Predicted thiopental concentration in blood following 25-mg/kg iv injection. b. Comparison of predicted and experimental values for adipose tissue. ■ = Injection duration; ● = dog. [*From* ref 21. Reproduced with permission of the copyright owner.]

lipid) tissue also has concentrations close to the blood after the initial distribution time caused by the large differences in tissue perfusion. This again illustrates, with a realistic example, how all the body water might be lumped into a single compartment for long drug residence times in the body.

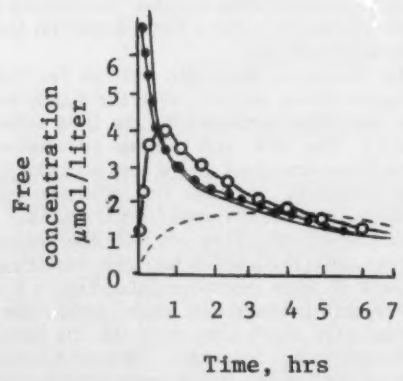

FIGURE 9.—Thiopental long-time behavior: free concentration. ——— = Viscera; - - - - - - = adipose tissue; -○-○-○-○- = lean tissue; -●-●-●-●- = blood. [*From* ref 21. Reproduced with permission of the copyright owner.]

ALTERNATE FORMS OF MASS BALANCES

Even though the above models provide a rational and rigorous (to within the carefully defined approximations) basis for predicting drug concentrations, they do require quite a bit of information for their use. For example, often only the total (free plus bound) concentrations are actually measured, and if the drug is essentially linearly bound, ie, far from the saturation region, this may be an adequate measure of the drug effect. Thus, the models might be more useful in many applications if they were further simplified.

The total concentrations are properly defined as follows:

$$\tilde{C}_B = w_B C_B + p_B x_B \qquad (6.1a)$$

$$\tilde{C}_{Bl} = w_{Bl} C_{Bl} + p_{Bl} x_{Bl} \qquad (6.1b)$$

$$\tilde{C}_l = \frac{(w_{Bl} V_{Bl} + w_{Tl} V_{Tl}) C_l + p_{Bl} V_{Bl} x_{Bl} + p_{Tl} V_{Tl} x_{Tl}}{V_{Bl} + V_{Tl}} \qquad (6.1c)$$

The latter equation assumes that the typical tissue biopsy sample includes both tissue and equilibrium blood. Also note that it does *not* assume the necessity of using the effective protein amounts. The total concentration of a tissue is most often reported as a tissue/blood distribution ratio

$$R_i = \frac{\tilde{C}_i}{\tilde{C}_{Bt}} = \left(\frac{\tilde{C}_i}{\tilde{C}_B}\right)_{\text{equilibrium, } C_i = C_B} \qquad (6.2)$$

With nonlinear binding, R_i is not a constant but is a function of the concentration levels. However, for linear binding, R_i is a constant, as can be seen by substituting equation (6.1) into (6.2), and this is its most convenient application. The second equality in equation (6.2) indicates that the blood pool concentration can replace the tissue venous outflow concentration only under equilibrium conditions, ie, long-time constant infusion. This has been discussed for the two-compartment model by Gibaldi (26) as well as Bischoff and Dedrick (9), who have shown the difference between R_i and the long-time slopes ratio from a bolus injection; for many situations, the values of the parameters are such that essentially equivalent values for R_i are obtained by either approach. Dedrick, Zaharko, and Lutz (27) have shown how well these concepts work for the linearly bound cancer chemotherapeutic agent, methotrexate.[4]

If equations (6.1) and (6.2) for each tissue region are substituted into the rigorous mass balance equation (5.1), the following alternate simpler form is obtained:

$$V_B \frac{d\tilde{C}_B}{dt} = -Q_B \tilde{C}_B + \sum_i Q_i \frac{\tilde{C}_i}{R_i} + \text{(injection)} \qquad (6.3)$$

$$\left(V_{Bt} + V_{Ti}\right)\frac{d\tilde{C}_i}{dt} = Q_i\left(\tilde{C}_B - \frac{\tilde{C}_i}{R_i}\right) + r_i\left(\underset{\uparrow}{C_i}\right)$$

$$\text{with } Q_B = \sum_i Q_i \qquad (6.4)$$

In these equations, R_i =constant only for linear binding, x = KC. It should be emphasized that equations (6.3) and (6.4) involve *no* further assumptions beyond that of flow-limited conditions, which is really the only situation where the total tissue concentration has a unique meaning. Equations (6.3) and (6.4) are valid for either a variable or constant R_i, although they are much more useful in the latter case. The arrow under the metabolic rate term indicates the question that the enzyme reactions presumably depend upon the free concentration, and for nonlinear binding this has no simple relationship to the toal concentrations in the rest of the mass balance. The practical importance of ignoring this and just re-defining the rates in terms of $\tilde{C}_i$ is not presently known.

Let us again consider the application of these concepts to specific examples. Bischoff, Dedrick, and Zaharko (28-31) considered in some detail the pharmacokinetics of methotrexate. Since this drug appears to be linearly bound, the simplified equations (6.3) and (6.4) could be used in conjunction with the flow diagram shown in figure 7. The mass balance equations are as follows:

plasma

$$V_P \frac{dC_P}{dt} = \text{(injection)} + Q_L \frac{C_L}{R_L} + Q_K \frac{C_K}{R_K} + Q_M \frac{C_M}{R_M} - (Q_L + Q_K + Q_M) C_P \qquad \text{a}$$

muscle

$$V_M \frac{dC_M}{dt} = Q_M \left(C_P - \frac{C_M}{R_M}\right) \qquad \text{b}$$

kidney

$$V_K \frac{dC_K}{dt} = Q_K \left(C_P - \frac{C_K}{R_K}\right) - k_K \frac{C_K}{R_K} \qquad \text{c}$$

liver

$$V_L \frac{dC_L}{dt} = (Q_L - Q_G)\left(C_P - \frac{C_L}{R_L}\right) + Q_G\left(\frac{C_G}{R_G} - \frac{C_L}{R_L}\right) - r_o \qquad \text{d}$$

where

$$r_o = \frac{k_L C_L/R_L}{K_L + C_L/R_L} \qquad (6.5)$$

bile ducts

$$\tau \frac{dr_i}{dt} = r_{i-1} - r_i \; (i = 1, 2, 3) \qquad \text{e}$$

gut tissue

$$V_G \frac{dC_G}{dt} = Q_G\left(C_P - \frac{C_G}{R_G}\right) + \sum_{i=1}^{4} \frac{1}{4}\left[\frac{k_G C_i}{K_G + C_i} + bC_i\right] \qquad \text{f}$$

gut lumen

$$\frac{dC_{GL}}{dt} = \frac{1}{4}\sum_{i=1}^{4} \frac{dC_i}{dt} \qquad \text{g}$$

$$\frac{V_{GL}}{4}\frac{dC_1}{dt} = r_3 - k_P V_{GL} C_1 - \frac{1}{4}\left[\frac{k_G C_1}{K_G + C_1} + bC_1\right] \qquad \text{h}$$

$$\frac{V_{GL}}{4}\frac{dC_i}{dt} = k_P V_{GL}(C_{i-1} - C_i) - \frac{1}{4}\left[\frac{k_G C_i}{K_G + C_i} + bC_i\right] \qquad \text{i}$$

$$(i = 2, 3, 4)$$

Most of the terms and their origins should now be clear. The new ones are: in equation (6.5[c]) the term $k_K C_K/R_K$ represents the renal excretion of methotrexate, which is close to the glomerular filtration rate; in equation (6.5 [d,e]), r_i is the bile flow of the drug, with the liver secretion being saturable at high doses (the three compartments-in-series again represent the actual tubular or distributed nature of the real system); in equation (6.5 [f-i]), the motion down the gut lumen is modeled by four compart-

[4]Methotrexate: NSC-740; CAS reg. No. 59-05-2; glutamic acid, *N*-[*p*-[[(2,4-diamino-6-pteridinyl)methyl]methylamino]benzoyl]-.

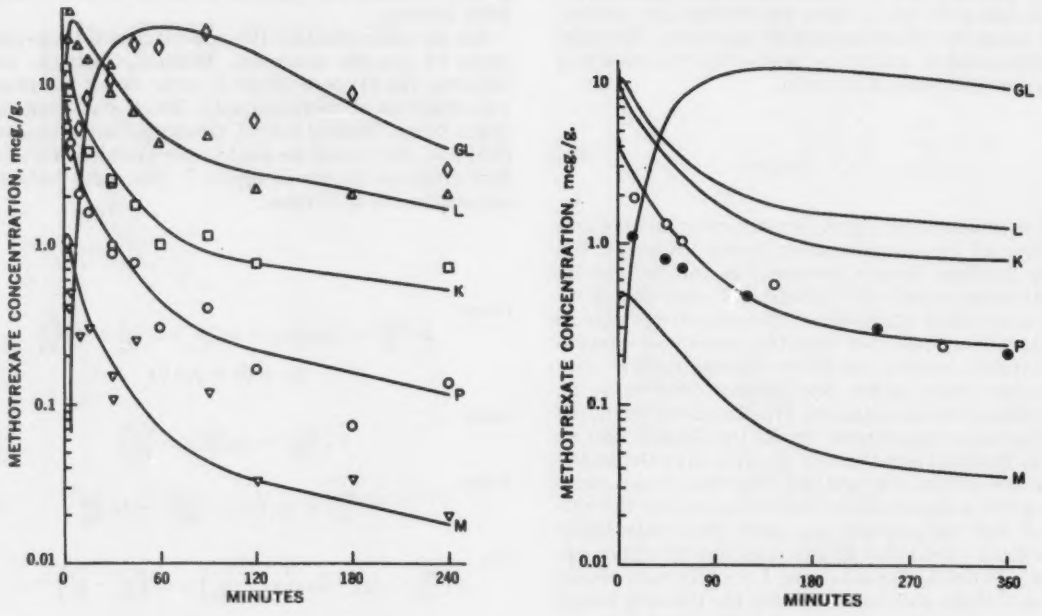

FIGURE 10.—a. Model prediction vs experimental results, mice, 3 mg/kg iv. Solid lines are model predictions; symbols are experimental data. GL (◇) = small intestine; L (△) = liver; K (□) kidney; P (○) = plasma; and M (▽) = muscle. b. Man, 1 mg/kg iv. Open and closed symbols are results of 2 separate experiments. [*From* ref 31. Reproduced with permission of the copyright owner.]

ments, and the absorption term has both a saturable and a nonsaturable component that is important only for very high doses, presumably passive diffusion.

The various parameters in equation (6.5) were either estimated from the values given earlier or were independently measured in the case of the complex secretion steps. Then, the pharmacokinetic behavior was able to be predicted in mice, rats, dogs, monkeys, and man over a dose range of 3000, all with the same model and with a consistent set of parameters. Two examples are shown in figure 10. Thus, it is felt that the details of this model must be a reasonably faithful representation of the actual physiologic and pharmacologic events, and should be of aid in interpreting experiments. Also, valid predictions of local drug concentrations for various dosage regimens are possible.

The flow diagram of figure 7 has a rather complicated configuration because of the importance of the enterohepatic cycle in the methotrexate pharmacokinetics. However, there was essentially no direct metabolism of the drug, and the ultimate excretion was by the renal or fecal route. A final example considers the opposite extreme, where a straightforward anatomic flow diagram is the basis but the metabolism is dominant. Dedrick, Forrester, and Ho (32) have considered the drug cytosine arabinoside[5] on the basis of the compartments seen in figure 11. The sizes of the boxes signify the relative importance of the various regions. Again, the same types of balances were used, but with metabolic terms in each based on known enzyme kinetics and levels. Figure 12 shows one prediction of the concentrations of cytosine arabinoside and its metabolite, uracil arabinoside. In this case, the metabolism is so rapid that any drug presented to an organ is almost completely reacted, and so this is again a sort of a "flow limitation," and is probably part of the reason why the standard models work so well.

A final reduction in the complexity of the models is possible when the excretion/metabolism processes are relatively slow compared to the intra-compartment blood flows. In this case, the entire body has an essentially identical time-response, and a one-com-

[5]Cytosine arabinoside: NSC-63878; CAS reg. No. 69-74-9; cytosine, 1-β-D-arabinofuranosyl-, monohydrochloride.

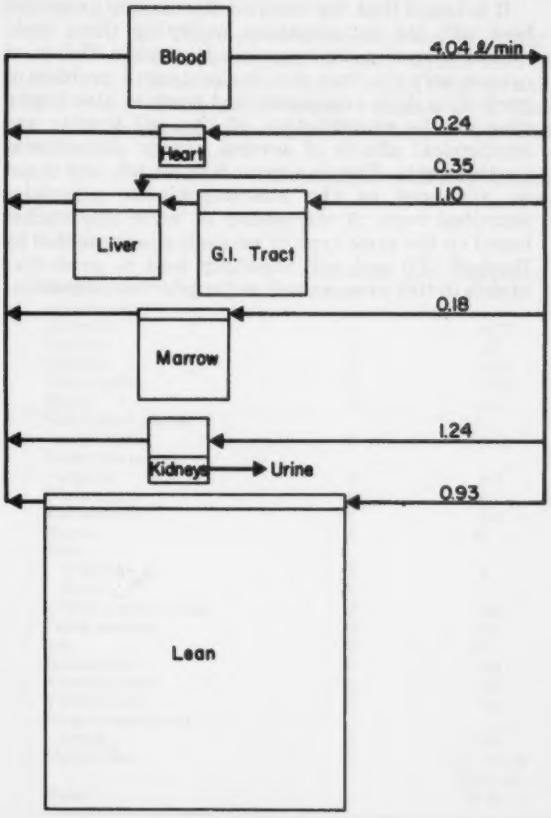

FIGURE 11.—Compartmental model for cytosine arabinoside distribution. [*From* ref 32.]

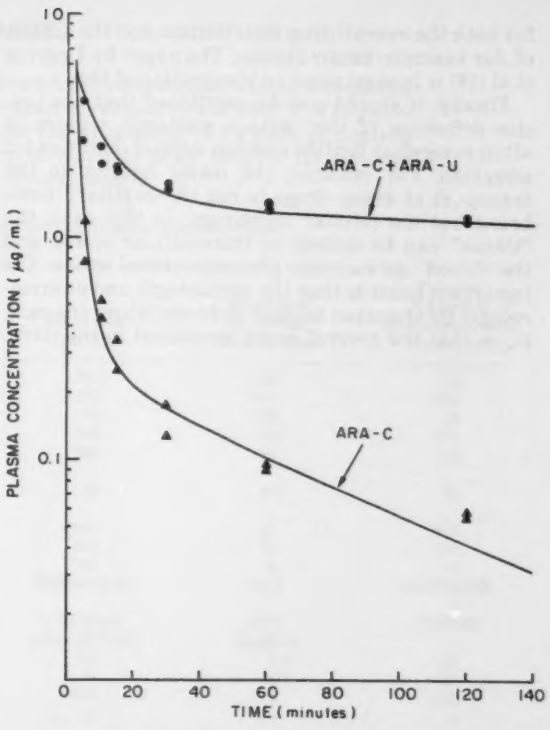

FIGURE 12.—Comparison between curves predicted by model and observed data in man at 1.2 mg/kg of cytosine arabinoside. [*From* ref 32.]

partment whole-body model is useful. In terms of equations (6.3) and (6.4) this implies that

$$r_i << Q_i \longrightarrow \infty, \quad \tilde{C}_B \simeq \frac{\tilde{C}_i}{R_i}$$

and then adding all the tissue mass balances to that for blood gives

$$\left[V_B + \sum_i \left(V_{Bi} + V_{Ti}\right) R_i\right] \frac{d\tilde{C}_B}{dt} = \sum \text{(injections)} + \sum_i r_i \left(C_i\right) \qquad (6.6)$$

The term in brackets would be the theoretic basis of the volume of distribution. An alternate form can be derived from equations (4.1) and (5.6) in terms of free concentrations, where the condition is now $C_B \simeq C_i$:

$$\left[V_1 + V_2 \frac{d\phi}{dC_B}\right] \frac{dC_B}{dt} = \sum \text{(injections)} + \sum_i r_i \left(C_B\right) \qquad (6.7)$$

where

$$V_1 = w_B V_B + \sum_i \left(w_{Bi} V_{Bi} + w_{Ti} V_{Ti}\right) = V_{water}$$

$$V_2 = p_B V_B + \sum_i \left(p_{Bi} V_{Bi} + p_{Ti} V_{Ti}\right) = V_{protein,\ effective}$$

Again, the value in brackets is the predicted volume of distribution but based on free concentrations. These types of equations are very familiar in pharmacology, although they are usually used with empirical parameters, and therefore no specific examples will be given.

DISCUSSION

Various special situations can require the use of combinations of all of the above types of mass balances. The examples have shown the type of reasoning used for several instances, although they have all used the flow-limited case. It appears that this quite often gives a good estimate of the overall drug concentrations throughout the body, even though the drug may be membrane limited in certain specific organs. Thus, a combination of the analysis illustrated in the examples, plus the use of equation (5.4) for the specific region, might be a reasonable scheme

for both the overall drug distribution and the details of, for example, tumor uptake. The paper by Dedrick et al (18) is in some ways an illustration of this.

Finally, it should also be mentioned that the precise definition of the various anatomic regions is often somewhat flexible and can depend on the exact situation. For example, the major barrier to the transport of many drugs is not the capillary membrane but the cellular membrane; in this case, the "tissue" can be defined as intracellular space, and the "blood" as vascular plus interstitial space. The important point is that the physiologic and pharmacologic information be used in formulating the model, so that the several goals mentioned in the introductory parts of this paper might be achieved.

It is hoped that the detailed discussions presented here will aid investigators in trying these techniques to develop pharmacokinetic models. This is, of course, only the first step in the overall problem of predicting drug responses, and work is also beginning on the quantitation of the cell kinetic and biochemical effects of several cancer chemotherapeutic agents. This is a more difficult job, and is not as advanced as the pharmacokinetic principles described here. A discussion of some approaches based on the same type of reasoning is presented by Bischoff (33) and will hopefully lead to predictive models in this area, as well as for pharmacokinetics.

APPENDIX

This Appendix contains the following three sets of information that are needed to use the pharmacokinetic models that have been developed in the text: I. A comprehensive collection of organ volumes and flows for a standard 70-kg man. II. Scaling relations for organ volumes as a function of mammal body weight. III. Scaling graphs for organ blood flows as a function of body weight.

I. Volumes and blood supplies of different body regions for a standard man* (*from* ref 19)

Tissue	Reference letters	Volume (liters)	Blood flow (ml/min)	Blood flow (ml/100 ml; tissue × min)	Volume of blood in equilibrium with tissue (ml)
Adrenals	A	0.02	100	500	62
Kidneys	B	0.3	1240	410	765
Thyroid	C	0.02	80	400	49
Gray matter	D	0.75	600	80	371
Heart	E	0.3	240	80	148
Other small glands and organs	F	0.16	80	50	50
Liver plus portal system	G	3.9	1580	41	976
White matter	H	0.75	160	21	100
Red marrow	I	1.4	120	9	74
Muscle	J	30	300/600/1500	1/2/5	185/370/925
Skin					
Nutritive	K	3	30/60/150	1/2/5	18/37/92
Shunt	L		1620/1290/300	54/43/10	
Nonfat subcutaneous	M	4.8	70	1.5	43
Fatty marrow	N	2.2	60	2.7	37
Fat	O	10	200	2	123
Bone cortex	P	6.4	0	0	0
Arterial blood	Q	1.4			
Venous blood	R	4.0			
Lung parenchymal tissue	S	0.6			
Air in lungs	T	2.5 + half tidal vol			1400†
					999/795/185‡
Total		70.0§	6480		5400

*Standard man = 70 kg body wt, 1.83 m² surface area, 30-39 yrs.
† Arterial blood.
‡ Skin-shunt venous blood.
§ Excluding air in the lung.

II. Scaling relations for organ volumes as a function of mammal body weight (*from* ref 31)

$V_{Plasma} = 44\ W^{0.99}$ $V_{Kidney} = 7.5\ W^{0.85}$ $V_{Muscle} \simeq 500\ W$

$V_{Liver} = 34\ W^{0.87}$ $V_{Gut} = 49\ W^{0.94}$

V in ml, W in kg

III. Scaling graphs for organ blood flows as a function of body weight
(*from* ref 31)

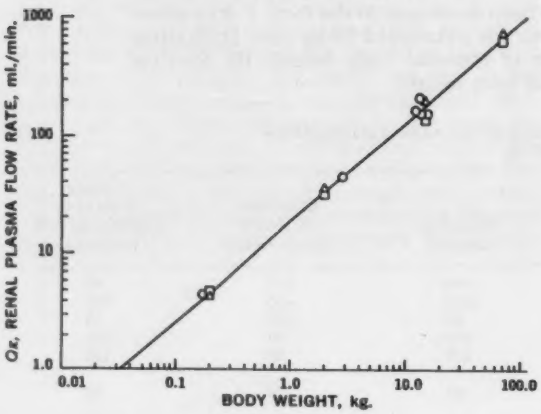

FIGURE A1.—Renal plasma flow rate.

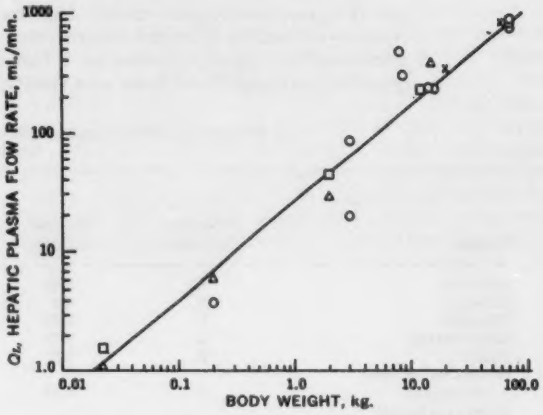

FIGURE A2.—Hepatic plasma flow rate.

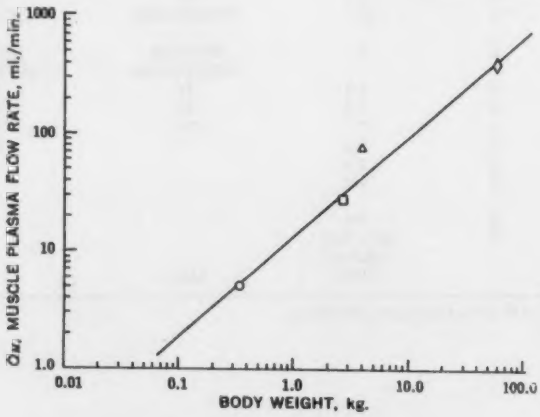

FIGURE A3.—Muscle plasma flow rate.

NOTATION

A = area
C = concentration of free drug
C^* = concentration of ionized drug
$\tilde{C}$ = total concentration, free plus bound
$g(t)$ = time course of drug injection
k_i = permeability coefficient of membrane "i"
K = equilibrium constant
l = capillary length
l = vacant binding sites
M = amount of drug injected
p_i = protein concentration in tissue "i"
P = membrane permeability
Q_i = volumetric flow rate to tissue "i"
r = reaction rate
R_i = distribution ratio between tissue "i" and blood (or plasma)
t = time
V_i = volume of tissue "i"
w_i = fraction water in tissue "i"
x = bound concentration per unit amount of protein
z = length coordinate
$\psi(C)$ = functional form of binding dependence on free concentration C

Subscripts

A = adipose tissue
A, B = chemical species "A," "B"
Al = bound species "A"
B = blood
C = cellular
G = gut tissue
GL = gut lumen
i = interstitial
K = kidney
l = vacant binding site
L = lean tissue
M = muscle tissue
P = plasma
T = tissue
V = visceral tissue

REFERENCES

1. Dedrick RL. Animal scale-up. J Pharmacokinet Biopharm 1:435-461, 1973.
2. Freireich EJ, Gehan EA, Rall DP, et al. Quantitative comparison of toxicity of anticancer agents in mouse, rat, hamster, dog, monkey, and man. Cancer Chemother Rep 50:219-244, 1966.
3. Teorell T. Kinetics of distribution of substances administered to the body. Arch Int Pharmacodyn Ther 57:205-240, 1937.
4. Krüger-Thiemer E. Formal theory of drug dosage regimens. II. The exact plateau effect. J Theor Biol 13:212-235, 1966; 23:169-170, 1969.
5. ———. Pharmacokinetics and dose-concentration relationships. Proceedings of the 3rd International Pharmacological Meeting, Sao Paulo, Brazil, 1966. *In* Physico-Chemical Aspects of Drug Actions. New York, Pergamon Press, 1968, vol 7, pp 63-113.
6. Riegelman S, Loo J, and Rowland M. Shortcomings in pharmacokinetic analysis by conceiving the body to exhibit properties of a single compartment. J Pharm Sci 57:117-123, 1968.
7. ———. Concept of a volume of distribution and possible errors in evaluation of this parameter. J Pharm Sci 57:128-133, 1968.
8. Bischoff KB, and Dedrick RL. Generalized solution to linear, two-compartment, open model for drug distribution. J Theor Biol 29:63-83, 1970.
9. Wagner JG. Biopharmaceutics and relevant pharmacokinetics. Hamilton, Ill, Drug Intelligence Publications, 1971.
10. Leonard EF, and Jorgensen SB. The analysis of convection and diffusion in capillary beds. Annu Rev Biophys Bioeng 3:293-339, 1974.
11. Bellman R, Kalaba R, and Jacquez JA. Some mathematical aspects of chemotherapy. Bull Math Biophys 22:181-190, 309-322, 1960.
12. Bischoff KB, and Brown RG. Drug distribution in mammals. Chemical Engineering Program Symposium, Series No. 66, vol 62:33-45, 1966.
13. Himmelblau DM, and Bischoff KB. Process Analysis and Simulation. New York, John Wiley, 1968.
14. Bischoff KB. Applications of a mathematical model for drug distribution in mammals. *In* Chemical Engineering in Medicine and Biology (Hershey D, ed). New York, Plenum Press, 1967.
15. Goldstein A, Aronow L, and Kalman SM. Principles of Drug Action. New York, Harper and Row, 1969.
16. Ariens EM, ed. Molecular Pharmacology. New York, Academic Press, 1964.
17. Dedrick RL, and Bischoff KB. Pharmacokinetics in applications of the artificial kidney. Chemical Engineering Program Symposium, Series No. 84, vol 64:32-44, 1968.
18. Dedrick RL, Zaharko DS, Bender RA, et al. Pharmacokinetic considerations on resistance to anticancer drugs. Cancer Chemother Rep 59:795-804, 1975.
19. Mapleson WW. An electric analogue for uptake and exchange of inert gases and other agents. J Appl Physiol 18:197-204, 1963.
20. Krüger-Thiemer E. Die Lösung chemotherapeutischer Probleme durch programmgesteuerte Ziffernrechenautomaten. 5: Systematik der pharmakokinetischen Modelle und Interpretation der Verteilungsvolumina. Arzneim Forsch 14:1334-1343, 1964.
21. Bischoff KB, and Dedrick RL. Thiopental pharmacokinetics. J Pharm Sci 57:1346-1351, 1968.
22. Shen D, and Gibaldi M. Critical evaluation of use of effective protein fractions in developing pharmacokinetic models for drug distribution. J Pharm Sci 63:1698-1703, 1974.
23. Price HL, Kovnat PJ, Safer JN, et al. The uptake of thiopental by body tissues and its relation to the duration of narcosis. Clin Pharmacol Ther 1:16-22, 1960.
24. Rackow H, Salanitre E, Epstein RM, et al. Simultaneous uptake of N_2O and cyclopropane in man as a test of compartment model. J Appl Physiol 20:611-620, 1965.
25. Goldbaum LR, and Smith PK. The interaction of barbiturates with serum albumin and its possible relation to their disposition and pharmacological actions. J Pharmacol Exp Ther 111:197-209, 1954.
26. Gibaldi M. Effect of mode of administration on drug distribution in a two-compartment open system. J Pharm Sci 58:327-331, 1969.
27. Dedrick RL, Zaharko DS, and Lutz RJ. Transport and binding of methotrexate in vivo. J Pharm Sci 62:882-890, 1973.
28. Bischoff KB, Dedrick RL, and Zaharko DS. Preliminary model for methotrexate pharmacokinetics. J Pharm Sci 59:149-154, 1970.
29. Dedrick RL, Bischoff KB, and Zaharko DS. Interspecies correlation of plasma concentration history of methotrexate (NSC-740). Cancer Chemother Rep 54:95-101, 1970.
30. Zaharko DS, Dedrick RL, Bischoff KB, et al. Methotrexate tissue distribution: prediction by a mathematical model. J Natl Cancer Inst 46:775-784, 1971.
31. Bischoff KB, Dedrick RL, Zaharko DS, et al. Methotrexate pharmacokinetics. J Pharm Sci 60:1128-1133, 1971.
32. Dedrick RL, Forrester DD, and Ho DHW. In vitro-in vivo correlation of drug metabolism—deamination of 1-β-D-arabinofuranosylcytosine. Biochem Pharmacol 21:1-16, 1972.
33. Bischoff KB. Pharmacokinetics and cancer chemotherapy. J Pharmacokinet Biopharm 1:465-480, 1973.

Pharmacokinetic Considerations on Resistance to Anticancer Drugs

Robert L. Dedrick,[1] Daniel S. Zaharko,[2] Richard A. Bender,[3] W. Archie Bleyer,[4] and Robert J. Lutz[1, 5]

SUMMARY

A model framework is discussed for a quantitative description of intercompartment drug transport in terms of individual processes involved. It permits joint consideration of blood flow, membrane transport, binding, and enzyme synthesis. Illustrations are drawn from the pharmacokinetics and pharmacodynamics of methotrexate. Special cases include flow and membrane limitation, and a simple expression is derived to estimate the time required for intracellular drug to reach the concentration of high-affinity binding sites. Transport parameters between blood and cerebrospinal fluid are inferred from new clinical data. Lumbar injection provided a reservoir effect which maintained plasma concentration for a prolonged time compared with intravenous injection.

[Cancer Chemother Rep 59:795-804, 1975]

For an anticancer drug to be effective, it must reach a desired site of action and remain there in sufficient concentration and for sufficient time to produce a useful tumor cell kill. Generally, a biochemical process is blocked, which is common to both certain normal and neoplastic cells; therefore, the therapeutic framework is one of destroying cancer cells more rapidly than they can be produced within constraints imposed by the toxicity to the host. Optimization, then, must consider biologic factors such as sensitivity of various cell lines, cytokinetics, and the influence of repair processes. It must also consider physical phenomena such as the transport of a drug to its site of action and interactions at that site. This paper is concerned with the physical (pharmacokinetic) phenomena.

Numerous pharmacokinetic reasons have been suggested for the ineffectiveness of certain drugs or dose schedules in the treatment of cancer. These include "poor" tumor perfusion, "slow" transport of drug to its site of action, "high" enzyme levels, and "rapid" enzyme synthesis. Such concepts have no intrinsic meaning; they are significant only as they relate to the time scale of other kinetic processes which occur simultaneously. They are illustrated and placed in quantitative perspective by a discussion of the pharmacokinetics and pharmacodynamics of methotrexate.[6]

MECHANISM OF ACTION

The mechanism of action of methotrexate has been reviewed by Bertino and Johns (1). It is a very strong inhibitor of the enzyme dihydrofolate reductase, which catalyzes the formation of tetrahydrofolate. If tetrahydrofolate is not available for the production of a cofactor necessary for thymidylate formation, DNA synthesis is inhibited. Additional sites of action have been proposed, and these complicate the complete description of the biochemical events leading to cell death or recovery following exposure to methotrexate.

It is generally assumed that the fundamental effect of a reversibly acting inhibitor is determined by its free concentration at the site of action. (Gross observable effects may not exhibit simple temporal relationships; they are frequently delayed.) For some drugs, such as certain barbiturates, the plasma concentration is a good index of effect. For others, such as methotrexate, a number of physical limitations may cause the free concentration in some

[1]Biomedical Engineering and Instrumentation Branch (BEI), Division of Research Services (DRS), National Institutes of Health (NIH), Bethesda, Md.

[2]Pharmacokinetics and Pharmacodynamics Section, Laboratory of Chemical Pharmacology, Experimental Therapeutics, Division of Cancer Treatment (DCT), National Cancer Institute (NCI), Bethesda, Md.

[3]Medicine Branch, DCT, NCI, Bethesda, Md.

[4]Department of Pediatrics, Division of Hematology/Oncology, Children's Orthopedic Hospital and Medical Center, University of Washington, Seattle.

[5]*Reprint requests to:* Dr. Robert L. Dedrick, BEI, DRS, NIH, Bldg 13, Rm 3W13, Bethesda, Md 20014.

[6]Methotrexate: NSC-740; CAS reg. No. 59-05-2; glutamic acid, N-[p-[[(2,4-diamino-6-pteridinyl)methyl]methylamino]benzoyl]-; MTX.

compartments of the body to differ significantly from that in the plasma.

INTERCOMPARTMENT TRANSPORT

A drug usually is transported to a given region of the body with the flowing blood. Figure 1 is a schematic diagram of a typical region divided into plasma, interstitial fluid, and intracellular fluid compartments. Mass balance equations can be written on each of the compartments as follows:

$$V_1 \frac{dq_1}{dt} = Q\,(q_P - q_1) - (jA)_{12} \quad (1)$$

$$V_2 \frac{dq_2}{dt} = (jA)_{12} - (jA)_{23} \quad (2)$$

$$V_3 \frac{dq_3}{dt} = (jA)_{23} \quad (3)$$

where V = compartment volume, ml; q = total (free + bound) concentration, μg/ml; Q = plasma flow rate, ml/min; j = flux between compartments, μg/(min) (cm^2); and A = area for transport, cm^2. The subscripts represent the compartment or direction of transport. The terms j and A are often not separated in practice, but they could be in principle.

Solution of equations (1)-(3) requires information of several types:

Anatomic—compartment volumes, V.

Physiologic—plasma flow rate, Q.

Thermodynamic—binding isotherm, $q = q(C)$, where C is the free concentration.

Transport—description of (jA) in terms of local free concentrations.

Initial concentrations in each compartment and the plasma concentration as a function of time are also required. Frequently, not all of these must be known accurately. In some regions, the capillary membrane is much more permeable than the cell membrane so that compartments 1 and 2 may be combined and the three compartments reduced to two, extracellular and intracellular fluid. Algebraic details and attendant assumptions have been discussed (2).

An appropriate number of regions such as those shown in figure 1 may be organized into a flow diagram which provides the basis for a complete pharmacokinetic model. Alternatively, it is often necessary to obtain detailed information about the behavior of only one or two compartments, and these can be simulated with measured plasma concentration data.

Flow-Limited Models

A particularly simple solution exists to equations (1)-(3) when the membrane permeabilities are much greater than the perfusion rate (3.4).

$$\frac{(PA)}{V} \gg \frac{Q}{V}.$$

Then, the pharmacokinetic model is completely characterized by volumes, flows, and binding data, and much can be said a priori about its sensitivity to changes in these. The development of flow-limited models has been discussed extensively (5-8).

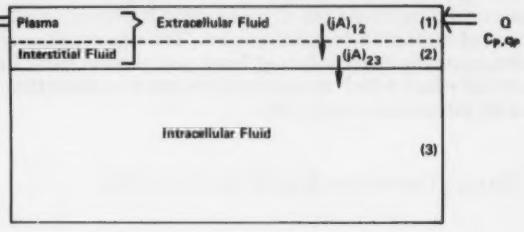

FIGURE 1.—Diagram of a compartment showing inter- and intra-tissue transport (2). Q = plasma flow rate; C_P and q_P are free and total drug concentrations in the plasma; (jA) = transmembrane rate of transport.

Table 1 includes a few selected blood flow rates in normal tissues and in tumors. Plasma flow rates are equal to (1-hematocrit)Q_B. The range of data in table 1 is striking, with three orders of magnitude separating the smallest from the largest values. Relatively little is known about tumor blood flows. They probably vary considerably as a function of tumor type. The relationship between spontaneous and implanted tumors is not clear. It has been reported (9) that the blood flow to Walker 256 carcinosarcoma increases with growth when this tumor is implanted in rat tails.

Membrane-Limited Models

When $Q/V >> PA/V$, the process is said to be membrane limited. This also applies formally to drug transport studies in tissue culture. Both can be solved within the framework of equations (1)-(3). Goldman et al (10) have analyzed the process of methotrexate transport in L1210 leukemia cells according to an asymmetric facilitated model:

$$jA = \frac{v_{max,en}\,C_e V}{K_{m,en} + C_e} - \frac{v_{max,ef}\,C_i V}{K_{m,ef} + C_i} \quad (4)$$

where v_{max} = maximum facilitated transport rate, K_m = Michaelis constant for the process, and the

TABLE 1.—Illustrative blood flow rates

Species	Organ	$\frac{Q_B}{V}$ (min^{-1})	Ref No.
Rat	Spleen	0.8	2
	Small intestine	0.9	2
	Bone marrow	0.29	2
	Transplanted Walker 256 carcinosarcoma	0.07	26
Rabbit	Transplanted VX-2 carcinoma	0.5	27
Dog	Spontaneous lymphosarcoma	1.2-18	28
Man	Adrenals	5	21
	Gray matter	0.8	21
	Liver plus portal system	0.41	21
	Red marrow	0.09	21
	Muscle	0.01/0.02/0.05	21

subscripts *e*, *i*, *en*, and *ef* refer respectively to extracellular, intracellular, entry, and efflux.

Methotrexate is bound very strongly to the intracellular enzyme dihydrofolate reductase. Werkheiser (11) observed a dissociation constant on the order of 10^{-11} M for rat liver preparations if it is a competitive inhibitor. It is not certain that this value is characteristic of intracellular dihydrofolate reductase, particularly in other species such as man, or that significant inter-tissue differences do not exist. This uncertainty is a key difficulty in the interpretation of methotrexate pharmacodynamics.

Figure 2 is a general diagram of uptake by cells in vitro if the transport is described by equation (4) and if the free intracellular concentration is negligibly small, until the dihydrofolate reductase capacity, a, is reached at the time t^*. The actual value of t^* can vary greatly. It depends upon the extracellular concentration (C_e), the dihydrofolate reductase capacity (a), and the cell permeability. For $C_i \simeq 0$

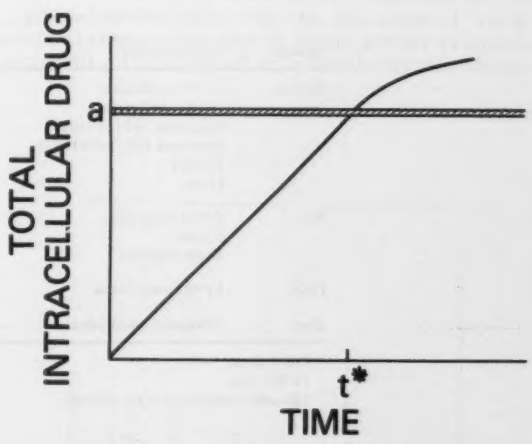

FIGURE 2.—Schematic diagram of methotrexate uptake by a cell or tissue exposed to a constant extracellular concentration. a = dihydrofolate reductase content; t^* = time at which strong binding capacity of dihydrofolate reductase is reached.

$$V\int_0^a dq = \frac{V_{max,en}V}{K_{m,en} + C_e}\int_0^{t^*} C_e\, dt \qquad (5)$$

or

$$t^* = \frac{a}{kC_e} \qquad (6)$$

$$\text{where } k = \frac{V_{max,en}}{K_{m,en} + C_e} = \frac{(PA)}{V}$$

Enzyme Synthesis

If t^* becomes significant compared with the time scale of dihydrofolate reductase synthesis, then a cannot be considered constant. An enzyme kinetic scheme which has been used successfully to model clotting factors includes a constant rate of production, k_o, and a first-order rate of removal by natural processes, $k_1 a$ (12).

Werkheiser and Ho (13) obtained a similar mechanism for dihydrofolate reductase in mouse liver. Hakala (14) considered the case of cells in logarithmic growth and developed the concept of "dynamic equilibrium" including drug-enzyme dissociation.

If a represents free enzyme which can be inactivated at a rate kC_e by influx of methotrexate, then

$$\frac{da}{dt} = k_o - k_1 a - kC_e \cdot \quad (7)$$

Since $a = a_o$ at $t = 0$ and $(k_o - k_1 a_o = 0)$ in the absence of prior drug effects,

$$t^* = \frac{1}{k_1} \ln \frac{kC_e}{kC_e - k_o} \cdot \quad (8)$$

Equation (8) produces a finite value for t^* only when the rate of drug influx, kC_e, is greater than the rate of enzyme synthesis, k_o.

Equation (8) can be written:

$$t^* = -\frac{1}{k_1} \ln\left[1 - \frac{k_o}{kC_e}\right]$$

so that for small k_o/kC_e

$$t^* \approx \frac{1}{k_1} \frac{k_o}{kC_e} = \frac{a_o}{kC_e}$$

since $a_o = k_o/k_1$. Equation (6) is thus a special case of equation (8) for $kC_e >> k_o$.

Illustrative Calculations

Tables 2 and 3 contain dihydrofolate reductase levels and cell membrane transport parameters for a

TABLE 2.—Selected dihydrofolate reductase concentrations

Species	Cell or tissue	Dihydrofolate reductase (μg methotrexate/g)	Ref No.
Mouse	L1210 leukemia	0.85	10
	L1210 leukemia	0.5	29
	Sarcoma 180 (parent)	0.17	14
	Sarcoma 180 (resistant)	12,*55†	14
	Kidney	0.3	7
	Liver	0.3	7
Rat	Small intestine	0.2	2‡
	Spleen	0.1	2‡
	Bone marrow	0.2	2‡
Dog	Lymphosarcoma	0.02-0.3	28
Man	"Induced" leukocytes	0.7	30

*22% free.
†2.6% free.
‡Based on intracellular volume.

TABLE 3.—Membrane transport of methotrexate

Species	Cell or tissue	$\frac{PA}{V}$ (min^{-1})	Ref No.
Mouse	L1210 leukemia	0.3	10*
		0.14	31†
	Sarcoma 180	0.005	14
	Skeletal muscle	0	2
Rat	Small intestine	0.031	2*
	Spleen	0.0082	2*
	Bone marrow	0.013	2*
Man	Granulocyte	0.01	32‡
	Small lymphocyte	0.003	32‡
	Lymphoblast (acute lymphocytic leukemia)	0.015	32§
		0.006	32§

*Ratio of v_{max} to K_m.
†Calculated from chart 1 of ref 31 (0.2 μM).
‡Calculated from chart 1 of ref 32 (0.2 μM).
§Calculated from chart 7 of ref 32 (0.2 μM).

number of tissues or cell types from several mammalian species. They were obtained or calculated from a variety of sources based upon both in vivo and in vitro data. The range is quite impressive: 0.02-55 μg methotrexate/g for a; 0-0.3 min^{-1} for k. This undoubtedly does not represent the extreme range that occurs. Dihydrofolate reductase levels are probably zero or very small in some nonproliferating tissues. Transport in kidney and liver has been modeled on the basis of flow limitation (6,7) which implies very high membrane permeabilities.

Example 1: rapid uptake.—Goldman et al (10) measured the rate of transport of methotrexate in L1210 leukemia cells in vitro.

$$k = (0.3\ \text{min}^{-1})\left(\frac{K_m}{K_m + C_e}\right) = \frac{(0.3)\ (1.8)}{1.8 + 1.0} = 0.19\ \text{min}^{-1}$$

$a = 0.85\ \mu\text{g MTX/g}$

$C_e = 1\ \mu\text{g/ml}$

From equation (6)

$$t^* = \frac{0.85}{(0.19)\ (1)} = 4.5\ \text{min.}$$

Under these conditions, the actual time required to reach nominal saturation of the dihydrofolate reductase would not be expected to have a significant influence on drug sensitivity under most conditions of incubation.

Example 2: slow uptake.—Zaharko et al (15) measured the rate of incorporation of deoxyuridine into several tissues of mice bearing Lewis lung carcinoma following implantation of a constant infusion drug cell. Plasma concentrations resulting from an infusion of 0.8 μg/hour are shown in figure 3. If the transient required to reach plateau values is neglected, C_e = 0.01 μg/ml. If transport parameters and enzyme levels for the small intestine are based on studies in the rat (2), from tables 2 and 3, a = 0.13 μg methotrexate/g (based on whole tissue) and k = 0.031 min^{-1}. From equation (6)

$$t^* = \frac{0.13}{(0.031)\ (0.01)} = 420\ \text{min} = 7\ \text{hr}.$$

This time is sufficiently long so that enzyme synthesis cannot be neglected. From Margolis et al (16, chart 6)

$a_0 = 0.15\ \mu\text{g MTX/g}$

$k_0 = 0.0074\ \mu\text{g/g hr}$

$k_1 = k_0/a_0 = 0.05\ \text{hr}^{-1}$

For k = 0.031 min^{-1} and C_e = 0.01 μg/ml, equation (8) yields

$$t^* = \frac{1}{0.05} \ln\left[\frac{(0.031)\ (0.01)\ (60)}{(0.031)\ (0.01)\ (60) - 0.0074}\right] = 10\ \text{hr}.$$

This estimate may be compared with experimental results shown in figure 4a. The deoxyuridine incorporation rate does reach its minimum value in mouse small intestine in the neighborhood of 10 hours. However, it does not go to zero even though a plasma concentration of 0.01 μg/ml is lethal to all mice if it is maintained.

It is interesting that incorporation of deoxyuridine into mouse bone marrow is depressed transiently but recovers and overshoots control values even in the presence of methotrexate (fig 4c). Rat bone marrow has an intercompartment transport parameter of only 0.013 min^{-1}, less than one half the value for small intestine with comparable enzyme levels.

Incorporation of deoxyuridine into Lewis lung tumors is essentially unaffected by exposure to 0.01 μg/ml of methotrexate (fig 4b). Estimates of transport parameters and enzyme levels are not available to permit an analysis of drug uptake by this tissue.

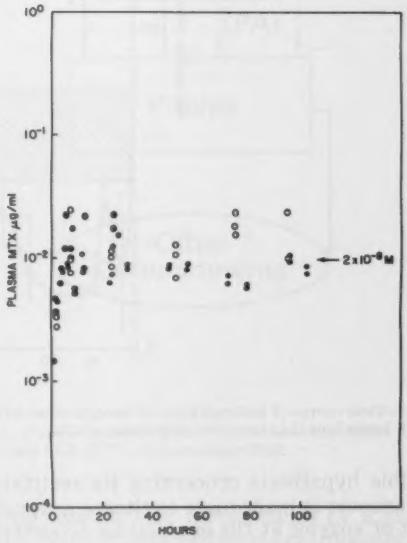

FIGURE 3.—Plasma concentration of methotrexate (MTX) in mice after subcutaneous implantation of 0.8 μg/hr cells (15). Each point represents a single mouse. Open circles = normal CDF$_1$ mice; closed circles = male CDF$_1$ mice bearing 0.5-1 g Lewis lung tumors.

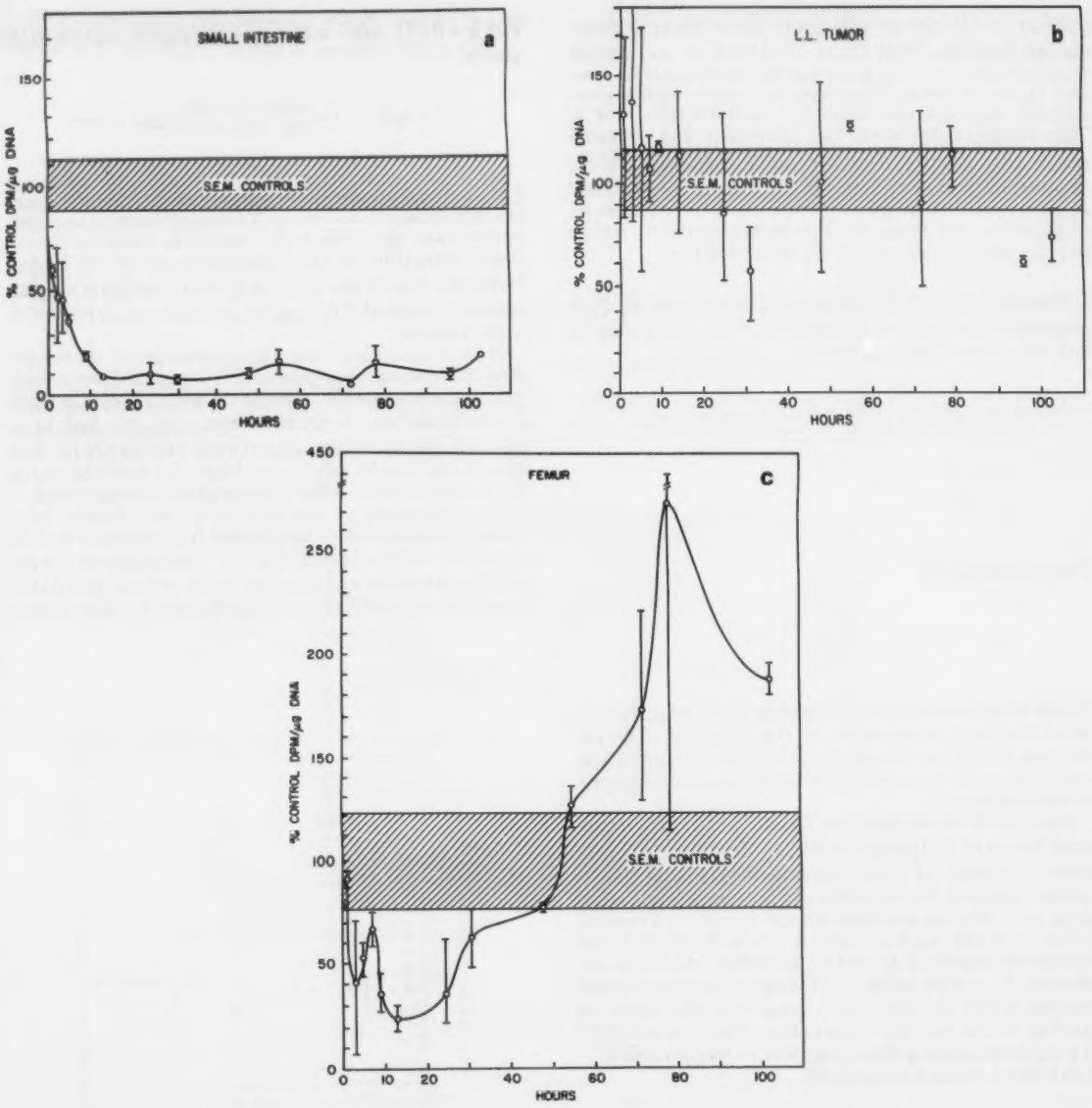

FIGURE 4.—Time course of incorporation of deoxyuridine-derived radioactivity into DNA after implantation of 0.8 μg/hr cells. Small intestine (a), Lewis lung (LL) tumor (b), and femur (c) (15).

A credible hypothesis concerning its resistance is that transport is inadequate to titrate a significant amount of enzyme at the low plasma concentration existing in the animals.

Transport Following Intravenous Pulse Injection

Tissues in the body are often exposed to rapidly changing plasma concentrations of a drug. The analysis of transport following an intravenous (iv) pulse injection is significantly more complex than when a constant plasma concentration is maintained. Even direct observations are difficult to interpret because flow and transport interact, and observed tissue concentrations include contributions from drug in both extracellular and intracellular space.

Figure 5 presents a model-dependent interpretation of the concentration dynamics in the bone marrow of a rat following an iv dose of 2.5 mg/kg (2,17).

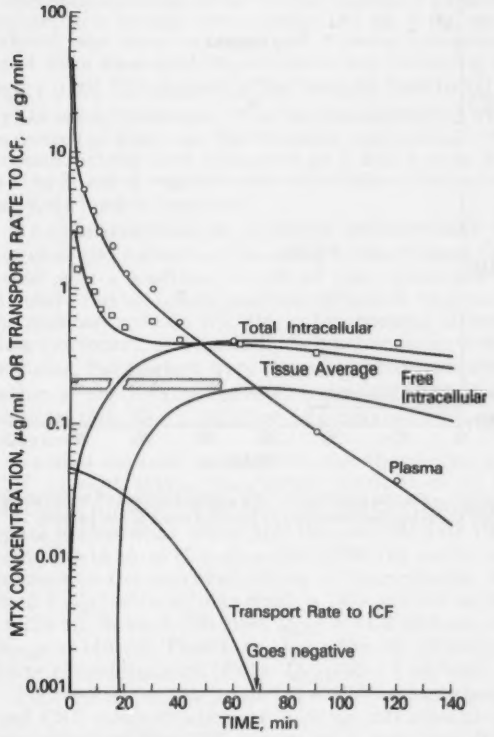

FIGURE 5.—Simulated concentrations and transmembrane transport rate of methotrexate (MTX) in rat bone marrow following 2.5 mg/kg iv. Observed data points represent one rat at each time interval. ICF = intracellular fluid. (Adapted from refs 2 and 17.)

Only plasma and average tissue concentrations were observed. We inferred the following from studies at several doses. At the perfusion rate of rat marrow, extracellular fluid concentration (not shown) follows plasma concentration quite closely. Methotrexate transport is facilitated and exhibits saturation kinetics with a Michaelis constant of 0.9 μg/ml; therefore, the high initial plasma (and extracellular fluid) concentrations do not produce a proportionately high drug influx.

Observed tissue concentrations are weighted averages of intracellular and extracellular drug; most of the drug in the tissues at short times is actually extracellular. The free intracellular concentration rises rapidly at about 20 minutes when the binding capacity of the intracellular dihydrofolate reductase is exceeded, but net influx continues until 70 minutes when the extracellular concentration falls below the free intracellular concentration. Then, a driving force for efflux exists.

Transport Between Plasma and Cerebrospinal Fluid

The previous intercompartment transport resistances occur at the level of the membrane separating intracellular from extracellular fluid. Certain macroscopic regions of the body such as ascites fluid, pleural fluid, and cerebrospinal fluid (CSF) would not be expected to follow closely changes in the plasma concentration.

Figure 6 is a simplified compartmental model to assess the magnitude of transport parameters between plasma and CSF. It is adapted from Gabelnick et al (18), who used it to model chloride transport in the cat brain. It is assumed that methotrexate distributes into a cerebral space, V_B, equal to brain tissue extracellular fluid plus CSF. Active transport in the choroid plexus or at extrachoroidal sites, passive transport, and removal of drug by bulk flow with the CSF may occur.

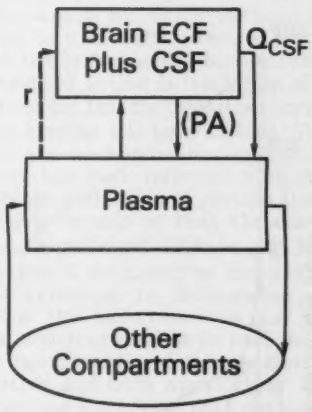

FIGURE 6.—Compartmental model to simulate transport between plasma and CSF. ECF = extracellular fluid.

Plasma kinetics may be simulated by a pharmacokinetic model or obtained from experimental measurements. A mass balance for the CSF compartment is

$$V_B \frac{dC_{CSF}}{dt} = r + (PA)(C_P - C_{CSF}) - Q_{CSF} C_{CSF} \qquad (9)$$

where r = rate of transport by active processes, (PA) = (permeability) (area) product for passive transport between plasma and CSF, and Q_{CSF} = CSF flow rate.

Some estimate of the magnitude of the terms in equation (9) can be obtained from inspection of the data shown in figure 7, which shows plasma and lumbar CSF concentrations of methotrexate during and following a constant iv infusion in one patient. If we neglect the effect of any active transport, eg, choroidal, on lumbar CSF concentrations, r may be assumed to be zero. At steady state, from equation (9),

$$(PA)\ (C_P - C_{CSF}) - Q_{CSF}\, C_{CSF} = 0.$$

Therefore, if 20 hours represents a substantial approach to steady state, from figure 7,

$$(PA) = Q_{CSF}\, \frac{C_{CSF}}{C_P - C_{CSF}} = \frac{Q_{CSF}}{30}.$$

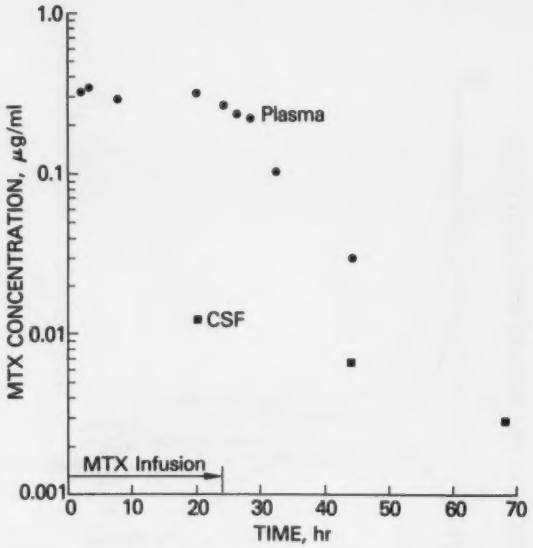

FIGURE 7.—Plasma and lumbar CSF concentrations of methotrexate (MTX) during and following 24-hr iv infusion in one patient.

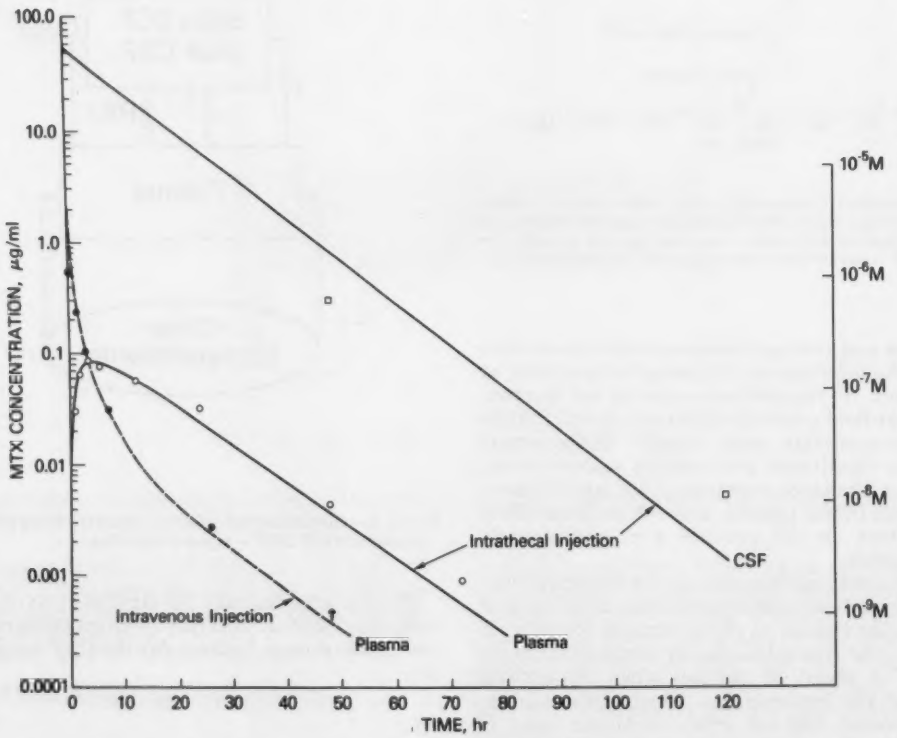

FIGURE 8.—Simulated and observed plasma concentrations following 20 mg of methotrexate (MTX) iv or intrathecally in one patient. Lumbar CSF concentrations are indicated following the intrathecal injection.

Patient Simulation

Methotrexate was given by two routes of administration to a young, very slender (53 kg, 6 ft), male patient who was in remission. Plasma concentrations were measured at selected times following 20 mg iv until the concentration became undetectable by the assay employed. Plasma concentrations were measured at intervals for 72 hours, and lumbar CSF concentrations were measured at 2 and 5 days following 20 mg of methotrexate administered intrathecally via lumbar puncture.

We characterized the systemic methotrexate kinetics of the patient on the basis of the iv dose. Our model was a modification (2) of that developed to simulate methotrexate pharmacokinetics in several mammalian species (7); the enterohepatic circulation was intact, and the CSF compartment (fig 6) was included. Parameters were chosen to produce a simulation of the plasma concentration following iv administration. The simulation is compared with data in figure 8.

We used the same model to predict the plasma and CSF concentrations that would result from an intrathecal (lumbar) injection. The brain extracellular space is somewhat uncertain. Davson (19) lists 10%-15%; Levin et al (20) give 18%-20% for inulin and sucrose in the cerebral cortex of four species. We used V_{ECF} (extracellular fluid) = 15% of 1500 ml (21) or 225 ml. Davson (19) cites Q_{CSF} = 31.2 ml/hour and V_{CSF} = 140 ml. Therefore, V_B =365 ml. From previous considerations, $(PA) = Q_{CSF}/30 = 1$ ml/hour.

Figure 8 shows the predicted and observed plasma and CSF concentrations following intrathecal administration. The CSF serves as a reservoir from which methotrexate is released slowly into the systemic circulation. The result is that the plasma concentration peaks at a much lower value following the intrathecal dose as compared with the iv dose but becomes and remains higher after 3 hours. The intrathecal route of administration could increase systemic toxicity because plasma concentrations on the order of 0.01 μg/ml or higher are maintained for about 36 hours compared with only 13 hours after the iv injection. Golman (22) has studied the pharmacokinetics of intrathecally administered metrizamide and analyzed his data with a one-compartmental open model with a delay in absorption from the CSF. His reported mean absorption rate constant (1.5 hr^{-1}) is considerably larger than our related value

$$\text{(approximately } \frac{PA + Q_{CSF}}{V_B} = 0.09\ hr^{-1}\text{)}.$$

The lumped CSF compartment we have used is clearly a grossly oversimplified basis for analysis of transport within the brain. Brain extracellular fluid and CSF cannot remain in equilibrium on the time scale of these observations (20). The CSF itself is not well mixed, and it is not certain how well lumbar concentrations mimic average CSF. Methotrexate may be taken up actively by the choroid plexus (23). We have observed that the concentration of methotrexate in ventricular CSF falls much more rapidly than the concentration in lumbar CSF during the first day after intraventricular injection. Also, disappearance from lumbar CSF is much more rapid during this time period than during the subsequent several days following lumbar administration.

DISCUSSION

We have discussed and attempted to interrelate a number of physical factors implicated in resistance to anticancer drugs. Formulations have been presented to assess the possible roles of blood or CSF flow, membrane transport, enzyme levels, and enzyme synthesis rates. Methotrexate serves as a useful model compound because of its clinical importance and because its transport and mechanism of action have been studied extensively in vitro and in vivo.

Attempts to optimize therapy must also include consideration of the cytokinetics of both tumor and sensitive normal tissue and how these may be affected by chemotherapeutic agents. Further, the actual detailed mechanism by which methotrexate exerts its cytocidal or cytostatic effect is not completely understood. It has frequently been assumed that its principal mode of action is inhibition of dihydrofolate reductase and that the inhibition correlates with very strong binding site interactions. The stability constant of the methotrexate:dihydrofolate reductase complex has been inferred from studies with soluble enzyme, and it is not certain that the same constant exists in cells or that variations between tissues are insignificant. Hakala (14) has stressed the importance of drug:enzyme dissociation as well as enzyme synthesis in determining sensitivity. Zaharko et al (15) have observed that plasma concentrations which are lethal to mice do not totally inhibit the incorporation of deoxyuridine into mouse small intestine and bone marrow (fig 4). Recently, Goldman (24) has postulated that methotrexate acts at both high- and low-affinity binding sites. The low-affinity sites require a relatively high concentration of free intracellular methotrexate for their effective inhibition. In addition, as reviewed by Goldman (25), membrane transport of methotrexate is complex and may involve both active efflux and coupling to a variety of other substances.

While pharmacokinetic considerations alone are not adequate for optimization of therapy, they provide an operational framework into which detailed biochemical and cytokinetic information can be incorporated. Pharmacokinetics permits quantitative descriptions of the local environment in selected tissues and provides a basis for manipulation of dose, schedule, and route of administration to exploit known or suspected differences between normal and malignant tissues.

REFERENCES

1. Bertino JR, and Johns DG. Folate antagonists. *In* Cancer Chemotherapy II, 22nd Hahnemann Symposium (Brodsky I, Kahn SB, and Moyer JH, eds). New York, Grune and Stratton, 1972, pp 9-22.
2. Dedrick RL, Zaharko DS, and Lutz RJ. Transport and binding of methotrexate in vivo. J Pharm Sci 62:882-890, 1973.
3. Dedrick RL, and Bischoff KB. Pharmacokinetics in applications of the artificial kidney. Chem Eng Progress Symposium Series 64, No. 84:32-44, 1968.
4. Dedrick RL, Forrester DD, and Ho DHW. In vitro-in vivo correlation of drug metabolism—deamination of 1-β-D-arabinofuranosylcytosine. Biochem Pharmacol 21:1-16, 1972.
5. Bischoff KB, and Dedrick RL. Thiopental pharmacokinetics. J Pharm Sci 57:1346-1351, 1968.
6. Bischoff KB, Dedrick RL, and Zaharko DS. Preliminary model for methotrexate pharmacokinetics. J Pharm Sci 59:149-154, 1970.
7. Bischoff KB, Dedrick RL, Zaharko DS, et al. Methotrexate pharmacokinetics. J Pharm Sci 60:1128-1133, 1971.
8. Dedrick RL. Animal scale-up. J Pharmacokinet Biopharm 1:435-461, 1973.
9. Oikawa M, and Milne ENC. A morphological and quantitative study of tumour blood flow during growth and immune rejection. Tohoku J Exp Med 112:325-338, 1974.
10. Goldman ID, Lichtenstein NS, and Oliverio VT. Carrier-mediated transport of the folic acid analogue, methotrexate, in the L1210 leukemia cell. J Biol Chem 243:5007-5017, 1968.
11. Werkheiser WC. Specific binding of 4-amino folic acid analogues by folic acid reductase. J Biol Chem 236:888-893, 1964.
12. Levy G. Comparative pharmacokinetics of the anticoagulant effect of coumarin drugs in man and rat. *In* Pharmacology and Pharmacokinetics (Teorell T, Dedrick RL, and Condliffe PG, eds). New York, IFI/Plenum, 1974, pp 339-348.
13. Werkheiser WC, and Ho DHW. Rates of synthesis and decay of dihydrofolate reductase (FH_2R) in mouse liver: influence of methotrexate (MTX) on the decay rate. Fed Proc 27:780, 1968.
14. Hakala MT. On the role of drug penetration in amethopterin resistance of Sarcoma-180 cells in vitro. Biochim Biophys Acta 102:198-209, 1965.
15. Zaharko DS, Dedrick RL, Peale AL, et al. Relative toxicity of methotrexate in several tissues of mice bearing Lewis lung carcinoma. J Pharmacol Exp Ther 189:585-592, 1974.
16. Margolis S, Philips FS, and Sternberg SS. The cytotoxicity of methotrexate in mouse small intestine in relation to inhibition of folic acid reductase and of DNA synthesis. Cancer Res 31:2037-2046, 1971.
17. Zaharko DS, and Dedrick RL. Applications of pharmacokinetics to cancer chemotherapy. *In* Pharmacology and the Future of Man (Proceedings of the 5th International Congress of Pharmacology, San Francisco, 1972). Basel, Karger, 1973, vol 3, pp 316-331.
18. Gabelnick HL, Dedrick RL, and Bourke RS. In vivo mass transfer of chloride during exchange hemodialysis. J Appl Physiol 28:636-641, 1970.
19. Davson H. Physiology of the Cerebrospinal Fluid. Boston, Little, Brown, 1967.
20. Levin VA, Fenstermacher JD, and Patlak CS. Sucrose and inulin space measurements of cerebral cortex in four mammalian species. Am J Physiol 219:1528-1533, 1970.
21. Mapleson WW. An electric analogue for uptake and exchange of inert gases and other agents. J Appl Physiol 18:197-204, 1963.
22. Golman K. Absorption of metrizamide from cerebrospinal fluid to blood. A pharmacokinetic study in man. J Pharm Sci. In press.
23. Rubin R, Owens E, and Rall D. Transport of methotrexate by the choroid plexus. Cancer Res 28:689-694, 1968.
24. Goldman ID. The mechanism of action of methotrexate. I. Interaction with a low-affinity intracellular site required for maximum inhibition of deoxyribonucleic acid synthesis in L-cell mouse fibroblasts. Mol Pharmacol 10:257-274, 1974.
25. ——.The characteristics of the membrane transport of amethopterin and the naturally occurring folates. Ann NY Acad Sci 186:400-422, 1971.
26. Gullino PM. The internal milieu of tumors. Prog Exp Tumor Res 8:1-25, 1966.
27. Edlich RF, Borner J, and Buchin RJ. Microcirculation of tumor. Influence of implantation site on tumor blood flow. Arch Surg 98:233-234, 1969.
28. Straw JA, Hart MM, Klubes P, et al. Distribution of anticancer agents in spontaneous animal tumors. I. Regional blood flow and methotrexate distribution in canine lymphosarcoma. J Natl Cancer Inst 52:1327-1331, 1974.
29. Zager RF, Frisby SA, and Oliverio VT. The effects of antibiotics and cancer chemotherapeutic agents on the cellular transport and antitumor activity of methotrexate in L1210 murine leukemia. Cancer Res 33:1670-1676, 1973.
30. Bertino JR, Cashmore AR, and Hillcoat BL. "Induction" of dihydrofolate reductase: purification and properties of the "induced" human erythrocyte and leukocyte enzyme and normal bone marrow enzyme. Cancer Res 30:2372-2378, 1970.
31. Kessel D, and Hall TC. Amethopterin transport in Ehrlich ascites carcinoma and L1210 cells. Cancer Res 27:1539-1543, 1967.
32. Kessel D, Hall TC, and Roberts D. Modes of uptake of methotrexate by normal and leukemic human leukocytes in vitro and their relation to drug response. Cancer Res 28:564-570, 1968.

Cytokinetic Aspects of Clinical Drug Resistance

Richard A. Bender[1] and Robert L. Dedrick[2,3,4]

Clinical resistance to antineoplastic chemotherapy continues to be one of the major problems in cancer treatment today. Such resistance may represent intrinsic properties of the tumor cell itself, although certain host factors such as drug activation and metabolism can also play a role. Tumor cell resistance generally results from cytokinetic, pharmacokinetic, or biochemical alterations in a sensitive cell population and may be natural or acquired. A consideration of cytokinetics and of the cytokinetic basis for resistance is the subject of this paper.

The Cell Cycle

Dividing cells traverse four phases during one cell division. These phases are illustrated in figure 1. Using tritiated thymidine incorporated into cells synthesizing deoxyribonucleic acid (DNA), it is possible to estimate the duration of these phases. Tritiated thymidine is incorporated during S phase, the DNA synthetic phase. In addition, ribonucleic acid (RNA) and protein synthesis probably continue as well. S phase is fairly constant for most cells in both normal and malignant tissue, lasting from 10 to 20 hours, although periods of up to 60 hours have been reported as seen in table 1. Following DNA replication, the cells enter a pre-mitotic period termed G_2 which is usually quickly followed by mitosis (M phase) lasting 30-90 minutes in most mammalian cells. However, recent studies suggest that there may be a considerable delay in the G_2 to M transition under certain circumstances (9,10). After mitosis several possible kinetic alternatives exist: (*a*) cells may continue in the proliferative cycle and enter the G_1 period; (*b*) they may move to one or more nondividing compartments where they undergo differentiation; (*c*) they may enter a nonproliferating compartment of cells which can no longer replicate and hence are "pre-terminal"; or (*d*) they may enter a similar compartment of cells that have not lost their replicative ability, the G_0 cells (11). In fact, some investigators (12-14) feel that a distinction between cells in G_0 and cells in a prolonged G_1 phase is artificial in that the period from the end of M to the commencement of S is a continuum of finite duration with cells leaving to enter S phase at various times (*see* fig 2). In any case, this group of cells proliferates slowly, a fact which limits their chemotherapeutic responsiveness as will be seen later. The time required for a given cell to traverse one cycle (T_c) in most human tumors is largely dependent on the duration of its G_1 and is quite variable. The T_c's for several of these tumors are summarized in table 1 where this range is evident.

Thus far, this paper has dealt with cell proliferation without considering cell attrition. Cell loss occurs from all three subgroups of a given cell population as seen in figure 3. Subgroups A and B comprise the viable cell mass with A representing the more rapidly cycling cells and B representing the "resting" cells in G_0 or a prolonged G_1. Cell loss from these groups is presumably small when compared to that from subgroup C, the preterminal subgroup

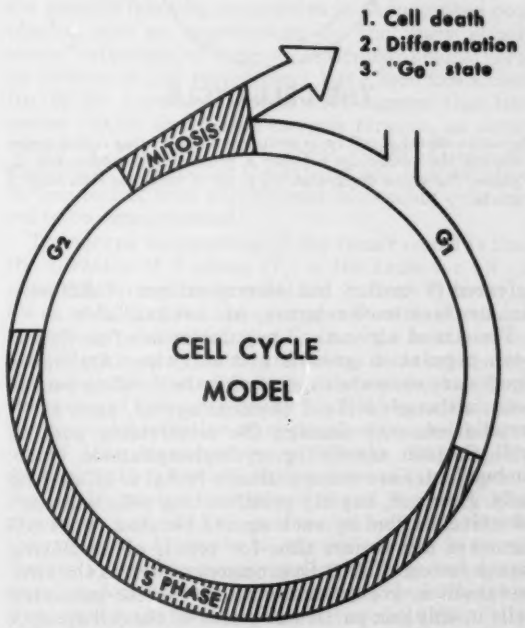

FIGURE 1.—Phases of cell cycle during one cell division.

[1]Laboratory of Chemical Pharmacology (LCHPH), Experimental Therapeutics (EXT), and Medicine Branch, Medical Oncology, Division of Cancer Treatment (DCT), National Cancer Institute (NCI), Bethesda, Md.

[2]Bio-Medical Engineering and Instrumentation Branch, Division of Research Services, National Institutes of Health, Bethesda, Md.

[3]We wish to thank Dr. Stanley Shackney for his helpful discussions and for the use of figures 5 and 6, and Dr. Vincent DeVita for allowing us to use figures 2 and 3.

[4]*Reprint requests to:* Richard A. Bender, MD, LCHPH, EXT, DCT, NCI, Bldg 10, Rm 12N226, National Institutes of Health, Bethesda, Md 20014.

TABLE 1.—Kinetic parameters of human neoplasms

Tissue	T_s (hr)	T_c (hr)	Growth fraction	Ref No.
Endometrial carcinoma	60	110	0.20	1
Lymphosarcoma	17	91	0.24	1
Basal cell carcinoma	19	36-96	0.29	2, 3
Epidermoid carcinoma	11	24-48	0.40	2, 3
Breast carcinoma	24	51	0.48-0.57	4
Acute myelogenous leukemia	10-20	15-134	0.11-0.65	5-7
Acute lymphocytic leukemia	10-20	15-134	0.15-0.65	5-8
Malignant melanoma	24	47	0.33-0.68	4
Stomach carcinoma	20	72-110	0.93	1

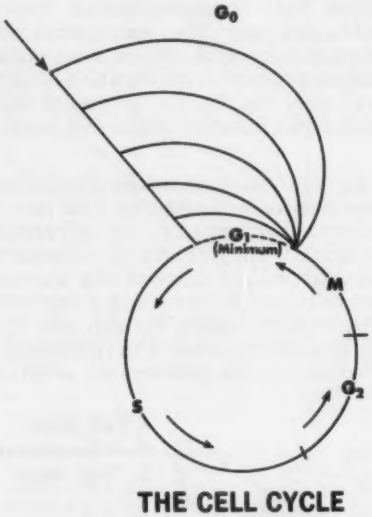

FIGURE 2.—Model of cell cycle with arcs of increasing radius representing the continuum between a prolonged G_1 phase and G_0 phase. The arrow designates the point at which the cells enter S phase.

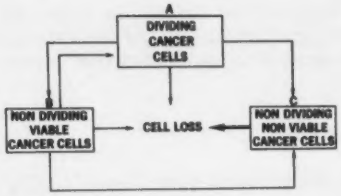

FIGURE 3.—Schematic representation of intercompartment mobility and differential cell loss.

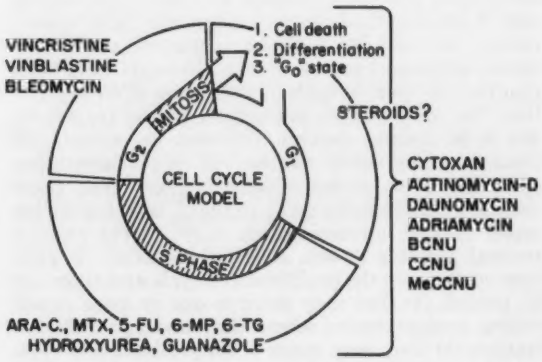

FIGURE 4.—Model of cell cycle demonstrating the specificity of various antitumor agents.

referred to earlier, but determinations of differential loss from each subgroup are not available.

The size of a given cell population is a function of both population growth and attrition. Antitumor agents are somewhat specific for the dividing pool of cells, although certain physical agents, such as X-irradiation, may damage the nondividing pool as well. Certain agents (eg, cyclophosphamide, chlorambucil, etc) are nonspecifically lethal to all cycling cells. However, rapidly proliferating cells are more effectively killed by such agents because rapid cell turnover allows less time for repair of alkylating agent-damaged DNA. Other agents, such as the antimetabolites, are generally phase-specific poisoning cells in only one particular phase of the cell cycle. A summary of the common antitumor agents and their specificity is illustrated in figure 4.

Chemotherapy Model

To illustrate the aforementioned concepts consider the following example: Two tumors of fixed population size, designated "A" and "B," are proliferating in a host and have cell cycle times of 16 and 24 hours respectively. In the first situation (fig 5), an S-phase-specific agent is given as a pulse at time = 0.

All those cells in S phase are lethally injured and drop out leaving the G_1 and G_2-M cells to continue to divide. Eight hours later the cell population appears as seen at "time = 8 hours, pre Rx." A second pulse of an S-phase-active agent is given killing all the remaining cells in tumor A, all of which happen to be in S phase, but only 56% of those cells in tumor B, since not all the cells were in S phase. Now, consider

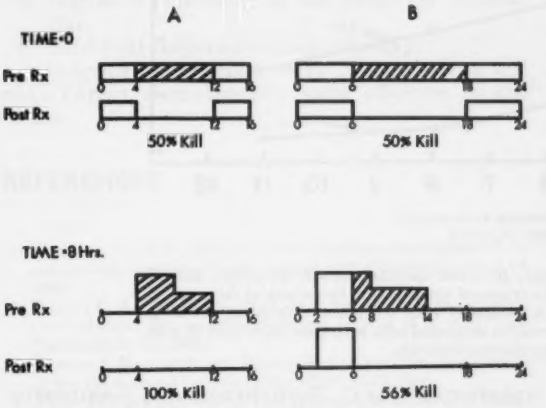

FIGURE 5.—Theoretic cell kill for tumors A and B with 16- and 24-hr cycle times, respectively, treated with an S-phase-specific agent every 8 hrs.

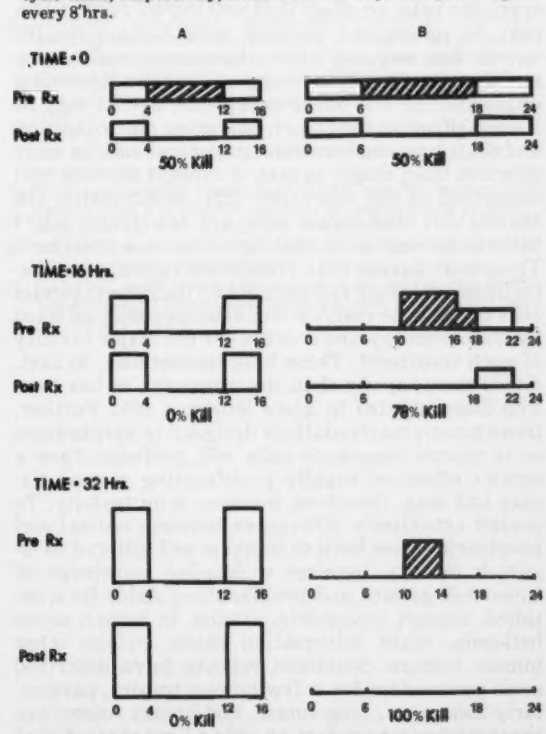

FIGURE 6.—Theoretic cell kill for tumors A and B with 16- and 24-hr cycle times, respectively, treated with an S-phase-specific agent every 16 hrs.

the same two tumors, but exposed to an S-phase-specific agent given on a different schedule, every 16 hours (fig 6). Such a schedule allows tumor A to divide and to increase in size following an initial 50% kill, whereas tumor B is eliminated following three doses of drug. The importance of scheduling antitumor chemotherapy, a point previously made by Skipper et al (15), is well illustrated by this example; however, the example relies on several assumptions whose validity we will now examine.

First, the model assumes that cells in tumors A and B are dividing regularly every 16 or 24 hours and that all the dividing cells have the same T_c. In fact, as mentioned earlier, T_c varies over a wide range. This point is illustrated by figure 7 where the observed tritiated thymidine labeling curve deviates from the expected one because of the wide variation in T_c for both murine and human leukemia (15). Further, such factors as population density may influence the T_c of a particular tumor in a Gompertzian fashion, where volume doubling time increases as tumor mass increases. Perhaps the most erroneous assumption is that all the tumor cells are cycling. In fact, as previously mentioned, a large portion of the total tumor cell population may actually be in G_0 or in a prolonged G_1 and hence these cells are somewhat insensitive to most antitumor agents. The portion of cells actually proliferating is called the "growth fraction" and its variability from tumor to tumor is illustrated in table 1. Increasing the growth fraction of a given tumor is termed "recruitment," and it is schematically represented in figure 8. An increase in the growth fraction eventuates in an increased population size as represented by the "new steady state." Attempts to improve antitumor chemotherapy in man by cell recruitment have been unsuccessful (16-18). Investigations in mice suggest that hormones (19,20) and tissue oxygen tension, as determined by proximity to a blood vessel (21,22), are capable of influencing the rate of cell proliferation in tissues but true recruitment of resting cells has yet to be demonstrated.

The second assumption of the tumor model is that the duration of S phase (T_s) is the same for all cycling cells in a given population. In fact, T_s is variable as well. Further, the cycling cells of most tumors are not synchronized, that is they do not traverse the cell cycle as a cohort, but rather do so separately and hence are "out of phase" with one another. Both the range of times necessary for DNA synthesis and the desynchronization of cycling cells make the timing of drug treatment very difficult. Only rapidly dividing animal tumors, such as exponentially growing L1210 murine leukemia (15) and Burkitt's lymphoma in man (23,24), conform to our illustrative assumptions. Attempts to improve cell kill in human tumors by synchronizing cycling cells have experienced modest success experimentally, but improved treatment responses have not followed (16,25).

The third assumption of our model is that all tumor cells in S phase are killed by exposure to chemotherapy. Further, it is assumed that those cells not

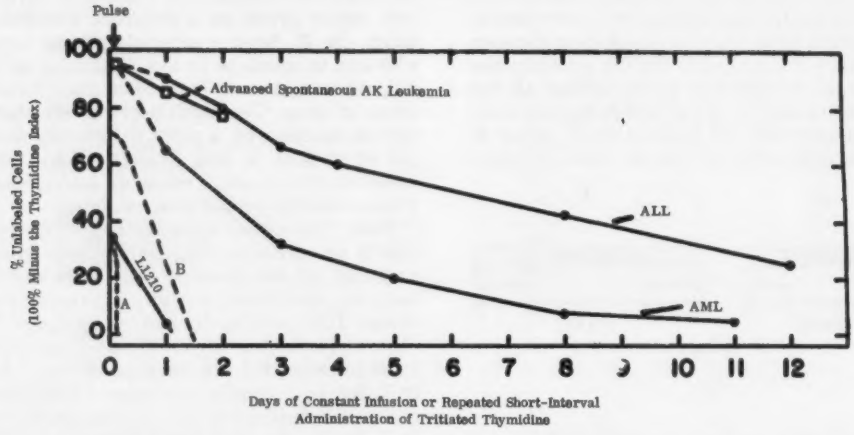

FIGURE 7.—Decrease in unlabeled cells of L1210 leukemia, advanced spontaneous AK lymphoma, and advanced human acute leukemias on constant exposure to tritiated thymidine vs hypothetical decreases calculated on a no-range. A. Hypothetical decrease in unlabeled cells with time calculated on a no-range basis for L1210 leukemia. B. Hypothetical decrease in unlabeled cells with time calculated on a no-range basis for acute lymphocytic leukemia or acute myelocytic leukemia.

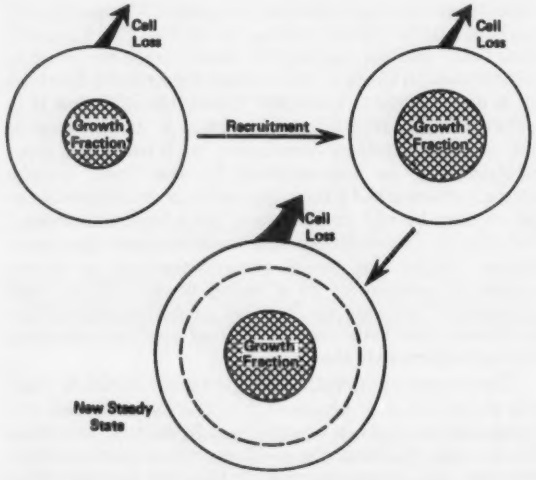

FIGURE 8.—Schematic representation of the effect of recruitment on both growth fraction and population size.

in S phase are unaffected by S-phase-specific chemotherapy. Neither of these assumptions is correct. In fact, not all cells in S phase will be lethally injured; some will only be damaged and others, perhaps, may be unaffected due either to resistance or to residence in a "pharmacologic refuge," such as the central nervous system or the center of a large tumor mass, where inhibitory drug levels may never be reached (26-28). Those damaged cells may continue to divide, but at a slower rate, due perhaps to prolongation of T_s or G_1. Such changes may compromise responsiveness to further chemotherapy. An increase in T_s results from retardation of the DNA synthetic rate, an effect that will impair responsiveness to subsequent therapy with S-phase-specific agents but may not alter phase-nonspecific agent responsiveness. This suggests that combining phase-specific and phase-nonspecific agents may be a more effective method of delivering chemotherapy and that drug combinations in general may be more effective than single agents, a concept already well supported in the literature (29). Additionally, the assumption that tumor cells are selectively killed without damage to normal host tissues is incorrect. Those host tissues that proliferate rapidly, the gastrointestinal tract epithelium and the hematopoietic cells of the bone marrow, are often severely affected by chemotherapy and account for the major toxicity of such treatment. These host tissues may, in fact, divide more rapidly than the neoplasm, as has been well demonstrated in acute leukemia (30). Further, those kinetic manipulations designed to synchronize or to recruit neoplastic cells will, perforce, have a similar effect on rapidly proliferating normal tissues and may, therefore, increase drug toxicity. To exploit cytokinetic differences between normal and neoplastic tissue both to increase cell kill and to diminish toxicity requires a detailed knowledge of tumor cell growth and proliferation. Aside from detailed, though incomplete, studies in human acute leukemia, scant information exists on the other human tumors. Scattered reports have described some parameters for a few human tumors, particularly melanoma, lung tumor, and breast tumor, but these studies report data on only a limited number of patients. Most other human tumors remain poorly characterized.

In summary, then, an analysis of tumor cell cytokinetics has revealed that chemotherapy responsiveness is a function of several interrelated factors. These are:

1. Tumor size and location.
2. Rate of cell proliferation.
3. Distribution of T_c and T_s in the cell population.
4. Variation in the growth fraction.
5. Degree of synchrony of the tumor cell population.
6. Sublethal response to chemotherapy.

It is hoped that further work in these areas will make cancer chemotherapy more effective in the future.

REFERENCES

1. Clarkson B, Ota K, Ohkita T, et al. Kinetics of proliferation of cancer cells in neoplastic effusions in man. Cancer 18:1189-1213, 1965.
2. Frindel E, Malaise E, Vassort F, et al. La cinétique de prolifération cellulaire des tumeurs humaines in vivo et in vitro. Bull Cancer 55:51-62, 1968.
3. Frindel E, Malaise E, and Tubiana M. Cell proliferation kinetics in five human solid tumors. Cancer 22:611-620, 1968.
4. Young RC, and DeVita VT. Cell cycle characteristics of human solid tumors in vivo. Cell Tissue Kinet 3:285-290, 1970.
5. Ota K. Kinetics of cellular proliferation in leukemia and cancer. Acta Haematol Jap 27:693-704, 1964.
6. Gavosto F, Pileri A, and Gabutti V. Effects of radiation on cellular proliferation and differentiation. *In* Proceedings of the International Atomic Energy Agency, Vienna, 1968, pp 275-281.
7. Mauer AM, and Fisher V. Characteristics of cell proliferation in four patients with untreated acute leukemia. Blood 28:428-445, 1966.
8. Gavosto F, Pileri A, Gabutti U, et al. Unusual blast proliferation and kinetics in acute lymphoblastic leukaemia. Eur J Cancer 5:343-348, 1969.
9. Wickramasinghe SN, Chalmers DG, and Cooper EH. Arrest of cell proliferation and protein synthesis in megaloblasts of pernicious anaemia. Acta Haematol 41:65-75, 1969.
10. Gelfant S, and Smith JG, Jr. Aging: noncycling cells—an explanation. Science 178:357-361, 1972.
11. Gavosto F, and Pileri A. Cell cycle of cancer cells in man. *In* The Cell Cycle and Cancer (Berserga R, ed). New York, Marcel Dekker, Inc., 1971, pp 97-128.
12. Haas RJ, Bohne F, and Fliedner TM. Cytokinetic analysis of slowly proliferating bone marrow cells during recovery from radiation injury. Cell Tissue Kinet 4:31-45, 1971.
13. Rosse C. Two morphologically and kinetically distinct populations of lymphoid cells in the bone marrow. Nature 227:73-75, 1970.
14. Yoshida Y, and Osmond DG. Identity and proliferation of small lymphocyte precursors in cultures of lymphocyte-rich fractions of guinea pig bone marrow. Blood 37:73-86, 1971.
15. Skipper HE, Schabel FM, Jr, Mellett LB, et al. Implications of biochemical, cytokinetic, pharmacologic, and toxicologic relationships in the design of optimal therapeutic schedules. Cancer Chemother Rep 54:431-450, 1970.
16. Lampkin BC, Nagao T, and Mauer AM. Synchronization and recruitment in acute leukemia. J Clin Invest 50:2204-2214, 1971.
17. Saunders EF, and Mauer AM. Reentry of nondividing leukemic cells into a proliferative phase in acute childhood leukemia. J Clin Invest 48:1299-1305, 1969.
18. Ernst P, and Killmann SA. Perturbation of generation cycle of human leukemic myeloblasts in vivo by methotrexate. Blood 38:689-705, 1971.
19. Perrotta CA. Effect of x-irradiation on DNA synthesis in the uterine epithelium. Radiat Res 28:232-242, 1966.
20. Bullough WS. Mitotic and functional homeostasis. A speculative review. Cancer Res 25:1683-1727, 1965.
21. Tannock IF. The relation between cell proliferation and the vascular system in a transplanted mouse mammary tumour. Br J Cancer 22:258-273, 1968.
22. Tannock IF, and Steel GG. Tumor growth and cell kinetics in chronically hypoxic animals. J Natl Cancer Inst 45:123-133, 1970.
23. Iversen OH, Iversen U, and Ziegler JL. Cell kinetics in Burkitt lymphoma. Eur J Cancer 10:155-163, 1974.
24. Ziegler JL, Morrow RH, Jr, Fass L, et al. Treatment of Burkitt's lymphoma with cyclophosphamide. Cancer 26:474-484, 1970.
25. Lampkin BC, McWilliams NB, and Mauer AM. Cell kinetics and chemotherapy in acute leukemia. Semin Hematol 9:211-223, 1972.
26. Henderson ES. Acute lymphoblastic leukemia. *In* Cancer Medicine (Holland JF, and Frei E, eds). Philadelphia, Lea and Febiger, 1973, pp 1173-1198.
27. Goldacre RJ, and Sylvén B. On the access of blood-borne dyes to various tumour regions. Br J Cancer 16:306-322, 1962.
28. Goldacre RJ, and Whisson ME. The biology of large solid tumours regressing with nitrogen mustard treatment: a study of the mouse plasma cell tumour ADJ-PC-5 and the Walker carcinosarcoma 256. Br J Cancer 20: 801-812, 1966.
29. Henderson ES, and Samaha RJ. Evidence that drugs in multiple combinations have materially advanced the treatment of human malignancies. Cancer Res 29:2272-2280, 1969.
30. Killmann SA. Acute leukemia. The kinetics of leukemic blast cells in man. An analytical review. Ser Haematol 1:38-102, 1968.

Kinetic Model for the Disposition and Metabolism of Moderate and High-Dose Methotrexate (NSC-740) in Man[1]

Paulo R. Leme,[2,3] Patrick J. Creaven,[4] Larry M. Allen,[4] and Mones Berman[2,5]

SUMMARY

A compartmental model was developed to describe the kinetics of the antimetabolite methotrexate in five patients who had carcinoma. Each patient received 80 mg/m² of the drug and three patients subsequently received a second higher dose (up to 1800 mg/m²). Methotrexate containing 250 microcuries of ^3H shown radiochromatographically to be better than 98% pure was given by rapid intravenous injection and plasma and urinary radioactivities were measured from 5 minutes to 90 hours after injection. The results were analyzed and modeled by means of the program SAAM, on a UNIVAC 1108 computer. The analysis shows that plasma activity consists of at least two distinct moieties, only one of which (defined as fast) serves as the dominant precursor to urine. The relative magnitude of the second moiety, defined as the slow one (half-life of 40-240 hours), increases with the larger doses of methotrexate administered, and because of this and the purity of the administered radioactivity it is believed not to be due to a contaminant. A two-compartment model was necessary to explain the first plasma moiety, considered as the methotrexate subsystem. These compartments seem to correlate in magnitude with the extracellular and intracellular body spaces. The second plasma moiety does not exchange with the two-compartment methotrexate subsystem and kinetically cannot be methotrexate. It is therefore suggested that the slow plasma moiety is a byproduct of methotrexate. Only about 60%-90% of the injected methotrexate was recovered in the urine after 4 days. A smaller fraction was recovered at the higher doses than at the lower ones. Considering that relatively little methotrexate is lost in the feces, a significant amount of the administered methotrexate is retained in the body for relatively long periods of time and could be the precursor for the slow plasma moiety observed. It was not possible to confirm this fully in our present studies, but if true, this could influence the estimation of the clinical effects of methotrexate over long periods of time. The paired studies on three of the patients (each at two dose levels) suggest that at least two methotrexate transports are nonlinear. At the higher plasma methotrexate levels the apparent initial space of distribution of methotrexate is increased and urinary clearance is reduced. The former suggests a rapid nonlinear distribution of methotrexate. These concentration-dependent transports have been incorporated into a single nonlinear model applicable to all methotrexate studies.

[Cancer Chemother Rep 59:811-817, 1975]

Folic acid analogs have been one of the most important groups of anticancer drugs since the introduction by Farber et al in the late 1940s of aminopterin[6] for the treatment of acute lymphoblastic leukemia (1). Methotrexate, the 10-methyl analog of aminopterin, is now the clinically used drug and has activity against leukemia and solid tumors including cancer of the breast and of the head and neck; it is dramatically effective against the rare trophoblastic tumor (for a review of the clinical activity of methotrexate, *see* Livingston et al [2]). Its activity is notably schedule dependent both against leukemia L1210 in mice (3) and clinically in the remission maintenance of acute lymphoblastic leukemia (4). It is also used in some nonneoplastic disorders, notably in severe psoriasis (5). Its action can be reversed by citrovorum factor[7] and the therapeutic advantage of giving very high doses of metho-

[1] Methotrexate: CAS reg. No. 59-05-2; glutamic acid, *N*-[*p*-[[(2,4-diamino-6-pteridinyl)methyl]methylamino]benzoyl]-; MTX; amethopterin.

[2] Laboratory of Theoretical Biology, Division of Cancer Biology and Diagnosis, National Cancer Institute (NCI), Bethesda, Md.

[3] *Present address:* Servico de Radioisótopos, Hospital do Servidor Público Estadual, São Paulo, Brazil.

[4] NCI-Veterans' Administration (VA) Medical Oncology Branch, VA Hospital, Washington, DC.

[5] *Reprint requests to:* Dr. Mones Berman, Laboratory of Theoretical Biology, Division of Cancer Biology and Diagnosis, NCI, Bg 10, Rm 4B56, National Institutes of Health, Bethesda, Md 20014.

[6] Aminopterin: NSC-739; CAS reg. No. 54-62-6; glutamic acid, *N*-[*p*-[[(2,4-diamino-6-pteridinyl]methyl]amino)benzoyl]-.

[7] Citrovorum factor: NSC-3590; CAS reg. No. 6035-86-5; glutamic acid, *N*-[*p*-[[(2-amino-5-formyl-5,6,7,8-tetrahydro-4-hydroxy-6-pteridinyl)methyl]amino]benzoyl]-, calcium salt; leucovorin; *N*⁵-formyltetrahydrofolate.

trexate followed by citrovorum factor rescue is under active investigation.

Methotrexate acts by binding very tightly to dihydrofolate reductase (6) and thus shutting off the synthesis of thymidine essential for the production of DNA.

The clinical pharmacology of this drug was first reported nearly 10 years ago by Henderson et al (7) and has been more recently investigated by Huffman et al (8). Extensive pharmacokinetic modeling has been carried out by Bischoff et al (9) and Zaharko et al (10) in lower animals, and these models have been more recently extended to man. In the course of pharmacologic investigations of moderate and high-dose methotrexate in man we initially developed a linear compartmental model which is described in this paper. Based on the results of the linear analysis in dual dose experiments it was concluded that a nonlinear model is more appropriate.

Five patients with advanced cancer (table 1) were studied at moderate doses (usually 80 mg/m^2); subsequently, three of these patients received a higher ($\geq$ 240 mg/m^2) intravenous (iv) dose of methotrexate labelled with radiochromatographically pure methotrexate. Plasma decay and urinary excretion were followed for 72 hours (figs 1 and 2). The ability to study three patients at two different dose levels each enabled us to use each patient as his own control and thus greatly enhance the sensitivity of the analysis.

All the modeling and data analysis was carried out on a UNIVAC 1108 computer using the SAAM computer program (11-13).

DEVELOPMENT OF THE MODEL AND RESULTS

One basic assumption inherent in the present analysis is the compartmental nature of the system. In order to identify the sites where concentration-dependent transport may occur, the kinetic data for each of the two studies on a single patient (figs 1 and 2 [patient No. 2] for lower and higher methotrexate doses) were first analyzed separately under the assumption that each followed linear (first-order) kinetics. This analysis led to a common model in which some parameter values had to be different between the high- and the low-dose kinetics, since the data, expressed as fraction of administered dose, do not superimpose. Based on the observed differences and known (or speculative) mechanisms of transport, concentration-dependent nonlinearities were introduced and a common model with identical parameter values for both lower and higher doses was developed.

Linear Model

In analyzing the data in terms of a first-order kinetic model, the transport of drug into and out of compartments is described by linear first-order differential equations with constant coefficients:

$$\frac{df_i}{dt} = L_{11}f_1 + L_{12}f_2 + \ldots - L_{1i}f_i - L_{2i}f_i - \ldots, \quad (i = 1, 2, \ldots, n)$$

where f_i is the amount of drug in compartment i and L_{ij} is the fractional rate of the drug transfer into compartment i from compartment j, in units of time^{-1}.

Three exponential terms were necessary and sufficient to satisfy the plasma data. Hence, a minimal three-compartment model was required (14). It was observed in all studies that the cumulative urinary methotrexate elimination curve was not proportional to the integral of the plasma curve. The ratio of plasma concentration to rate of urine excretion changed with the transition of the plasma curve from the fast to the slow phase. Since it is reasonable that urinary methotrexate derives from plasma, it was necessary to postulate that plasma methotrexate consists of at least two moieties and that the plasma data are a linear combination of these. It was further postulated that only one of the moieties served as a precursor for urinary methotrexate. In addition, a delay had to be introduced between plasma and urine to account for the slow initial build-up in the urine.

TABLE 1.—Patient diagnoses and previous treatment

Patient No.	Age (yrs)	Diagnosis	Prior therapy
1	56	Epidermoid carcinoma, oropharynx	Radiotherapy, surgery
2	42	Epidermoid carcinoma, tongue	Radiotherapy
3	64	Epidermoid carcinoma, floor of mouth	Radiotherapy, surgery
4	47	Epidermoid carcinoma, unknown primary	Streptozotocin, bleomycin
5	55	Carcinosarcoma, pyriform sinus	Surgery

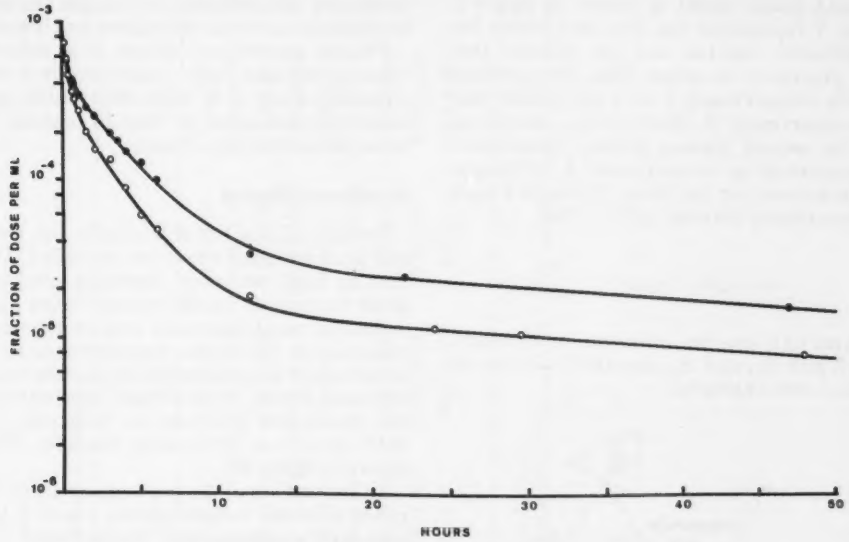

FIGURE 1.—Representive data (patient No. 2): plasma. Tracer concentrations in plasma for doses of 105 mg (○) and 350 mg (●) of methotrexate. Solid lines are computer-generated least squares model solutions.

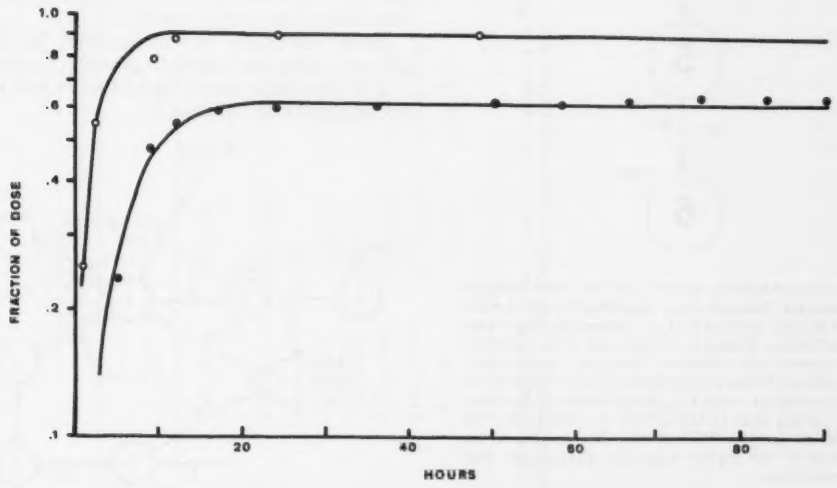

FIGURE 2.—Representative data (patient No. 2): urine. Cumulative urinary excretion after the administration of 105 mg (○) and 350 mg (●) of [^{3}H]-methotrexate. Solid lines are computer-generated least squares model solutions.

The proposed linear model is shown in figure 3. Compartment 1 represents the site into which the drug was initially injected and the moiety that serves as a precursor to urine. This compartment interacts with compartment 2 in a reversible way and with compartment 3 irreversibly, which accounts for the second plasma moiety. Cumulative urine is represented by compartment 6, with compartment 5 to account for the delay. Triangle 4 is, by definition, the sampled plasma, $q_4(t)$, so that

$$q_4(t) = S_{41}f_1(t) + S_{43}f_3(t)$$

where $f_1(t)$ and $f_3(t)$ are the contents in compartments 1 and 3 and S_{41} and S_{43} are the fractions of compartments 1 and 3 sampled.

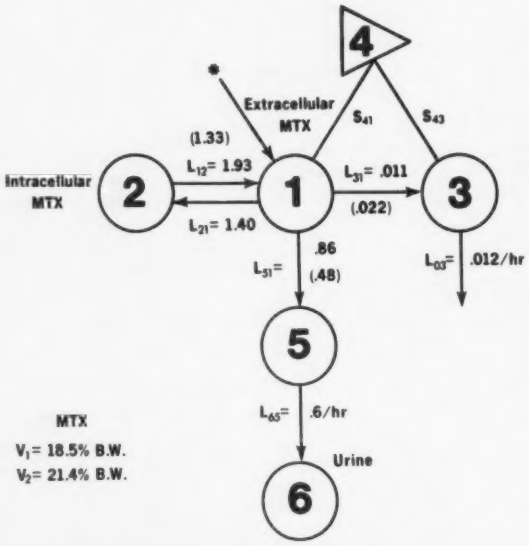

FIGURE 3.—Linear compartmental model used for methotrexate (MTX) kinetics analysis. Starred arrow identifies the site of tracer injection. Other arrows, marked by L_{ij}'s, represent drug transfer between compartments, defined by circles, and to the exterior. L_{ij} is fractional transfer rate constant. Triangle 4 is an operational unit representing plasma sampling as a linear combination of material in compartments 1 and 3. S_{ij} is coefficient of the linear combination. The values next to the arrows are means for the population studied at the low MTX levels. The values in the brackets are means at the higher doses for parameters that required a change in value.

For patients in whom studies were carried out at two dose levels, the parameter values were first calculated for each study separately. Attempts were then made to determine which parameters (based on their uncertainties) might have the same values at both dose levels. This was determined by fitting both sets of data simultaneously under the constraints that some parameters remain invariant (15). This procedure was followed for various parameter combinations in order to establish the changes that were necessary and sufficient to explain the differences in the kinetics between the higher and lower doses.

Plasma equivalent spaces (V_i), defined as hypothetical volumes that a substance in a compartment i would occupy if it were distributed at a uniform concentration equal to that in plasma, were calculated for each compartment.

Nonlinear Model

Results of the linear analysis for the individual and paired studies are given in table 2. They suggest that at least two rate constants need to change in order to explain the differences in the kinetics: a decrease in renal clearance and an increase in tissue retention at the higher methotrexate levels. Since a single set of parameters must satisfy both high- and low-dose levels, a nonlinear concentration-dependent model was proposed to integrate the changes with dose in a continuous manner. This model is shown in figure 4.

In the nonlinear model, compartment 7 was interposed between compartments 1 and 3 to provide a very rapid exchange with compartment 1. A Michaelis-Menten type saturation in the return from compartment 7 to compartment 1 was introduced which, at high doses, favors the accumulation of methotrexate in compartments 7 and 3. Compartment 8 was also added in this model to represent the slow plasma component being supplied by compartment 3. Compartment 8 is assumed to occupy the same space (extracellular) as compartment 1.

Renal excretion is represented by a nonlinear process using the function given in figure 4.

The nonlinear model is tentative and requires additional data to validate it.

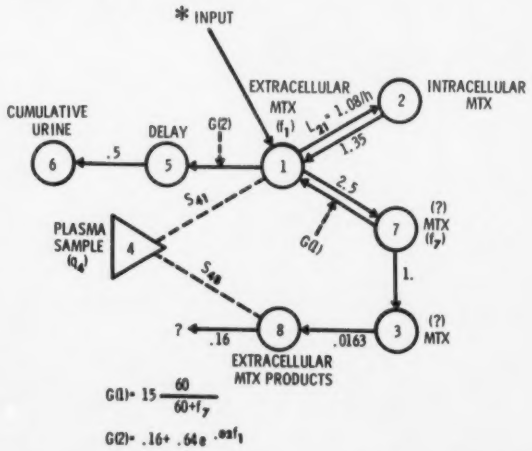

FIGURE 4.—Nonlinear compartmental model for methotrexate (MTX). Conventions are the same as in fig 3. *G(1)* and *G(2)* are control functions for the transports L_{51} and L_{17}. ? Indicates uncertainty as to whether compartment contains MTX or a byproduct of MTX. The question mark next to the loss from compartment 8 indicates an unknown loss route. *See* Discussion section for further explanations.

TABLE 2.—Calculated compartmental model parameters from 5 patient studies*

	Patient No.	1		2		3		5	4
Parameters	Dose (mg)	122	540	105	350	110	2400	105	142
L_{21}		1.81±0.34	1.52±0.18	1.63±0.14	0.71±0.08	1.95±0.15	1.76±0.14	2.07±0.46	2.19±0.25
L_{12}		1.44±0.13		1.55±0.14		1.28±0.09		1.33±0.19	1.40±0.18
L_{31}		0.056±0.051	0.161±0.031	0.102±0.044	0.169±0.012	0.190±0.047	[0.442-0.056]†	0.110±0.053	[0.526-0.067]†
L_{03}		0.0120±0.0015		0.0175±0.0025		0.0025±0.0005		0.0060±0.0047	0.021±0.005
L_{51}		0.98±0.06	0.71±0.03	0.86±0.05	0.32±0.02	0.75±0.05	0.4±0.1	0.84±0.01	[0.319±0.778]
L_{05}		0.31±0.05	0.46±0.09	2.0±0.5	0.23±0.03	1.26±0.30	—	0.170±0.086	—
V_1		0.156±0.004	0.169±0.003	0.185±0.005	0.278±0.006	0.164±0.005	0.128±0.002	0.226±0.023	0.175±0.003
V_2		0.194±0.006	0.177±0.005	0.194±0.008	0.127±0.004	0.248±0.008	0.176±0.018	0.35±0.03	0.273±0.006
V_3		0.72±0.7	2.3±0.4	1.08±0.51	2.7±0.4	1.24±0.30	[22.0−2.9]	4.1±3.7	[4.4-0.56]

*Values for dose are in mg of methotrexate, for L_{ij} in hour^{-1}, and for V_i in fraction of body weight; errors associated are SD.

†Due to lack of data on urinary excretion from these studies, all values within brackets are calculated ranges based on the lower and higher urine recovery found in the literature: 37.8% and 93%, respectively.

DISCUSSION

The average plasma equivalent volume (PEV) of distribution of compartment 1 (18.5% of body weight) approximates extracellular space and is in agreement with recent results of Freeman (16). Henderson et al (7) reported a much higher value; however, it was based on the average from studies in which the doses were administered both iv and orally and the authors did not take into account the "fast" component of the plasma clearance in half of the studies. We recalculated the volume of distribution from their iv data alone and found an average value of about 21% of body weight.

Compartment 2 washes out almost completely during the first 24 hours after administration of the drug. Chromatography performed by Johns et al (17) showed that the radioactivity eliminated in the urine during the first 48 hours consisted almost entirely of unchanged methotrexate. This suggests that compartment 2 in our model consists predominantly of unbound or lightly bound methotrexate.

Since compartment 1 already accounts for practically all of the extracellular spaces, compartment 2 most likely represents an intracellular space. It has a plasma equivalent space of about 21% body weight and is lower than total intracellular space. From the studies of Fountain et al (18) it is known that in small animals methotrexate concentrates primarily in the liver and the kidney and to a lesser extent in other tissues. This may also be true in man.

Compartment 7 (fig 4) is not identified physiologically. It is relatively small at low plasma methotrexate levels but becomes larger at higher levels. We shall consider some possibilities for this later.

Compartment 3 accounts for the slowest exponential term in the plasma curve contributing, through compartment 8, a concentration of only about 2% of the initial concentration. We know from the urine excretion data that compartment 8 is not methotrexate. We also do not think that it is a contaminant introduced with the initial injection for several reasons. First, chromatographic analysis of the injected material showed that at least 98% of the label was in the form of methotrexate. Second, the slow component is not a constant fraction of the injected activity at the higher and lower dose levels. Third, there is a consistent failure to account for up to 30% of the injected activity in urine at the higher dose levels, consistent with concomitant increases in plasma levels of the slow component.

An attempt to feed the output from compartment 8 to urine resulted in too much radioactivity in the urine. Only a fraction of this could be allowed, with the rest most likely going to feces.

It is not known what compartment 3 represents. It could be intracellular methotrexate bound to dihydrofolate reductase. Fountain et al (18) demonstrated that injected methotrexate persists for periods up to 8 months in certain mouse tissues such as liver and kidney, and it has been suggested (18-20) that this long retention is due to the binding of the drug to this enzyme. Studies carried out by Johns et al (17) have shown that, in man, tritiated methotrexate binds to the enzyme dihydrofolate reductase and that it can readily be displaced unchanged by other compounds having affinity for the enzyme for up to 26 days after methotrexate administration. Compartment 3 in the model turns over somewhat faster than the enzyme-bound intracellular methotrexate mentioned in the studies here. It is possible, however, that it represents a combination of enzyme and other less specific binding.

There is no evidence that intracellular methotrexate is metabolized to yield plasma byproducts. On the other hand, bacteria in the intestinal flora are known to take up methotrexate and to degrade it. Such a mechanism could explain compartments 3 and 8, and the increased uptake to methotrexate by compartment 3 at the higher dose levels. Methotrexate enters the gastrointestinal tract through biliary secretion and may be either reabsorbed, excreted, or taken up by bacteria and be degraded. At high methotrexate levels however, reabsorption saturates, making more methotrexate available for bacterial absorption and subsequent degradation. Under this scheme, compartment 7 of the model corresponds to the methotrexate in the intestinal lumen available for recycling, and L_{17} is the saturable reabsorption path. Compartment 3 would correspond to bacteria-absorbed methotrexate and compartment 8 would correspond to the released degradation products. Obviously the physiologic nature of compartments 7 and 3 could have important implications relative to the therapeutic efficacy of methotrexate at high and low doses.

A delay in the urinary excretion was observed in some but not all studies. At present, no physiologic explanation can be given for this delay.

A decrease in the urinary clearance rate with increasing methotrexate concentrations is in line with previously reported kidney clearance studies by Leigler et al (21). At high concentrations, the clearance is comparable to the filtration rate and at low concentrations it is about five times higher. Thus, at low concentrations there is a considerable loss of methotrexate through an active secretion process. The decrease in urinary clearance at higher methotrexate levels still further enhances the accumulation of methotrexate in the tissues and the intestinal flora.

REFERENCES

1. Farber S, Diamond LK, Mercer RD, et al. Temporary remissions in acute leukemia in children produced by folic acid antagonist, 4-aminopteroylglutamic acid (aminopterin). N Engl J Med 238:787-793, 1948.
2. Livingston RB, and Carter SK. Single Agents in Cancer Chemotherapy. New York, IFI/Plenum, 1970.
3. Goldin A, Venditti JM, Humphreys SR, et al. Modification of treatment schedules in the management of advanced mouse leukemia with amethopterin. J Natl Cancer Inst 17:203-212, 1956.

4. Selawry OS, Hananian J, Wolman IJ, et al. New treatment schedule with improved survival in childhood leukemia. JAMA 194:75-81, 1965.
5. Van Scott EJ, Auerbach R, and Weinstein GD. Parenteral methotrexate in psoriasis. Arch Dermatol 89:550-556, 1964.
6. Osborn MJ, Freeman M, and Huennekens FM. Inhibition of dihydrofolic reductase by aminopterin and amethopterin. Proc Soc Exp Biol Med 97:429-431, 1958.
7. Henderson ES, Adamson RH, and Oliverio VT. The metabolic fate of tritiated methotrexate. II. Absorption and excretion in man. Cancer Res 25:1018-1025, 1965.
8. Huffman DH, Wan SH, Azarnoff DL, et al. Pharmacokinetics of methotrexate. Clin Pharmacol Ther 14:572-579, 1973.
9. Bischoff KB, Dedrick RL, Zaharko DS, et al. Methotrexate pharmacokinetics. J Pharm Sci 60:1128-1133, 1971.
10. Zaharko DS, Dedrick RL, Bischoff KB, et al. Methotrexate tissue distribution: prediction by a mathematical model. J Natl Cancer Inst 46:775-784, 1971.
11. Berman M, and Weiss MF. Users' Manual for SAAM. Public Health Service Publication No. 1703, Bethesda, Md, National Institutes of Health, 1967.
12. Berman M, Shahn E, and Weiss MF. The routine fitting of kinetic data to models. A mathematical formulism for digital computers. Biophys J 2:275, 1962.
13. Berman M, Weiss MF, and Shahn E. Some formal approaches to the analysis of kinetic data in terms of linear compartmental systems. Biophys J 2:289, 1962.
14. Berman M, and Schoenfeld R. Invariants in experimental data on linear kinetics and the formulation of models. J Appl Physics 27:1361-1370, 1956.
15. Berman M. A postulate to aid in model building. J Theor Biol 4:229, 1963.
16. Freeman MV. The fluorometric measurement of the absorption, distribution, and excretion of single doses of 4-amino-10-methyl pteroylglutamic acid (amethopterin) in man. J Pharmacol Exp Ther 122:i54, 1958.
17. Johns DG, Hollingsworth JW, Cashmore AR, et al. Methotrexate displacement in man. J Clin Invest 43:621, 1964.
18. Fountain JR, Hutchison DJ, Waring GB, et al. Persistence of amethopterin in normal mouse tissues. Proc Soc Exp Biol Med 83:369, 1953.
19. Nichols CA, and Welch AD. On the mechanism of action of aminopterin. Proc Soc Exp Biol Med 74:403, 1950.
20. Greenspan EM, Goldin A, and Schoenbach EB. Influence of the citrovorum factor and folic acid on the toxic manifestations of aminopterin. Cancer 4:619, 1951.
21. Leigler DG, Henderson ES, Hahn MA, et al. The effect of organic acids on renal clearance of methotrexate in man. Clin Pharmacol Ther 10:849, 1967.

Preliminary Pharmacokinetic Model for Adriamycin (NSC-123127)[1,2]

Phillip A. Harris[3] and Joseph F. Gross[4,5,6,7]

SUMMARY

The systematic chemical control of cancer requires a quantitative knowledge of the pharmacologic disposition of antitumor drugs in both healthy and malignant tissues in the body. Pharmacokinetic models can predict the drug concentration in both tumor sites and healthy organs and hence may provide a predictive capability regarding both antitumor action and concomitant toxicity. Adriamycin is an anthracycline antibiotic that has been demonstrated to possess a broad spectrum of antitumor activity against malignancies in animals and man, particularly solid tumors. Its major toxicity is manifested by the depression of normal cell proliferation in the bone marrow and a delayed dose-dependent cardiac toxicity eventually resulting in congestive heart failure. This study is concerned with the development of a predictive analytic model for the pharmacokinetics of adriamycin. The analytic approach embodies a physiologic multicompartmental model as a framework. This model postulates that specific organs or tissue masses may be simulated by a compartment whose elements consist of physiologic properties such as tissue volume and blood flow and pharmacologic behavior such as tissue binding and metabolic activity. A mass balance is set up across each compartment and all compartments are linked by an independent blood compartment. The mass balance includes terms representing inflow and outflow of the drug as well as its metabolism, protein-binding, and other pharmacologic behavior. A model has been developed that has ten compartments which represent the plasma, heart, liver, kidney, lung, lean tissue, adipose tissue, gut, bone marrow, and spleen. Solutions of the system of equations yield the time course of the drug in each organ. Predictions of adriamycin concentration-time curves in the ten tissues after intravenous (iv) administration were generated using this model. With few exceptions, agreement between predicted and actual tissue data in rabbits was excellent. Human plasma levels of adriamycin were predicted and comparison with patient data demonstrated a reasonable first approximation.

INTRODUCTION

Clinical trials have demonstrated the broad and significant antineoplastic activity of the anthracycline antibiotic, adriamycin (1-4). This drug is derived from *Streptomyces peucetius* var. *caesius* (5) and is the 14-hydroxy derivative of daunorubicin,[8] a chemotherapeutic agent primarily used in the treatment of acute leukemia. The major toxic effect of adriamycin is the depression of normal cell proliferation (1-3,6) in the bone marrow and a delayed cumulative dose-dependent cardiomyopathy (7,8) resulting in congestive heart failure. The therapeutic potential of adriamycin is seriously limited by these toxic effects. In order to optimize the therapeutic utilization of adriamycin, a thorough understanding of the pharmacokinetics of this drug appears to be desirable.

Arena et al (9) were the first investigators to report on the pharmacokinetics of adriamycin in mice and rabbits. They used a fluorometric method and showed that the drug was extensively incorporated into tissues and that the concentrations remained substantially constant from 4 to 24 hours. The concentrations in most organs were at least one to two orders of magnitude greater than blood levels. Further, it was demonstrated that biliary excretion was the primary route of elimination. Similar results were obtained by Di Fronzo et al (10) and Yesair et al (11) who used ^{3}H-labeled adriamycin and total fluorescence respectively. In mice, the uptake of adriamycin into most tissues appeared to be greater than the daunorubicin uptake (10) and it has been suggested this may account for the higher in vivo cytotoxicity at equal doses and greater antitumor activity of adriamycin. In addition, neither adriamycin nor daunorubicin readily penetrates into the brain (10). More recently, Bachur et al (12) have reported data that compares the disposition of adriamycin and daunorubicin in rabbits. They used analytic methods which appeared to be more specific than those used in previous investigations in that unchanged drug and metabolites are separated before being quantified. Both adriamycin and daunorubicin were shown to be extensively metabolized in rabbits. There was no consistent striking difference in tissue concentrations of the two unchanged drugs although most organs contained greater amounts of total fluorescent daunorubicin metabolites than total fluorescent adriamycin metabolites.

[1]Supported by contract N01-CM-23241 from the Division of Cancer Treatment (DCT), National Cancer Institute (NCI), National Institutes of Health, Department of Health, Education, and Welfare.

[2]Adriamycin: CAS reg. No. 23214-92-8; doxorubicin. Supplied by the Drug Development Branch, Drug Research and Development, DCT, NCI.

[3]University of California at Los Angeles, Harbor General Hospital, Torrance, and University of Southern California, Los Angeles.

[4]University of Arizona, Tucson.

[5]The authors wish to express thanks to Mr. Owen Nelson for his assistance and excellence in computer programming and Dr. Robert Dedrick of the NIH for his assistance and many valuable suggestions.

[6]Requests for assistance in the utilization of the model described in this paper and associated computer program are welcome.

[7]*Reprint requests to:* Dr. Phillip A. Harris, Division of Medical Oncology, Department of Medicine, Harbor General Hospital, 1124 West Carson St, Torrance, Calif 90502.

[8]Daunorubicin: NSC-82151; CAS reg. No. 23541-50-6.

The concentration-time course of adriamycin (and quite possibly metabolites) in normal tissues and tumors is important in the toxic events and therapeutic outcome that accompany adriamycin treatment. Prediction of adriamycin concentrations can only be accomplished if a model for the pharmacokinetics is available, and necessarily, these predictions must first be made in animals so that extensive verification is possible. This paper presents an initial model for the pharmacokinetics of adriamycin in rabbits. Our approach is based on a physiologic multicompartmental model which has been described elsewhere in detail (13-15).

MODEL DEVELOPMENT

A multicompartment physiologic approach to the pharmacokinetic modeling of adriamycin was selected on the basis of previously published information that established the high tissue affinity for adriamycin (9-11). It seemed unlikely that a model based only on a fit of the plasma concentration-time curve would be beneficial in predicting other specific target organs or tumor concentrations of adriamycin. In order to establish a physiologic model, the parameters governing the behavior of a drug in any given tissue must be defined. A blood flow-limited distribution rate model was used as a first approximation. Average blood flow values were obtained from previously reported data. The volume of each tissue was determined in order to compute concentration. Parameters describing the interaction of adriamycin with the tissues were obtained by experimentation. These included intestinal absorption, plasma protein binding, tissue affinity, and elimination.

Ten compartments including the plasma were modeled. The total mass of these compartments constituted approximately 80% of the total body mass. The skeleton (except for the marrow) and the central nervous system were the major tissues not included. Of particular importance was the inclusion of the heart and bone marrow as compartments in the model since these tissues are the major sites of life-threatening adriamycin toxicity. The organization of the compartments is shown in figure 1. The lines connecting the compartments represent the flow of blood (Q). The blood flow to the liver consists of the hepatic arterial supply and the outflow of the spleen and gut, the hepatic portal venous supply. These flows were considered to act equivalently in the liver with regard to adriamycin uptake and elimination. The hepatic arterial flow was assumed to represent 25% of the total hepatic flow. All adriamycin elimination processes were summed and are depicted as the dotted line from the liver.

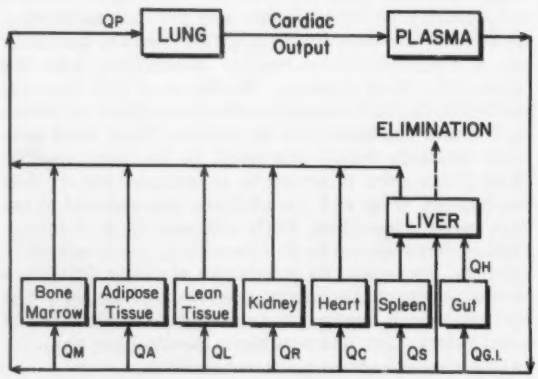

FIGURE 1.—Schematic diagram of the 10-compartment pharmacokinetic model for adriamycin; see text for details.

A conservation equation is written for each compartment that includes the physiologic and disposition parameters relevant to the compartment. A general form of such a conservation equation for a compartment, α, is given by:

$$\frac{dC_\alpha}{dt}\left\{\gamma_{\alpha B} V_{\alpha B} + \gamma_{\alpha T} V_{\alpha T}\right\} = Q_\alpha \left\{\phi_{\alpha B} C_B - \phi_{\alpha T} C_\alpha\right\} + Z_\alpha$$

where: $\gamma_{\alpha B} = f_B + (1 - f_B)(K_B + \lambda'_{\alpha B})$

$$\gamma_{\alpha T} = f_\alpha + (1 - f_\alpha)(K_\alpha + \lambda'_{\alpha T})$$

$$\lambda'_{\alpha B} = \frac{K_{B1} B_{B1}}{(1 + K_{B1} C_\alpha)^2} + \cdots\cdots + \frac{K_{Bn} B_{Bn}}{(1 + K_{Bn} C_\alpha)^2}$$

$$\lambda'_{\alpha T} = \frac{K_{\alpha 1} B_{\alpha 1}}{(1 + K_{\alpha 1} C_\alpha)^2} + \cdots\cdots + \frac{K_{\alpha n} B_{\alpha n}}{(1 + K_{\alpha n} C_\alpha)^2}$$

$$\phi_{\alpha B} = f_B + (1 - f_B)(K_B + \lambda_{\alpha B})$$

$$\phi_{\alpha T} = f_\alpha + (1 - f_\alpha)(K_\alpha + \lambda_{\alpha T})$$

$$\lambda_{\alpha T} = \frac{K_{\alpha 1} B_{\alpha 1}}{(1 + K_{\alpha 1} C_\alpha)} + \cdots\cdots + \frac{K_{\alpha n} B_{\alpha n}}{(1 + K_{\alpha n} C_\alpha)}$$

$$\lambda_{\alpha B} = \frac{K_{B1} B_{B1}}{(1 + K_{B1} C_\alpha)} + \cdots\cdots + \frac{K_{Bn} B_{Bn}}{(1 + K_{Bn} C_\alpha)}$$

Z_α = metabolism, transport term

C_α, C_B = free concentration in α and blood

Q_α = blood flow in α

$V_{\alpha B}$, $V_{\alpha T}$ = volume of blood and tissue in α

This formulation is for a flow-limited model and it provides a very general representation for including linear and nonlinear binding in tissue, equilibrium blood, and the blood compartment. The rate of change of the drug in the α-compartment is given by the term on the left-hand side of the equation. The first term on the right-hand side represents the flow of drug into and out of the compartment. This particular equation involves both equilibrium blood and tissue binding. The terms γ, λ', ϕ, and λ are expressions that contain provisions for linear and nonlinear binding. In our modeling we have considered only linear binding in the blood and tissues. The $Z\alpha$ term will have a mathematical representation based on the phenomenologic expression characteristic of the specific metabolism or transport occurring. A specific transport phenomenon for adriamycin was not defined or used at this point in the development of the model. The $Z\alpha$ term was included only in the equation describing the liver compartment for

the elimination clearance which includes both transport out of the liver (excretion into the bile) and biotransformation to metabolites. The equations for each of the ten compartments were interrelated according to figure 1 and were solved simultaneously by a computer modeling program to obtain values of predicted adriamycin concentrations with time in each of the compartments.

METHODS AND PARAMETERS

Four parameters of adriamycin disposition in rabbits were defined by experimentation: the intestinal absorption, the tissue/plasma equilibrium concentration ratios, the plasma protein binding, and the elimination clearance. The details of the experimental approaches will be reported elsewhere. We will briefly describe the methods utilized in determining these parameters. Adriamycin analysis was performed by combined thin-layer chromatography and spectrofluorometry according to a previously published method (16).

Elimination Clearance

The clearance for adriamycin in rabbits was determined by using two approaches. The adriamycin concentration of the plasma (Cp) as a function of time was observed and used to establish the total clearance by dividing the dose by the integral

$$\int_0^\infty C_p dt.$$

This approach yielded a total clearance of 71 ml/minute. A second method involved the observation of serial lung concentrations with both iv and hepatic portal vein infusions of adriamycin. The results of this method are shown in figure 2. It can be shown by comparison of the areas under the respective concentration-time curves that the hepatic portal vein infusion resulted in a loss of 60% of the adriamycin on the first pass through the liver. The calculated hepatic elimination fraction of 0.6 together with the estimated hepatic plasma flow yielded an hepatic clearance of 68 ml/minute (17). The close agreement between the total clearance and the hepatic clearance indicates that the primary source of adriamycin elimination resides in the liver. Urinary excretion of unchanged adriamycin in rabbits has been reported to be about 1% of the dose over an 8-hour period (12). Therefore, a renal clearance term was not considered in this model.

Plasma Protein Binding

Plasma protein binding of adriamycin has been investigated by using ultracentrifugation. This method examines the adriamycin concentrations in the supernatant fractions of different protein solutions after ultracentrifugation for 18 hours in a swinging bucket rotor (Spinco SW 50.1 rotor and L3-50 ultracentrifuge, Beckman Instruments, Palo Alto, Calif). Adriamycin appeared to be bound to rabbit and human plasma proteins to an extent of 50%. Subsequent measurements using an equilibrium dialysis method yielded a complex binding relationship as demonstrated by a curvilinear behavior on a Scatchard plot. No analysis of the binding-site relationships has been attempted because interpretation of the data is difficult due to the binding of adriamycin to the cellulose dialysis bag. A constant value of 50% protein-binding was used in the model.

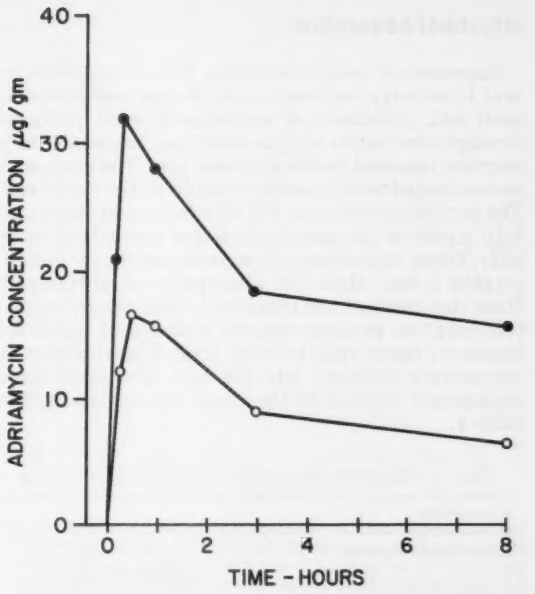

FIGURE 2.—Lung concentrations of adriamycin vs time resulting from 30-min infusions of 3-mg/kg doses of adriamycin in rabbits. ● = Peripheral iv infusion and ○ = hepatic portal venous infusion.

Tissue/Plasma Concentration Ratios

The equilibrium tissue/plasma concentration ratios were obtained experimentally for each of the compartments. Adriamycin concentrations representing the compartments in rabbit tissue were obtained at 15 minutes and 1, 3, 8, 24, and 48 hours after a 3-mg/kg dose of adriamycin was given iv over 1 minute. The tissue/plasma concentration ratios at 8, 24, and 48 hours were substantially constant, although variable due to experimental error. The values at these three times were averaged to obtain the equilibrium binding ratio for each compartment to be used in the model.

Intestinal Absorption

Segments of rabbit intestine, 25 cm long with intact blood supplies, were isolated and transected at each end. Solutions of adriamycin were perfused through the lumen of the intestinal segment via a cannula inserted in the proximal end. The perfusate was collected with another cannula at the distal end. The perfusion rate was 0.5 ml/minute and contained 1-10 μg/ml of adriamycin in either normal saline or bile. These experimental approaches have demonstrated a less than 5% absorption of adriamycin from the lumen of the intestinal tract. An intestinal reabsorption process was not included in the model based on these results even though adriamycin is extensively excreted into the bile. The disposition parameters utilized in the model are summarized in table 1.

TABLE 1.—Disposition parameters of adriamycin in the rabbit

Parameters	
Elimination clearance	70 ml/min (assigned totally to liver compartment)
Plasma protein bound fraction	0.5 (constant)
Intestinal absorption	0
Equilibrium tissue/plasma concentration ratios (±SE)	
Retroperitoneal fat pad (adipose tissue)	19 ± 3.5
Skeletal muscle (lean tissue)	29 ± 3.6
Liver	45 ± 8.3
Small intestine (gut)	51 ± 7.7
Heart	57 ± 5.0
Femur marrow (red marrow)	91 ± 13
Lungs	155 ± 24
Kidney	512 ± 45
Spleen	556 ± 46

The physiologic parameters of blood flow in rabbits were obtained from the data of Neutze et al (18) and Alexander and De Quattro (19). Neutze et al used the radioactive microsphere-trapping method and Alexander and De Quattro used the rubidium-uptake method for determining blood flow. These two methods generally agreed. Plasma flows were used in the model and were calculated from the blood flows using a hematocrit value of 35%. Compartmental volumes for rabbits were estimated from the actual weights of organs obtained in this laboratory for rabbits weighing 2.2-2.4 kg. Other compartmental volumes such as lean tissue, adipose tissue, bone marrow, and plasma volumes were estimated through an appropriate scaling from data of other species given by Dedrick et al (20). A specific gravity of 1 was assumed for all tissue compartments. Equilibrium blood of the tissues was included as part of the total compartmental volume. The values of the equilibrium blood were obtained from a reference source (21). The value of the adipose tissue equilibrium blood was arbitrarily assigned as one half that of lean tissue per unit of mass. Red marrow equilibrium blood was assigned a value equivalent to that reported for the spleen. The sum of the equilibrium blood was subtracted from total blood volume for calculating the plasma compartment size. The physiologic parameters used in the model for the rabbit are given in table 2.

The values for human tissue blood flows and tissue volumes that we used (derived from previous studies) are also shown in table 2. Again, plasma flow was utilized in the human model for adriamycin and a hematocrit value of 45% was assumed. The adipose tissue volume was calculated on the basis of 11.4% of body weight as reported by Forbes et al (22). The volumes of lung, red marrow, and lean tissue were those reported by Mapleson (23). Lean tissue included skeletal muscle, skin, and non-fat subcutaneous tissue. The spleen volume used was that published by Blendis et al (24) based on spleen weight from a human necropsy series of 58. The blood flows for red marrow, adipose tissue, and lean tissue are from a report by Mapleson (23). The flows to the lungs and plasma were assumed equivalent to cardiac output (25). Estimation of spleen blood flow was taken from Blendis et al (26) and Gitlin et al (27). All other blood flow and tissue volume values are from Dedrick et al (20).

TABLE 2.—Physiologic parameters for adriamycin modeling

Parameter	Rabbit*	Man
Body weight (kg)	2.33	70†
Tissue volume (ml)		
Plasma	70	2670
Lungs	17 (3.4)	600
Liver	100 (12)	1700
Kidney	15 (3)	1060
Heart	6 (0.72)	450
Red marrow	47 (7.5)	1400
Adipose tissue	120 (1.2)	7980
Lean tissue	1350 (27)	38,250
Gut	120 (3)	3180
Spleen	1 (0.16)	200
Blood flow (ml/min)		
Plasma	520	5600
Lungs	520	5600
Liver	177	1450
Kidney	80	1240
Heart	16	240
Red marrow	11	120
Adipose tissue	32	200
Lean tissue	155	730
Gut	111	1100
Spleen	9	200

*Values in parentheses are equilibrium blood in tissue.
†1.83 m^2 surface area.

The tissue samples used to represent the compartments were as follows: plasma from aortic blood, lung from the soft parenchymous areas away from the central bronchus region, liver from all lobes (with care taken to avoid the gall bladder), a section across the kidney including both medullary and cortical regions, ventricular areas of the heart, bone marrow obtained from the femur by cracking the bone open and scraping out the soft tissue (considered to be primarily red marrow since animals were young), adipose tissue from retroperitoneal fat pads, lean tissue represented by skeletal muscle from around the femur, gut samples from the upper small intestines, and whole spleens.

RESULTS AND DISCUSSION

The predictions of adriamycin concentration with time in rabbits in each of the compartments are shown in figures 3-6 in addition to the actual concentrations after an iv adriamycin dose of 3 mg/kg in rabbits from 15 minutes to 48 hours. The dose of adriamycin for the computer predictions was also 3 mg/kg. Most of the actual data represent an average of three rabbits at any given time; a few represent an average of four.

The plasma curve is shown in figure 3 and indicates the rapid distribution of the drug dropping to a value of 0.2 μg/ml in the first hour. Subsequently, the second part of the biphasic curve is reached at about 5 hours where the plasma concentration decrease occurs much more slowly with a predicted half-life of 16.5 hours. The fit between actual and predicted values of plasma and liver compartments is quite adequate during both the pre- and post-equilibrative phases. The later bone marrow concentrations are clearly above those predicted by the model for which no explanation is presently apparent. Further investigations are in progress to more adequately define adriamycin uptake and retention by this tissue.

It appears from figures 4-6 that the model overestimates the early time-concentration behavior of the drug in the kidney, gut, adipose tissue, lung, heart, and spleen. The major disagreement appears in the kidney and spleen. These two organs also have the highest estimated blood flow (table 2) per unit of tissue volume. This combination may challenge the perfusion-limited concept by producing a diffusion limitation in addition. Drug diffusion rate may also be a factor in the adipose tissue since adriamycin is quite polar and has a low lipid/water partition coefficient.[9] Long-time predictions for all of these tissues agree quite well with the data. In the case of muscle tissue, the early prediction checks closely with the data with intermediate points being rather low. This may be due to the nonhomogeneity of the muscle tissue and the sampling technique.

The heart is an organ of particular interest in this analysis because of the known cardiotoxicity of adriamycin (7,8). The model shows excellent agreement with experimental data and could be used to provide predictive concentrations for animal toxicity experiments. The lungs were included because of the demonstrated high uptake of adriamycin in lung tissue. Although clinically evident pulmonary toxicity has not been demonstrated in adriamycin therapy, the successful inclusion of the lungs in this model shows that its application to drugs in which strong pulmonary toxicity exists (eg, bleomycin) is warranted.

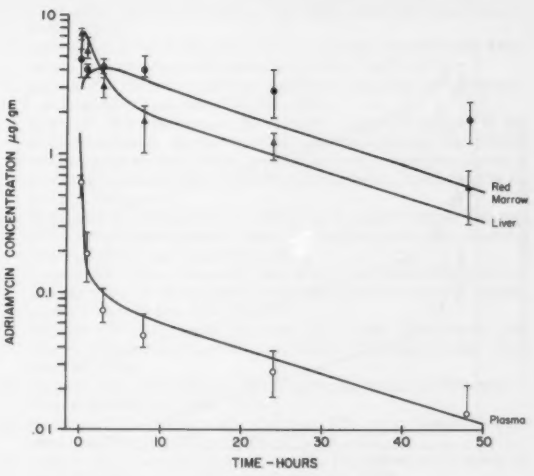

FIGURE 3.—Continuous curves represent computer-generated predictions of adriamycin in the indicated compartment based on the model after a 3-mg/kg iv injection of adriamycin. Point symbols represent actual tissue concentrations of adriamycin after a 3-mg/kg iv injection in rabbits. The range of these concentrations is represented by the T bars. ● = Marrow, ▲ = liver, and ○ = plasma concentrations.

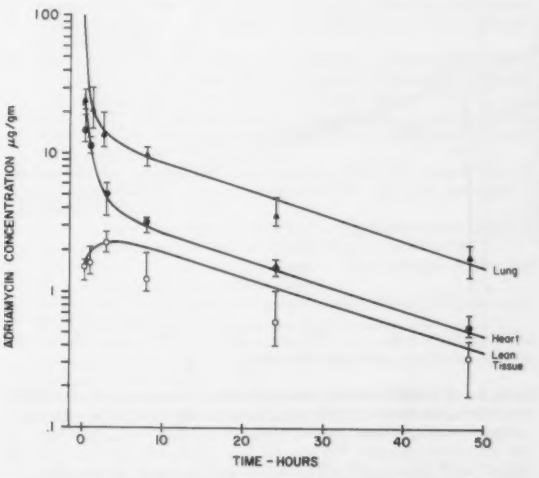

FIGURE 4.—Same as fig 3 except ▲ = lung, ● = heart, and ○ = lean tissue concentrations.

[9]Unpublished data.

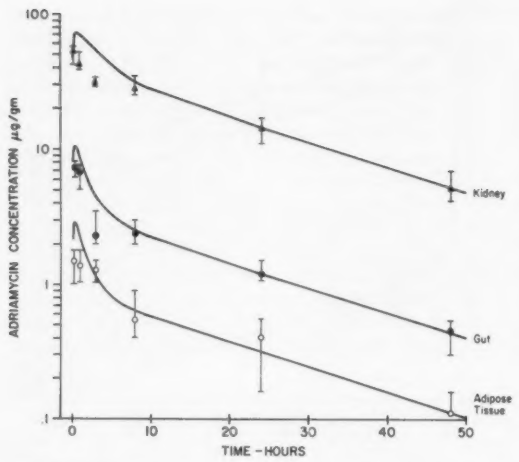

FIGURE 5.—Same as fig 3 except ▲ = kidney, ● = gut, and ○ = adipose tissue concentrations.

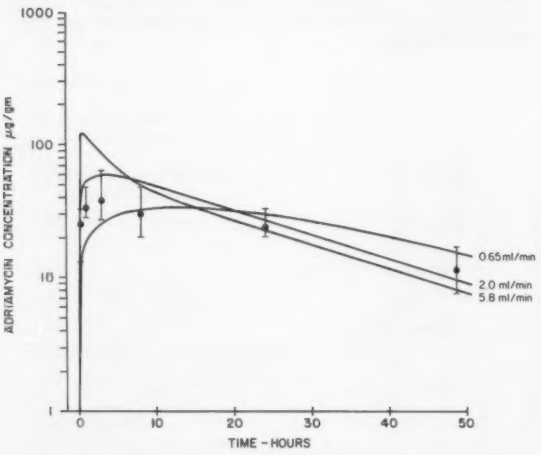

FIGURE 6.—Predicted spleen concentrations of adriamycin at 3 different plasma flows as indicated. Same as fig 3 except ● = actual spleen concentrations.

The concentration behavior in the spleen is shown for three different plasma flows in figure 6. It is known that the flow in the spleen may vary substantially; the reported values for rabbits range from 9 ml/minute/g (18) to 0.85 ml/minute/g (19). The extreme range makes it difficult to estimate blood flow a priori. The higher value was chosen for initial predictions. The model can provide an estimate based on matching concentration-time history of the drug in the spleen. The value of 5.8 ml/minute is based on the reported 9 ml/minute of blood flow for rabbit spleen. The lower value was selected as an equivalent rabbit plasma flow based on the reported human blood flow (26,27). The intermediate value was an arbitrary choice between the two extremes. It does seem that the intermediate plasma flow may be a more realistic estimate if diffusion limitations can be ruled out.

The interplay between blood flow and possible diffusional resistance is shown in the results we have presented. The present model is flow limited and does not include membrane resistance to drug transfer. Resistance to drug transfer would be manifested by lower tissue concentration than that predicted by the model. Furthermore, the magnitude of this discrepancy would be amplified with increasing blood flow. It is evident from an examination of figures 3-6 that organs with a low flow rate (muscle) or a low endothelial resistance (liver) show good agreement with very early time estimates. In the case of rapid flow rates, especially combined with high drug affinity, the early time values are overestimated and some level of membrane resistance could be postulated. Work is currently under way to establish the possible existence and magnitude of a membrane resistance to adriamycin diffusion.

Figure 7 demonstrates our initial attempts to predict adriamycin levels in man. The data points shown are the actual values from Benjamin et al (28) and the curve shown in the figure is the prediction utilizing the human physiologic values given in table 2 and the rabbit disposition parameters given in table 1. The human elimination clearance was calculated from the human hepatic plasma flow and the hepatic elimination fraction of 0.6 obtained in rabbits. The slope of the curve at later times is lower than the actual data in man. Considering the number of other variables that cannot be accounted for here, the prediction is a reasonable first approximation. The position and slope of the curve in relation to the actual data indicate that the tissue binding in humans may not be as great as the binding to rabbit tissue. The binding affinity of human tissues for adriamycin is currently under investigation in order to develop a model that will predict the tissue and plasma levels in man more accurately.

There are many considerations in the pharmacokinetic modeling of adriamycin that need further investigation. A total model must consider the metabolites of adriamycin. One or more of these metabolites may have an active role in the cytotoxic action (12). The dose dependency of adriamycin kinetics in the tissues and the effect of repetitive doses of adriamycin on its own kinetics have not been carefully investigated. Published data on the uptake and retention of adriamycin in both experimental and human tumors are meager to nonexistent.

A reliably predictive pharmacokinetic model for adriamycin would contribute significantly to the understanding and clinical use of this drug. For instance, radiation therapists may be able to more effectively decide the time to administer radiation when used in combination with adriamycin. Tumor resistance to adriamycin on the basis of inadequate uptake may be predictable in some cases, thereby

avoiding an expensive and dangerous drug and saving time for other modes of treatment. The model presented in this report is preliminary; more investigation is needed and is in progress to refine and improve its capability. However, the model in its present form may be utilized for certain applications by other investigators.

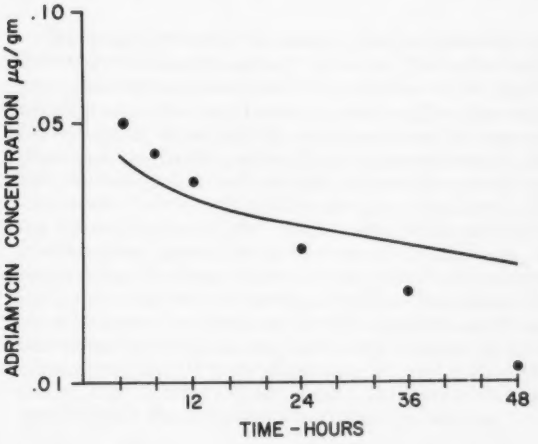

FIGURE 7.—Continuous curve represents predicted adriamycin plasma concentrations in man after a 60-mg/m^2 iv dose of adriamycin. ● = Actual adriamycin plasma concentrations in man after the same dose (*from* ref 28).

REFERENCES

1. BONADONNA G, MONFARDINI S, DELENA M, ET AL. Clinical trials with adriamycin. Results of a three year study. *In* International Symposium on Adriamycin (Carter SK, DiMarco A, Ghione M, et al, eds). New York, Springer-Verlag New York, Inc., 1972, pp 139-152.
2. O'BRYAN RM, LUCE JK, TALLEY RW, ET AL. Phase II evaluation of adriamycin in human neoplasia. Cancer 32:1, 1973.
3. TAN C, ETCUBANAS E, WOLLNER N, ET AL. Adriamycin—an antitumor antibiotic in the treatment of neoplastic disease. Cancer 32:9, 1973.
4. BLUM RH, and CARTER SK. Adriamycin—a new anticancer drug with significant clinical activity. Ann Intern Med 80:249, 1974.
5. ARCAMONE F, CASSINELLI G, FRANCESCHI G, ET AL. Structure and physiochemical properties of adriamycin (doxorubicin). *In* Proceedings of International Symposium on Adriamycin (Carter SK, DiMarco A, Ghione M, et al, eds). New York, Springer-Verlag New York, Inc., 1972, pp 9-22.
6. WANG J, CORTES EP, SINKS L, ET AL. Therapeutic effect and toxicity of adriamycin in patients with neoplastic diseases. Cancer 28:837, 1971.
7. LEFRAK EA, PITHA J, ROSENHEIM S, ET AL. A clinicopathologic analysis of adriamycin cardiotoxicity. Cancer 32:302, 1973.
8. JAENKE RS. An anthracycline antibiotic-induced cardiomyopathy in rabbits. Lab Invest 30:292, 1974.
9. ARENA E, D'ALESSANDRO N, DUSONCHET L, ET AL. Analysis of the pharmacokinetic characteristics, pharmacological and chemotherapeutic activity of 14-hydroxydaunomycin (adriamycin), a new drug endowed with an antitumour activity. Arzneim Forsch 21:1258, 1971.
10. DI FRONZO G, GAMBETTA RA, and LENAZ L. Distribution and metabolism of adriamycin in mice. Comparison with daunomycin. Rev Eur Etud Clin Biol 16:572, 1971.
11. YESAIR DW, SCHWARTZBACH E, SHUCK D, ET AL. Comparative pharmacokinetics of daunomycin and adriamycin in several animal species. Cancer Res 32:1177, 1972.
12. BACHUR NR, HILDEBRAND RC, and JAENKE RS. Adriamycin and daunorubicin disposition in the rabbit. J Pharmacol Exp Ther 191:331, 1974.
13. BISCHOFF KB, and DEDRICK RL. Thiopental pharmacokinetics. J Pharm Sci 57:1346, 1968.
14. BISCHOFF KB, DEDRICK RL, ZAHARKO DS, ET AL. Methotrexate pharmacokinetics. J Pharm Sci 60:1128, 1971.
15. DEDRICK RL, ZAHARKO DS, and LUTZ FJ. Transport and binding of methotrexate in vivo. J Pharm Sci 62:882, 1973.
16. CHAN KK, and HARRIS PA. A fluorometric determination of adriamycin and its metabolites in biological tissues. Res Commun Chem Pathol Pharmacol 6:447, 1973.
17. HARRIS PA. The kinetics of specific organ metabolism in relation to the overall fate of a drug in the body. PhD Dissertation, University of California, 1968.
18. NEUTZE JM, WYLER F, and RUDOLPH AM. Use of radioactive microspheres to assess distribution of cardiac output in rabbits. Am J Physiol 215:486, 1968.
19. ALEXANDER N, and DE QUATTRO V. Regional and systemic hemodynamic patterns in rabbits with neurogenic hypertension. Circ Res 35:636, 1974.
20. DEDRICK RL, FORRESTER DD, CANNON JN, ET AL. Pharmacokinetics of 1-β-D-arabinofuranosylcytosine (ara-C) deamination in several species. Biochem Pharmacol 22:2405, 1973.
21. ALTMAN PL, and DITTMER DS, eds. Respiration and Circulation. Bethesda, Md, Federation of the American Society of Biology, 1971, p 386.
22. FORBES RM, COOPER AR, and MITCHELL HH. The composition of the adult human body as determined by chemical analysis. J Biol Chem 203:359, 1953.
23. MAPLESON WW. An electric analogue for uptake and exchange of inert gases and other agents. J Appl Physiol 18:197, 1963.
24. BLENDIS LM, WILLIAMS R, and KREEL L. Radiological determination of spleen size. Gut 10:433, 1969.
25. GUYTON AC. Function of the Human Body, 3rd ed. Philadelphia, W. B. Saunders Co., 1969.
26. BLENDIS LM, BANKS DC, RAMBOER C, ET AL. Spleen blood flow and splanchnic haemodynamics in blood dyscrasia and other splenomegalies. Clin Sci 38:73, 1971.
27. GITLIN N, GRAHAME GR, KREEL L, ET AL. Splenic blood flow and resistance in patients with cirrhosis before and after portacaval anastomoses. Gastroenterology 59:208, 1970.
28. BENJAMIN RS, RIGGS CE, and BACHUR NR. Pharmacokinetics and metabolism of adriamycin in man. Clin Pharmacol Ther 14:592, 1973.

Mathematic Models For Cancer Chemotherapy: Pharmacokinetic and Cell Kinetic Considerations[1]

Shui-Nan Chuang[2,3,4]

SUMMARY

This paper presents a theoretic study of pharmacokinetic and cell kinetic models for cancer chemotherapeutic systems. The mathematic analysis is based on a modified procedure deduced from DeVita's scheme of the relationship between the cellular kinetics of normal and tumor tissues and the pharmacokinetics of antitumor agents for designing an optimal dose and schedule for cancer treatment. In this scheme pharmacokinetic data and cell-drug interactions at the tumor site are incorporated into the cell cycle kinetic models to form the cancer chemotherapeutic model systems. Three cell cycle kinetic models are presented under alternative hypotheses concerning the mechanism of the resting cells, while each tumor mass is comprised of cells in proliferating (consisting of the four cycle phases G_1, S, G_2, and M), resting (G_0), and nondividing (D, dead) states. An algorithm and a computer program for simulating the tumor populations during scheduled treatments have been prepared. By a suitable selection of expressions for cell-drug interactions, the program is able to simulate tumor behavior during scheduled treatments with different classes of anticancer agents such as cell cycle phase-specific, cell cycle-specific, or cell cycle-nonspecific drugs. A preliminary study of the L1210-ara-C therapeutic system is included to demonstrate the computer simulation procedures.

[Cancer Chemother Rep 59:827-842, 1975]

Pharmacokinetic and cell kinetic studies have been well developed and have become two major branches of research in cancer chemotherapy during the past decade. From these studies we have learned that to maximize the kill of neoplastic cells and minimize the damage to the host, an optimal dosage regimen design should include studies of tumor population growth kinetics, cell cycle phase specificity of anticancer drugs, and cell cycle kinetic behavior of target tumor cells and sensitive normal cells subjected to drug treatments. However, since Teorell (1) introduced compartment models in pharmacokinetics and Quastler and Sherman (2) carried out the percentage labeled mitosis technique to estimate the cell cycle phase parameters for proliferating cells, investigators engaged in mathematic studies of pharmacokinetics or cell kinetics have confined their research topics to one field or the other and have never combined them. It has only been recently that some preliminary studies on predicting cell kill by drugs were made by Himmelstein and Bischoff (3,4) and Jusko (5). They recognized the importance of the cell cycle phase specificity of anticancer drugs, but phase parameters of cell cycle kinetics are not clearly expressed in their models.

A mathematic model has been proposed (6) in which the cell populations in the resting state and four consecutive proliferating phases during the scheduled treatment are represented by separate equations to express explicitly their different responses to the drug treatment. It is assumed that in the tumor model the resting state is conceived to act as a reservoir in which a cell may remain for any length of time and re-enter into G_1 phase with a constant probability. The computer simulations of chemotherapeutic responses of some ascites and solid tumor systems treated with a number of anticancer agents at different doses and schedules are being planned. The simulations will also suggest the "best" schedules for those cancer chemotherapeutic systems.

However, presently the gross mechanism of cellular proliferation in cancer is not fully known, eg, the kinetic aspects of resting cells, such as their positions relative to the proliferating cycle and their biochemical activities, are not clear. These uncertainties would affect the estimations of the kinetic parameters of the cycle phases and, hence, the evaluations of cancer chemotherapeutic effects. It is the purpose of this paper to discuss the alternative hypotheses concerning the kinetic aspects of resting

[1]Supported by contract NO1-CM-12098 from the Division of Cancer Treatment, National Cancer Institute, National Institute of Health, Department of Health, Education, and Welfare.

[2]Kettering-Meyer Laboratory, Southern Research Institute, Birmingham, Ala.

[3]The author wishes to thank Dr. Harris H. Lloyd for his interest and encouragement in this work. His many valuable discussions have helped to formulate this paper.

[4]*Reprint requests to:* Dr. Shui-Nan Chuang, Southern Research Institute, 2000 9th Ave S, Birmingham, Ala 35205.

cells and, based on these hypotheses, to propose three mathematic models for the tumor systems. A comparison of computer simulations of cancer chemotherapeutic effects under these hypotheses deserves a full discussion.

HYPOTHESES AND ASSUMPTIONS BEHIND THE MODEL SYSTEMS

It is clear that a single cancer cell is capable of multiplying and eventually killing the host, and that to cure cancer it is necessary to choose doses and intervals between doses that kill tumor cells faster than they are being replaced (for long enough to reduce the number of cancer cells to zero) without overdosing the host. It is also clear that the currently used anticancer drugs kill cancer cells as well as the sensitive normal cells and thus have adverse effects on the normal tissues. Therefore, biomedical studies in cancer chemotherapy should include (*a*) pharmacokinetics (to determine the concentration-time curves of anticancer drugs in tumor sites and sensitive normal tissues); (*b*) cell-drug interactions (to determine the drug dependency of cell population loss); (*c*) cell kinetics (to determine the cell cycle phase parameter, the population growth rate, and the tumor behavior during the treatment); and (*d*) host toxicity (to investigate the adverse drug effects on the sensitive normal tissues such as bone marrow, gastrointestinal tract, central nervous system, and renal and hepatic functions). From these interlaced studies in cancer chemotherapy, DeVita (7) proposed a scheme (shown in fig 1) to obtain the optimal dose and schedule. For the present study, we have redrawn this chart (fig 2) and have defined the "best" (which is deduced only from the cell kinetic study of tumors alone or together with sensitive normal tissues) and optimal dosage designs in cancer chemotherapy. The route leading to the "best" schedule sketches the structure of this paper.

The tumor models proposed in this mathematic analysis follow Skipper's scheme (8) of the proliferative state in cancer (fig 3), where each tumor mass is composed of three cell types: proliferating (consisting of the four cycle phases G_1, S, G_2, and M), temporarily nonproliferating (resting), and permanently nonproliferating cells. The cells remaining in

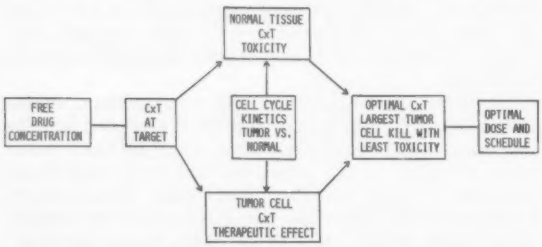
NORMAL TISSUE CxT TOXICITY
FREE DRUG CONCENTRATION
CxT AT TARGET
CELL CYCLE KINETICS TUMOR VS. NORMAL
OPTIMAL CxT LARGEST TUMOR CELL KILL WITH LEAST TOXICITY
OPTIMAL DOSE AND SCHEDULE
TUMOR CELL CxT THERAPEUTIC EFFECT

FIGURE 1.—DeVita's ideal scheme of the relationships between the cellular kinetics of normal and tumor tissues and the effective blood levels of anticancer agents (*from* ref 7).

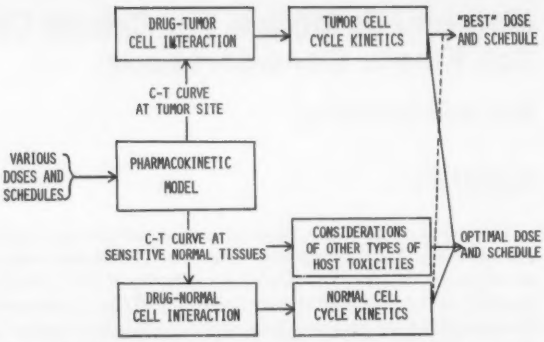
DRUG-TUMOR CELL INTERACTION
TUMOR CELL CYCLE KINETICS
"BEST" DOSE AND SCHEDULE
C-T CURVE AT TUMOR SITE
VARIOUS DOSES AND SCHEDULES
PHARMACOKINETIC MODEL
C-T CURVE AT SENSITIVE NORMAL TISSUES
CONSIDERATIONS OF OTHER TYPES OF HOST TOXICITIES
OPTIMAL DOSE AND SCHEDULE
DRUG-NORMAL CELL INTERACTION
NORMAL CELL CYCLE KINETICS

FIGURE 2.—"Best" and optimal dosage regimen designs in cancer chemotherapy.

the four consecutive proliferating phases are relatively sensitive to all agents. The permanently nonproliferating (sterile) cells have lost the ability to divide and are of no concern to chemotherapists, but their physical presence is still reflected in the measure of tumor size for solid tumor and cell count for leukemias. The resting cells do not respond to antimetabolites and are less sensitive than proliferating cells to chemically reactive compounds. They can be triggered at any time and can go back into the cycle. Therefore, these nonproliferating but still viable cells form a protected reservoir of cancer cells. This is one of the reasons for chemotherapeutic failure. In this study, three mathematic models designated models I, II, and III are proposed to analyze cancer chemotherapeutic effects. They are based on three alternative hypotheses concerning the kinetics of the resting cells.

The hypothesis behind model I (fig 4) (6), as mentioned previously, assumes that G_0 phase is conceived to act as a reservoir in which a cell may remain for any length of time and re-enter into G_1 phase with a constant probability per unit time. For model II (fig 5) the hypothesis says that there is no mark for the transition between G_1 and G_0, and cells will have a minimum sojourn time before reinstituting DNA synthesis. Thus, the combined G_1 phase will have a widely spread duration. This hypothesis was first induced by Burns and Tannock (9) and Smith and Martin (10) who argued that unless biochemical detection is possible, G_0 cells are indistinguishable

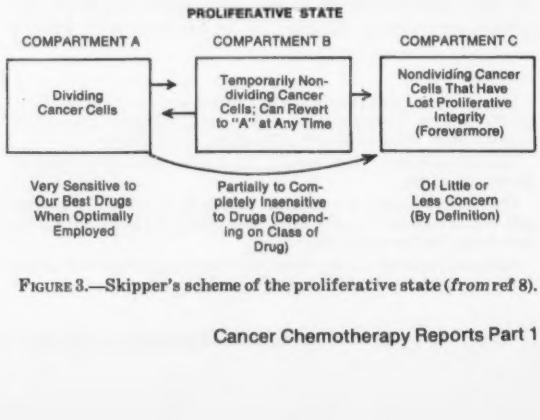
PROLIFERATIVE STATE
COMPARTMENT A
COMPARTMENT B
COMPARTMENT C
Dividing Cancer Cells
Temporarily Non-dividing Cancer Cells; Can Revert to "A" at Any Time
Nondividing Cancer Cells That Have Lost Proliferative Integrity (Forevermore)
Very Sensitive to Our Best Drugs When Optimally Employed
Partially to Completely Insensitive to Drugs (Depending on Class of Drug)
Of Little or Less Concern (By Definition)

FIGURE 3.—Skipper's scheme of the proliferative state (*from* ref 8).

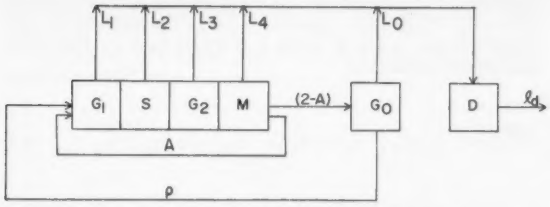

FIGURE 4.—Cancer chemotherapeutic model system I.

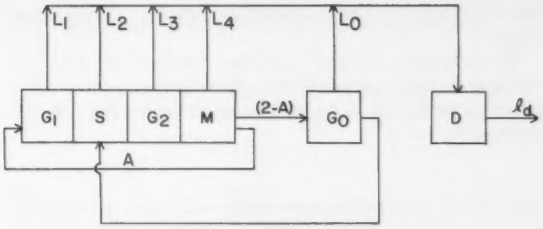

FIGURE 6.—Cancer chemotherapeutic model system III.

from the "true" G_1 cells and together comprise the G_1 phase (for convenience, we will use the term G'_1 phase in this paper). The major difference between the "true" G_1 phase and the G_0 state is that the former has a relatively uniform duration while the latter has a widely spread duration. These investigators also argued that the durations of S and G_2 phases are uniform for particular tumor types and usually do not show much intrapopulation variation, while the duration of G'_1 phase is extremely variable and, consequently, changes in generation time are attributed to changes in G'_1 phase duration. However, their second argument is not obvious, and in this study we will assume stochastic durations for all phases and we will consider as special cases those situations in which tumors have constant durations of S, G_2, and M phases. The hypothesis of model III (fig 6) is intermediate between those of models I and II; in this model the G_0 phase is considered as a separate phase (but parallel to the G_1 phase) with a much longer and more widely spread duration. The relationship between the G_1 and G_0 phases of the cell cycle assumed in the hypotheses of models II and III is well depicted in figures 3 and 4 of reference 7.

In all of the models, the following general assumptions hold:

1. The proliferating cells go through a binary fission following mitosis.

In models I and III, after each binary fission, 2-A cells enter the resting compartment (G_0) and A cells continue in the proliferative cycle, where $1 \leq A \leq 2$ and 1-(A/2) is called the decycling probability.

2. The cells in G_1, S, G_2, M, or G_0 phase may enter the permanently nonproliferative (D) compartment and die either after exposure to cytotoxic drugs or by natural attrition.

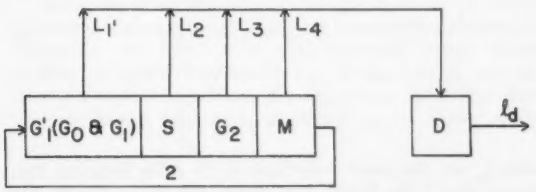

FIGURE 5.—Cancer chemotherapeutic model system II.

3. The transit times of cells in each proliferating phase (or resting phase in model III) can be described by independently distributed probability density functions.

The present mathematic analysis and the relevant computer simulation programs are able to deal with the situations where cells surviving treatment do undergo an alteration of kinetic parameters. However, data which have been obtained on a number of classes of anticancer agents (11) suggest that probably neither drug-induced lag phase nor drug-induced alteration in generation time plays a major role in drug-induced increase in lifespan of BDF_1 mice bearing L1210 leukemia. Also, there is some evidence that the alteration of tumor growth characteristics during drug treatment is due to death of a large percent of cells, thus causing the redistribution of cells within the proliferating cycle and the resting state.

MATHEMATIC REPRESENTATIONS OF THE MODEL SYSTEMS

The mathematic representations of the proposed cancer chemotherapeutic model systems shown in figures 4-6 are formulated on the basis of Von Foerster's population balance equation (12) and the compartment equation, so that the population density functions $n_i(t,a_i)$ of the resting phase (except in model I) and of each of the proliferating phases are governed by the age-time representation of cell population kinetics

$$\frac{\partial n_i(t,a_i)}{\partial t} + \frac{\partial n_i(t,a_i)}{\partial a_i} = -[\lambda_i(a_i) + L_i(t)]n_i(t,a_i) \qquad (1)$$

where a_i represents cell age within each phase. The expected cell population in each phase will be

$$N_i(t) = \int_{a_i=0}^{\infty} n_i(t,a_i)\,da_i \qquad (2)$$

the integral of the population density function $n_i(t,a_i)$.

In equation (1), the transfer coefficient $\lambda_i(a_i)$ is related to the independently distributed probability density function $f_i(a_i)$ of phase duration by the expression

$$\lambda_i(a_i) = \frac{f_i(a_i)}{\phi_i(a_i)} \tag{3}$$

with

$$\phi_i(a_i) = 1 - \int_{x=0}^{a_i} f_i(x)dx \tag{4}$$

The loss function $L_i(t)$ is the rate constant for cells randomly losing their ability to divide, due to drug treatment or natural attrition. In an untreated tumor system $L_i(t) = l_i$ are small constant coefficients, while for tumors receiving chemotherapy they are functions of drug concentration at the tumor site. This cell-drug interaction will be discussed later. In the following equations the subscripts 1, 2, 3, 4, 0, and d will be used to index those quantities associated with G_1, S, G_2, M, G_0, and D cells respectively, and 1′ will be used in model II for those quantities of G'_1 cells which comprise the G_0 and "true" G_1 cells. The notation I, II, or III following an equation number will indicate that the equation is valid only for that particular model. Equations (1)-(4) are valid with i = 1-4 for model I, i = 1′,2-4 for model II, and i = 1-4,0 for model III.

The initial conditions (the initial age distributions) associated with equation (1) are defined as

$$n_i(0,a_i) = \beta_i(a_i) \tag{5}$$

The expressions for $\beta_i(a_i)$ deserve some discussion which will be given later when we analyze the scheduled treatments.

The boundary conditions (the birth rate functions) defined as

$$n_i(t,0) = \alpha_i(t) \tag{6}$$

play the essential role in characterizing the alternative hypotheses for the proposed models. For model I,

$$\begin{cases} \alpha_1(t) = A\displaystyle\int_{a_4=0}^{\infty} \lambda_4(a_4)n_4(t,a_4)da_4 + \rho N_0(t) \\ \alpha_{i+1}(t) = \displaystyle\int_{a_i=0}^{\infty} \lambda_i(a_i)n_i(t,a_i)da_i, \quad i=1,2,3 \end{cases} \tag{7.I}$$

in which $\rho N_0(t)$ is the rate at which G_0 cells revert to the proliferating cycle, ie, ρ is the rate constant of G_0 cells entering G_1 phase. The expected cell population $N_0(t)$ in G_0 at time t is governed by the compartment equation

$$\frac{dN_0(t)}{dt} = -[\rho+L_0(t)]N_0(t)+(2-A)\int_{a_4=0}^{\infty} \lambda_4(a_4)n_4(t,a_4)da_4 \tag{8.I}$$

For tumors receiving treatment with cycle phase-nonspecific anticancer drugs, $L_0(t)$ is also a function of drug concentration while for untreated periods it is a small constant. The initial condition $N_0(0)$ should be chosen according to known or evaluated tumor characteristics. For models II and III, the boundary conditions are

$$\begin{cases} \alpha_{1'}(t) = 2\displaystyle\int_{a_4=0}^{\infty} \lambda_4(a_4)n_4(t,a_4)da_4 \\ \alpha_{i+1}(t) = \displaystyle\int_{a_i=0}^{\infty} \lambda_i(a_i)n_i(t,a_i)da_i, \quad i = 1',2,3 \end{cases} \tag{7.II}$$

and

$$\begin{cases} \alpha_0(t) = (2-A)\displaystyle\int_{a_4=0}^{\infty} \lambda_4(a_4)n_4(t,a_4)da_4 \\ \alpha_1(t) = A\displaystyle\int_{a_4=0}^{\infty} \lambda_4(a_4)n_4(t,a_4)da_4 \\ \alpha_2(t) = \displaystyle\int_{a_0=0}^{\infty} \lambda_0(a_0)n_0(t,a_0)da_0 + \int_{a_1=0}^{\infty} \lambda_1(a_1)n_1(t,a_1)da_1 \\ \alpha_{i+1}(t) = \displaystyle\int_{a_i=0}^{\infty} \lambda_i(a_i)n_i(t,a_i)da_i, \quad i=2,3 \end{cases} \tag{7.III}$$

The third expression in equation (7.III) reunites G_0 and G_1 cells into S phase.

The expected cell population in the D compartment is governed by

$$\frac{dN_d(t)}{dt} = -l_d N_d(t) + \sum_i L_i(t)N_i(t) \tag{9}$$

with l_d as the rate constant of D cells leaving the tumor site. Like $N_0(0)$, the initial condition $N_d(0)$ will be chosen from known or evaluated tumor charac-

teristics. The subscript i in the summation includes those of resting and proliferating phases.

The expected total population of the tumor mass at time t will be

$$N(t) = \sum_i N_i(t) \tag{10}$$

Here, the summation is understood to include all compartments.

The mathematic representations formulated above are designated to simulate the tumor behaviors under the cytotoxic drug treatments. The models are also able to describe the kinetics of normal but drug-sensitive tissues. To simulate various dosage regimens (chosen in some cases from the available toxicity data) to suggest a "best" dosage and schedule for multiple-dose treatments, a discussion on pharmacokinetics of anticancer drugs, cell-drug interaction relationships, cell cycle kinetic study, and host toxicity study are needed. They will be discussed in the next four sections.

PHARMACOKINETIC CONSIDERATIONS

Pharmacokinetic data for most of the currently used anticancer agents for animals (and sometimes for man) are available for our use in this series of studies. When the drug level at the tumor site is not available and cannot be measured directly, a prediction from the compartment analysis (identification and descriptive analysis) is needed. The identification problem deals with the determination of biochemical, physiologic, and patient parameters for pharmacokinetic modeling, while descriptive analysis predicts numerically the consequences of the established model. Some multicompartment models for various anticancer drugs have been published in the literature. Among them, the one derived by Bischoff et al (13) for methotrexate[5] is one of the most successful models. However, for most practical situations, two- or three-compartment models will provide sufficient information. An approach with particular emphasis on two- and three-compartment models is suggested by Chuang and Lloyd (14), from both stochastic and deterministic points of view, to identify the compartment models from the measured urine excretion rate and the observations on only one of the compartments and to evaluate the drug levels at the unobservable tumor sites.

Here, we describe briefly the procedures of deterministic compartment analysis in pharmacokinetics. Suppose we have the three-compartment model shown in figure 7 in which C_{10} is the initial concentration resulting from an injection into the first compartment which is assumed to be observable. The system can be expressed by the equation

$$\dot{\underline{C}}(t) = \begin{bmatrix} K_{11} & K_{12} & K_{13} \\ K_{21} & K_{22} & K_{23} \\ K_{31} & K_{32} & K_{33} \end{bmatrix} \underline{C}(t); \quad \underline{C}(0) = \begin{bmatrix} C_{10} \\ 0 \\ 0 \end{bmatrix} \tag{11}$$

Assuming that the drug concentration in the observed compartment takes the form

$$C_1(t) = A_{11}e^{\Lambda_1 t} + A_{12}e^{\Lambda_2 t} + A_{13}e^{\Lambda_3 t} \tag{12}$$

then the unknown parameters A_{1i} and Λ_i (i = 1-3) can be estimated by a computer least-squares procedure to minimize the function

$$\sum_{j=1}^{N} \sum_{k=1}^{n_j} \left[C_{1,k}(t_j) - \sum_{i=1}^{3} A_{1i}e^{\Lambda_i t_j} \right]^2 \tag{13}$$

$C_{1,k}(t_j)$ is the k^{th} data point at the sample time t_j and N is the total number of sampling times. Having determined the parameters A_{1i} and Λ_i (i = 1-3), the value of the rate constant K_{ij} can be evaluated from table 2 of reference 14 under 11 different physical and physiologic conditions. Therefore, the drug concentrations in the other two unobservable compartments can be predicted from the following expressions

$$\begin{cases} C_2(t) = \left(C_{10} \dfrac{R_{1,321}}{S_{123}} e^{\Lambda_1 t} + \dfrac{R_{2,321}}{S_{231}} e^{\Lambda_2 t} + \dfrac{R_{3,321}}{S_{312}} e^{\Lambda_3 t} \right) \\ C_3(t) = \left(C_{10} \dfrac{R_{1,231}}{S_{123}} e^{\Lambda_1 t} + \dfrac{R_{2,231}}{S_{231}} e^{\Lambda_2 t} + \dfrac{R_{3,231}}{S_{312}} e^{\Lambda_3 t} \right) \end{cases} \tag{14}$$

with

$$\begin{cases} R_{\ell,ijk} = (\Lambda_\ell - K_{ii})K_{jk} + K_{ji}K_{ik} \\ S_{ijk} = (\Lambda_i - \Lambda_j)(\Lambda_i - \Lambda_k) \end{cases} \tag{15}$$

The above-described compartment analysis in pharmacokinetics is based on the concept of first-order kinetics. However, the present study for cancer chemotherapy does not rule out the possible incorporations of nonlinear pharmacokinetics. In

[5]Methotrexate: NSC-740; CAS reg. No. 59-05-2; glutamic acid, *N*-[*p*-[[(2,4-diamino-6-pteridinyl)methyl]methylamino]benzoyl]-.

fact, the Michaelis-Menton-type pharmacokinetics which have been discussed by many investigators (ref 13 is one of them) can be incorporated as easily as the linear pharmacokinetics in the following evaluation of cell-drug interactions on a modern computer.

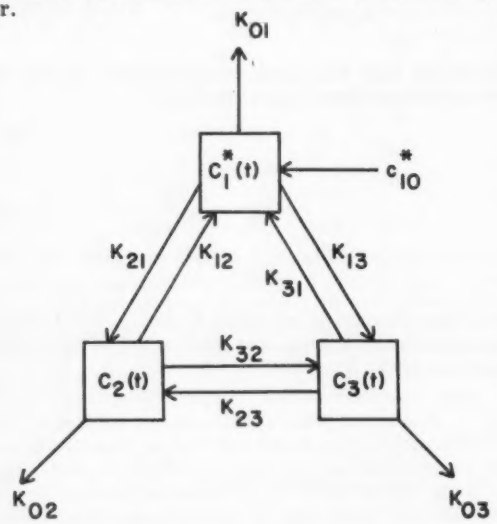

FIGURE 7.—Three-compartment open model in pharmacokinetics.

CELL-DRUG INTERACTIONS

As in reference 6, the cell-drug interaction relationships are proposed according to two factors. The first factor is the cell-kill hypothesis of Skipper et al (11) which states that for most drugs a clear relationship exists between the drug dose and the extent of eradication of tumor cells within the limits of toxicity to the host, and that a given dose of a drug kills a constant fraction of cells (not a constant number) regardless of the cell numbers present at the time of therapy. The second factor is the assumption that, in a drug-sensitive phase, when the drug concentration is below a threshold cytotoxic level, the cell loss is due to the natural attrition as in the untreated period; after that level, the rate constants of cell loss increase as concentration increases until it reaches a maximum effective level above which the rate constants of cell loss remain at that fraction. Hence, the loss functions in equations (1) and (8.I) can be expressed mathematically by the general form

$$L_i(t) = \begin{cases} l_{max,i} & C(t) \geq C_{max,i} \\ l_{max,i}[C(t) - C_{min,i}] + l_i[C_{max,i} - C(t)] \\ \hline C_{max,i} - C_{min,i} & C_{max,i} > C(t) > C_{min,i} \\ l_i & C(t) \leq C_{min,i} \end{cases} \quad (16)$$

where $C_{min,i}$ is the threshold cytotoxic concentration for phase i, and $C_{max,i}$ is the concentration at and above which the rate constant of cell kill is $l_{max,i}$. The values $C_{max,i}$, $C_{min,i}$, and $l_{max,i}$ depend on the sensitivity of cells in each state to the chemotherapeutic agents.

For simulating the cell kinetic behavior after treatment with S-phase-specific drugs, only $L_2(t)$ is defined by equation (16) and other values for $L_i(t)$ are equal to l_i as in the untreated case. For cell cycle-specific drugs, the simulation would be required to define $L_i(t)$, except for resting cells, by equation (16).

By the above-proposed cell-drug interactions, we will see later that our derived expressions for cell kill by drug will agree with the conclusion of DeVita (7), derived from experimental observations, that the effectiveness of an anticancer agent is directly related to the concentration in the tumor site and the duration of time that an effective level is maintained.

CELL CYCLE KINETIC STUDIES

With the proposed mathematic representations for the cancer chemotherapeutic systems and the preceding developments of cell-drug interaction relationships, we are ready to analyze the chemotherapeutic effects on population kinetics of tumor systems. A single dose of an anticancer drug will provide cytotoxic concentrations for some interval depending upon the characteristics and pharmacokinetics of the drug; however, for many drugs, fractionated doses provide greater therapeutic effectiveness with relatively less host toxicity. Therefore, the following analysis or simulation of treatment is accomplished over a series of time intervals. These include the intervals of growth before treatment, the intervals during which the drug level is above the threshold cytotoxic concentration, and the intervals of regrowth during which the drug concentration is less than the minimum effective concentration. During the simulation, only gross drug characteristics such as cell cycle phase specificity and serum concentration with time are required. In this paper we will skip the detailed mathematic derivations (6) and present the equations which are essential to the computer simulation.

From equations (1), (4), (5), and (6), the population density functions can be expressed as follows

$$n_i(t,a_i) = \begin{cases} \alpha_i(t-a_i)\phi_i(a_i)\dfrac{U_i(t)}{U_i(t-a_i)}, & t \geq a_i \\ \beta_i(a_i-t)\dfrac{\phi_i(a_i)}{\phi_i(a_i-t)}U_i(t), & t \leq a_i \end{cases} \quad (17)$$

with $U_i(t)$ defined by

$$U_i(t) = \exp\left[-\int_{\tau=0}^{t} L_i(\tau)d\tau\right] \quad (18)$$

For the growth period before treatment and the regrowth periods between treatment intervals, $L_i(t) = l_i$ in equation (18). For the treatment intervals, if C(t) and the four parameters defining $L_i(t)$ of equation (16) are known, it is a simple matter to calculate $U_i(t)$ by numerical integrations. The detailed form of $U_i(t)$ needed in the computer simulation is derived in reference 6. Then, the expected cell populations in each phase (including the resting state in models II and III) are

$$N_i(t) = U_i(t)\left\{\int_{a_i=0}^{t} \frac{\alpha_i(t-a_i)}{U_i(t-a_i)}\,\phi_i(a_i)da_i + \int_{a_i=t}^{\infty} \frac{\beta_i(a_i-t)}{\phi_i(a_i-t)}\,\phi_i(a_i)da_i\right\} \tag{19}$$

in which the birth rate functions $\alpha_i(t)$ obey the recursive relationships

$$\begin{cases} \alpha_1(t) = AU_4(t)\left\{\int_{a_4=0}^{t} \frac{\alpha_4(t-a_4)}{U_4(t-a_4)}\,f_4(a_4)da_4 + \int_{a_4=t}^{\infty} \frac{\beta_4(a_4-t)}{\phi_4(a_4-t)}\,f_4(a_4)da_4\right\} \\ \quad + \rho e^{-\rho t}U_0(t)\left[N_0(0)+(2-A)\int_{\tau=0}^{t} e^{\rho\tau}\frac{U_4(\tau)}{U_0(\tau)}\left\{\int_{a_4=0}^{\tau} \frac{\alpha_4(\tau-a_4)}{U_4(\tau-a_4)}\,f_4(a_4)da_4 \right.\right. \\ \quad \left.\left. + \int_{a_4=\tau}^{\infty} \frac{\beta_4(a_4-\tau)}{\phi_4(a_4-\tau)}\,f_4(a_4)da_4\right\}d\tau\right] \\ \alpha_{i+1}(t) = U_i(t)\left\{\int_{a_i=0}^{t} \frac{\alpha_i(t-a_i)}{U_i(t-a_i)}\,f_i(a_i)da_i + \int_{a_i=t}^{\infty} \frac{\beta_i(a_i-t)}{\phi_i(a_i-t)}\,f_i(a_i)da_i\right\} \\ \qquad i=1,2,3 \end{cases} \tag{20.I}$$

$$\begin{cases} \alpha_1(t) = 2U_4(t)\left\{\int_{a_4=0}^{t} \frac{\alpha_4(t-a_4)}{U_4(t-a_4)}\,f_4(a_4)da_4 + \int_{a_4=t}^{\infty} \frac{\beta_4(a_4-t)}{\phi_4(a_4-t)}\,f_4(a_4)da_4\right\} \\ \alpha_{i+1}(t) = U_i(t)\left\{\int_{a_i=0}^{t} \frac{\alpha_i(t-a_i)}{U_i(t-a_i)}\,f_i(a_i)da_i + \int_{a_i=t}^{\infty} \frac{\beta_i(a_i-t)}{\phi_i(a_i-t)}\,f_i(a_i)da_i\right\} \\ \qquad i=1,2,3 \end{cases} \tag{20.II}$$

or

$$\begin{cases} \alpha_0(t) = (2-A)U_4(t)\left\{\int_{a_4=0}^{t} \frac{\alpha_4(t-a_4)}{U_4(t-a_4)}\,f_4(a_4)da_4 + \int_{a_4=t}^{\infty} \frac{\beta_4(a_4-t)}{\phi_4(a_4-t)}\,f_4(a_4)da_4\right\} \\ \alpha_1(t) = \frac{A}{(2-A)}\,\alpha_0(t) \\ \alpha_2(t) = \frac{1}{2}\sum_{j=0}^{3} U_j(t)\left\{\int_{a_j=0}^{t} \frac{\alpha_j(t-a_j)}{U_j(t-a_j)}\,f_j(a_j)da_j + \int_{a_j=t}^{\infty} \frac{\beta_j(a_j-t)}{\phi_j(a_j-t)}\,f_j(a_j)da_j\right\} \\ \alpha_{i+1}(t) = U_i(t)\left\{\int_{a_i=0}^{t} \frac{\alpha_i(t-a_i)}{U_i(t-a_i)}\,f_i(a_i)da_i + \int_{a_i=t}^{\infty} \frac{\beta_i(a_i-t)}{\phi_i(a_i-t)}\,f_i(a_i)da_i\right\}, \\ \qquad i=2,3 \end{cases} \tag{20.III}$$

for models I, II, and III respectively. Equation (20) can only be solved iteratively by numerical methods with a digital computer and an appropriate chosen starting function.

The expected cell population in the resting state of model I can be evaluated from

$$N_0(t) = e^{-\rho t}U_0(t)\left[N_0(0) + (2-A)\int_{\tau=0}^{t} e^{\rho\tau}\frac{U_4(\tau)}{U_0(\tau)}\cdot \left\{\int_{a_4=0}^{\tau} \frac{\alpha_4(\tau-a_4)}{U_4(\tau-a_4)}\,f_4(a_4)da_4 + \int_{a_4=\tau}^{\infty} \frac{\beta_4(a_4-\tau)}{\phi_4(a_4-\tau)}\,f_4(a_4)da_4\right\}d\tau\right] \tag{21.I}$$

The numerical calculations of the convolution integrals in equations (19)-(21) can be easily and quickly performed by the fast Fourier transformation technique developed by Cooley and Tukey (15).

Finally, the expected cell population in the D compartment is computed by numerical integration of the following expression

$$N_d(t) = e^{-\delta_d t}\left\{N_d(0) + \int_{\tau=0}^{t} e^{\delta_d\tau}\left[\sum_{i} L_i(\tau)N_i(\tau)\right]d\tau\right\} \tag{22}$$

and the expected total population of tumor mass is the sum of cells in each compartment.

To begin the simulation, it is reasonable to assume exponential growth with negligible cell loss when the untreated tumor is small. Thus the initial age distributions for the growth period before treatment take the form

$$\beta_i(a_i) = K_i e^{-ca_i}\phi_i(a_i) \tag{23}$$

where c is the specific growth rate of the tumor in the early stage of exponential growth, and K_i is the constant defined as the birth rate at time 0, depending on the size of the initial population. If the specific growth rate c and the cell cycle phase parameters are available from the current research literature, then K_i can be evaluated from the recursive relationships

$$\begin{cases} K_1 = AK_4\tilde{f}_4(c) + \rho N_0(0) \\ K_{i+1} = K_i\tilde{f}_i(c), \qquad i=1,2,3 \end{cases} \tag{24.I}$$

$$\begin{cases} K_1 = 2K_4\tilde{f}_4(c) \\ K_{i+1} = K_i\tilde{f}_i(c), \quad i=1',2,3 \end{cases} \tag{24.II}$$

or

$$\begin{cases} K_0 = (2-A)K_4\tilde{f}_4(c) \\ K_1 = AK_4\tilde{f}_4(c) \\ K_2 = K_0\tilde{f}_0(c) + K_1\tilde{f}_1(c) \\ K_{i+1} = K_i\tilde{f}_i(c), \quad i=2,3 \end{cases} \tag{24.III}$$

for models I, II, and III respectively, with one of them as the scaling factor obtained from experimental data. Usually, it is K_2 which could be determined, based on the experimental thymidine labeling index (TI) defined as

$$TI = \frac{N_2(0)}{N(0)} = \frac{K_2\tilde{\phi}_2(c)}{N(0)} \tag{25}$$

In equations (24) and (25), $\tilde{f}_i(\cdot)$ and $\tilde{\phi}_i(\cdot)$ are the Laplace transforms of $f_i(a_i)$ and $\phi_i(a_i)$.

For the subsequent treatment and regrowth periods, the initial age distribution $\beta_i(a_i)$, the initial population $N_0(0)$ in model I, and $N_d(0)$ are equal to those at the end of the previous simulation interval, ie,

$$\begin{cases} \beta_i(a_i) = n_i(t_f,a_i) \\ N_i(0) = N_i(t_f), \ i=0 \text{ in Model I and } i=d \end{cases} \tag{26}$$

where t_f is the final time of the previous simulation.

However, the cell cycle phase parameters are not available for every tumor system. In order to make our computer simulation possible, the prediction of cell cycle phase parameters is required. This may be done by the percentage labeled mitosis technique and the automatic curve-fitting procedure which fits the theoretic fraction labeled mitosis (FLM) function to the observed data with least-squares or maximum-likelihood criteria. Let the quantities associated with labeled cells be denoted by an asterisk (*); then the theoretic FLM function defined by

$$FLM(t) = \frac{N_4^*(t)}{N_4(t)} \tag{27}$$

can be derived for any period of the scheduled treatment. In equation (27), the expression for $N_4^*(t)$ can be derived, in the same way as for $N_4(t)$ in equations (19) and (20), with the initial age distributions

$$\begin{cases} n_2^*(0,a_2) = \beta_2(a_2) \\ n_i^*(0,a_i) = 0, \quad i\neq 2 \end{cases} \tag{28}$$

However, most of the available FLM data in the literature are taken under the control period. For this situation, in addition to the above-mentioned numerical approach, the analytic expressions of $\tilde{N}_4^*(S)$ and $\tilde{N}_4(S)$ can be obtained by solving the recursive integral equation (20) and equation (19) with the Laplace transformation method. In order to write a general program to include periods of growth and periods of drug treatment in computer simulations we will only use the former approach here. Those who are interested in the analytic solutions are directed to reference 6 in which the detailed derivations for model I are demonstrated.

During the process of automatic prediction of cell cycle phase parameters, any reasonable type of distribution can be chosen for $f_i(a_i)$. However, gamma and log-normal distributions are most commonly used to describe random variables which are constrained to be nonnegative. The deterministic phase duration $f_i(a_i)$, which is usually assumed for M phase and is also assumed for S and G_2 phases in the special case of model II, is defined by the Dirac delta functions.

REMARKS ON HOST TOXICITY

Toxicity is usually a limiting factor in determining the schedule of an anticancer drug. Therefore, as shown in figure 2, an optimal dosage regimen design in cancer chemotherapy should consider not only the tumor cell kill by the drug, but also the cell kill in certain sensitive normal tissues as well as many other types of host toxicities, as mentioned previously. The normal cell kill by the drug may possibly be handled by the proposed models, with an appropriate selection of parameters, while other types of host toxicities are difficult to express in mathematic terms. Hence, the present analysis will be confined to the "best" dosage regimen design defined in figure 2. However, the toxicity data, if they are available, do help us in selecting a series of doses and schedules to be simulated and to suggest a "best" schedule.

PRELIMINARY RESULTS OF COMPUTER SIMULATION

In this section, an example of L1210 mouse leukemia being treated with arabinosylcytosine (ara-C)[6]

[6]Arabinosylcytosine: NSC-63878; CAS reg. No. 69-74-9; cytosine, 1-β-D-arabinofuranosyl-, monohydrochloride; ara-C.

is considered. Some preliminary results from the automatic simulation of the proposed model I are shown to demonstrate the simulated cancer chemotherapeutic effects. The choice of a "best" schedule deduced from the simulations of a series of different schedules is discussed.

Biochemical data (16) suggested that ara-C specifically blocks DNA synthesis. This mechanism of action implies that ara-C is an S-phase-specific anticancer agent, ie, cell death results only when cells exposed to ara-C are passing through the S phase of their proliferating cycle. In the BDF_1 mouse, ara-C has a half-life of about 25 minutes. Experimental data for L1210-ara-C interactions are listed in table 1. Some of the data used here were obtained from the cell culture studies of Wilkoff et al (17) and other unpublished data. Also, some observations show that treatment of mice bearing L1210 leukemia with representatives of the major classes of known antileukemic agents does not increase the average doubling time of the L1210 cells that survive therapy, nor does it induce a significant lag in the growth rate of these surviving cells. Therefore, we will use the same cell cycle kinetic parameters for both treated and untreated periods for this therapeutic system.

TABLE 1.—Experimental data for cell-drug interactions of L1210 leukemia in BDF_1 mice treated with ara-C (S-phase-specific agent)

Parameter	Observed value
l_i (hr^{-1}), i = 1-4	$\approx$ 0.0
l_o (hr^{-1})	—
l_d (hr^{-1})	$\geq$0.01
$C_{min,2}$ (μg/ml)	0.1-0.3
$C_{max,2}$ (μg/ml)	1-3
$l_{max,2}$ (hr^{-1})	0.8-1.2
Overall average rate constant of cell kill (hr^{-1})	$\approx$ 0.4

In the simulations of the following two cases, the kinetic parameters chosen for the random-phase durations with log-normal distributions and for the cell-drug interactions are displayed in figure 8. Another two parameters which are not shown in the figure are $C_{max,2}$ = 1.5 μg/ml and $C_{min,2}$ = 0.3 μg/ml. The first situation we consider here is a case with a 93% observed cure rate in L1210 leukemia (ip inoculum of 10^5 cells) after treatment with ara-C (15 mg/kg/dose, q3h × 8 on Days 2, 6, 10, and 14). Seventy-five percent of this inoculum is assumed to be D cells. Also, ara-C at a dose of 15 mg/kg will induce the highest serum level of 15 μg/ml in the BDF_1 mouse. The pharmacokinetic information and the computer-simulated expected cell populations of proliferating phases during the scheduled treatment are plotted in figure 9, while those of the total tumor mass and the resting, dead, and proliferating compartments are plotted in figure 10. Figures 9 and 10 show that there is a 2.8-log kill of S cells for each treatment day and a net 0.35-log kill for each dose. The cell kill in S phase makes the populations in other proliferating phases oscillate periodically during the regrowth

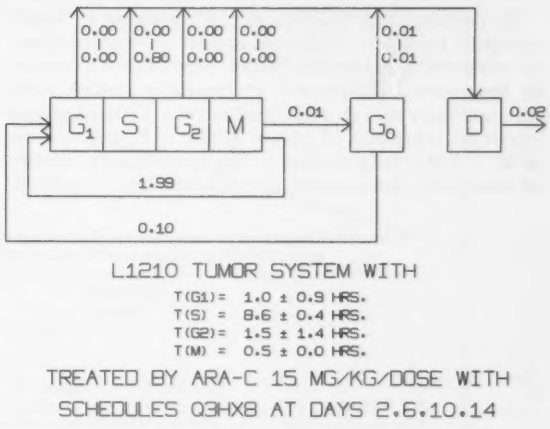

FIGURE 8.—Parameters of L1210-ara-C therapeutic system.

periods and with a different time lag in growth. At the end of the treatment on Day 14, the cells in each proliferating phase are reduced to less than one cell. The tumor mass consists of only dead cells, and no more proliferating or resting cells appear. The time lag in regrowth of G_0 cells is a function of random-phase durations and other kinetic parameters. The reason that a 93% (instead of 100%) cure rate was observed in these experimental data is probably because of the development of drug-resistant cell lines and the lesser chance of killing the last surviving cancer cell. These two factors had been discussed by Wilcox (18) and are not considered in our models. The second case involves BDF_1 mice receiving an inoculum of 10^7 cells and treated with the same dose and schedule. The L1210 leukemia is no more curable. The expected cell populations during the scheduled treatment for this situation are shown in figures 11 and 12. Although there is an equal log kill of S cells for each treatment day as in the previous case, at the end of treatment more than one cell appears in each of the proliferating phases and in the resting state. These cells will regrow to a lethal number of 10^9 cells between Days 27 and 28. The lifespan predicted by the simulation is 2-3 days shorter than the observed value. This can be explained by some observations that when tumor cells grow to a number of about 10^8, the growth rate decreases and it takes two or three times longer than ever to let a tumor grow 1 log from 10^8 to 10^9 cells. This is probably because at the time when the leukemic cell population grows to 10^8 cells or more, the cancer cell population in the tumor mass is so crowded that the nutritional state around the proliferating cells is not sufficient for cancer cells to remain in an active proliferative state. However, choosing a "best" schedule from the simulations of a series of different schedules will not give any serious misjudgment since the difference in the predicted and true lifespans will be consistent throughout all the schedules.

To demonstrate the process of choosing a "best" schedule from the simulated cancer chemotherapeutic effects of a series of different schedules, we consider the same L1210-ara-C therapeutic system with an inoculum of 10^5 cells and with a 15-mg/kg/dose given on schedules of q1h × 8, q3h × 8, q6h × 8, or q12h × 8 starting on Day 2. The preliminary results of computer simulations are summarized in table 2.

The computer simulations also show that for the q1h × 8 schedule, the accumulated drug concentrations within 8 hours of treatment are higher than $C_{max,2}$ and there is no population regrowth between any two doses of treatment. The regrowth period before the next dose in the q6h × 8 schedule is much longer than that in the q3h × 8 schedule. For the q12h × 8 schedule, the expected cell population in S phase

TABLE 2.—Comparison of simulated and observed chemotherapeutic effects on L1210 leukemia in animals given 10^5-cell ip inoculum and treated with ara-C (15 mg/kg/dose) at different schedules

Schedule	Lifespan (days)		Net log kill of S-phase cells per dose	Proliferating cell population at end of treatment
	Simulated (expected)	Observed (median)		
q1h × 8, Day 2	11.3	13.0	0.21	7.0×10^3
q3h × 8, Day 2	13.8	17.0	0.35	4.8×10^2
q6h × 8, Day 2	13.77	17.0	0.262	2.0×10^3
q12h × 8, Day 2	11.9	15.5	0.012	2.4×10^5

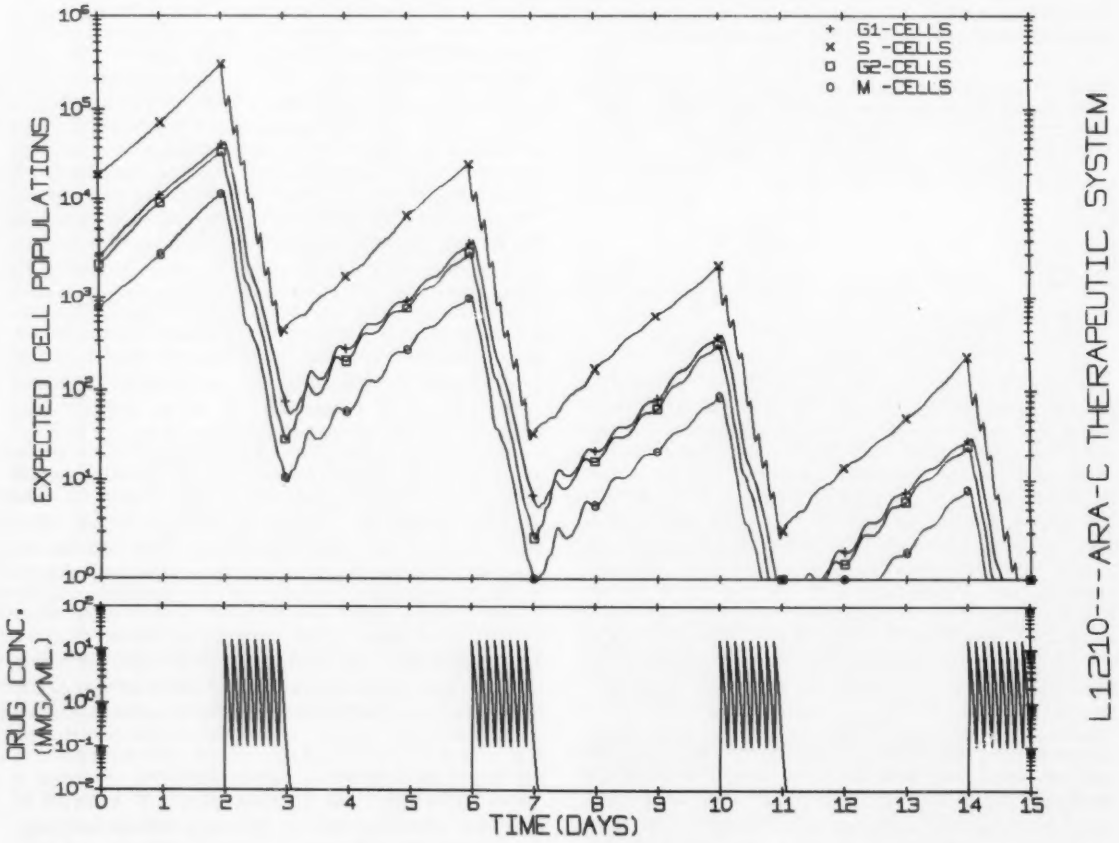

FIGURE 9.—Concentration of ara-C and expected cell populations in proliferating phases of L1210 leukemia. Animals received a 10^5-cell inoculum and were treated on a schedule of 15 mg/kg/dose q3h × 8 on Days 2, 6, 10, and 14.

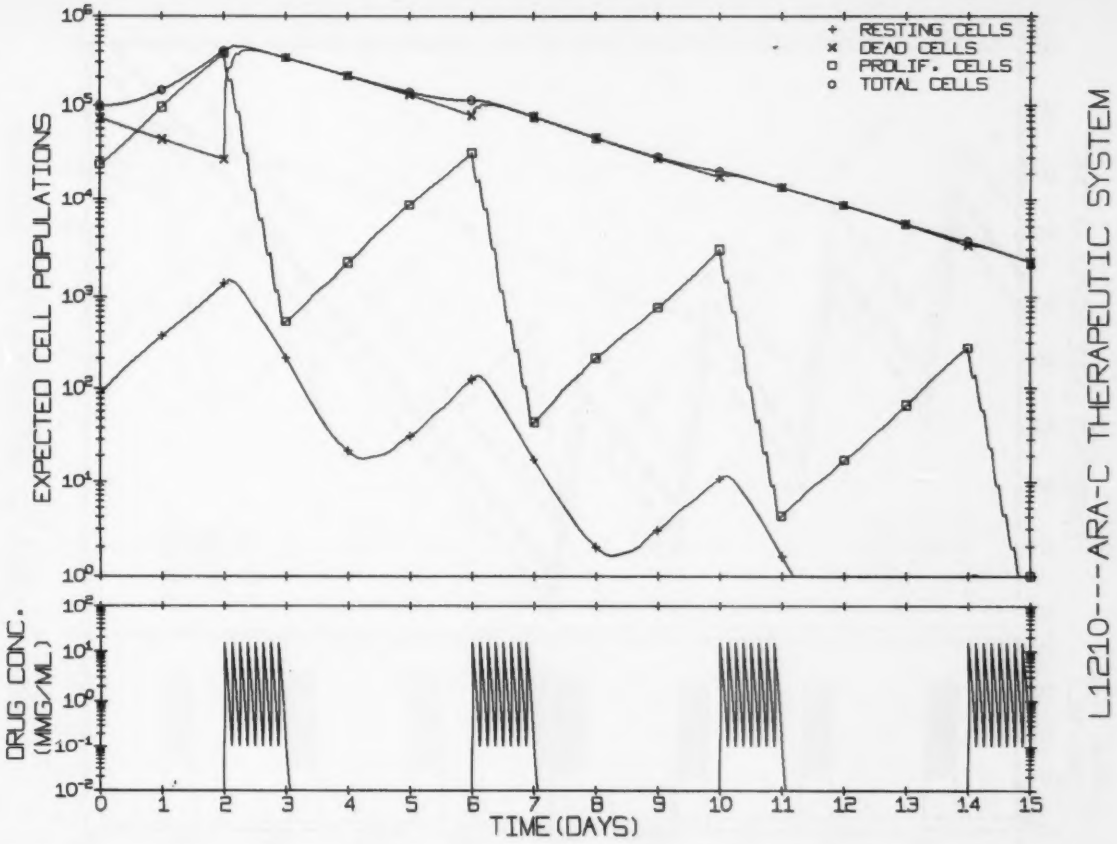

FIGURE 10.—Concentration of ara-C and expected cell populations of proliferating, resting, and dead compartments of L1210 leukemia. Animals received a 10^5-cell inoculum and were treated on a schedule of 15 mg/kg/dose q3h × 8 on Days 2, 6, 10, and 14.

within those 4 days of treatment oscillates around a constant number of 1.3×10^5, just as the expected cell populations in other proliferating phases and in the resting compartment oscillate around certain constant numbers. (The simulation charts for the q12h × 8 schedule look quite different from the others and are shown in figs 13 and 14.) From the above discussions, the q3h × 8 schedule is chosen to be the "best" schedule, among these four simulated schedules, for the treatment of L1210 leukemic mice (10^5-cell inoculum) with ara-C at a dose of 15 mg/kg.

In synchronized cultures of Chinese hamster cells, Tobey (19) found that ara-C grossly reduces the transition of cells from G_1 phase to an active S phase and causes accumulation of cells in the vicinity of the G_1-S boundary. This blocking effect is not considered in the present models and may cause us to underestimate the parameter $l_{max,2}$. However, the blocking effects can be included in our computer simulations with some modifications and may be the topic of a future work.

CONCLUDING REMARKS

This mathematic study for cancer chemotherapy was intended to obtain some results which are usually difficult or impossible to measure, and to help experimental therapists explore further the tumor behavior during scheduled treatment. The models not only incorporate the known parameters but also suggest some additional parameters which are important in interpreting the phenomena and which need to be further investigated. For example, in discussing the cell-drug interactions, the fraction cell-kill hypothesis (11) stimulates the formulation of equation (16) to express the drug dependency of loss

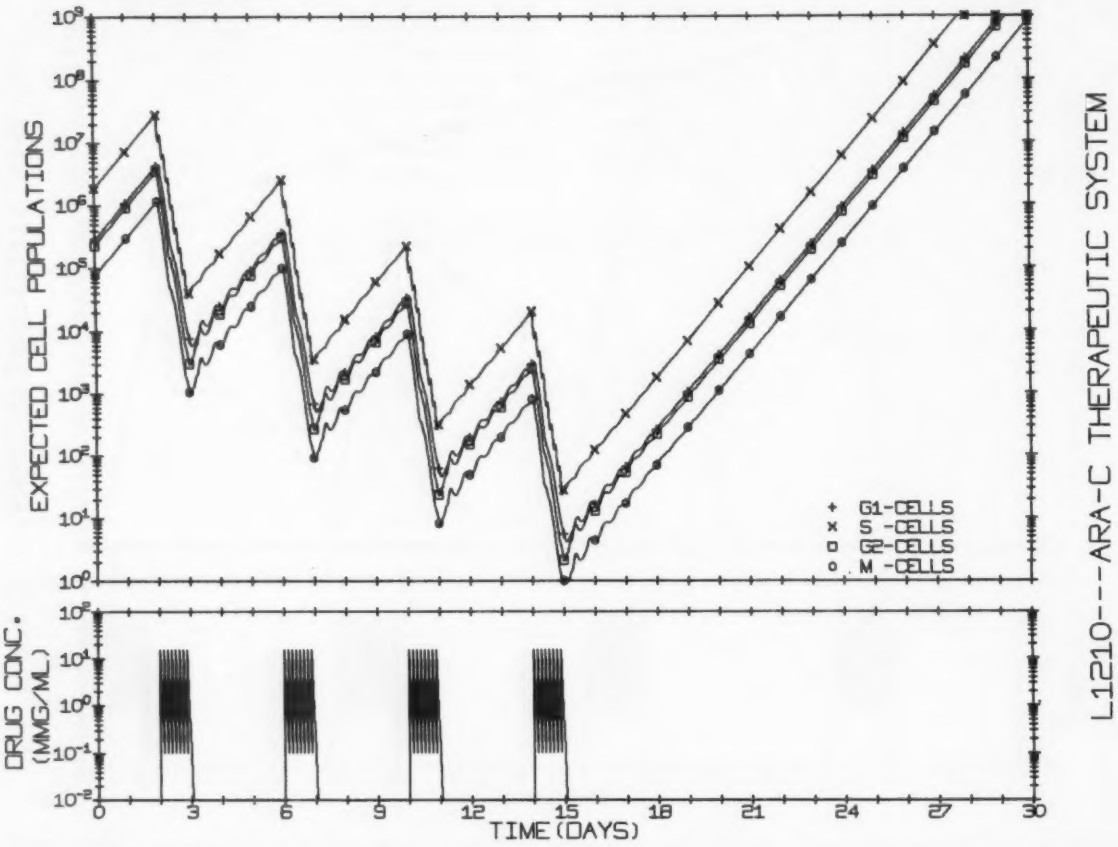

FIGURE 11.—Concentration of ara-C and expected cell populations in proliferating phases of L1210 leukemia. Animals received a 10^7-cell inoculum and were treated on a schedule of 15 mg/kg/dose q3h × 8 on Days 2, 6, 10, and 14.

functions. Although some preliminary investigations of some of the involved parameters ($C_{max,i}$, $C_{min,i}$, $l_{max,i}$, and l_i) in cell culture for some tumor systems have been done in this laboratory by Wilkoff et al (17), thorough and massive information in this area is not yet available and needs further investigation. Also, the experimental percentage labeled mitosis technique initiates the derivation of the theoretic FLM function to provide a more accurate prediction of the cell cycle phase parameters. In turn, this derivation suggests some additional parameters, associated with the resting and nondividing cells, whose biologic aspects need to be further investigated experimentally.

In evaluating the cancer chemotherapeutic effects, the approach we take in this study with separate formulations for cancer cell populations in each of the proliferating phases and the resting state has the following advantages: (*a*) it provides the theoretic FLM functions which may be used to predict the cell cycle phase parameters for any period of a scheduled treatment if the observed FLM curves are available; (*b*) the cell cycle phase specificity of anticancer drugs is incorporated in the simulation of a scheduled treatment; and (*c*) it makes possible the analysis of the blocking effects of some anticancer agents.

This study also provides a more systematic approach to model construction for cancer chemotherapy. This approach includes the pharmacokinetic considerations, the proposed cell-drug interaction relationships, the prediction of cell cycle kinetic parameters, and the computer simulation of cancer chemotherapeutic effects of scheduled treatments. The three mathematic models developed in this paper are based on three different hypotheses. It is most likely that the proliferative mechanisms might vary

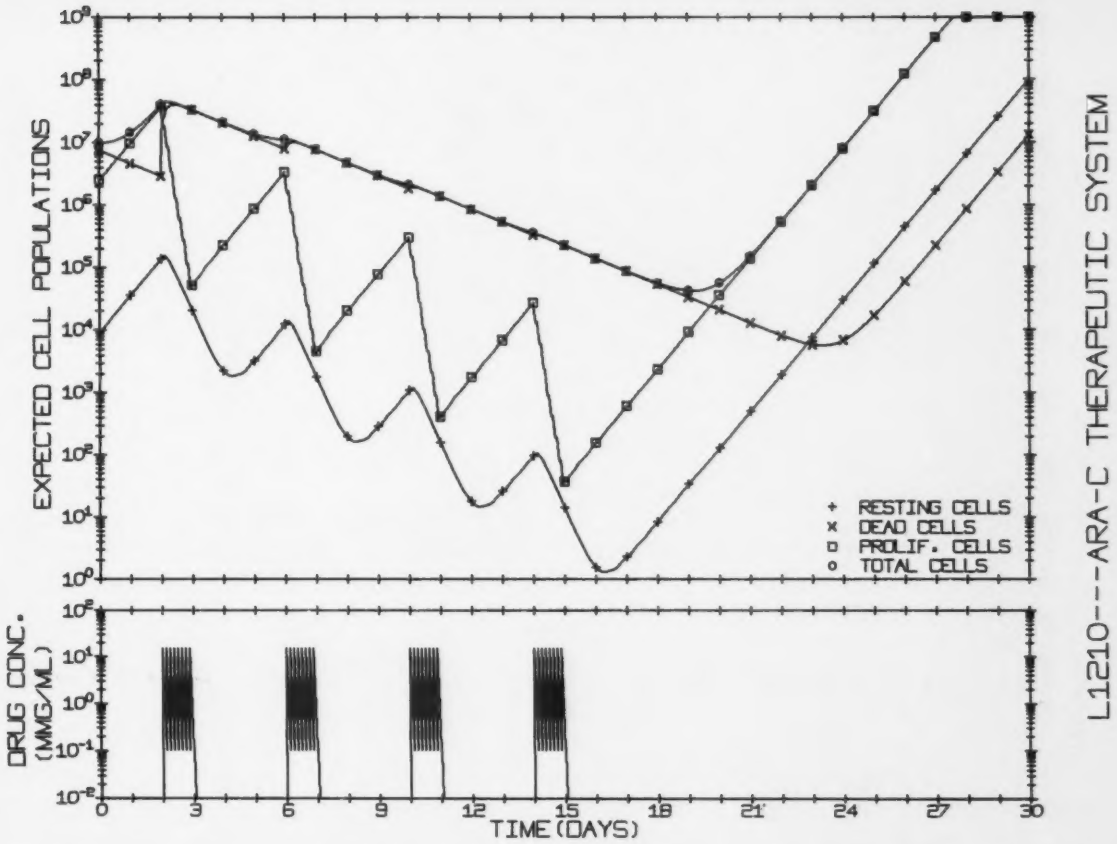

FIGURE 12.—Concentration of ara-C and expected cell populations of proliferating, resting, and dead compartments of L1210 leukemia. Animals received a 10^7-cell inoculum and were treated on a schedule of 15 mg/kg/dose q3h × 8 on Days 2, 6, 10, and 14.

partially from one class of tumors to another. The cell cycle kinetic models proposed according to observations in some experimental tumor systems might be suitable only for a similar class of tumors but not for others. The degree of applicability of each model to a particular therapeutic system is hard to justify unless we actually perform the simulation and judge from the available data. Therefore, a comparison of numerical results after applying these models to some real systems will be essential.

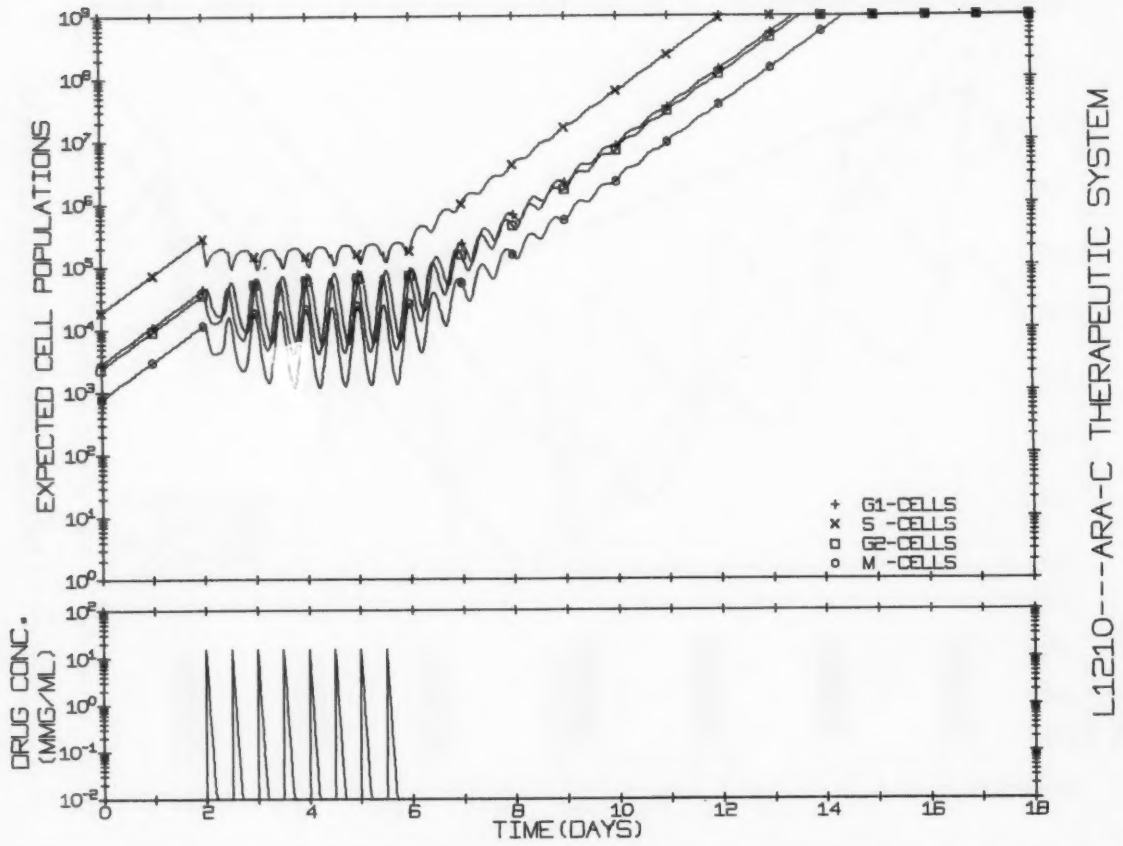

FIGURE 13.—Concentration of ara-C and expected cell populations in proliferating phases of L1210 leukemia. Animals received a 10^5-cell inoculum and were treated on a schedule of 15 mg/kg/dose q12h × 8 starting on Day 2.

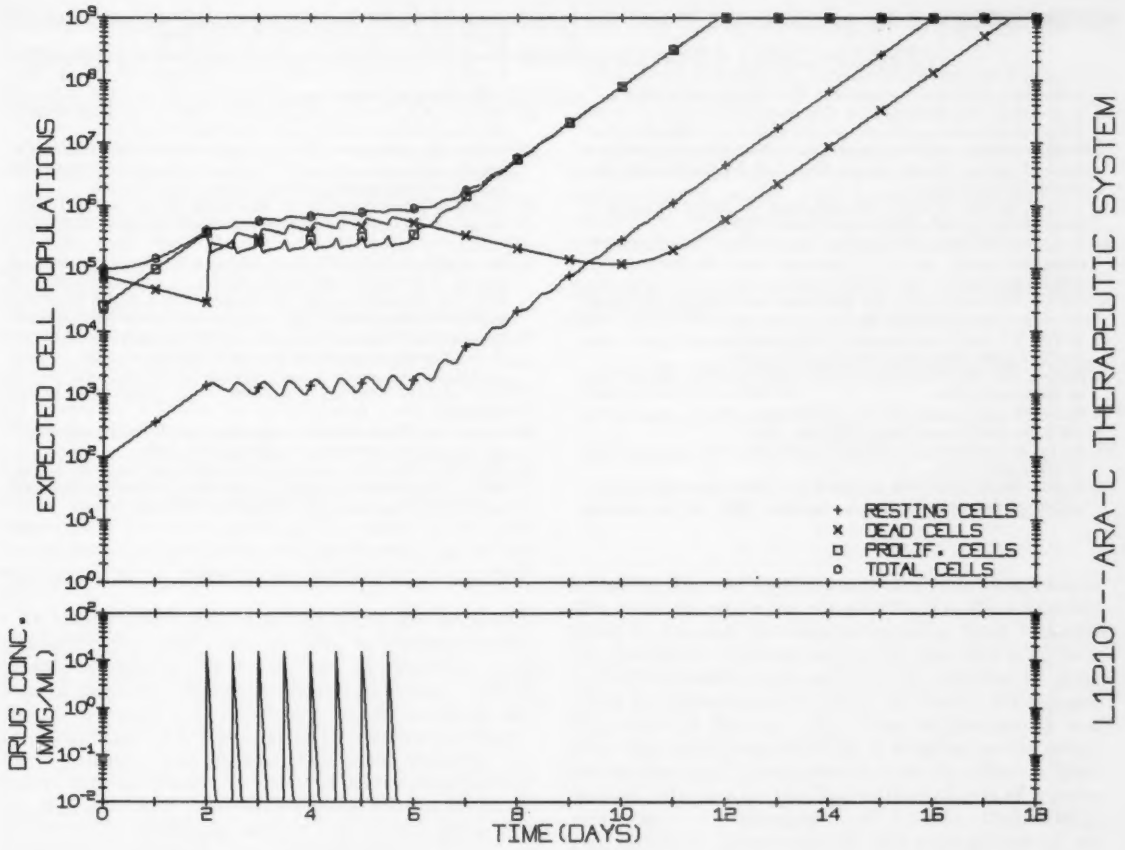

FIGURE 14.—Concentration of ara-C and expected cell populations of proliferating, resting, and dead compartments of L1210 leukemia. Animals received a 10^5-cell inoculum and were treated on a schedule of 15 mg/kg/dose q12h × 8 starting on Day 2.

REFERENCES

1. Teorell T. Kinetics of distribution of substances administered in the body. Arch Int Pharmacodyn Ther 57:205-240, 1937.
2. Quastler H, and Sherman FG. Cell population kinetics in the intestine epithelium of the mouse. Exp Cell Res 17:420-438, 1959.
3. Himmelstein KJ, and Bischoff KB. Mathematical representations of cancer chemotherapy effects. J Pharmacokinet Biopharm 1:51-68, 1973.
4. ———. Models of ara-c chemotherapy of L1210 leukemia in mice. J Pharmacokinet Biopharm 1:69-81, 1973.
5. Jusko WJ. A pharmacodynamic model for cell-cycle-specific chemotherapeutic agents. J Pharmacokinet Biopharm 1:175-200, 1973.
6. Chuang SN, and Lloyd HH. Mathematical analysis of cancer chemotherapy. Bull Math Biol 37:147-160, 1975.
7. DeVita VT. Cell kinetics and the chemotherapy of cancer. Cancer Chemother Rep Part 3, vol 2(1):23-33, 1971.
8. Skipper HE. Improvement of the model systems. Cancer Res 29:2329-2333, 1969.
9. Burns FJ, and Tannock IF. On the existence of a G_0-phase in the cell cycle. Cell Tissue Kinet 3:321-334, 1970.
10. Smith JA, and Martin L. Do cells cycle? Proc Natl Acad Sci USA 70:1263-1267, 1973.
11. Skipper HE, Schabel FM, Jr, and Wilcox WS. Experimental evaluation of potential anticancer agents. XIII. On the criteria and kinetics associated with "curability" of experimental leukemia. Cancer Chemother Rep 35:1-111, 1964.
12. Von Foerster H. Some remarks on changing populations. *In* The Kinetics of Cellular Proliferation (Stohlman F, Jr, ed). New York, Grune and Stratton, 1959, pp 382-407.
13. Bischoff KB, Dedrick RL, Zaharko DS, et al. Methotrexate pharmacokinetics. J Pharm Sci 60:1128-1133, 1971.
14. Chuang SN, and Lloyd HH. Analysis and identification of stochastic compartment models in pharmacokinetics: implication for cancer chemotherapy. Math Biosci 22:57-74, 1974.
15. Cooley JW, and Tukey JS. An algorithm for the machine calculation of complex Fourier series. Math Comput 19:297-301, 1965.
16. Skipper HE, Schabel FM, Jr, and Wilcox WS. Experimental evaluation of potential anticancer agents. XXI. Scheduling of arabinosylcytosine to take advantage of its S-phase specificity against leukemia cells. Cancer Chemother Rep 51:125-165, 1967.
17. Wilkoff LJ, Dulmadge EA, and Lloyd HH. Kinetics of effect of 1-β-D-arabinofuranosylcytosine, its 5′-palmitoyl ester, 1-β-D-arabinofuranosyluracil, and tritiated thymidine on the viability of cultured leukemia L1210 cells. J Natl Cancer Inst 48:685-695, 1972.
18. Wilcox WS. The last surviving cancer cell: the chances of killing it. Cancer Chemother Rep 50:541-542, 1966.
19. Tobey RA. Effects of cytosine arabinoside, daunomycin, mithramycin, azacytidine, adriamycin, and camptothecin on mammalian cell cycle traverse. Cancer Res 32:2720-2725, 1972.

Stochastic Compartmental Modeling of the Disposition of 5-(3,3-Dimethyl-1-triazeno)imidazole-4-carboxamide (NSC-45388)[1,2]

Bayliss McInnis,[3] Asha Kapadia,[4] Souhail El-Asfouri,[3] and Ti Li Loo[5,6]

Deterministic compartmental modeling has become an established method of studying the pharmacokinetics of cancer drugs. For example, a three-compartment model has been used by Loo et al (1) to describe the distribution of 5-(3,3-dimethyl-1-triazeno)imidazole-4-carboxamide (NSC-45388). Bischoff, Dedrick, and Zaharko (2) have developed a compartmental model for methotrexate[7] pharmacokinetics. On the other hand, stochastic compartmental analysis remains in the evolvement stage. The theory of illness-death processes as given by Chiang (3) provides a basis for stochastic compartmental analysis. Significant results have recently been obtained by Matis and Hartley (4) for a discrete population of particles in a system of *m* compartments. These authors have reported on a procedure for identifying the parameters of the model when time-series data are available only on the passage of the total quantity of material to the exterior of the model.

In pharmacokinetic modeling, data are generally available for only one of the *m* compartments. Measurements of the total loss of material from human subjects are inconvenient to obtain, but on the other hand, it is relatively simple to assay the concentration of a material in the central compartment, namely, the plasma. We have recently obtained results similar to those of Matis and Hartley (4); however, our treatment can be applied to pharmacokinetic modeling when time-series data are available for a single compartment only.

In the deterministic theory the parameters of the model are estimated by the least-squares technique. Following Matis and Hartley we have derived the variance covariance matrix for the observations from the single compartment. We then incorporate the covariance kernel in a generalized least-squares estimation of the parameters from time-series data.

In the following sections we illustrate our treatment with a two-compartment model. This can easily be generalized to the case of *m* compartments. As an example of the application of the stochastic two-compartment model and parameter-identification procedure, we consider time-series data for the new cancer chemotherapeutic agent NSC-45388.

DERIVATION OF DIFFERENTIAL DIFFERENCE EQUATIONS

Consider the following two-compartment system with three parameters:

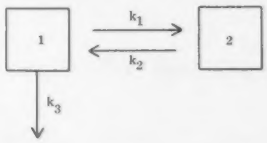

where k_1, k_2, and k_3 represent the time-independent flux rates between the compartments. We are interested in tracing the disposition of a drug through the system at various points in time. Let $n_i(t)$ be a random variable representing the number of drug units in compartment i ($i = 1,2$) at time t. We assume that each of the $n_i(t)$ units acts independently and that the underlying pattern of drug molecule movements from one compartment into the other is Markovian. In other words, future transitions of a molecule are independent of past transitions. Furthermore, given $n_i(t)=R$, the probability of exactly one drug molecule transferring from compartment 1 to compartment 2 in an interval $(t, t+\Delta t)$ is $R k_1 \Delta t + o(\Delta t)$. The probability of exactly one exit from compartment 1 to the exterior of the system is $Rk_3 \Delta t + o(\Delta t)$. Similarly, for $n_2(t)= S$, the probability of exactly one drug molecule transferring back from compartment 2 to compartment 1 in $(t, t+\Delta t)$ is $Sk_2 \Delta t + o(\Delta t)$. Clearly, $1-(k_1 + k_2)\Delta t+0(\Delta t)$ denotes the probability that a particle in compartment 1 will remain there during $(t, t+\Delta t)$.

Let $P_{n_1,n_2}(t)$ be the probability that $n_i(t)=n_i (i=1,2)$. Direct enumeration of possible events in $(t, t+\Delta t)$ yields the following differential difference equation:

$$\begin{aligned}\frac{dP_{n_1,n_2}(t)}{dt} &= -\left(n_1k_1 + n_2k_2 + n_1k_3\right)P_{n_1,n_2}(t) \\ &+ \left(n_1 + 1\right)k_3P_{n_1+1,n_2}(t) \\ &+ \left(n_1 + 1\right)k_1P_{n_1+1,n_2-1}(t) \\ &+ \left(n_2 + 1\right)k_2P_{n_1-1,n_2+1}(t) \\ & n_1, n_2 \geq 0\end{aligned} \qquad (1)$$

We assume that the initial value $n_1(0)$ of the number of drug molecules in compartment 1 has a normal distribution with a mean equal to N_1 and an

[1]Supported in part by contract NO1-CM-61156 from the Division of Cancer Treatment, National Cancer Institute, National Institutes of Health, Department of Health, Education, and Welfare; and in part by NSF grant No. DCR 74-17282.

[2]NSC-45388: CAS reg. No. 4342-03-4; DIC. Supplied by Drug Research and Development, DCT, NCI.

[3]Department of Electrical Engineering, University of Houston, Tex.

[4]The University of Texas System Health Science Center at Houston, School of Public Health, and University of Houston.

[5]The University of Texas System Cancer Center, M. D. Anderson Hospital and Tumor Institute, Houston.

[6]*Reprint requests to:* Dr. Ti Li Loo, The University of Texas System Cancer Center, M. D. Anderson Hospital and Tumor Institute, Houston, Tex 77025.

[7]Methotrexate: NSC-740; CAS reg. No. 59-05-2; glutamic acid, *N*-[*p*-[[(2,4-diamino-6-pteridinyl)methyl]methylamino]benzoyl]-.

SD (σ) equal to cN_1 where $0 \leq c \leq 1$. The initial number of drug molecules $n_2(0)$ in compartment 2 is assumed to be equal to 0. Let $K(\theta_1, \theta_2, t)$ = cumulant generating function of the joint distribution of $n_1(t)$ and $n_2(t)$. Then

$$K(\theta_1, \theta_2, t) = \log E\left[e^{\theta_1 n_1(t) + \theta_2 n_2(t)}\right]$$

with the initial conditions

$$K(\theta_1, \theta_2, 0) = \frac{\sigma^2 \theta_1^2}{2} + N_1 \theta_1,$$

$$n_2(0) = 0.$$

Then

$$K(\theta_1, \theta_2, t) = \left[\frac{\sigma^2 \theta_1^2}{2} + N_1\right] \log\left[1 + \left(e^{\theta_1} - 1\right) p_{11}(t) + \left(e^{\theta_2} - 1\right) p_{21}(t)\right]$$

where[8]

$$p_{ij}(t) = \frac{1}{\mathrm{Det}F} \sum_{j=1}^{2} f_{ij} f_{kj} e^{-\alpha_j t} \qquad (2)$$

$\alpha_i = i^{th}$, characteristic root of β

$$\beta = \begin{pmatrix} k_3 + k_1 & -k_1 \\ -k_2 & k_2 \end{pmatrix}$$

and $F = (f_{ij})$ is the matrix of the characteristic vectors corresponding to α_i. The cofactor of f_{ij} is denoted by F_{ij}. The mean and variance of $n_i(t)$ $(i = 1,2)$ are found to be

$$\mu_1(t) = N_1 p_{11}(t) \qquad (3)$$

$$\sigma_1^2(t) = N_1 p_{11}(t)\,[1 - p_{11}(t)] + \sigma^2 p_{11}(t)\,\delta_{11} \qquad (4)$$

where δ_{11} is the Kronecker delta.

Since measured data are obtained in terms of concentrations in compartment 1 (central compartment), it is convenient to express the results in terms of concentrations. The expected value and SDs of the concentrations in the two compartments are then obtained by dividing the expected number and SDs by their respective volumes.

[8]It can be easily shown (3) that $p_{ij}(t)$ = prob [a drug molecule in compartment j at time 0 will be in compartment i at time t]. Clearly, $0 \leq p_{ij}(t) \leq 1$ for all i, j and t. $p_{21}(\Delta t) = k_1 \Delta t$; $p_{12}(\Delta t) = k_2 \Delta t$.

GENERALIZED LEAST-SQUARES IDENTIFICATION OF THE PARAMETERS

The values of the parameters in a pharmacokinetic model are usually assumed to be unknown and are identified by least-squares estimation using time-series data. For the generalized least-squares parameter estimation procedure given in this paper, we utilize the variance covariance matrix, Σ, whose elements are determined by equations (5) and (6)

$$\mathrm{Var}\left[n_1(t_a)\right] = \sigma_{aa} = N_1 p_{11}(t_a)\left[1 - p_{11}(t_a)\right] + \sigma^2 p_{11}(t_a) \qquad (5)$$

$$\mathrm{Cov}\left[n_1(t_a), n_1(t_b)\right] = N_1 p_{11}(t_b - t_a)\, p_{11}(t_a)\left[1 - p_{11}(t_a)\right] + \sigma^2 p_{11}(t_b - t_a)\, p_{11}(t_a) \qquad (6)$$

The identification of the parameters of the model is carried out as follows:

1. Let ${}_0\Omega$ denote the vector of unknown parameter k_i where ${}_0\Omega = [{}_0k_1, {}_0k_2, {}_0k_3]$. Then obtain ${}_1\Omega$, the initial estimate of Ω, using the ordinary least-squares criterion.
2. Substitute the ${}_1\Omega$ $({}_k\Omega)$ estimates into the matrix β and determine its characteristic roots, α_i, and characteristic vectors, f^i.
3. Determine the parameters $p_{ij}(t)$ from equation (2).
4. Determine an estimate for the covariance matrix ${}_1\Sigma$ $({}_k\Sigma)$ from equations (5) and (6).
5. Iterate for new parameter estimates ${}_2\Omega$ $({}_{k+1}\Omega)$ using ${}_1\Sigma$ $({}_k\Sigma)$ in the following formula (*see* ref 5, p 233)

$$\underset{\sim}{D} = \left[{}_1G^T \Sigma^{-1}\, {}_1G\right]^{-1} {}_1G^T \Sigma^{-1} \left[Y - g(t, {}_1\Omega)\right]$$

where

$${}_1D^T = \left[{}_1d_1, {}_1d_2, {}_1d_3\right]$$

is the vector of differences

$$[{}_2k_i - {}_1k_i],$$

$${}_1G = [\partial g(t_i, \Omega)]/(\partial k_j)]\Omega = {}_1\Omega$$

$$\underset{\sim}{g}^t(t, \Omega) = [g(t_1), g(t_2), \ldots\ldots, g(t_n)]$$

is the n-vector of expected values

$$\mu_1(t_1), \mu_1(t_2), \ldots\ldots, \mu_1(t_n), \quad Y = [y_1, y_2, \ldots\ldots, y_n]$$

is the n-vector of observations

$$n_1(t_1), n_1(t_2), \ldots\ldots, n_1(t_n).$$

6. Repeat steps 2-5 obtaining ${}_i\Sigma$ and ${}_i\Omega$ estimates successively until the process converges.

7. Estimates of the SDs of k_1, k_2, and k_3 are obtained from the formula

$$\Sigma_{\Omega\Omega} = s^2\left[G^T\Sigma^{-1}G\right]$$

where

$$s^2 = \epsilon^t\Sigma^{-1}\epsilon/(n-3),$$

n is the number of data points, and ϵ is the vector of the errors.

RESULTS

In this section the estimation procedure is illustrated with previously published data for NSC-45388 in the dog (1). The procedure yields the distribution for the estimates of the concentrations in the compartments as well as the distribution of the estimates of the parameters. The estimates of the parameters of the two-compartment model are shown in table 1. The SDs for the values of the parameters can be reduced by increasing the number of data points. However, for clinical applications it is desirable to use the minimum number of data points. The predictions of the concentrations of the drug in the central compartment and the data points are shown in figure 1. Curves representing the predictions plus and minus 1 SD are also shown. Clearly the stochastic considerations improve parameter estimation and goodness-of-fit criteria; they also render it easy to compute drug distribution in each compartment.

DISCUSSION

In the present study, k_1 and k_2 are about the same size, but both are significantly larger than k_3. Similar relationships also hold for the same constants computed on the basis of the deterministic model previously described by us (1). It may therefore be inferred that the rates of influx and efflux of NSC-45388 between the central (plasma) and the peripheral (tissue) compartments are nearly identical. However, the rate of elimination of NSC-45388 from the central compartment is definitely slower than the rates of the intercompartmental fluxes. Myelosuppression in patients treated with NSC-45388 is often delayed; this is probably caused by the persistence of the drug in the body as a result of its delayed elimination from the body.

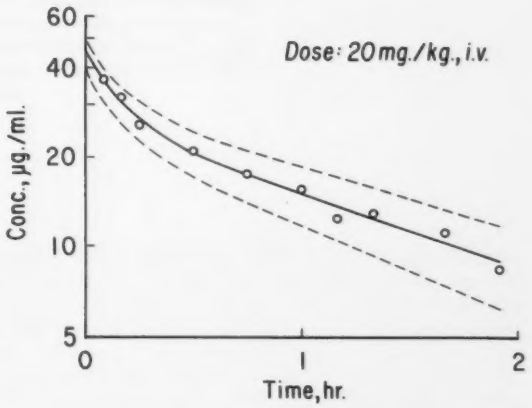

FIGURE 1.—Plasma disappearance of NSC-45388 in a dog.

TABLE 1.—Pharmacokinetic parameters of NSC-45388 (20 mg/kg, iv) in dogs

Dog No.	No. of iterations	$k_1 \pm$ SD (hr^{-1})	$k_2 \pm$ SD (hr^{-1})	$k_3 \pm$ SD (hr^{-1})	S^2
63	7	2.511 ± 0.5571	2.298 ± 1.536	1.482 ± 0.6152	4.79
72	4	3.016 ± 0.4347	2.156 ± 0.5653	3.032 ± 0.2585	2.482
91	5	2.846 ± 0.6073	3.453 ± 1.638	1.744 ± 0.3593	5.476
87	5	4.643 ± 1.009	3.699 ± 1.212	1.025 ± 0.2068	14.64
57	4	2.807 ± 0.1234	2.138 ± 0.1996	1.026 ± 0.0633	0.6692
76	5	1.970 ± 0.6056	3.834 ± 1.623	0.9082 ± 0.1298	5.599
Mean		2.966	2.930	1.536	

REFERENCES

1. LOO TL, TANNER BB, HOUSHOLDER GE, ET AL. Some pharmacokinetic aspects of 5-(dimethyltriazeno)-imidazole-4-carboxamide in the dog. J Pharm Sci 57:2126-2131, 1968.
2. BISCHOFF KB, DEDRICK RL, and ZAHARKO DS. Preliminary model for methotrexate pharmacokinetics. J Pharm Sci 50:149-154, 1970.
3. CHIANG CL. Introduction to Stochastic Processes in Biostatistics. New York, Wiley, 1968.
4. MATIS JH, and HARTLEY HO. Stochastic compartmental analysis; model and least squares estimation from time series data. Biometrics 27:77-102, 1971.
5. GOLDBERGER AS. Econometric Theory. New York, Wiley, 1964.

Analysis of the Effects of Antitumor Drugs on Cell Cycle Kinetics

Kwang B. Woo,[1] Larry B. Brenkus,[2] and Karl M. Wiig[2,3,4]

SUMMARY

A cell cycle stage-specific multicompartmental model has been developed and used to investigate the effects of antitumor drugs on the proliferation of tumors. The drug effects simultaneously considered are (*a*) non-cycle-specific killing and cycle stage-specific killing of cells, (*b*) progression delay of cells through the cell cycle phases which may bring about an accumulation of cells in various phases of the cell cycle, and (*c*) prolongation of cell cycle times. These effects are analyzed in terms of possible variations in the behavior of cell kinetic parameters (namely, cell cycle times, cell loss rate, and growth fraction) and are implemented in the model specifying proper functional forms for the parameters. The time-course of drug distribution in a tumor-host system is also described by a two-compartment model and the factors affecting drug action are quantitatively formulated as a function of drug concentration. Simulation is carried out to examine the effects of BCNU, cytosine arabinoside, and methotrexate on the cell cycle and proliferation kinetics of L1210 leukemia, and the results of the simulation compare favorably with available experimental data. Also discussed are the sensitivity of drug effects to variation in dosage schedule and the different modes of drug actions exerted on each cell cycle phase.

[Cancer Chemother Rep 59:847-860, 1975]

Cell cycle and proliferation kinetics are concerned with the distribution of generation times plus a variety of other kinetic parameters describing both normal and tumor tissues, including the rate of cell loss and the growth fraction. Some of the kinetic studies are directed at animals and patients with cancer before and after therapy, and they deal specifically with dose- and time-survival curves to antitumor drugs, the effect of antitumor drugs on the interrelationship between functionally different cell compartments, and the effect of antitumor drugs on cell progression through the cell cycle.

A number of mathematical models and computer techniques have been developed to obtain various kinetic parameters of tumor growth kinetics, and these have been extensively reviewed (1). By treating each cell cycle phase as a separate compartment, a mathematical model has been developed and used to simulate the kinetic behavior of experimental tumor growth and associated changes in cell kinetic parameters.[5] The results obtained using the model were in good agreement with experimental data on Ehrlich ascites tumor, L1210 leukemia, JB-1 ascites tumor, and Sarcoma 180. In the present study, the model is extended to allow for the kinetic analysis of the effects of antitumor drugs on the cell cycle. These effects are characterized as (*a*) non-cycle-specific killing and cycle stage-specific killing of cells, (*b*) blocking or at least slowing down the progression of cells through the cell cycle phases which may bring about an accumulation of cells in various phases of the cell cycle, and (*c*) prolonging cell cycle times. Efforts are presently under way to relate these effects quantitatively to possible changes in three cell kinetic parameters (the cell cycle time, the rate of cell loss, and the growth fraction) and to compare them with available experimental data.

METHODS OF ANALYSIS

Compartmental Modeling: Tumor Growth Kinetics

The multicompartmental (cycle stage-specific) model is shown schematically in figure 1. The model is similar to the one used by Dombernowsky and Hartmann (2) except for the parameters δ_1 and δ_2 which represent the fractions of cells cycling in G_1 and G_2 respectively. These parameters were also defined as the cell proliferation parameters (3,4) and are related to the growth fraction of the tumor cell population. It is assumed that cell loss in the system occurs from all the compartments at the same rate

[1]Division of Cancer Treatment (DCT), National Cancer Institute (NCI), Bethesda, Md.

[2]Arthur D. Little, Inc., Cambridge, Mass.

[3]We wish to thank Dr. Seymour Perry for his encouragement and support of this work.

[4]*Reprint requests to:* Dr. Kwang B. Woo, DCT, NCI, Bldg 37, Rm 5D16, National Institutes of Health, Bethesda, Md 20014.

[5]Wiig KM, Brenkus LM, and Woo KB. A mathematical analysis of tumor growth kinetics. Submitted to *Mathematical Biosciences.*

Woo KB, Wiig KM, and Brenkus LM. A compartment model analysis of the cell cycle and proliferation kinetics of tumor cell populations. In preparation.

and that the cells in the Q_1 and Q_2 compartments do not return to the cycling phases. Using a conservation law for the balance of cells in each compartment, the dynamics of the tumor growth are described by a set of nonlinear differential equations with cell population-dependent kinetic parameters as follows:

$$M: \frac{dx_m}{dt} = F_2x_2 + \Gamma_2x_{q2} - F_mx_m - \beta_mx_m \quad (1)$$

$$G_1: \frac{dx_1}{dt} = 2\delta_1 F_mx_m - F_1x_1 - \beta_1x_1 \quad (2)$$

$$S: \frac{dx_s}{dt} = F_1x_1 + \Gamma_1x_{q1} - F_sx_s - \beta_sx_s \quad (3)$$

$$G_2: \frac{dx_2}{dt} = \delta_2F_sx_s - F_2x_2 - \beta_2x_2 \quad (4)$$

$$Q_1: \frac{dx_{q1}}{dt} = 2(1 - \delta_1) F_mx_m - \Gamma_1x_{q1} - \beta_{q1}x_{q1} \quad (5)$$

$$Q_2: \frac{dx_{q2}}{dt} = (1 - \delta_2) F_sx_s - \Gamma_2x_{q2} - \beta_{q2}x_{q2} \quad (6)$$

where x denotes the number of cells at time t in each compartment: x_m = the number of cells in M, x_1 = the number of cells in G_1, x_s = the number of cells in S, x_2 = the number of cells in G_2, x_{q1} = the number of cells in Q_1, and x_{q2} = the number of cells in Q_2. β_i is the rate of cell loss from each compartment, and F_i is the cell growth activity factor that is inversely related to the mean cell transit time (τ) in each cycle phase, where i = m, 1, s, 2, q_1, and q_2. δ_1 is the fraction of dividing cells returning to the cycling phases with $(1-\delta_1)$ representing the fraction of cells transferring to Q_1, and δ_2 is the fraction of cycling cells remaining in the cycling phases with $(1-\delta_2)$ representing the fraction of cells transferring to Q_2. Γ_1 and Γ_2 are functions representing the mechanisms of the transfer of noncycling cells in Q_1 and Q_2 to the cycling phases respectively.

As noted before, all kinetic parameters associated with tumor growth are tumor population dependent; for computer simulation, these are first derived in logarithmic form and are characterized for two parts of the growth pattern, (*a*) exponential growth and (*b*) non-exponential growth. Details of the derivation and biologic implications will be given elsewhere.[6] The cell population-dependent kinetic parameters are quantitatively related to the pattern of tumor growth; they are implemented computationally by an iterative scheme and are adjusted until the model predicts the growth curve as well as the cell cycle time, the growth fraction, and the cell loss rate. Computer programs are written in Fortran IV.

Compartmental Modeling: Drug Effects on Tumor Growth Kinetics

The multicompartmental model used to study the kinetics of tumor growth is extended to deal with the effects of antitumor drugs on the proliferation of tumor. Special emphasis is given to characterize possible variation in the behavior of three cell kinetic parameters (cell cycle time, cell loss rate, and growth fraction) brought about by the drugs in a tumor cell population. The relationship between

[6] See footnote 5.

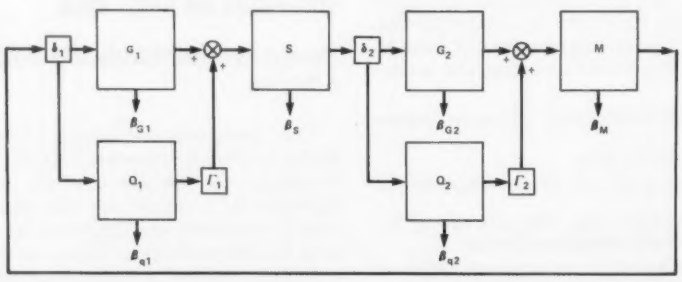

FIGURE 1.—Schematic diagram of a cell cycle stage-specific model for the cell cycle and proliferation kinetics of tumor cell populations.

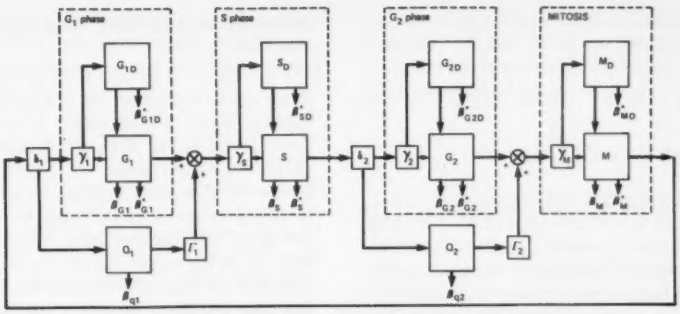

FIGURE 2.—Schematic diagram of the relationship between drug-tumor interactions illustrated by the cell cycle stage-specific model. Each block enclosed by broken lines represents three possible modes of drug action within each cell cycle-phase; β^* denotes the drug-induced cell kill rate, γ the fraction of cells accumulating in the drug-induced quiescent compartment, and τ^* the elongated transit time in each phase.

drug-tumor interactions may be established (fig 2) based on the dynamics of the kinetic parameters associated with the proliferating and quiescent compartments.

This schematic diagram may illustrate three modes of drug action: (*a*) cell kill, (*b*) delay of cell progression or accumulation of cells in various cell cycle phases, and (*c*) elongation of cell cycle times. First, for cell kill following drug administration, we simply introduce an additional β for each phase, β^*, which denotes the rate of cell kill. This may be defined as drug-induced cell loss and may be combined with the rate of natural cell loss. This is a drug dose-dependent mode of action and its relation to the dose is essentially determined by the shape of the time-survival curve or the dose-effect curve (5,6). Second, delay of cell progression is formulated by means of an accumulation of cells in the drug-induced quiescent compartments, G_{1D}, S_D, G_{2D}, and M_D. The accumulation of cells in G_1 or G_2 is, thus, implemented in terms of the fraction of cells transferring to G_{1D} or G_{2D}, which results in a change in the growth fraction. Four inhibitory factors, γ_1, γ_s, γ_2, and γ_m, are introduced which behave like δ_1 and δ_2 in that they split off into the drug-induced quiescent compartments a fixed fraction of the number of cells flowing in from the preceding cycle phase. Since the length of progression delay is dose dependent as demonstrated in a number of studies (7), the behavior of these parameters is drug-concentration dependent. The return of cells from the drug-induced quiescent compartments to the cycling phases is controlled by four factors: F_{I1}, F_{Is}, F_{I2}, and F_{Im}. As long as the drug continues to affect the tumor, no cells leave the quiescent compartments, that is, $F_{Ii} = 0$. When the cells do return, it is assumed that the rates of return are equal to the rates at which cells leave the cycling phases. Thus, it may be described that the growth fraction and the transfer rates of cells from G_{iD} are specifically affected by the drug concentration. Third, experimental observations of a progressive prolongation of generation time or S phase caused by increasing doses of antitumor drug (eg, BCNU[7] in L1210 leukemia [8,9]) are characterized through modification of the specific cell growth activities, such that elongation of the transit time through one or more cycle phases does not actually hold up any cells but does decrease the number of cells which leave these phases.

When we integrate all of these drug effects into the multicompartmental model consisting of ten compartments, a set of ten nonlinear differential equations is derived, including cell population-dependent parameters as well as drug-dependent parameters.

$$\frac{dx_m}{dt} = \gamma_m (F_2 x_2 + F_{I2} x_{I2} + F_{20} x_{20}) - (F_m + \beta_m + \beta_m^*) x_m \quad (7)$$

$$\frac{dx_{Im}}{dt} = (1 - \gamma_m) (F_2 x_2 + F_{I2} x_{I2} + F_{20} x_{20}) - (F_{Im} + \beta_{Im} + \beta_{Im}^*) x_{Im} \quad (8)$$

$$\frac{dx_1}{dt} = 2\delta_1\gamma_1 (F_m x_m + F_{Im} + x_{Im}) - (F_1 + \beta_1 + \beta_2^*) x_1 \quad (9)$$

$$\frac{dx_{I1}}{dt} = 2\delta_1 (1 - \gamma_1) (F_m x_m + F_{Im} x_{Im}) - (F_{I1} + \beta_{I1} + \beta_{I1}^*) x_{I1} \quad (10)$$

$$\frac{dx_{10}}{dt} = 2 (1 - \delta_1) (F_m x_m + F_{Im} x_{Im}) - (F_{10} + \beta_{10} + \beta_{10}^*) x_{10} \quad (11)$$

[7]BCNU: NSC-409962; CAS reg. No. 154-93-8; urea, 1,3-bis(2-chloroethyl)-1-nitroso-.

$$\frac{dx_s}{dt} = \gamma_s (F_1 x_1 + F_{11} x_{11} + F_{10} x_{10}) - (F_s + \beta_s + \beta_s^*) x_s \quad (12)$$

$$\frac{dx_{Is}}{dt} = (1 - \gamma_s) (F_1 x_1 + F_{11} x_{11} + F_{10} x_{10}) - (F_{Is} + \beta_{Is} + \beta_{Is}^*) x_{Is} \quad (13)$$

$$\frac{dx_2}{dt} = \delta_2 \gamma_2 (F_s x_s + F_{Is} x_{Is}) - (F_2 + \beta_2 + \beta_2^*) x_2 \quad (14)$$

$$\frac{dx_{I2}}{dt} = \delta_2 (1 - \gamma_2) (F_s x_s + F_{Is} x_{Is}) - (F_{I2} + \beta_{I2} + \beta_{I2}^*) x_{I2} \quad (15)$$

$$\frac{dx_{20}}{dt} = (1 - \delta_2) (F_s x_s + F_{Is} x_{Is}) - (F_{20} + \beta_{20} + \beta_{20}^*) x_{20} \quad (16)$$

However, in practice the model may be considerably simplified, since no drug kills cells and delays their progress in all phases at the same time. BCNU, for example, kills cells in all phases of the proliferative cycle at equal rates, and kills nonproliferating cells as well at a slower rate (10-14). On the other hand, cytosine arabinoside[8] only kills cells in S phase (7,-11,15-17), so that all the β^*'s are 0 except for β_s^*. For BCNU, all the α's are equal to 1, since there is no progression delay. When drugs, such as hydroxyurea (18),[9] cause delay in cell progression mainly in G_1, γ_1 is set to be less than 1. Cytosine arabinoside causes progression delay through all phases to a slight extent (but notably in G_1) and all γ's are equal to less than 1. BCNU is the only drug, of those we have considered, which elongates cell cycle time, and it increases the transit time in S.

EXPERIMENTAL DATA FOR ANALYSIS OF DRUG-DEPENDENT KINETIC PARAMETERS

Just as the main concern in the kinetic analysis of free-growing tumors was to specify proper functional forms for cell kinetic parameters of tumor population dependence, the drug effect study also requires the establishment of functional forms representing mechanisms of drug action expressed in terms of drug concentration. For computer simulation, a number of functional forms are derived for the kinetic parameters. Experimental data reported on BCNU, cytosine arabinoside, and methotrexate[10] are used in the following sections to illustrate the results.

For the rate of cell kill, β^*, the range of effective drug concentration is determined based on experimental data which show a saturation type of the functional form with minimum and maximum effective concentrations. Within these extremes of the effective concentrations, it is assumed that except where available experimental data may be expressed in terms of a power law, cell kill is linearly dependent on drug concentration. In relating the rate of cell kill to the effective drug concentration, it may thus be required to have the maximum effective value of β^*, which depends on the different nature of drug action. For non-cycle-stage-specific agents like BCNU there is no maximum effective value; on the other hand, for cycle-stage-specific agents like cytosine arabinoside, which kills cells in the S phase, there is a maximum effective value. Within the region of linearity, the relationship between cell kill rate (β^*) and drug concentration (C) is given by

$$\beta^* = K_B [C]^{\mu} \quad (17)$$

where K_B and μ are the constants to be determined by experimental observations.

The inhibitory factors (γ's) also have a linear dependence on drug concentration and are known to be inversely related to it. One must know the value of γ_{min} at the maximum effective concentration of drug to determine the pattern of the dependence, but it is not easily extractable from reported data. Attempts are made to carry out simulation using various values of γ_{min}, and to find the best agreement of the surviving fraction curve to the reported data.

It should be noted that elongation of cell cycle time results in an increase, $\tau^* - \tau$, and is linearly dependent on drug concentration. For BCNU, Young and DeVita (8) measured increases in transit time in S at various initial doses, D_o, which is expressed by the relationship

$$\tau_s^* = \tau_s + K_T [D_o]^{\eta} \quad (18)$$

where K_T and η are the constants to be determined by experimental observations. Equation (18) implies that the increased transit time, τ_s^*, is a step function; thus, it is equal to τ_s before drug effects begin and is equal to some constant afterwards, which is determined not by concentration but by initial dose. This mode of drug action has been characterized analytically by modifying the cell growth activity factor in $\Im$ (F_s) based on equilibrium between the tumor cells and the drugs assuming the constant number of drug receptor sites in a single tumor cell (19).

[8]Cytosine arabinoside: NSC-63878; CAS reg. No. 69-74-9; cytosine, 1-β-D-arabinofuranosyl-, monohydrochloride; ara-C.

[9]Hydroxyurea: NSC-32065; CAS reg. No. 127-07-1.

[10]Methotrexate: NSC-740; CAS reg. No. 59-05-2; glutamic acid, *N*-[p-[[(2,4-diamino-6-pteridinyl) methyl]methylamino]benzoyl]-.

The drug concentration in plasma is modeled by assuming that the mouse plasma under study consists of two compartments, one for faster decay and another for slow decay. This enables us to derive two differential equations for the dependence of concentration on initial dosage and time, given the following four parameters: (*a*) the ratio between the original amounts of drug in the two compartments, Δ; (*b*) the half-lives of the drug in the two compartments, $T_{½F}$ and $T_{½s}$ (readily obtained from the graph); and (*c*) the correction factor, θ, to convert a drug dosage (D) given in mg/kg to the equivalent dose in μg/ml.

$$\frac{dC_F}{dt} = \Delta \ \theta \ D \ - \frac{\ln 2}{T_{½F}} \ C_F \qquad (19)$$

$$\frac{dC_s}{dt} = (1-\Delta) \ \theta \ D \ - \frac{\ln 2}{T_{½s}} \ C_s \qquad (20)$$

where C_F denotes the drug concentration in the faster decay compartment, and C_s is the drug concentration in the slow decay compartment. A two-compartment model of drug distribution from a similar viewpoint has been discussed by Gillette (20) and Jusko (36).

There are two other effects of delayed drug response which must be taken into account: (*a*) a lag period (t_{lag}) before any drug effects begin, even at maximum concentration; and (*b*) a linger period (t_{ling}) after the concentration has fallen below minimum concentration, notably for drugs that cause progression delay before any cells are released from the drug-induced quiescent compartment. Both the lag period and the linger period depend not on the immediate concentration but on the concentration for a preceding period of time.

It is assumed that the length of the lag period is the time it takes for the integral of drug concentration to reach a threshold value, A_{lag}, and this agrees with experimental evidence. As the dosage administered decreases, the lag time increases such that

$$\int_0^{t_{lag}} C \cdot dt \doteq C \cdot t_{lag} = A_{lag}$$

where A_{lag} is constant. Before the time integral of concentration C reaches A_{lag}, no drug effect is seen; thus, all β^*'s are equal to 0, all γ's are equal to 1, and all τ^*'s become τ's. If the drug concentration falls below the minimum effective concentration (C_{min}) before a new dose is administered, the time integral is set at 0, so that there will be a lag effect for every dose of the drug.

The linger period only controls the release of cells from progression delay. It is assumed again that the length of the linger period is the time it takes for the integral of the drug concentration which is below C_{min} to reach a threshold value, A_{ling}. For the concentration above C_{min},

$$\int_0^{t_{ling}} (C_{min} - C) \cdot dt$$

is set at 0, so that it will only measure the appropriate part of the dose-effect curve. Before the integral is equal to A_{ling}, there is no return of cells from the drug-induced quiescent compartments. After that, the rates of return are equal to the rates that cells leave the cycling phases.

RESULTS: APPLICATION OF THE COMPARTMENTAL MODEL

The following is a scheme for utilizing the multicompartmental model in analyzing the effects of antitumor drugs on tumor growth kinetics. First, the model simulates L1210 leukemia ascites tumor as reported earlier by Yankee, DeVita, and Perry (21). The simulated results are illustrated in figure 3 (growth curve) and figure 4 (the cell population-dependent kinetic parameters) respectively. The present study emphasizes mainly the exponential phase

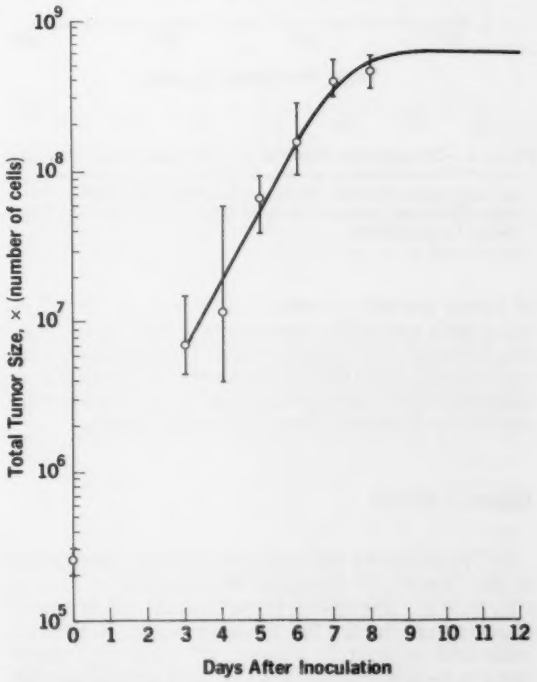

FIGURE 3.—Growth curve of L1210 leukemia ascites tumor after inoculation of 2 to 3 × 10^5 cells. Experimental data points (○) are from Yankee, DeVita, and Perry (21). Results of computer simulation of the model are represented by solid line. For simulation purposes, the exponential phase of tumor growth was set to occur up to the tumor size of 1.6 × 10^8 cells.

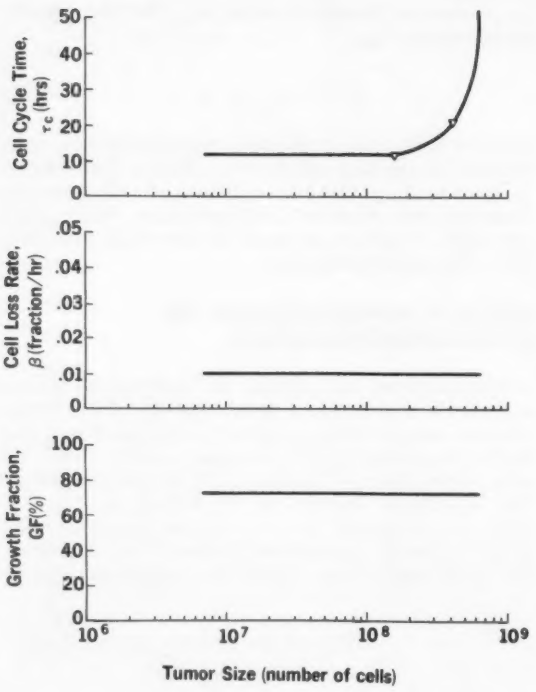

FIGURE 4.—Cell population dependence of cell kinetic parameters during L1210 ascites tumor growth. Experimental data points of the cell cycle time obtained (21) are superimposed by simulation results. Solid lines represent model prediction of cell kinetic parameters (τ_c, β, and GF).

of tumor growth in order to validate the model results with available experimental data (8,12-14,22-26), although investigation is under way on possible variation in these kinetic parameters following drug administration throughout the entire exponential and non-exponential phases of tumor growth.

Effect of BCNU

BCNU is known to be non-cycle-stage specific and is also known to elongate the duration of transit time in S (8). Therefore, there is equal cell kill in all four cycling phases. The rates of cell kill in both cycling and noncycling phases, β_p^* and β_q^*, would have to be determined as a function of drug concentration.

Based on the experimental data reported by Wilkoff et al (13) and Skipper et al (14) for proliferating cells and by Schabel et al (12) for nonproliferating cells, a relationship between the drug concentration and the cell kill rate is established from survival fraction curves at different dosage levels. Since the time-course of the surviving fraction shows a first-order decay (ie, surviving fraction = $e^{-\beta_p^* t}$), one measures the slopes of these decay lines and estimates the values of β_p^* for five different levels of drug concentration. The values of β_q^* are obtained in the same manner.

$$\beta_p^* = 1.074\ [C]^{1.4}$$

$$\beta_q^* = .25\ [C]^{1.77}$$

Such relationships are given in figure 5 where solid circles represent the data points of Skipper et al (14), solid triangles represent those of Wilkoff et al (13), and solid squares represent those of Schabel et al (12), all in L1210 leukemia in culture.

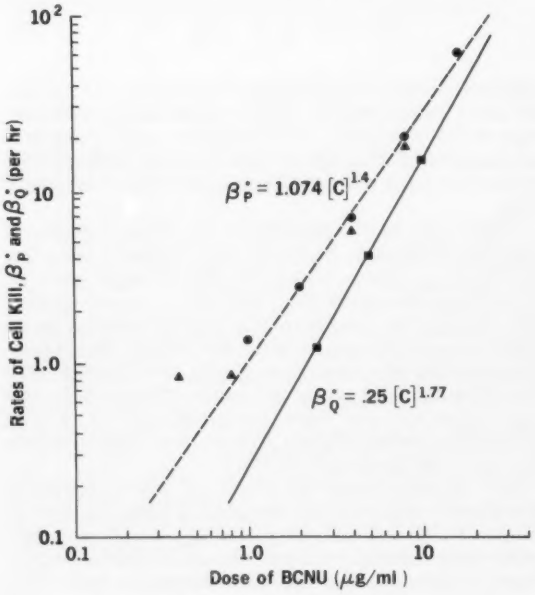

FIGURE 5.—Cell kill rate of cultured L1210 leukemia cells as a function of the concentration of BCNU. ● = Data points obtained from survival fraction curves at different dosage levels by Skipper et al (14), ▲ = data points by Wilkoff et al (13), and ■ = data points by Schabel et al (12). ———— and ----- are the best-fit lines to these data points.

As reported by Young and DeVita (8), a single dose of BCNU increased the transit time in S long enough for a percent labeled mitoses curve to be measured. Since this takes a minimum of 22 hours (τ_c), elongation effect of the transit time persists long after the concentration of BCNU has fallen below 0.2 μg/ml. It is assumed then that the increase in S-phase transit time depends on the initial dose of the drug,

not on the concentration. Based on the reported data (fig 6), the best-fit straight line is given by

$$\tau_s^* = \tau_s + 1.1\ [D\ ]^{.737}$$

In a sample run of a single dose of 6 mg/kg of BCNU, there was almost no significant difference between the survival fraction with the transit time elongation in S and the survival fraction without the transit time elongation in S.

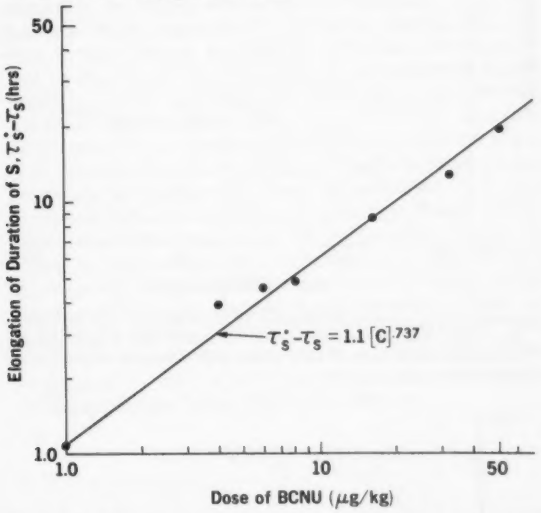

FIGURE 6.—Elongation of the transit time in S of cultured L1210 leukemia cells as a function of the concentration of BCNU. ● = Data points reported by Young and DeVita (8). ——— = Best-fit line to these data points.

Since the data by Schabel et al (12) and Wilkoff et al (13) generally showed a t_{lag} which decreased with increasing concentration, it is approximated by assuming that $\beta_p^* = 0$ until $c \cdot t_{lag} = A_{lag}$ = constant, and then estimated that this constant be 0.5 (hour·μg/ml).

The functional forms of β^* have been generated and confirmed by Wilkoff's experiments. Since these experiments were carried out with a single injection of drug, two simulations have been performed: (*a*) continuous infusion of drug (constant concentration), and (*b*) single dose with half-life of 54 minutes, which is the value reported. The continuous infusion simulation would provide a strict lower bound for how fast the surviving fraction can fall. Both of two simulated results (fig 7) are in acceptable ranges.

Effect of Cytosine Arabinoside

The drug action of cytosine arabinoside results from S-phase-specific cell killing and from affecting the progression rate of cells from S to G_2 phase to a greater extent than from G_1 to S (15). In cell killing,

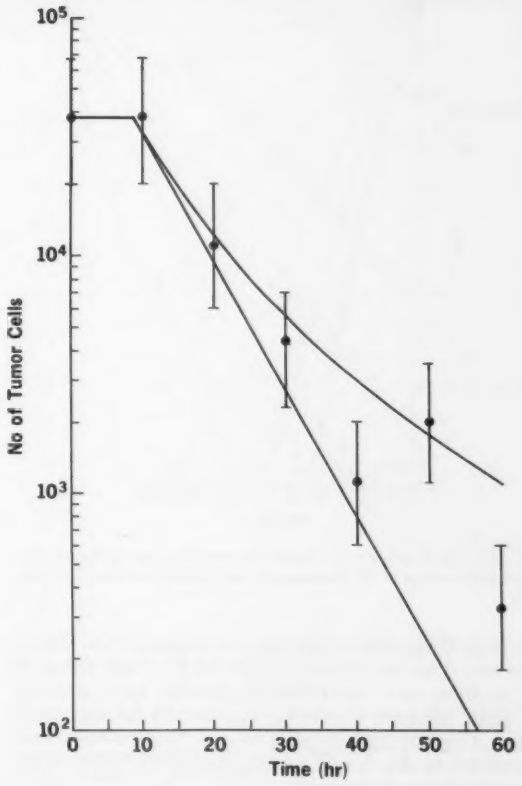

FIGURE 7.—Time-course behavior of the number of surviving tumor cells after BCNU is administered at 4 μg/ml at time 0. ●= Data points (25). Model prediction of the time-course behavior: upper curve = single dose of 4 μg/ml with half-life of 54 mins; lower curve = constant infusion of 4 g/ml.

it is modeled with only one $\beta_s^* > 0$ and other β^*'s = 0. As with BCNU, a relationship between an observed survival fraction curve and the kinetic parameters associated with the drug effect of cytosine arabinoside was established, in particular a plot of the observed β^* versus various concentrations of cytosine arabinoside. Because cytosine arabinoside is cell cycle stage specific, the relationship is not simply derived. Using the L1210 model, computer simulation is carried out for various constant values of β_s^* to find the patterns of the resulting survival fraction curves (fig 8). Notice that after some initial curvature (due to the fast killing of the cells then in S phase), the survival fraction curves become straight lines.

A plot of the slopes of these curves versus the values of β_s^* can be interpolated to a smooth curve. This relationship now gives us the necessary tie between the compartmental model for S-phase cell kill and the observed experimental results. By plotting the available in vitro survival fraction data at

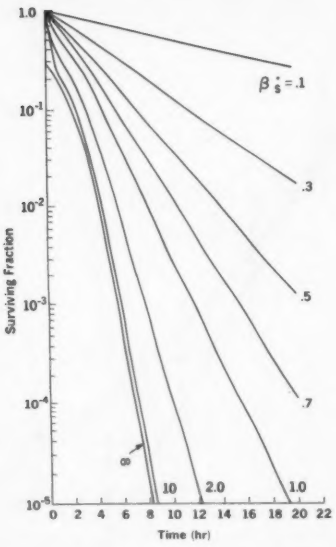

FIGURE 8.—Model prediction of survival fraction curves for various constant values of β^* for cytosine arabinoside in the L1210 model.

various drug concentrations, we measure the slopes and use them to obtain a value of β^*_s. This value of β^*_s is then, as a scattergram, plotted as a function of drug concentration (fig 9). As will be discussed later, the kinetic behavior of the system is rather sensitive to β^*_s, which is now specified to be drug-concentration dependent.

In order to generate an initial sharp decline in the surviving fraction after treatment with the maximum cytotoxic concentration of cytosine arabinoside, a straight line is fitted to data points (fig 9) by taking into account the fact that β^*_s should be fairly high when the concentration reaches 10 μg/ml. The approximate dependence is given by

$$\beta^*_s = 1.18\ [C]^{.532} \qquad \text{for } C_{min} \leq C \leq C_{max}$$

$$= 1.18\ [C_{max}]^{.532} \qquad \text{for } C > C_{max}$$

The maximum and minimum effective concentrations are obtained from the surviving fraction (26) in which change in the fraction is not observed for concentrations greater than 10 μg/ml, while no cell kill is measured with a concentration of 0.01 μg/ml even after exposure for 24 hours. It is chosen that $C_{min} = 0.01$ and $C_{max} = 10.0$.

The lag period of drug response is implemented into the system by computing A_{lag}, the value which must be exceeded before drug effects begin. It is designed that $C \cdot t_{lag} = A_{lag}$ with a line of slope = -1 (fig 10); this yields an A_{lag} of 1.05.

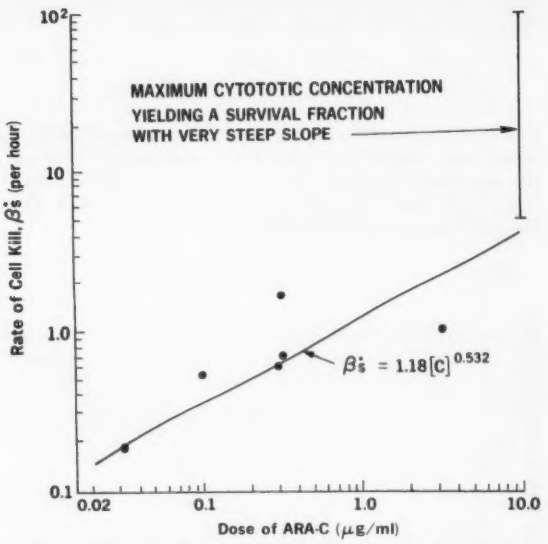

FIGURE 9.—Cell kill rate of cultured L1210 leukemia cells as a function of the concentration of cytosine arabinoside. A straight line fitted with experimental data points (26) is used to mimic the observed surviving fraction.

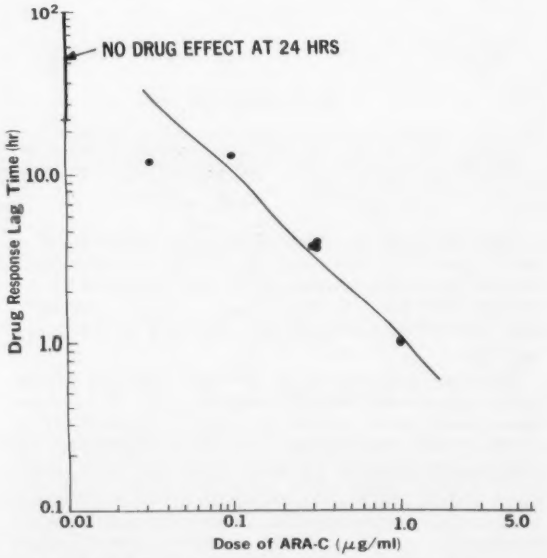

FIGURE 10.—Lag period of drug response as a function of the concentration of cytosine arabinoside. A straight line fitted with experimental data points (26) is used to mimic the observed surviving fraction.

For biologic half-lives, Mellett (27) stated that the serum half-lives of cytosine arabinoside were between 27 and 39 minutes in the mouse, depending on the amount of drug infused. Both values have been used in the present study to test sensitivities.

The inhibitory factor γ which controls the entry of cells into the drug-induced quiescent compartment is determined in the following way. The survival fraction data for maximum cytotoxic concentrations of cytosine arabinoside are primarily represented in a Gompertzian shape (fig 11; note 3.2 μg/ml and especially 10 to 30,000 μg/ml). This shape could be explained as follows: (*a*) For concentrations between 10 and 30,000 μg/ml all cells in S are assumed to be killed; the survival fraction curves resulting from exposure to cytosine arabinoside at this concentration are thus a reflection of the cells left in G_1, M, and G_2. (*b*) Cytosine arabinoside might slightly inhibit protein and RNA syntheses, which would be equivalent in our model to γ's $\neq 1$, and this would result in a Gompertzian form of survival fraction curves. (Due to the holdup of cells in other phases which prevents cells from being killed in S, the action of cytosine arabinoside produces a lower limit to the survival fractions.) In the present study, we chose to implement the mechanism described in (*b*), because although the distribution of transit times could not be easily altered, the progression delay of cells in the cell cycle could be easily integrated. As a result of computer simulation, it is found that a lower limit of γ_1 when C = 10 μg/ml produces the proper Gompertzian form. Thus, one obtains

$$\gamma_1 = 1 - 0.001 \cdot \frac{C - C_{min}}{C_{max} - C_{min}} \qquad \text{for } C_{min} \leq C \leq C_{max}$$

$$= 0 \qquad \text{for } C < C_{min}$$

$$= 0.999 \qquad \text{for } C > C_{max}$$

The validity of the model is then examined by comparing its performance to observed experimental results (fig 11). The model works well for the concentrations 0.1, 0.32, and the concentration-independent range of 10 to 30,000 μg/ml. However, note that the model predicts no cell kill after a 24-hour exposure to 0.032 μg/ml, while Wilkoff et al (26) actually measured cell kill. This is explained by figure 10, where one sees that the data point for lag time at 0.032 μg/ml was the only one far from the regression line, and thus a larger lag was used than was actually observed. Further, the model has much greater cell kill at the concentrations of 1.0 and 3.2 μg/ml than observed, and even more important, both of these end up falling to lower levels than would be seen from exposure to the maximum cytotoxic concentration. It is easily understood that they fall too fast because the too-large value of β_s^* was used (fig 9) where the selection of a large value for β_s^* is designed for simulation at concentrations greater than 10 μg/ml. The survival fraction curves falling lower than anticipated at lower concentrations were due to less inhibition which causes the progression delay. Overall, however, agreement is reasonable, and further characterization of the system dynamics is under way to various functional forms of β_s^*.

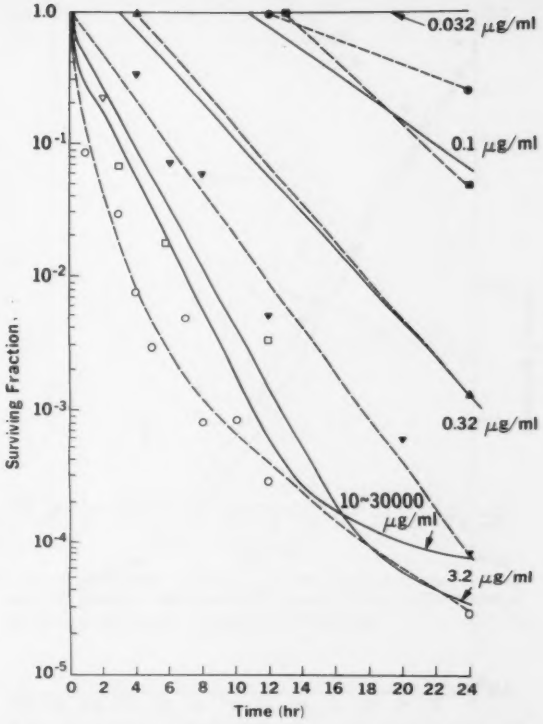

FIGURE 11.—Survival fraction curves at various concentrations of cytosine arabinoside.--- = Estimation of surviving fractions representing data points (● = 0.032 μg/ml; ■ = 0.1; ▲ = 0.32; ▼ = 3.2, □ and ○ = 10 to 30,000) reported by Wilkoff et al (26) and Skipper et al (14); ———— model prediction.

Several attempts have been made to simulate in vivo experiments by the model, and one set of experimental data (28) has been used to verify the model results (fig 12), where 15 mg/kg of cytosine arabinoside was injected every 3 hours during a 24-hour period. In figure 12, the solid line represents the model prediction with a half-life of 27 minutes, and the broken line represents a prediction with a half-life of 39 minutes. The model prediction is reasonable and could be improved by slightly decreasing the β_s^* for the maximum concentration of drug.

Effect of Methotrexate

As a first attempt to define the action of methotrexate the model was utilized to examine two survival fraction curves from Skipper et al (14) in an in vitro constant concentration study with 2 μg/ml and 5 to 60 μg/ml respectively. The system behavior is illustrated in figure 13. It is shown that the prediction with $\beta_s^* = 2.0$ and $\gamma = 0.992$ fits the survival fraction curve of 5 to 60 μg/ml rather well, although more cells must be inhibited to replicate the curve of the lower dose. $\beta_s^* = 0.7$ and $\gamma = 0.93$ gave a moderately good fit to 2 μg/ml, although more inhibition is still needed (γ should be < 0.93).

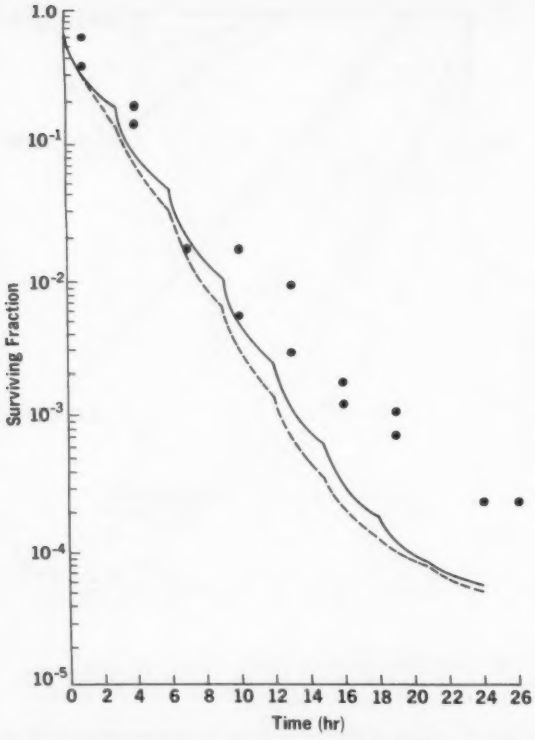

FIGURE 12.—Survival fraction curves of L1210 leukemia cells when 15 mg/kg of cytosine arabinoside was injected every 3 hrs during a 24-hr period. _____ = Model prediction with half-life of 27 mins and - - - = prediction with half-life of 39 mins where ● = data points (28).

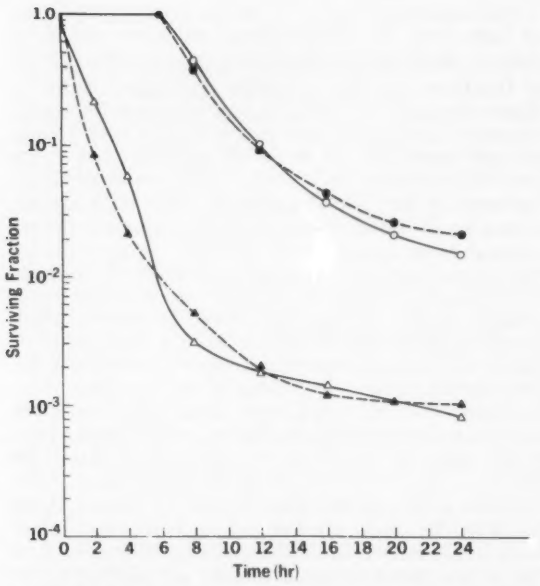

FIGURE 13.—Survival fraction curves of L1210 leukemia cells at constant methotrexate concentrations of 2 μg/ml (●) and 5 to 60 μg/ml (▲) (14). _____ = Estimation of data points and - - - - - = model prediction.

Dosage Schedule of Cell Cycle Stage-Specific Drugs and System Sensitivity

The computer simulation of the multicompartmental model presented above gives insights into the system performance of tumor-drug interactions and enables one to analyze the effects of various drugs on tumor growth kinetics. It is now illustrated how drug effects expressed in terms of survival fraction curves vary with mechanisms of drug action in the cell cycle (namely, [*a*] progression delay or accumulation of cells, or [*b*] elongation of cell cycle times together with drug-induced cell kill), and to what extent the drug effects are sensitive to variation in dosage schedules and different modes of drug actions exerted on each cell cycle phase.

In the system of tumor-drug interactions (fig 2), the geometry and configuration of the model are important in predicting drug effects. The relative placement of which phase(s) will exhibit progression delay and which phase(s) will exhibit drug-induced cell kill is significant in determining the modes of the effects produced. By taking into account the mechanisms of progression delay and elongation of cell cycle times and the relative position operating in the cell cycle, the system performance is examined for several dosage schedules and is compared by the resulting survival fraction curves.

If progression delay occurs immediately before cell kill, as in the case of G_1 accumulation and S killing, the cell kill is important because it instantaneously reduces cell population in S by several logs in an hour, but after that period it is the progression delay which is all-important. Schedule dependency rests on cell killing after progression delay is eased and cells enter the sensitive compartment. Figure 14 illustrates this type of drug action with the dosage schedules of every 11 hours, every 12 hours, every 14 hours, and every 21 hours during a period of 32 hours. Cell fractions in G_1 and S for each dosage schedule are summarized in figure 15. This type of a self-limiting drug action is expected for cytosine arabinoside, methotrexate, and other drugs. For every 12 and every 14 hours, when the progression delay is suddenly reduced, cells are flowing into S, and as a result there is a sharp peak in S fraction. The second dose of drug kills this cohort of delayed cells. For every 21 hours, a considerable fraction of cells remains in S until the first dose is administered. Comparison of the survival fraction curves (fig 14) indicates that every 14 hours appears to be more effective than other schedules.

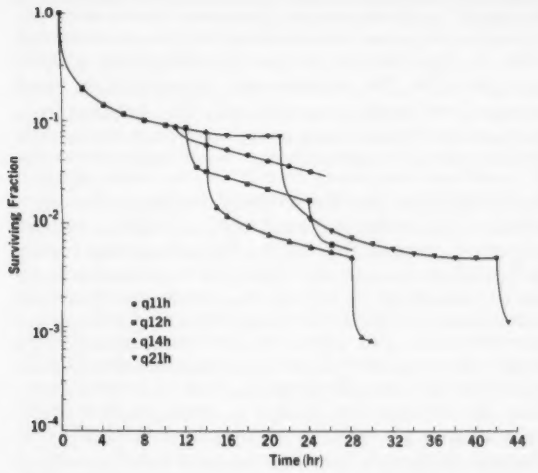

FIGURE 14.—Computer simulation of the survival fraction curves with the dosage schedules of q11h (●), q12h (■), q14h (▲), and q21h (▼), during a period of 32 hrs. The modes of the drug action are G_1 accumulation and S killing.

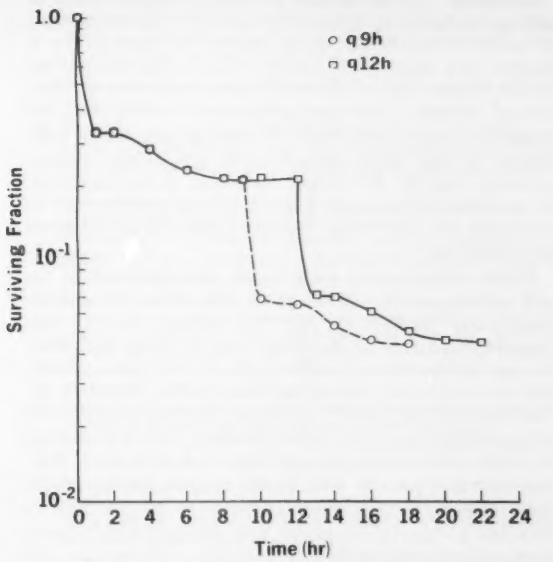

FIGURE 16.—Computer simulation of the survival fraction curves with the dosage schedules of q9h (○) and q12h (□). The modes of the drug action are G_1 elongation and S killing.

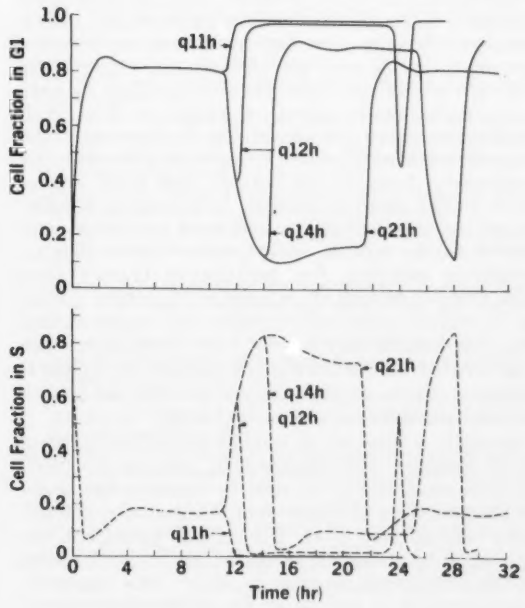

FIGURE 15.—Computer simulation of the time-course behavior of cell fractions in G_1 and S (see fig 14).

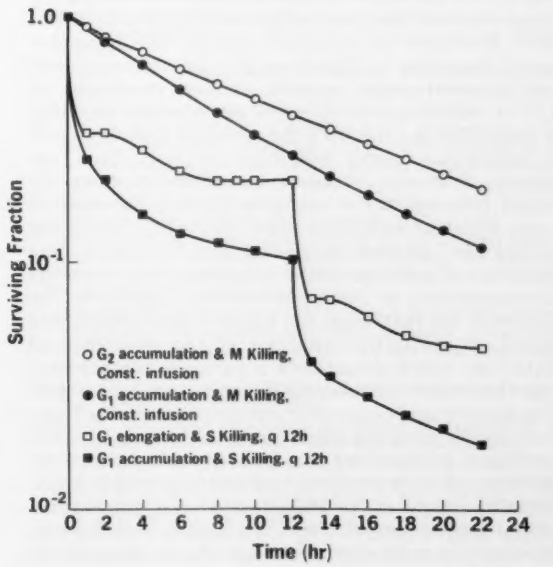
Surviving Fraction
○ G_2 accumulation & M Killing, Const. infusion
● G_1 accumulation & M Killing, Const. infusion
□ G_1 elongation & S Killing, q 12h
■ G_1 accumulation & S Killing, q 12h
Time (hr)

FIGURE 17.—Comparison of the survival fraction curves for different modes of the drug action.

The mode of drug action with G_1 elongation and S killing is shown in figure 16, in which the reduction of cells is less sensitive to every 12 than every 9 hours; this was not the case with G_1 accumulation and S killing (fig 14). The difference between elongation of transit times and progression delay may be quantitatively described by comparing these two modes of the drug action with the same dosage schedule (fig 17). For every 12 hours, it reveals that G_1 accumulation and S killing are more effective in reducing the surviving fraction than G_1 elongation and S killing.

When drugs cause cells to be accumulated in G_2 and subsequently killed in M, the effect is almost completely ineffective (fig 17), mainly due to the shorter duration of M-phase transit time and thus the small fraction of cells in M. In the G/S system, one can wait until the delay has ended, and then allow most of the cells to proceed into the sensitive S phase before applying another dose. This scheduling depends on a longer transit time in S. It is seen that the effectiveness of cell cycle stage-specific drugs rests heavily upon the exact mode of drug action in relation to the mechanisms and configuration functioning in the cell cycle.

DISCUSSION

A variety of mathematical models have been used to represent dose-response curves for the drug effects on tumor cell populations and to analyze subsequent cell populations with varying degrees of fidelity to the underlying cell kinetics. Relatively simple models have been proposed (5,22,29,30) to deal with dose-time-cell survival curves. The computer model described by Shackney (31) for tumor growth and chemotherapy, applied to the treatment of L1210 leukemia with cytosine arabinoside, provided a means for dealing with the schedule dependency of a particular tumor-drug-host system. This approach, however, requires considerably more detailed information to evaluate its key parameters than might be available experimentally. One of the widely used schemes in dealing with the time-course behavior of cells surviving treatment was to utilize an exponential or Gompertz function (18,25,26). The choice of the mathematical form of the kinetics was based on statistical analysis of the experimental data (18), which determines a parameter representing the extent of retardation in tumor regression. The growth and regression curves of Gompertz function can be obtained when the growth equation with nonlinear parameters of a time-dependent mean cycle time, growth fraction, and cell loss rate is simulated by computer (4). The selection of a simple functional dependence of these cell kinetic parameters, however, is arbitrary, although the model predicts the time variation of the tumor volume after radiotherapy.

The multicompartmental models are relatively easy to formulate by treating different functional cell groups separately, but it is difficult to obtain analytic solutions because cell kinetic parameters of the model are in nonlinear functional forms. A deterministic, two-compartment model which accounts for cells in proliferating and nonproliferating phases can describe the exponential, Gompertzian, and steady-state proliferation of cells (32). Another two-compartment model was proposed which deals with the homeostatic mechanism involved in the dynamics of proliferative and nonproliferative cells (33,34). By integrating the compartment for biomarker synthesis with the two-compartment cell model, tumor-polyamine interactions in the Ehrlich ascites tumor cells were characterized which led to an estimate of the total number as well as the size or proliferation rate of tumor cells by the measurement of polyamine concentration (35). However, the two-compartment models were not able to provide insights into details of kinetic factors affecting the rate of growth fraction. In the present study, a cycle stage-specific compartmental model was proposed to deal with changes in the cell kinetic parameters during tumor growth and regression before and after treatment. Because of the limited experimental data available, emphasis was mainly given to the exponential phase of growth, and investigation is presently under way to characterize the effects of antitumor drugs on the cell kinetic parameters throughout the entire period of growth. It should be noted that in the cycle stage-specific model (fig 1), the transit time in each phase is in an exponential form while the actual transit time distribution is in a bell-shaped form. As presented elsewhere,[11] the model with the exponential transit time describes the time-dependent and population-dependent cell kinetic parameters as well as the tumor growth of experimental observations. However, in analyzing the effects of drugs on tumor cell populations using the model (fig 2), especially the progression delay of cells through the cell cycle, the distribution form of the transit time is of importance. In the case of cytosine arabinoside, simulation of the exponential transit time results in survival fraction curves with less sensitive shapes; simulation utilizing the bell-shaped transit time gives much more sensitive survival fraction curves (fig 11) which compare favorably with experimental data. The bell-shaped transit time distribution can be generated by increasing the number of compartments per phase, ie, three compartments per phase; the results will be presented elsewhere.

Recently, a number of studies have been carried out to combine pharmacokinetic parameters with cell cycle parameters in order to characterize in detail the dynamics of tumor-drug interactions (36-40). Jusko (36) derived four differential equations describing a pharmacodynamic model for cell cycle-specific antitumor agents in which two compartments are used to characterize cell kinetics and an-

[11] See footnote 5.

other two compartments are used to represent the time-course of drug levels. Himmelstein and Bischoff (38) used a form of the partial differential equation and derived the specific cell death rate as a function of drug concentration and, for a cell cycle-specific drug, the cell maturity. However, the drug action considered was mainly cell-killing effect. It is rather difficult to determine from these models the specific effects of drugs on the cell cycle time and the growth fraction.

One of the practical values of the cell cycle stage-specific model would be that it can be readily expanded to integrate various reactions occurring in each cycle phase, ie, including the known biochemical pathways into the model and their perturbation resulting from administration of drugs as previously exploited (5,42,43). The schedule dependency of the model performance (fig 14), even though it is a preliminary result, is also of considerable interest, and further evaluation of the system with respect to available experimental data (44,45) should give some details on the dose-cell cycle kinetic relationship. With this information we may be able to formulate a framework necessary for the design of optimal dosage schedules (46).

REFERENCES

1. Aroesty J, Lincoln T, Shapiro N, et al. Tumor growth and chemotherapy: mathematical methods, computer simulations, and experimental foundations. Math Biosci 17:243-300, 1973.
2. Dombernowsky P, and Hartmann NR. Analysis of variations in the cell population kinetics with tumor age in the L1210 ascites tumor. Cancer Res 32:2452-2458, 1972.
3. Steel GG. Cell loss from experimental tumours. Cell Tissue Kinet 1:193-207, 1968.
4. Curtis SB, Barendsen GW, and Hermens AF. Cell kinetic model of tumour growth and regression for a rhabdomyosarcoma in the rat: undisturbed growth and radiation response to large single doses. Eur J Cancer 9:81-87, 1973.
5. Valeriote FA, Bruce WR, and Meeker BE. A model for the action of vinblastine in vivo. Biophys J 6:145-152, 1966.
6. van Putten LM. Are cell kinetic data relevant for the design of tumor chemotherapy schedules? Cell Tissue Kinet 7:493-504, 1974.
7. Momparler RL. A model for the chemotherapy of acute leukemia with 1-β-D-arabinofuranosylcytosine. Cancer Res 34:1775-1787, 1974.
8. Young RC, and DeVita VT. The effect of chemotherapy on the growth characteristics and cellular kinetics of leukemia L1210. Cancer Res 30:1789-1794, 1970.
9. Young RC. The effect of methyl CCNU (NSC-95441) on the cellular kinetics of normal and leukemic murine tissues in vivo. Cell Tissue Kinet 6:35-43, 1973.
10. Borsa J, and Whitmore GF. Cell killing studies on the mode of action of methotrexate on L-cells in vitro. Cancer Res 29:737-744, 1969.
11. Borsa J, Whitmore GF, Valeriote FA, et al. Studies on the persistence of methotrexate, cytosine arabinoside, and leucovorin in serum of mice. J Natl Cancer Inst 42:235-242, 1969.
12. Schabel FM, Jr, Skipper HE, Trader MW, et al. Experimental evaluation of potential anticancer agents. XIX. Sensitivity of nondividing leukemic cell populations to certain classes of drugs in vivo. Cancer Chemother Rep 48:17-30, 1965.
13. Wilkoff LJ, Dixon GJ, Dulmadge EA, et al. Effect of 1,3-bis(2-chloroethyl)-1-nitrosourea (NSC-409962) and nitrogen mustard (NSC-762) on kinetic behavior of cultured L1210 leukemic cells. Cancer Chemother Rep 51:7-18, 1967.
14. Skipper HE, Schabel FM, Jr, Mellett LB, et al. Implications of biochemical, cytokinetic, pharmacologic, and toxicologic relationships in the design of optimal therapeutic schedules. Cancer Chemother Rep 54:431-450, 1970.
15. Karon M, and Shirakawa S. The locus of action of 1-β-d-arabinofuranosylcytosine in the cell cycle. Cancer Res 29:687-696, 1969.
16. Barranco SC, and Novak JK. Survival responses of dividing and nondividing mammalian cells after treatment with hydroxyurea, arabinosylcytosine, or adriamycin. Cancer Res 34:1616-1618, 1974.
17. Bhuyan BK, Fraser TJ, Gray LG, et al. Cell-kill kinetics of several S-phase-specific drugs. Cancer Res 33:888-894, 1973.
18. Wilkoff LJ, Lloyd HH, Dulmadge EA, et al. Kinetic evaluation of the effect of hydroxyurea on viability of replicating cultured leukemia L1210 cells. J Natl Cancer Inst 44:201-209, 1970.
19. Woo KB, and Wiig KM. Analysis of the effect of antitumor drugs on kinetics of tumor cell-biomarker relationship. *In* The Cell Cycle in Malignancy and Immunity (Hampton JC, ed). The Atomic Energy Commission Symposium Series (CONF-731005). Springfield, Va, National Technical Information Service, US Dept of Commerce, 1975, pp 485-503.
20. Gillette JR. The importance of tissue distribution in pharmacokinetics. J Pharmacokinet Biopharm 1:497-520, 1973.
21. Yankee RA, DeVita VT, and Perry S. The cell cycle of leukemia L1210 cells in vivo. Cancer Res 27:2381-2385, 1967.
22. Skipper HE, Schabel FM, Jr, and Wilcox WS. Experimental evaluation of potential anticancer agents. XIII. On the criteria and kinetics associated with "curability" of experimental leukemia. Cancer Chemother Rep 35:3-111, 1964.
23. ———. Experimental evaluation of potential anticancer agents. XIV. Further study of certain basic concepts underlying chemotherapy of leukemia. Cancer Chemother Rep 45:5-28, 1965.
24. Dixon GJ, Dulmadge EA, and Schabel FM, Jr. Growth requirements and biologic characteristics of leukemia L1210 cells in culture. Cancer Chemother Rep 50:247-254, 1966.
25. Wilkoff LJ, Wilcox WS, Burdeshaw JA, et al. Effect of antimetabolites on kinetic behavior of proliferating cultured L1210 leukemia cells. J Natl Cancer Inst 39:965-976, 1967.
26. Wilkoff LJ, Dulmadge EA, and Lloyd HH. Kinetics of effect of 1-β-D-arabinofuranosylcytosine, its 5′-palmitoyl ester, 1-β-d-arabinofuranosyluracil, and tritiated thymidine on the viability of cultured leukemia L1210 cells. J Natl Cancer Inst 48:685-695, 1972.
27. Mellett LB. Consideration in design of optimal therapeutic schedules. *In* Proceedings of the 5th International Congress on Pharmacology, San Francisco, 1972, vol 3, pp 332-353.
28. Skipper HE, Schabel FM, Jr, and Wilcox WS. Experimental evaluation of potential anticancer agents. XXI. Scheduling of arabinosylcytosine to take advantage of its S-phase specificity against leukemia cells. Cancer Chemother Rep 51:125-165, 1967.
29. Bagshawe KD. Tumour growth and anti-mitotic action. The role of spontaneous cell losses. Br J Cancer 22:698-713, 1968.
30. Berenbaum MC. Dose-response curves for agents that impair cell reproductive integrity. The relation between dose-response curves and the design of selective regimens in cancer chemotherapy. Br J Cancer 23:434-445, 1969.
31. Shackney SE. A computer model for tumor growth and chemotherapy, and its application to L1210 leukemia treated with cytosine arabinoside (NSC-63878). Cancer Chemother Rep 54:399-429, 1970.
32. Good PI. Homeostatic mechanisms and the loss of mitotic potential. J Theor Biol 34:99-102, 1972.
33. ———. Alternative mechanisms for homeostatic regulation of mammalian cell populations. J Theor Biol 40:543-552, 1973.
34. Woo KB, and Simon RM. A quantitative model for relating tumor cell number to polyamine concentrations. *In* Polyamines in Normal and Neoplastic Growth (Russell DH, ed). New York, Raven Press, 1973, pp 381-393.
35. Jusko WJ. Interpretation of cell proliferation curves using a two-compartment cell model. Math Biosci 21:31-37, 1974.
36. ———. A pharmacodynamic model for cell-cycle-specific chemotherapeutic agents. J Pharmacokinet Biopharm 1:175-200, 1973.
37. Bischoff KB. Pharmacokinetics and cancer chemotherapy. J Pharmacokinet Biopharm 1:465-480, 1973.

38. Himmelstein KJ, and Bischoff KB. Models of ara-C chemotherapy of L1210 leukemia in mice. J Pharmacokinet Biopharm 1:69-81, 1973.
39. Bischoff KB, Himmelstein KJ, Dedrick RL, et al. Pharmacokinetics and cell population growth models in cancer chemotherapy. *In* Advances in Chemistry, Series No. 118, Chemical Engineering in Medicine. Washington, DC, American Chemical Society, 1973, pp 47-64.
40. Zaharko DS, and Dedrick RL. Applications of pharmacokinetics to cancer chemotherapy. *In* Proceedings of the 5th International Congress on Pharmacology, San Francisco, 1972, vol 3, pp 316-331.
41. Werkheiser WC. Mathematical simulation in chemotherapy. Ann NY Acad Sci 186:343-358, 1971.
42. Werkheiser WC, Grindey GB, Moran RG, et al. Mathematical simulation of the interaction of drugs that inhibit deoxyribonucleic acid biosynthesis. Mol Pharmacol 9:320-329, 1973.
43. Venditti JM. Treatment schedule dependency of experimentally active antileukemic (L1210) drugs. Cancer Chemother Rep Part 3, vol 2(1):35-59, 1971.
44. Neil GL, and Homan ER. The effect of dose interval on the survival of L1210 leukemic mice treated with DNA synthesis inhibitors. Cancer Res 33:895-901, 1973.
45. Karon M, and Shirakawa S. Effect of 1-β-D-arabinofuranosylcytosine on cell cycle passage time. J Natl Cancer Inst 45:861-867, 1970.
46. Lamerton LF. Tumour cell kinetics. Br Med Bull 29:23-28, 1973.

Disposition of Cytosine Arabinoside (NSC-63878) and its Metabolites: A Pharmacokinetic Simulation[1,2]

P. F. Morrison, T. L. Lincoln, and J. Aroesty[3,4]

SUMMARY

A computer-based model of the pharmacokinetics of cytosine arabinoside (ara-C) and its active metabolite, ara-CTP, has been developed. This model, which is an intracellular extension of the Bischoff-Dedrick model of multi-organ pharmacokinetics, gives predictions which are in agreement with the recent measurements of Chou et al on tissue concentrations of ara-CTP and Borsa et al on blood levels of ara-C. It is shown that the ara-CTP halving time in tissue is much greater than the ara-C halving time in blood because of low tissue levels of phosphatase. For a single dose at the LD10 level in mice, significant splenic DNA inhibition is calculated to occur for 26 hours, while the ara-C levels are negligible in 6 hours. The calculated duration of cytostatic effect at lower dosages (2.5 mg/kg) is 10 or 12 hours, while ara-C blood levels are negligible within 3 hours. Implications for cell kinetics and scheduling studies are also briefly described.

[Cancer Chemother Rep 59:861-876, 1975]

The objective of cancer chemotherapy is to eliminate or at least suppress a population of neoplastic cells without undue toxicity to the host. Pharmacokinetic simulation seeks to put this effort on a firm rational basis based on the physiology, molecular biology, and biochemistry of drug distribution and metabolism. As a result of such simulations, we should be able to calculate tissue-specific drug exposures which would make available to the chemotherapist the same kind of dosimetry which is already available to the radiologist. We are studying the pharmacokinetics of cytosine arabinoside (ara-C) as one example of this approach. We have chosen ara-C because of its theoretic interest, the amount of experimental data on hand, and the drug's demonstrated clinical usefulness.

The pioneering work in the simulation of the multicompartment pharmacokinetics of anticancer agents is by Bischoff, Dedrick, and their co-workers (1-3). Our work extends theirs to include the simulation and prediction of intracellular metabolites and enzyme kinetics within those target cells which are the site of the ultimate cytotoxic and cytostatic effects. The next step, to be discussed in a later paper, is to relate intracellular concentrations to cell death and the inhibition of DNA synthesis. In this way, a realistic approach to the prediction and interpretation of optimal schedules is being developed.

[1]Supported by Public Health Service grants CA-12369 and CA-14088 from the National Cancer Institute (NCI), National Institutes of Health, Department of Health, Education, and Welfare.

[2]Cytosine arabinoside: CAS reg. No. 69-74-9; cytosine, 1-β-D-arabinofuranosyl-, monohydrochloride; ara-C.

[3]Physical Sciences Department, The Rand Corporation, Santa Monica, Calif.

[4]*Reprint requests to*: Dr. Thomas L. Lincoln, Physical Sciences Department, The Rand Corporation, 1700 Main St, Santa Monica, Calif 90406.

In this paper we report on the pharmacokinetic baseline simulations which allow us to interpret the experimental and clinical impact of ara-C. We wish to show the consistency of the experimental data on the pharmacology of ara-C by applying our models to the detailed measurements of Chou et al (4) for the DBA hybrid mouse.

Blood levels of ara-C have already been measured in mice, rabbits, and man as a function of dose and route of administration. Typical of these measurements are the results of Borsa et al (5), which are shown as crosses in figure 1. These data correspond to blood levels of ara-C found in mice after a single intraperitoneal injection of 200 mg/kg. This is less than a tenth of the single LD10 cited by Skipper et al (6). The line through the data points is the ara-C decay curve predicted by our version of the Bischoff-Dedrick pharmacokinetic model. The prediction is made using standard handbook values of organ size and blood flow, available in vitro values of kinase and deaminase levels, and clearances based on the 1-hour drug nucleoside levels in blood measured by Chou et al (4). While this agreement between prediction and measurements is exemplary, Bischoff and Dedrick et al (1-3) have also verified that the basic pharmacokinetic model is an accurate predictor of ara-C and ara-U levels in blood and other tissues.

However, the active intracellular form of ara-C is the triphosphate, ara-CTP, not ara-C itself. Ara-CTP has its impact by blocking DNA synthesis and possibly by introducing ara-C moieties into the DNA coding sequences. At high intracellular concentrations ara-CTP is cytocidal, and at much lower concentrations there is still a pronounced cytostatic effect. It is important, then, for the therapeutic utilization of pharmacokinetic data on ara-C, to determine the corresponding ara-CTP concentration within target cells. Does it follow closely the levels

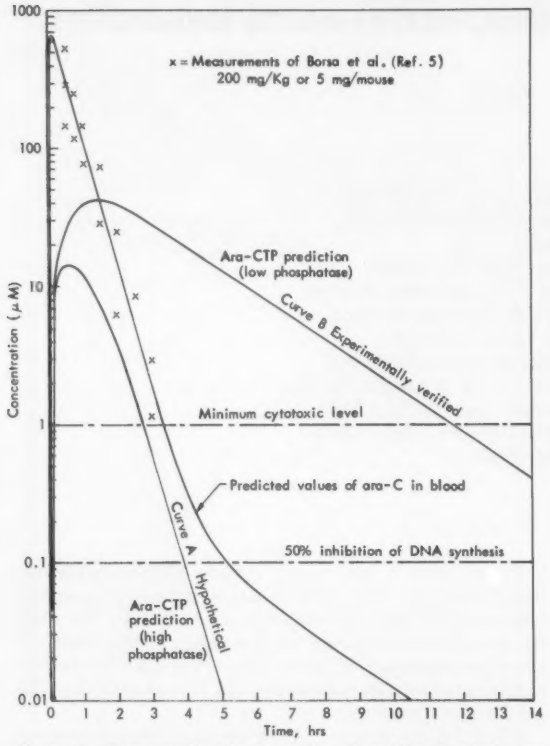

FIGURE 1.—Pharmacokinetic simulation of ara-C and splenic ara-CTP.

of ara-C within blood, as in curve A of figure 1, or does it continue to increase even while blood levels of ara-C are decreasing and ultimately decay with a long half-life as in curve B of figure 1? Estimates of the minimum cytotoxic concentrations of ara-CTP (1 μM) and the concentration which inhibits 50% of DNA synthesis (0.1 μM) are also shown in figure 1.

If the levels of phosphatase are high, then curve A is valid, the duration of the cytocidal and cytostatic effects can be estimated directly from the blood levels of ara-C, and a single pulse dose of 200 mg/kg of ara-C does not inhibit cell growth for more than 4 or 5 hours. If the levels of phosphatase are low, then curve B is valid and the situation is both different and more complex. The effective duration of activity would be much longer, between 12 and 16 hours, with corresponding implications for schedule and dosage studies. In this case, ara-C blood levels do not reveal the effective duration of drug action against target cells.

The main body of this paper will deal with the application of available information on the enzyme chemistry of ara-C to the prediction of intracellular concentrations of ara-CTP. As we show later, curve A is only hypothetical and curve B is much more realistic. We are able to verify the measurements of Chou by using phosphatase levels corresponding to that shown in curve B.

In the conference presentation of this paper, we considered a slightly different question. If the Bischoff-Dedrick model (1-3) of drug distribution to tissues can predict differences in tissue concentrations, how can such differences be utilized? We focused on the differences in ara-C tissue concentration which can be predicted in the testis and on how these concentrations may be altered by the manipulation of testicular blood flow.[5] Simulations show that tissue differences are greatest when the injection is given rapidly by intravenous (iv) bolus. The testis may be protected by cutting off the blood flow until the peak blood concentration has passed. Conversely, by decreasing blood flow at the time of peak testicular concentration, higher levels of drug can be maintained in the testis because less drug is returned to the blood stream. The peak tissue concentration may be found by simulation and the pharmacokinetics verified by sampling the testicular venous blood concentration and comparing it to predicted values. For ara-C, tissue distribution is pharmacologically simple because the principal rate-limiting features are tissue volume, tissue-specific blood flows, and the metabolic breakdown to ara-U.

Briefly, we touch on some of the implications of this work in connection with cell cycle specificity, optimum scheduling, and host resistance. It is sufficient to note that the curves for S-phase labeling using tritiated thymidine and the curves for cell death due to ara-C exposure are not the same.[6] More cells are killed by ara-C than are labeled with tritiated thymidine. It would appear that cells can form sufficient ara-CTP prior to entering S phase so that the exposure of cellular metabolism to ara-CTP exceeds the time of exposure to ara-C. Cells which have not entered S phase during an exposure time but which enter S phase while sufficient ara-CTP is present will be affected. This implies that sufficient deoxycytidine kinase is available prior to S phase to form ara-CTP, and that the half-life of ara-CTP is at least 1 or 2 hours (as indicated by present measurements) (7). From these considerations it is clear that calculations of pulse dose kill based only on the interactions of ara-C on S phase may be considerably oversimplified.

As we have indicated, low levels of ara-CTP are cytostatic. The rate of DNA synthesis may be slowed by a factor as great as 30 without killing the cells (8). Thus all the cells which are committed to divide, but which have not yet completed their passage through S phase, are nearly totally blocked. In this arrested state they are subject to any other cytocidal effects which may be present in their surroundings. As with the use of bacteriostatic agents, slow-

[5]Lincoln T, and Freireich E. Pharmacokinetic simulation, a future means for better control of cancer chemotherapy. Presented at the Annual Meeting of the European Organization for Research on Treatment of Cancer, Paris, June 1973.

[6]Steel GG. Descriptive and operational cytokinetics. Presented at the Symposium on Clinical Pharmacology, Jacksonville, Fla, Mar 1973.

ing the process of cell division magnifies host defenses even when they are relatively weak. Any immunologic resistance to tumor cells can thus be increased by cytostatic levels of ara-CTP. This may account for the clinical effectiveness of continuous iv infusion where blood levels (~ 0.07 μg/ml) (9) are not sufficient for direct cell death. The cytostatic activity of ara-C may also enhance the effectiveness of other therapeutic agents which for one reason or another tend to kill more tumor cells than normal cells. Simulation of this approach is under vigorous investigation.

THE PHARMACOKINETIC MODEL

In order to describe the distribution of ara-C and its pharmacologic action, we have extended the Bischoff-Dedrick multicompartment flow model (2) by adding another compartment and more metabolic detail. A schematic diagram of the flows appears in figure 2. We have used the same organ compartments as employed by Dedrick et al in their analysis of ara-C, namely the blood, liver, gut, heart, kidney, lean, and marrow, but have added the spleen to the portal circulation because this organ compartment has been shown to be metabolically very active with a high phosphorylating ability (10). For each compartment we have constructed mass balances which describe the organ concentrations of ara-C and its metabolites in terms of drug flow in and out of each compartment coupled with the important reactions within a compartment. The solution of these balances allows one to compare our simulated time-dependent nucleotide concentrations with those obtained from actual experiments. The model is calibrated to the DBA mouse, but is designed to be scaled to other animals and to man.

Because reaction terms describing the metabolism of ara-C are a part of each mass balance equation, we first discuss this metabolism and derive the appropriate enzyme kinetics. We return in the next section to the mass balance expressions themselves.

Ara-C Metabolism

The active form of ara-C is the triphosphate, ara-CTP. Thus we have selected as the pertinent ara-C biochemistry the minimal set of enzymatic steps which define the time-dependent concentration of ara-CTP. This approach has minimized the work required to solve the many simultaneous equations that arise in the model. It also reduces the problem of missing data posed by other enzyme systems that have only a marginal effect on ara-CTP levels and have not been fully characterized kinetically.

Using this approach, the key steps in the metabolism of ara-C are presented in figure 3. Steps 1-3 phosphorylate ara-C to ara-CTP. The initial phosphorylation is enzymatically controlled by deoxycytidine kinase (a "salvage" enzyme) (11,12); this initial step is rate determining. The second phosphorylation (13,14) by cytosine monophosphokinase and the third by nonspecific nucleoside diphosphokinase (15) exhibit activities much in excess of those found for deoxycytidine kinase. Several nucleotides may act as phosphate donors for these enzymes, but the primary donor is ATP, by virtue of its large steady-state level.

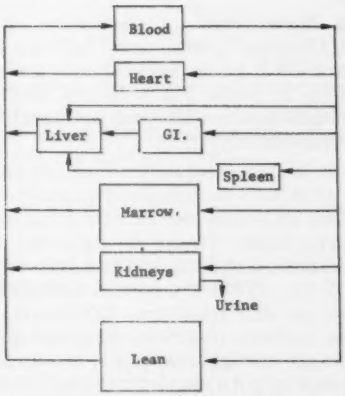

FIGURE 2.—Pharmacokinetic flow scheme.

The enzymes catalyzing dephosphorylation, steps 4-6 in figure 3, are less well studied. It is assumed that there are nucleoside triphosphatases and diphosphatases high in activity compared to deoxycytidine kinase so that the rate-determining dephosphorylation step is the ara-CMP to ara-C conver-

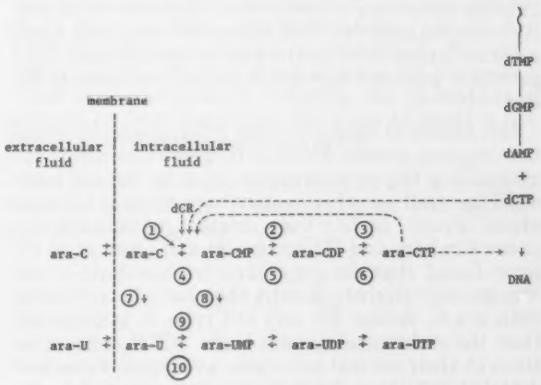

FIGURE 3.—Metabolism of ara-C.

sion. Schrecker (14) has indicated that in L1210 extracts this step is controlled in great part by a 5′-nucleotidase, while Tseng et al (16) has shown that this enzyme dephosphorylates 5′-UMP in rat liver slices. However, it is possible that other phosphomonoesterases present in the cytosol (5′-nucleotidase is bound to the plasma membrane) may also contribute to the dephosphorylation of ara-CMP nucleotide.

Ara-C is deaminated by pyrimidine nucleoside deaminase (17) (step 7), while ara-CMP may be deaminated to ara-UMP by deoxycytidylate aminohydrolase (18) (step 8). Steps 9 and 10 are controlled by deoxythymidine kinase (19) and presumably 5′-nucleotidase respectively.

Because it is also necessary to include the effects of enzyme inhibitors in deriving the kinetics of ara-C metabolism, we briefly mention the principal inhibitors. Deoxycytidine kinase is inhibited both by deoxycytidine triphosphate and to a lesser extent by ara-CTP (12,14). ATP is the normal phosphate donor in the reaction and these two inhibitors compete with it. The normal substrate, deoxycytidine, when present in large enough quantities, is also an inhibitor of the enzyme with respect to ara-C phosphorylation. Of the monophosphokinases, inhibition is observed among dCMP, CMP, UMP, and dUMP acting as competing substrates for dCMP kinase (13), and a similar situation also occurs with nucleoside diphosphokinase because of its lack of specificity. Naturally occurring inhibitors or activators for pyrimidine nucleoside deaminase are not known except the natural substrates deoxycytidine and cytidine (20).

The metabolic scheme actually employed in the present model includes the kinetics of steps 1-7 but generally ignores the deamination of ara-CMP and the phosphorylation steps of ara-U. Schrecker et al (19) have shown that such steps are small contributors to the overall kinetics in the L1210 system. Chou et al (4) have shown that the ara-U monophosphokinase and diphosphokinase steps are of minor importance in other murine tissues. The ara-UMP kinetics have only recently been shown to be of possible importance (4). The effects of including these kinetics (steps 8-10) in the present model have been partially explored and are discussed separately below.

Not shown in figure 3 is the ribonucleotide reductase enzyme system which is largely responsible for controlling the concentration level of the inhibitor dCTP (as well as other deoxyribonucleoside triphosphate levels). It has been omitted principally because Graham and Whitmore (8) and Chou et al (4) have found that deoxycytidine triphosphate levels change only slightly in cells that have been treated with ara-C. Hence, for any cell type, it is supposed that the reductase system holds dCTP concentrations at their normal (cell cycle-averaged) value and detailed reductase kinetics are not required to describe the formation of ara-CTP.

We now present the actual kinetic equations employed in our model by enzyme type, as well as the numerical values selected for the principal inhibitor concentrations.

Deoxycytidine kinase.—The kinetic equation for this enzyme has been derived from the data of Schrecker (14) and Momparler et al (12,21). Inhibition terms are particularly important here. We have employed as our kinetic scheme the mixed inhibition formalism of Dixon and Webb (22) since the reciprocal plots of ara-C phosphorylation in the presence of varying inhibitor (deoxycytidine triphosphate) concentrations do not intersect at either the ordinate or abscissa. An allosteric mechanism need not be invoked since these reciprocal plots *using ara-C as substrate* are linear over the physiologic concentration range. The mixed kinetics appear in figure 4 where the second substrate, ATP, is indicated. Inhibition by deoxycytidine triphosphate is equivalent to the direct replacement of ATP. The overall kinetic scheme of figure 4 has monosubstrate character since ATP in intact cells is maintained at a constant saturating level over time.

From figure 4, and from the additional condition that deoxycytidine may also bind to deoxycytidine kinase, the overall phosphorylation kinetic equation using mixed inhibition may be derived as

$$\dot{r}_p \equiv \left[\frac{d(ap_1 + ap_2 + ap_3)}{dt}\right]_p$$

$$= \frac{V_k}{1 + \frac{K_m}{a}\left(1 + \frac{c}{K_i} + \frac{dCR}{K_I} + \frac{ap_3}{K_i'}\right) + K_m\left(\frac{c}{K_i K_m'} + \frac{ap_3}{K_i' K_m''}\right)} \qquad (1a)$$

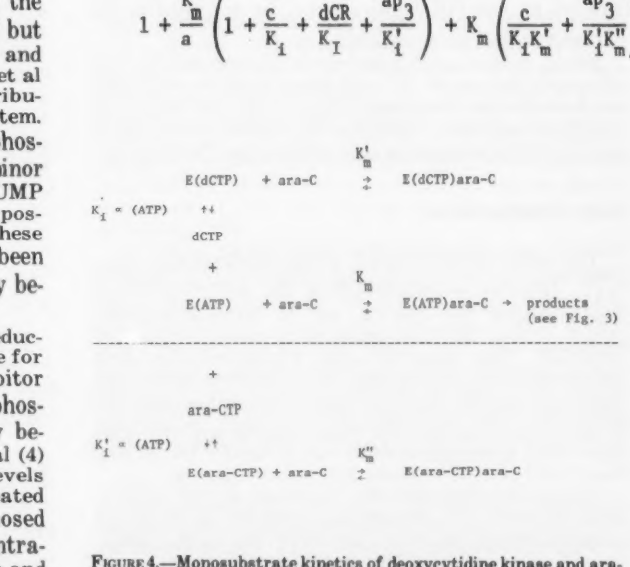

FIGURE 4.—Monosubstrate kinetics of deoxycytidine kinase and ara-C at saturating levels of ATP. The equilibrium constants are given here in the mixed inhibition notation used commonly in enzyme kinetics (22).

where a, ap_1, ap_2, and ap_3 are ara-C and its three nucleotides; c is deoxycytidine triphosphate; dCR is deoxycytidine; K_I is the deoxycytidine inhibitor constant; K_m corresponds to the usual competitive Michaelis constant; K_i, K_i', K_m', and K_m'' are the mixed inhibition constants of figure 3; and the p subscript denotes changes in total nucleotide level due to phosphorylation only. V_k is the kinase activity and depends on the individual tissues being considered.

Note that the left side of equation (1a) represents the time rate of change over the entire sum of ara-C nucleotides and not just ara-CMP. This results because the higher phosphorylations and dephosphorylations of ara-C are rapid compared to the first (13-15), thus causing the initial kinase product, ara-CMP, to immediately reapportion itself over all the higher nucleotide forms. This rapid reapportionment means that the various ara-C nucleotides will maintain constant steady-state ratios between themselves. Defining the ara-CTP/ara-CDP ratio as α_1 and the ara-CDP/ara-CMP ratio as α_2, the ara-C nucleotide sum ($ap_1 + ap_2 + ap_3$) may be written only in terms of ara-CTP and equation (1a) may be re-expressed as

$$\dot{r}_p = \left(1 + \frac{1}{\alpha_1} + \frac{1}{\alpha_1\alpha_2}\right)\left[\frac{d\ ap_3}{dt}\right]_p \qquad (1b)$$

The nucleotide ratios are calculable from the experimental nucleotide concentrations that have been determined for intact L1210 cells (19). Relative constancy of the ratios is in fact confirmed by the values obtained over a tenfold range of initial ara-C concentrations (ie, α_1 = 7.6, 7.8, and 4.2, α_2 = 4.7, 5.7, and 3.7 for initial drug concentrations of 10, 51, and 100 μM respectively).

Values for the Michaelis and inhibition constants in equation (1a) have been obtained by applying the mixed intercept values of Dixon and Webb (table VIII.1 of ref 22) first to the data on ara-C phosphorylation with dCTP present as inhibitor (fig 5 of ref 12; chart 2 of ref 14), then to the data with ara-CTP present as inhibitor (fig 1 of ref 21), and finally to the data with deoxycytidine present as inhibitor (fig 9 of ref 12). Depending on the data source, K_m was found to be equal to 40, 27, or 25 μM. Because it is only slightly below the mean of these three numbers, 27 μM was chosen for further use in our model. Values for the other deoxycytidine kinase constants appear in table 1.

TABLE 1.—Deoxycytidine kinase constants*

Constant	Value (μM)
K_m	27.0
K_m'	309.0
K_m''	101.9
K_i	1.00
K_i'	17.9
K_I†	0.84

*For an explanation of constants, see fig 4 and text.
†This differs slightly from Momparler's value of 1.3 μM since it was recalculated for a K_m equal to 27 μM.

Phosphatase.—5′-Nucleotidase is thought to be the primary phosphatase involved and hence the kinetics of phosphate hydrolysis are based on this enzyme. No inhibitors other than normal competing substrates are known. Hence a single Michaelis-Menten expression has been used,

$$\dot{r}_{dp} \equiv \left[\frac{d\ (ap_1 + ap_2 + ap_3)}{dt}\right]_{dp} = \left(1 + \frac{1}{\alpha_1\alpha_2} + \frac{1}{\alpha_1}\right)\left[\frac{d\ ap_3}{dt}\right]_{dp}$$

$$= \frac{-V_{dp}}{1 + \frac{\alpha_1\alpha_2 K_{dp}}{ap_3}} \qquad (2)$$

where K_{dp} is the Michaelis constant (equal to 900 μM) as determined by Schrecker et al (23) for 5′-nucleotidase, V_{dp} is the nucleotidase activity, the dp subscript denotes changes in total nucleotide level due to dephosphorylation only, and the rest of the symbols have the same meaning as above. This expression assumes that ara-CMP is the only form which reacts with the enzyme and that, as with deoxycytidine kinase, instantaneous reapportionment of the remaining nucleotides occurs in order to maintain time-independent nucleotide ratios. The competition due to other mononucleotides, principally AMP, has not been included in equation (2). It is estimated that the effect of this exclusion for the spleen would be equivalent to reducing the phosphatase activity by 50%. Currently, the activity itself is not known to within this degree of error.

The overall phosphorylation of ara-C in a cell is thus the sum of the phosphorylation and dephosphorylation equations, ie,

$$\dot{r}_x = \dot{r}_p + \dot{r}_{dp} \qquad (3)$$

Deaminase.—The kinetic equation employed for murine pyrimidine nucleoside deaminase is the same

as used by Dedrick et al (2) and is a single uninhibited Michaelis-Menten expression, ie,

$$\dot{r}_a \equiv \frac{da}{dt} = \frac{-V_{da}}{1 + \frac{K_{da}}{a}} \quad (4)$$

where K_{da} and V_{da} have their usual meanings. From Dedrick et al (3), K_{da} = 1011.7 μM (283 μg/ml). Inhibitions by the competing substrates deoxycytidine and cytidine have been omitted in equation (4) due to their estimated small effect. Using only inhibited Michaelis-Menten kinetics and the Michaelis constants of Creasey (24), we estimate that deoxycytidine concentrations in the normal murine 1-5-μM range are completely negligible and cytidine concentrations in the 50-μM range reduce the deaminase activity by only about 25%. In human systems, however, the K_{da} is reported to be lower (139 μM) and hence cytidine inhibition will then have to be included.

The effects of deoxycytidylate deaminase have not been included in the present model because Schrecker et al (19) have shown that this enzyme is not significantly active in the L1210 system against ara-CMP at concentrations that exceed any attained in our modeling, even though it is present and active against the normal substrate. However, there is the possibility that some tissues encountered in our work may have much higher dCMP deaminase activities than the L1210 system, and this may eventually require introduction of the kinetics of this enzyme into the present pharmacokinetic scheme.

Deoxycytidine triphosphate.—This species has been shown to be a relatively strong inhibitor of deoxycytidine kinase and thus its normal steady-state level in murine tissues must be estimated. A survey of the literature (8,11,25-27) shows that this concentration usually lies in the range of 3-30 μM. A midrange estimate for all murine tissues has accordingly been chosen at 10 μM.

Deoxycytidine.—Because deoxycytidine is the normal, more strongly bound substrate of deoxycytidine kinase, it is necessary to account for its presence in the kinase kinetics. The concentration has not been reported for a very large variety of species or tissue types but is about 40 μM (11,28) in rat blood. The data of Rotherham et al (28) indicate that levels in murine tissues are nearly an order of magnitude lower, and a recent study[7] has indicated that 1-4-μM levels are common in murine blood. Thus, for the present calculations, a value of 4 μM has been used for all tissues that contain significant levels of kinase.

[7]Momparler R. Personal communication, Feb 1975.

Pharmacokinetic Equations and Parameters

The method for constructing the mass balances has been described elsewhere (2) and hence we only present the results for the example compartments of kidney and blood. As in earlier works, the model presumes complete perfusion of the individual compartments and an organ blood/tissue partition ratio of 1.

The mass balances for kidney (K) are:

$$V_K \frac{da_K}{dt} = q_K (a_B - a_K) - k\, a_B + V_K \dot{r}_{a_K} - V_K \dot{r}_{x_K} \quad (5)$$

$$V_K \frac{du_K}{dt} = q_K (u_B - u_K) - k\, u_B - V_K \dot{r}_{a_K} \quad (6)$$

$$\frac{dx_K}{dt} = \dot{r}_{x_K} \quad (7)$$

where V_K is the total volume of the kidney, a_K is the ara-C concentration, u_K is the ara-U concentration, x_K is the total nucleotide concentration (ie, $ap_1 + ap_2 + ap_3$), k is clearance (assumed equal for ara-C and ara-U), and r_{aK} and r_{xK} are the kinetic expressions of equations (1)-(4) as applied to the kidney. The mass balances for blood (B) are:

$$V_B \frac{da_B}{dt} = q_H a_H + q_{Li} a_{Li} + q_M a_M + q_K a_K + q_{Le} a_{Le} - q_B a_B + M_1 g(t) \quad (8)$$

$$V_B \frac{du_B}{dt} = q_H u_H + q_{Li} u_{Li} + q_M u_M + q_K u_K + q_{Le} u_{Le} - q_B u_B \quad (9)$$

where H, Li, M, and Le denote heart, liver, marrow, and lean; M_1 is the total dose of drug; and g (t) is either the Bellman injection function (2) to simulate iv dosing or the exponential decay function of Dedrick et al (3) used here to simulate subcutaneous injection. No nucleotide expressions appear for the blood since deoxycytidine kinase is for all practical purposes absent in murine blood and nucleotides are not free to pass through cell membranes without first being dephosphorylated. Similar expressions may be derived for the other six compartments, giving a total of 22 equations including two representing ara-C and ara-U accumulation in the urine.

The parameters used in this model appear in table 2. The volumes and flows of each organ except the spleen have been taken from Dedrick et al (3) while

splenic values were scaled from rat data (29). Enzyme activities for pyrimidine nucleoside deaminase have also been obtained from Dedrick. These values compare well with those obtained by Ho (10) and may be considered representative of the DBA mouse (for liver, gut, and kidney, Dedrick's values are 16.45, 29.67, and 327.11 while Ho's values are 12.1, 70.83, and 317.33). The kinase activities, taken from Ho (10), are extract activities uncorrected for any intact cell differences (*see* Results below). The kidney clearance rate has been estimated from the data of Chou so that the total drug nucleoside concentration in blood agreed with the measured value after 60 minutes of exposure. The phosphatase activity has been derived from the L1210 extract data of Schrecker (14) using a phosphatase Michaelis constant (K_{dp}) of 900 μM and a value of 0.7 ml actual cell volume/ml of packed cells. Lacking accurate information for other tissue types, this value has currently been assumed to apply to all tissues. That the phosphatase level is in fact nearly constant over diverse tissue types is indicated by the data of Dixon and Webb (22), which show that 5'-nucleotidase activity is nearly constant in the liver, kidney, and small intestinal tissues of the rat. The various Michaelis and inhibitor constants discussed above have been assumed not to vary by tissue type.

For most of the 6- to 12-hour pharmacokinetic simulations, we have assumed that the time scale is too short to require corrections due to cell kinetic phenomena. For example, recruitment, cell lysis, and progression delay, which may result from ara-C exposure and which may in turn change enzyme concentrations, have been taken to be negligible over this time period.

RESULTS

The pharmacokinetic model presented above had been developed before the drug distribution data of Chou et al (4) became available. To assess the accuracy of the model, we wanted to see how well this extensive experimental data could be simulated. Thus, Chou's data became a consistency check on our previous formulation.

Certain requirements of the model immediately became evident when this simulation was attempted. The first was that the Dedrick kidney clearance value had to be increased to 0.66 ml/minute. This was necessary to fit the total blood nucleoside concentration and to better account for the total amount of ara-C and metabolites in the whole mouse as measured by Chou. The selection of this parameter is nearly independent of the deaminase and kinase activity values. To a first approximation, changing the deaminase activity causes a change in the relative proportions of ara-C and ara-U in the blood but not the total nucleoside concentration which is the actual quantity fitted in this calculation. Kinase activities, even boosted to levels tenfold higher than used in our model, are too low to make significant changes in blood nucleoside concentrations after only 60 minutes, principally because the volume of tissues containing kinase is relatively small. The method of selecting a clearance rate so that blood nucleoside levels are reproduced is the approach employed by Dedrick; it apparently remains a reasonable approach even if deoxycytidine kinase is present.

The second requirement is that enzyme activities close to the experimentally determined extract values be employed. Dedrick, Forrester, and Ho have previously shown that in vitro deaminase activities may be used successfully in in vivo simulations (2). In the case of kinase, the Ho extract values closely reproduce the ara-C nucleotide levels at 1-hour exposure in our pharmacokinetic simulation while values

TABLE 2.—Pharmacokinetic parameters

Item	Organ							
	Blood	Heart	Liver	Marrow	Kidney	Lean	Gut	Spleen
Volume (ml)	1.67	0.10	1.30	0.60	0.34	10.00	1.50	0.08
Flow (ml/min)	4.38	0.28	1.80	0.17	1.30	0.83	1.50	0.07
Deaminase activity (μM/min)	0	0	16.45* 400.00†	0	327.11	0	29.67	0
Kinase activity (μM/min)‡	0	0	0.65	1.28	0.02	0	0.10	4.00
Phosphatase activity (μM/min)‡	—	—	300.00	300.00	300.00	—	300.00	300.00
Clearance (ml/min)	0	0	0	0	0.66	0	0	0

*Value for Swiss mouse (3); similar to DBA/2 value of 12.1 μM/min obtained by Ho (10).
†Value for C3H mouse obtained by Ho (10).
‡Nucleotide ratios used in conjunction with these activities are $\alpha_1 = 7.83$ and $\alpha_2 = 5.67$.

NOTE: Activities and Michaelis constants have been expressed throughout this model in units of μM/min or μM (primarily to facilitate the calculation of nucleotide levels). The volume basis for the activities is total organ volume (rather than tissue volume) to be consistent with equations (5)-(9). The molecular weight of ara-C·HCl has been used to convert Dedrick's μg/ml units to μM.

16-fold higher (a multiplier that is required to convert Ho's [10] or Schrecker's [14] kinase extract activity to a value capable of reproducing Schrecker's [19] intact cell nucleotide levels) give splenic in vivo levels that are too high by a factor of 13.8 at dose levels of 2.5 mg/kg.

Furthermore, examination of the DNA synthesis curves obtained both by Chou et al (4) and Bhuyan et al (30) indicated that extract values can relate these curves. If equations (1)-(3) are used to predict ara-CTP concentrations, a value of V_K close to the Ho extract value will transform the ara-C percent inhibition curve of Bhuyan to the ara-CTP percent inhibition curve of Chou. It is possible, of course, that phosphatase activity may be altered to allow use of nonextract values, but the important observation to this point in time seems to be that extract activities for all three enzymes, deaminase, kinase, and phosphatase, form a consistent set for pharmacokinetic simulation.

The pharmacokinetic equations were solved by a Runge-Kutta integration procedure using step sizes of 0.1 minute for the first 20 minutes of simulation and 0.25 minute for the remainder.

After the clearance value and enzyme activities were chosen, the model was solved for the ara-C serum level corresponding to a dose of 5 mg/mouse. This is the dose used by Borsa et al (5) in their pharmacokinetic paper. Our simulation is in excellent agreement with this work since our calculated serum levels nearly perfectly reproduce the line drawn through their data.

For an ara-C dose of 2.5 mg/kg, the simulation results seen in table 3 and figures 5-10 were obtained using the DBA parameters of table 2. It can be seen in table 3 that the experimental and simulated liver and spleen ara-CTP values at 60 minutes agree to within 6%. The small intestine estimate is low by 1 order of magnitude, but it is possible that this may be accounted for by use of a kinase level determined for a tissue sample that does not exactly correspond histologically to that obtained in the pharmacologic study. The exact agreement between simulated and experimental blood nucleoside levels is not a prediction but comes about because the kidney clearance has been adjusted to do so. On the other hand, nucleoside concentrations in other organs are predicted and, except for the kidney, are in close agreement, especially when the published error bands of $\pm$ 0.2 μM are taken into account. The kidney values differ by a factor of two but this comparison is the weakest case since the experimental observation consisted of the analysis of only one mouse.

Figure 5 shows the ara-C and ara-U concentrations in blood, marrow, and lean compartments over a 5-hour period. As noted previously by Dedrick et al (2) the maximum of the ara-C concentration in the lean compartment occurs later than in blood or marrow compartments. The ara-C curves for all other compartments generally group around the three compartments shown here except the kidney. The kidney values are consistently found at a level 30% lower than shown in figure 5 due to the organ's high deaminase activity.

Figure 6 shows both the ara-C and ara-CTP concentrations in the spleen as a function of time for the DBA mouse. Results are shown for three levels of phosphatase activity (VDP), one set belonging to the extract value (VDP = 300 μM/min) in table 2 and the others belonging to phosphatase values that are fourfold higher and lower.

The most outstanding characteristic of these curves is that ara-C follows a much different time-course than ara-CTP, the nucleotide persisting at relatively high concentrations for long periods of time. For the extract phosphatase value of 300 μM/minute (which we take to be our best fit), ara-C has dropped three orders of magnitude from its peak concentration in 6 hours, while ara-CTP has fallen to only one sixth of its peak level.

TABLE 3.—Simulation results for DBA mouse at 60 minutes (ara-C dose = 2.5 mg/kg)

Organ	Type of result*	Tissue levels of— Ara-C (μM)	Ara-C + ara-U (μM)	Ara-CTP (μM)
Blood	S	1.10	1.44	0.0
	E	—	1.44	0.02
Liver	S	1.12	1.52	0.21
	E	1.36	1.45	0.22
Spleen	S	1.14	1.50	1.34
	E	—	2.05	1.26
Kidney	S	0.50	0.72	0.003
	E	—	1.50	0.05
Intestine	S	1.11	1.50	0.03
	E	—	1.65	0.46

*S = simulation and E = experimental (see ref 4).

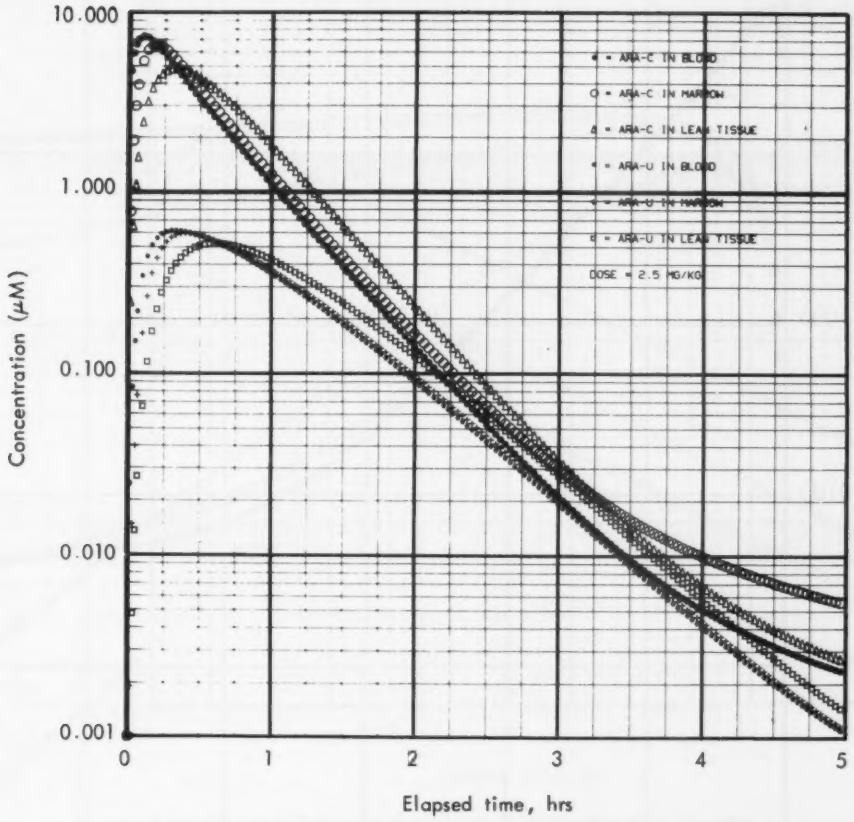

FIGURE 5.—Ara-C and ara-U concentration in blood, marrow, and lean tissue for DBA mice.

For low values of phosphatase activity, the ara-C curves flatten out after 3 hours instead of continuing their descent. This is so because nucleotide pools are built up during the first hour of exposure and continue to provide a source of ara-C by dephosphorylation. This maintains the serum concentrations at steady levels for a significant period of time. This effect does not appear for the higher value of 1200 μM/minute because at this rate the nucleoside source, ara-CMP, falls to such a low level after 3 hours that it cannot significantly affect ara-C concentrations in the serum.

Ara-CTP concentrations are plotted for the spleen, liver, and marrow compartments in figure 7 using the parameters of table 2. All three curves are parallel beyond 1 hour since we have assumed equal phosphatase activity in all the organ regions of this model.(The major exception to this would occur if the model included the testis which is known to have an extremely high 5′-nucleotidase activity [22].) The curve for the liver shows that the ara-CTP concentration decreases to about 0.02 μM 8 hours after a pulse dose of 2.5 mg/kg. According to the ara-CTP percent DNA inhibition curve determined by Chou, this computed 0.02 μM concentration corresponds to a DNA synthesis rate that is about 43% of normal. Chou experimentally measured the synthetic rate in liver at 8 hours and found a rate 20% of normal. These percentages are in relatively close agreement but could be brought into exact agreement by adjusting the dephosphorylation rate upwards by a factor of about two. We note that even if this adjustment were made, the time course of ara-C and ara-CTP would still remain quite different.

Figures 8 and 9 show the differences in ara-C and ara-CTP kinetics that occur when the DBA and C3H mouse strains are modeled. Results are shown for the blood and spleen compartments. Ho (10) measured deoxycytidine kinase and pyrimidine deaminase activities only in the liver of the C3H mouse, and hence our model of the C3H mouse has been limited to the assumption that all enzyme parameters are identical except the liver. Even so, the very large deaminase difference between DBA and C3H livers

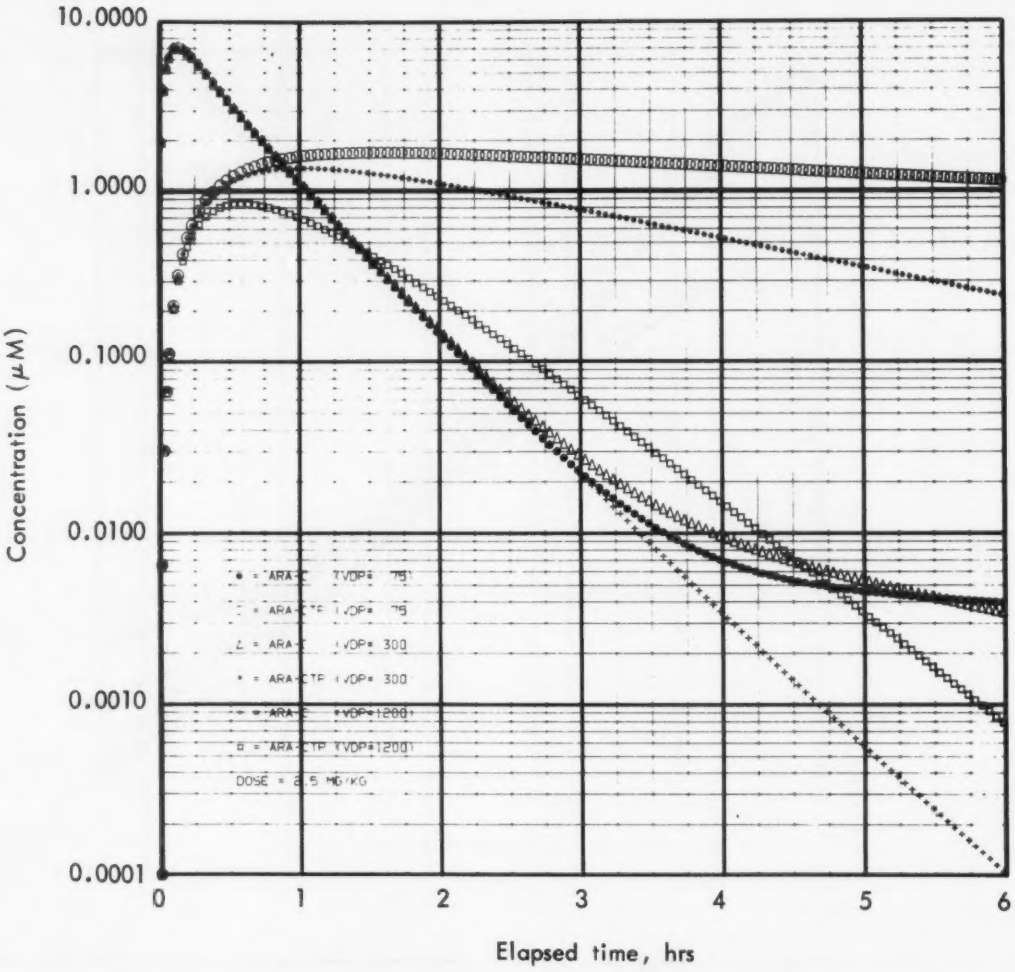

FIGURE 6.—Ara-C and ara-CTP concentration in spleen for DBA mice.

can be seen to make a substantial difference in the kinetics of ara-C. The ara-C nucleotide kinetics also differ but to a lesser degree. The C3H half-life of ara-C (based on the first 3 hours of exposure) is about five sixths the DBA value and this leads to a fourfold difference in serum ara-C concentration after only 2 hours. Ara-CTP concentrations differ by about 30% after 2 hours. The ara-CTP results are relatively insensitive to this deaminase variation because once the bulk of the triphosphate is formed (by the 1-hour point in fig 9), the ara-CTP kinetics lose their dependence on ara-C, including most of the interstrain variations shown in figure 8, and depend only on phosphatase activity.

The results of figure 10 anticipate the question of whether variations in enzyme activity in marrow, such as would result from synchronization due to progression delay or from an L1210 infiltration of bone marrow, lead to different whole-body pharmacokinetic estimates of drug concentrations in blood delivered to marrow. An activity increase due to progression delay is envisioned as resulting from a drug-induced buildup of cells in the early S-phase region where the deoxycytidine kinase activity is increased over the non-S-phase value by a factor of 1.5-2.2 (21). We have therefore chosen to model a marrow with an L1210 activity 50% of this value, where the 50% value may be taken as a maximum possible activity change. The ara-C concentrations in blood and marrow for normal marrow, L1210, and 50% L1210 deoxycytidine kinase activities are plotted in figure 10. The blood values differ only slightly

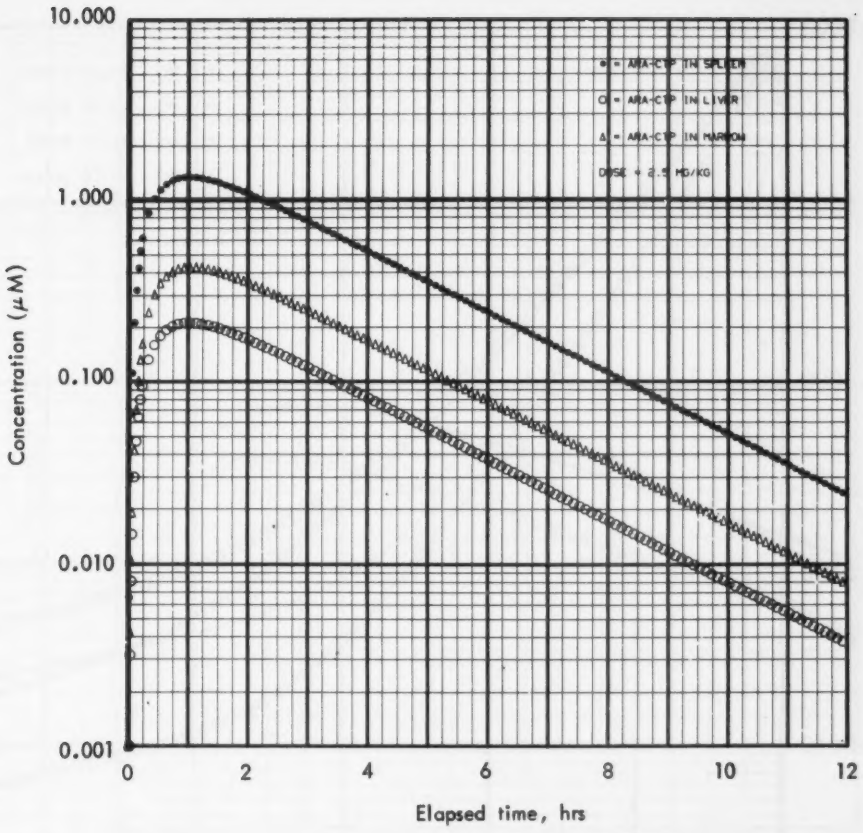

FIGURE 7.—Ara-CTP concentration in spleen, liver, and marrow for DBA mice.

during the first 3 hours when most of the ara-CTP is being produced from the ara-C. Even at 6 hours, the ara-C levels in the blood of the L1210 and the 50% L1210 cases differ by only a factor of two while ara-C levels of the normal and L1210 cases differ by a factor of five. Hence (at least at the dose of 2.5 mg/kg), variations in deoxycytidine kinase activity, particularly due to synchronization effects, have little effect on the ara-C supply delivered to the marrow.

DISCUSSION

The results obtained with the available data are accurate enough to provide us with an increased degree of confidence in our ability to compute ara-CTP levels for particular tissues in vivo.

The difference in the time-course of ara-C and that of ara-CTP is important. Skipper et al (6) estimated the cytotoxic impact of ara-C in terms of an exposure time to at least minimum cytotoxic concentrations in the blood. Concentrations above this threshold were considered lethal to cells carrying out DNA synthesis. These exposure times were used to interpret the effectiveness of particular dose schedules. The active compound, however, is ara-CTP, which is subject to different determinants of production, distribution, and decay than ara-C. Thus, the exposure time of a given cell or tissue to ara-CTP is generally different and not directly comparable, even if a new ara-C threshold were to be defined.

This difference in exposure time is particularly evident in cell culture viability studies which provide a constant level of extracellular exposure for a fixed period of time. These conditions focus sharply on the differences between the intracellular kinetics of the two drug forms. After exposure, cells are washed free of ara-C and viability is determined by plating or bioassay. Ara-C nucleotides are impermeable to cell membrane (19,32) and may dephosphorylate slowly, leading to ara-CTP exposures that are considerably larger than ara-C exposure. This extended toxicity partially explains the phenomenon

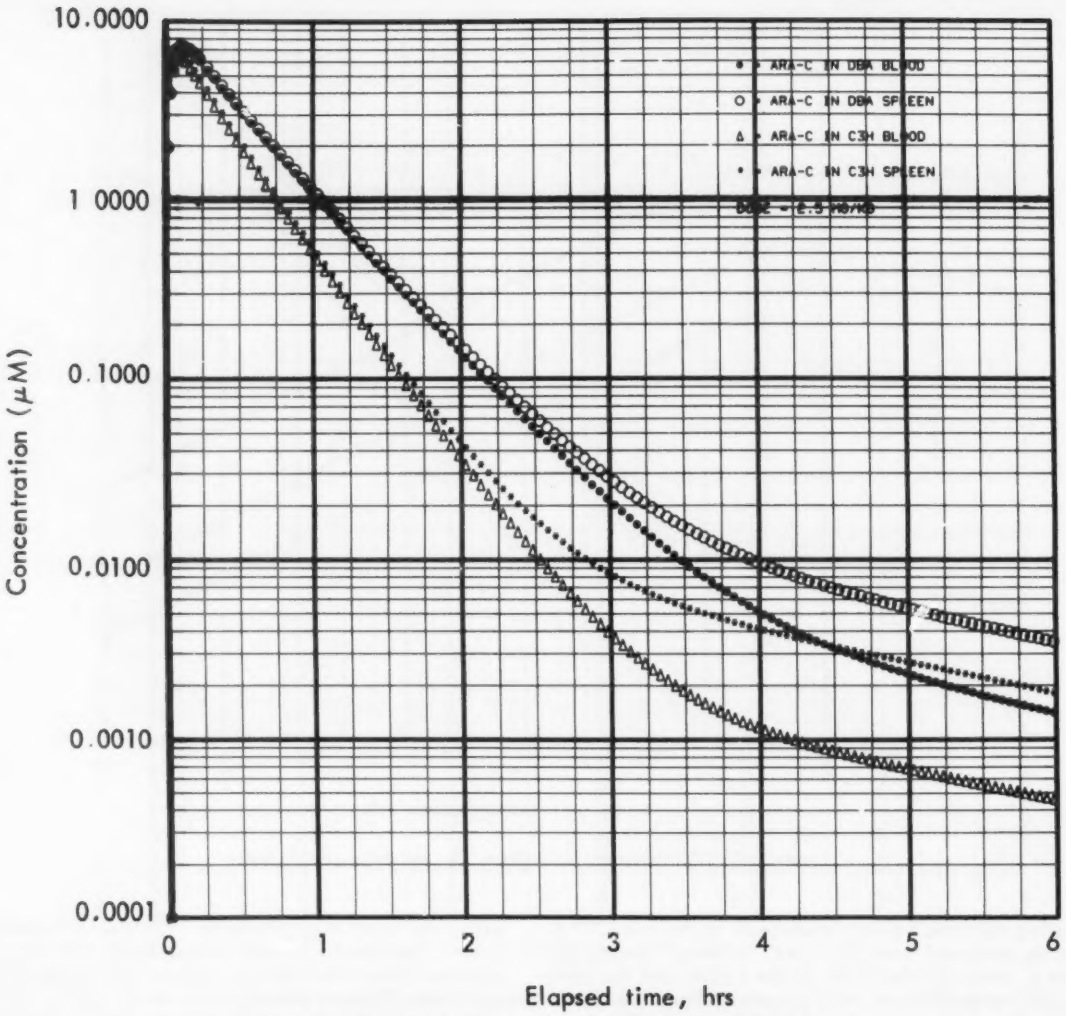

FIGURE 8.—Ara-C concentration in blood and spleen for DBA and C3H mice.

noted by Steel[8] that an exposure to ara-C is capable of killing more cells than are labeled by a similar exposure to tritiated thymidine, although thymidine label should identify all drug-sensitive cells passing through S phase. This may be verified by combining intracellular pharmacokinetics with cell-kinetic simulations of an appropriate cell population. Such simulations are in progress.

There are cytotoxic levels for ara-CTP which kill cells by altering DNA synthesis. There are lower levels in which DNA synthesis is inhibited so that progression through the cell cycle is prolonged leading to the phenomenon of progression delay. Chou et al (4) have measured an ara-CTP percent inhibition curve which shows that as the ara-CTP concentration falls to 0.01 μM DNA synthesis returns to 70% of its normal rate. We take this as a minimal threshold for inhibition. One may see from figure 7 that well over 8 hours are required at 2.5 mg of ara-C/kg before ara-CTP levels fall below this value. We note that this long-term inhibition due to ara-CTP is consistent with the lengths of inhibitions measured by Chou in ascites cells, liver, and small intestine.

By virtue of its inclusion of ara-CTP nucleotide kinetics, the pharmacokinetic model that we have developed is thus capable of providing the time-dependent function from which both cytotoxicity and progression delay may be estimated. Furthermore, the real anatomic and physiologic nature of each compartment in the Dedrick-type model allows one

[8] See footnote 6.

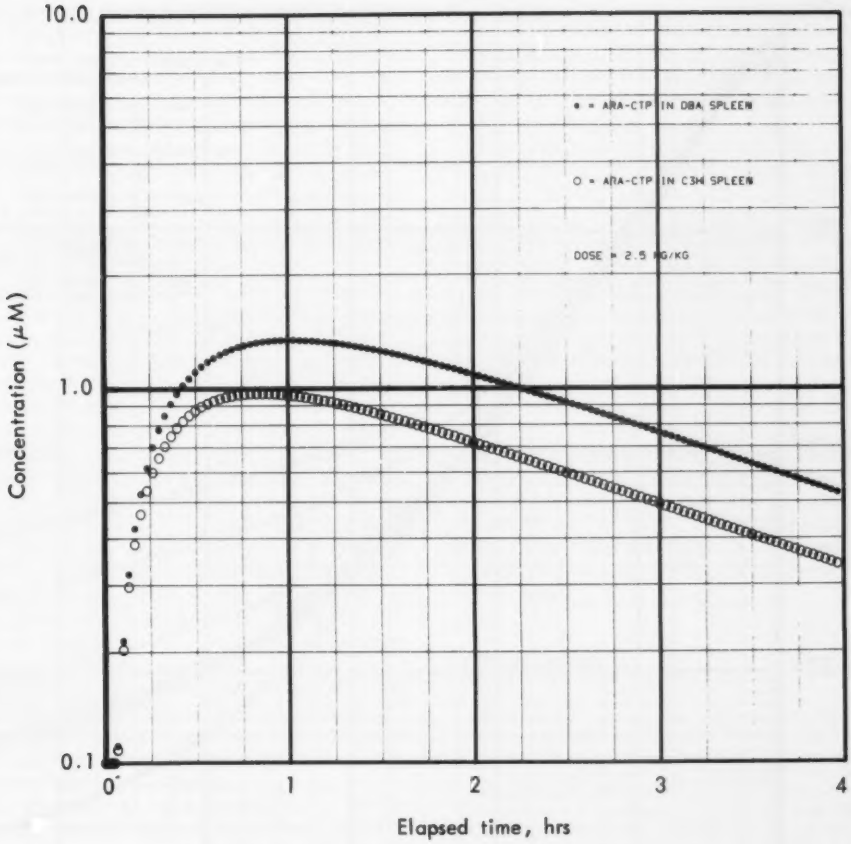

FIGURE 9.—Ara-CTP concentration in spleen for DBA and C3H mice.

to use ara-C and ara-CTP concentrations in the actual organ region of concern, rather than estimating drug concentrations for all compartments from blood serum levels. Finally, unlike earlier models, the present pharmacokinetic model allows one to more accurately investigate the case where tumors may be present in an organ region. The cells comprising this tumor generally have different deoxycytidine kinase and deaminase activities than the cells normally present in the tumor region, and these differences will lead to much different ara-C and particularly ara-CTP exposures. This can be handled to first order by simply changing the enzyme activity parameters of the model.

Development of the nucleotide-dependent pharmacokinetic model has shown us where our kinetic parameters are not well known, how they interact, and what experiments might be undertaken to improve the situation. An area of principal importance is the more accurate determination of the kinetics of dephosphorylation of ara-CTP, since this directly governs the length of exposure. From equation (2) one may derive an expression for the half-life of ara-CTP: half-life $= K_{dp}(1+ \alpha_2+ \alpha_1 \alpha_2)$ $(\ln 2)/V_{dp}$. It is apparent that this half-life depends on both the phosphatase activity, V_{dp}, and the ara-C nucleotide ratios, α_1 and α_2. Errors in these parameters are thus additive in their effects on the actual value of the half-life. There is evidence from Chou et al (4) and from Schrecker et al (19) that the nucleotide ratios employed in this modeling, particularly α_2, may be high. However, if the half-life is to remain relatively unchanged in order to keep the DNA synthesis rate depressed for as long as Chou has measured in liver (*see* fig 7 and Results section), the phosphatase activity would also have to be lowered. Hence an experiment that measures *both* ara-C nucleotide levels and phosphatase activities in different tissue types should provide us with the best kind of data to improve our half-life calculation.

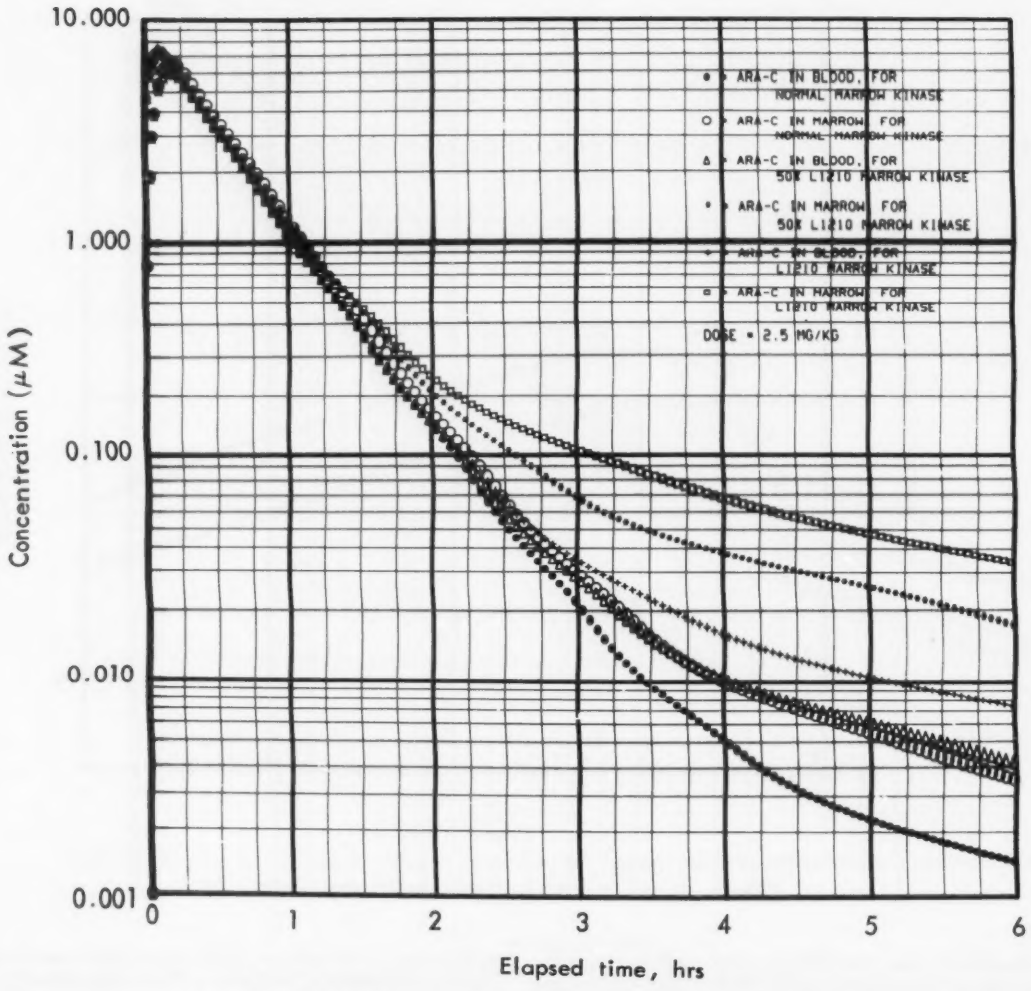

FIGURE 10.—Ara-C concentration in blood and marrow for DBA mice.

Chou et al (4) have stated that ara-UMP is a significant fraction of the ara-C mononucleotides in the blood, liver, and intestinal tissues of the mouse. If the presence of ara-UMP is confirmed at these high levels (in the range of 0.5 μM) in future experiments, reactions describing the production of this nucleotide will have to be added to the present model. Unfortunately, the route(s) by which ara-UMP is formed has not been fully clarified, and further experiments are needed. Two possible routes are: *(a)* by deamination of ara-CMP by deoxycytidylate (dCMP) deaminase, and *(b)* by phosphorylation of ara-U by deoxythymidine (TdR) kinase, but neither route is completely consistent with available data. In order for dCMP deaminase to be the active enzyme, significant activity of deoxycytidine kinase must be present in a tissue to form the ara-CMP substrate. Yet Chou found ara-UMP in all murine blood fractions and presumably in muscle, sites where Ho (10) or Durham and Ives (11) found little or no kinase activity in previous studies. Relatively high kinase levels have been found in human muscle (10), however, and reinvestigation of murine muscle could possibly reveal deoxycytidine kinase activities that, when combined with dCMP deaminase activities, are sufficiently high enough to produce Chou's ara-UMP levels.

The possibility of producing ara-UMP by TdR kinase phosphorylation of ara-U requires that ara-U first be formed by pyrimidine deaminase. If, how-

ever, the lean (muscle) compartment produces the levels of ara-UMP indicated by Chou, the total mass of ara-U derivatives in an anatomic region this large (nearly two thirds of the entire pharmacokinetic volume) would require that pyrimidine deaminase activities be increased greatly over present model values in order to produce this mass of ara-U in only 60 minutes. A very approximate simulation has shown that if only liver deaminase activity were changed, the activity would have to be increased from the DBA value of 16.45 to about 260 μM/minute (clearance rates would drop slightly to 0.46). The curves for $V_{dp} = 300$ μM/minute in figure 6 can be reproduced closely with these values.

The present results have shown that noticeable differences may arise in ara-C and ara-CTP concentrations in the organ regions of mice of different strains. For the 2.5-mg/kg dose in figure 9, the C3H ara-CTP concentration remains above 1 μM (taken here as an approximate lower cytotoxic level [4]) for nearly 2 hours while the DBA concentration never exceeds this value.

These kinds of differences, which may significantly change total exposure to cytotoxic levels of drug, suggest that the prevalence of interstrain enzyme variations be more fully investigated. For instance, the parameters of table 2 very accurately reproduce the serum ara-C curves of Borsa et al (5) obtained in AKR/J mice. However, if AKR/J mice have a liver deaminase level similar to the value for C3H mice and not DBA mice shown in table 2, a reasonably good reproduction of the serum curve may also be made by reducing the clearance value to about 0.2 ml/minute. Until pyrimidine deaminase activities are determined in AKR/J livers, we will not know which of these two possibilities is correct.

Ultimately, the murine pharmacokinetic model will be scaled for human application. Certain differences between the murine and human models have already become apparent. First, the deoxycytidine kinase and especially the pyrimidine deaminase activities are higher in human marrow relative to other organ sites than in the murine system (10). The marrow and variations in marrow activities will thus become a more important determinant of ara-C metabolism in the whole-body model. Secondly, the pyrimidine deaminase Michaelis constant is considerably lower in man (3), greatly increasing the importance of deoxycytidine and cytidine as inhibitors and requiring more accurate treatment of their inhibition than in the mouse. Particularly since deoxycytidine is also an inhibitor of deoxycytidine kinase, human application of this model will require that these two nucleoside concentrations be experimentally determined by tissue type.

The pharmacokinetic model described in this paper is currently being extended to include a peritoneal cavity, thereby allowing simulation of an L1210 tumor in that compartment. Perfusion of a tumor-laden peritoneum is not high, however, and thus an accurate kinetic description of the drug transport involved must be developed. Once present, the peritoneal cavity can be used to investigate the ara-CTP time history in both ara-C-sensitive and -resistant L1210 cells. Some work is also proceeding on more detailed modeling of ara-UMP production, assuming that high ara-UMP levels will continue to be found in murine tissues by other investigators, and assuming that it is produced by one of the two biochemical pathways discussed above.

In a preliminary study of toxicity, we have modeled Skipper's LD10 single dose of 3000 mg/kg. The increase in the exposure to ara-CTP above that achieved by a dose of 200 mg/kg is only 2 hours (see fig 1). The formation of ara-CTP is limited by the saturability of the kinase. The rapid clearance of ara-C together with the rate limitation imposed by kinase appears to protect the animal from a single dose unless that dose becomes so large that extreme physiologic effects not treated in this work come into play.

In summary, we have shown that the kinetics of ara-C and ara-CTP in vivo are quite different, and thus that the use of ara-C concentrations to predict states of the ara-CTP-dependent properties of toxicity or DNA inhibition can lead to large errors. The parameters of an ara-C nucleotide pharmacokinetic model have been described, as well as the need for various experimental data to improve the accuracy of the model.

REFERENCES

1. Bischoff KB, Dedrick RL, Zaharko DS, et al. Methotrexate pharmacokinetics. J Pharm Sci 60:1128-1133, 1971.
2. Dedrick RL, Forrester DD, and Ho DHW. In vitro-in vivo correlation of drug metabolism—deamination of 1-β-D-arabinofuranosylcytosine. Biochem Pharmacol 21:1-16, 1972.
3. Dedrick RL, Forrester DD, Cannon JN, et al. Pharmacokinetics of 1-β-D-arabinofuranosylcytosine (Ara-C) deamination in several species. Biochem Pharmacol 22:2405-2417, 1973.
4. Chou T-C, Hutchison DJ, Schmid FA, et al. Metabolism and selective effects in 1-β-D-arabinofuranosylcytosine in L1210 and host tissues in vivo. Cancer Res 35:225-236, 1975.
5. Borsa J, Whitmore GF, Valeriote FA, et al. Studies on the persistence of methotrexate, cytosine arabinoside and leucovorin in serum of mice. J Natl Cancer Inst 42:235-242, 1969.
6. Skipper HE, Schabel FM, Jr, Mellett LB, et al. Implications of biochemical, cytokinetic, pharmacologic, and toxicologic relationships in the design of optimal therapeutic schedules. Cancer Chemother Rep 54:431-450, 1970.
7. Momparler RL. Inhibition of cytotoxic action of 1-β-D-arabinofuranosylcytosine on S-phase HeLa cells by 5-fluorodeoxyuridine. Cancer Res 33:1754-1758, 1973.
8. Graham FL, and Whitmore GF. The effect of 1-β-D-arabinofuranosylcytosine on growth, viability, and DNA synthesis of mouse L-cells. Cancer Res 30:2627-2635, 1970.
9. Ho DHW, and Frei E, III. Clinical pharmacology of 1-β-D-arabinofuranosylcytosine. Clin Pharmacol Ther 12:944-954, 1971.
10. Ho DHW. Distribution of kinase and deaminase of 1-β-D-arabinofuranosylcytosine in tissues of man and mouse. Cancer Res 33:2816-2820, 1973.
11. Durham JP, and Ives DH. Deoxycytidine kinase. I. Distribution in normal and neoplastic tissues and interrelationships of deoxycytidine and 1-β-D-arabinofuranosylcytosine phosphorylation. Mol Pharmacol 5:358-375, 1969.
12. Momparler RL, and Fischer GA. Mammalian deoxynucleoside kinases. I. Deoxycytidine kinase: purification properties, and kinetic studies with cytosine arabinoside. J Biol Chem 243:4298-4304, 1968.

13. Sugino Y, Teraoka H, and Shimono H. Metabolism of deoxyribonucleotides. Purification and properties of deoxycytidine monophosphokinase of calf thymus. J Biol Chem 241:961-969, 1966.
14. Schrecker AW. Metabolism of 1-β-D-arabinofuranosylcytosine in leukemia L1210: nucleoside and nucleotide kinase in cell-free extracts. Cancer Res 30:632-641, 1970.
15. Nakamura H, and Sugino Y. Metabolism of deoxyribonucleotides. Purification and some properties of nucleoside diphosphokinase of calf thymus. J Biol Chem 241:4917-4922, 1966.
16. Tseng JK, and Gurpide E. Compartmentalization of uridine and uridine 5'-monophosphate in rat liver slices. J Biol Chem 248:5634-5640, 1973.
17. Camiener GW, and Smith CG. Studies of the enzymatic deamination of cytosine arabinoside-I. Biochem Pharmacol 14:1405, 1965.
18. Maley GF, and Maley F. Nucleotide interconversions in embryonic and neoplastic tissues, I. J Biol Chem 234:2975, 1959.
19. Schrecker AW, and Urshel MJ. Metabolism of 1-β-D-arabinofuranosylcytosine in leukemia L1210: studies with intact cells. Cancer Res 28:793-801, 1968.
20. Camiener GW. Studies of the enzymatic deamination of cytosine arabinoside. II. Properties of the deaminase of human liver. Biochem Pharmacol 16:1681-1689, 1967.
21. Momparler RL, Brent TP, Labitan A, et al. Studies on the phosphorylation of cytosine arabinoside in mammalian cells. Mol Pharmacol 7:413-419, 1971.
22. Dixon M, and Webb EC. Enzymes, 2nd ed. New York, Academic Press, 1964.
23. Schrecker AW, Mead JAR, and Urshel MJ. Isolation and antileukemic activity in mice of arabinofuranosylcytosine-5'-phosphate present in synthetic 5'-cytidylic acid. Biochem Pharmacol 15:1443-1452, 1966.
24. Creasey WA. Studies on the metabolism of 5-iodo-2'-deoxycytidine in vitro. Purification of nucleoside deaminase from mouse kidney. J Biol Chem 238:1772-1736, 1963.
25. Nordenskjold BA, Skoog L, Brown C, et al. Deoxyribonucleotide pools and deoxyribonucleic acid synthesis in cultured mouse embryo cells. J Biol Chem 245:5360-5368, 1970.
26. Bray G, and Brent TP. Deoxyribonucleoside 5'-triphosphate pool fluctuations during the mammalian cell cycle. Biochim Biophys Acta 269:184-191, 1971.
27. Weber MJ, and Edlin G. Phosphate transport, nucleotide pools, and ribonucleic acid synthesis in growing and in density-inhibited 3T3 cells. J Biol Chem 246:1828, 1971.
28. Rotherham J, and Schneider WC. Deoxyribosyl compounds in animal tissues. J Biol Chem 232:853-1833, 1958.
29. Dedrick RL, Zaharko DS, and Lutz RJ. Transport and binding of methotrexate in vivo. J Pharm Sci 62:882-890, 1973.
30. Bhuyan BK, Fraser T, Gray L, et al. Cell-kill kinetics of several S-phase-specific drugs. Cancer Res 33:888-894, 1973.
31. Neil GL, and Bhuyan BK. The utility and limitations of age-response curves in the design of effective dose schedules—studies in L1210 leukemia. *In* Proceedings of the Tumor Cell Kinetics and Chemotherapy Workshop, Radiobiological Institute TNO, Ryswijk, Netherlands, 1974, p 17.

Human Pharmacokinetic Model for Isophosphamide (NSC-109724)[1]

Larry M. Allen and Patrick J. Creaven[2,3]

Isophosphamide and the more well-known cyclophosphamide[4] (fig 1) are in a class of widely used cancer chemotherapeutic agents known as oxazaphosphorine nitrogen mustards. These compounds were developed in Germany nearly 20 years ago with two major objectives in mind (1). One objective was to reduce the reactivity of the β-chloroethyl side chain of the nitrogen mustards by reducing the nucleophilicity of the nitrogen through substitution of a strongly electrophilic group for the methyl of mechlorethamine.[5] The reduction in reactivity so produced was demonstrated by Brock who showed that the release of chloride ions after 24 hours in bicarbonate buffer was 1.02 mol/mol for *nor*-nitrogen mustard[6] but only 0.19 mol/mol for cyclophosphamide; the corresponding figure for isophosphamide was 0.06 mol/mol (2). The other objective was to synthesize a transport-carrier form of the nitrogen mustards because at that time it was thought that tumor cells had higher levels of phosphatases and phosphoamidases than normal tissue (3) and that by a process of enzymatic hydrolysis *nor*-nitrogen mustard would be preferentially released within the tumor cells, a form of lethal synthesis. Cyclophosphamide is in fact inherently inactive against tumor tissue in vitro. Against Yoshida ascites sarcoma for example, concentrations of more than 1 mg/ml of cyclophosphamide are required for an EC50, whereas less than 0.1 mg/ml is required for an EC50 with mechlorethamine (4). Instead, activation was found to occur predominantly in the liver by the mixed function oxidase system which is responsible for metabolism of other drugs (5-18). Several investigators have shown that the enzymatic activation of cyclophosphamide follows the reaction scheme shown in figure 2 (13,15-25). The initial oxidation occurs at the 4-position on the oxazaphosphorine ring with a subsequent ring opening to aldophosphamide, a cytotoxic product. Two other cytotoxic products which can also arise from aldophosphamide are acrolein (26,27) and *N,N*-bis(2-chloroethyl)phosphorodiamidic acid (19,28).

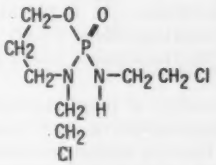

IFOSFAMIDE

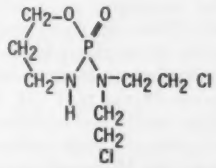

CYCLOPHOSPHAMIDE

FIGURE 1.—Chemical structures of ifosfamide (isophosphamide) and cyclophosphamide.

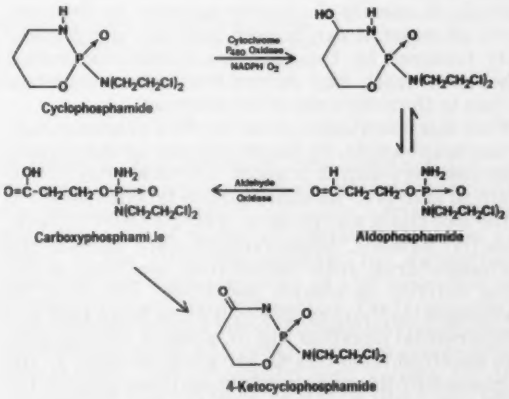

FIGURE 2.—Proposed route of cyclophosphamide metabolism (from refs 13,15-25).

Isophosphamide is a newer oxazaphosphorine which has been found to be superior to cyclophosphamide in several animal tumor systems, including

[1]Isophosphamide: CAS reg. No. 3778-73-2; 1,3,2-oxazaphosphorine, 3-(2-chloroethyl)-2-[(2-chloroethyl)amino]tetrahydro-, 2-oxide; ifosfamide.

[2]National Cancer Institute-Veterans' Administration (NCI-VA) Medical Oncology Branch, VA Hospital, Washington, DC.

[3]*Reprint requests to:* Larry M. Allen, PhD, NCI-VA Medical Oncology Branch, VA Hospital, 50 Irving St, NW, Washington, DC 20422.

[4]Cyclophosphamide: NSC-26271; CAS reg. No. 6055-19-2; 2*H*-1,3,2-oxazaphosphorine, 2-[bis(2-chloroethyl)amino]tetrahydro-, 2-oxide, monohydrate.

[5]Mechlorethamine: NSC-762; CAS reg. No. 55-86-7; diethylamine, 2,2'-dichloro-*N*-methyl-, hydrochloride; nitrogen mustard.

[6]*Nor*-nitrogen mustard: NSC-10873; CAS reg. No. 821-48-7; diethylamine, 2,2'-dichloro-, hydrochloride.

a highly chemotherapy-resistant DS-carcinosarcoma (29). There was also a suggestion that isophosphamide might be somewhat more active than cyclophosphamide in small-cell carcinoma of the lung in man (30). Early clinical trials of isophosphamide in the United States, Europe, and South Africa (30-32) revealed two major differences between isophosphamide and cyclophosphamide from a pharmacologic point of view, namely, that the moderately toxic dose of isophosphamide was approximately three to four times that of cyclophosphamide and that its major dose-limiting toxicity was in the kidney and bladder whereas that of cyclophosphamide was generally myelosuppression. As a result, we initiated pharmacologic investigations which were designed to elucidate the pharmacologic basis for these clinical observations.

In our initial studies of isophosphamide, we found that this oxazaphosphorine was also principally activated by the hepatic mixed function oxidase system and that only after microsomal activation did isophosphamide undergo classic alkylating reactions (33-36). For example, only after activation would it react with DNA (35, fig 3) and with proteins (36). The activation of isophosphamide behaves according to simple Michaelis-Menten kinetics as seen from the Lineweaver-Burke plot (34, fig 4). In figure 4 it can be seen that while the maximal velocities of activation of cyclophosphamide and isophosphamide are about the same, the Michaelis constant (K_m) for the two drugs differs by a factor of 5 (34). We have conjectured that the reason for this difference in substrate concentration for half maximal velocity is the presence of the bulky chloroethyl group on the endocyclic nitrogen of isophosphamide (34). If we assume that the site of initial enzymatic attack on isophosphamide is the same as for cyclophosphamide (fig 2), namely the carbon adjacent to the endocyclic nitrogen, it can be seen that this site is sterically hindered by the presence of the chloroethyl side chain which may reduce the approach of this carbon to the active site of the enzyme.

With this knowledge of the in vitro pharmacology of isophosphamide, we began a study of the clinical pharmacology during a phase I clinical trial of this agent in man (37). Isophosphamide labelled with ^{14}C in the side chain was given as a single short intravenous (iv) infusion. Measurements were made of the unchanged drug, total metabolites, and total alkylating activity in plasma and urine. The decay of unchanged isophosphamide in plasma fitted best to a biexponential equation (fig 5); some of the parameters obtained from this fit are given in table 1. The β-phase half-lives are two to three times greater for isophosphamide than for cyclophosphamide (38-40). Using the values for A, α, B, and β in table 1, we calculated the transfer constants for a two-compartment open model as was done for cyclophosphamide by Cohen et al (39). Table 2 shows the comparison of the two sets of results. A number of the parameters including the volumes of the central compartment, the elimination rate constant, and the pseudo-metabolic rate constant are markedly different for the two drugs. These differences were interesting enough for us to pursue the development of a multicompartment model for isophosphamide which includes a term for metabolism based on our in vitro investigations.[7]

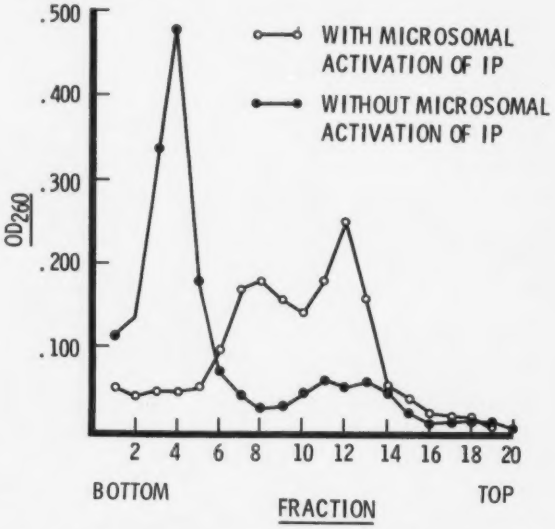

FIGURE 3.—Effect of microsomal activation of isophosphamide (IP) on calf thymus DNA showing sucrose zone sedimentation of calf thymus DNA as described (from ref 35).

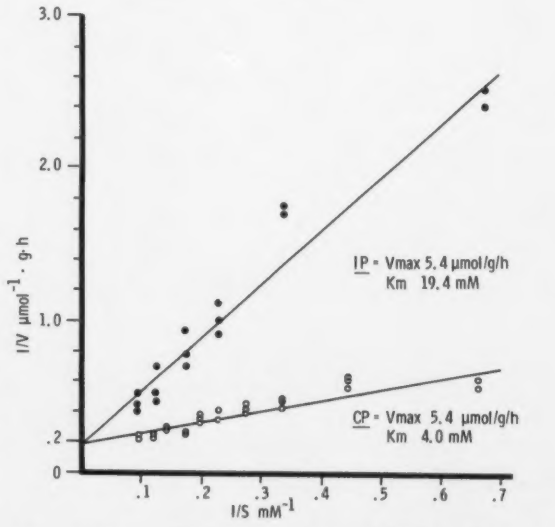

FIGURE 4.—Lineweaver-Burke plot of the activation of isophosphamide (IP) and cyclophosphamide (CP) as described (from ref 34).

[7]Allen LM, and Creaven PJ. A pharmacokinetic model for ifosfamide in man. Presented at the 11th International Cancer Congress, Florence, 1974.

TABLE 1.—Pharmacokinetic constants describing serum concentrations of isophosphamide after its iv infusion in man*

Constant†	Serum concentration in patient No.—‡				
	1	2	3	4	5
A, μg/ml	34.99 (7.60)	66.24 (16.69)	50.00 (20.53)	118.31 (10.93)	149.97 (7.00)
α, hr^{-1}	0.65 (0.16)	0.60 (0.34)	0.60 (0.29)	0.49 (0.12)	0.29 (0.02)
B, μg/ml	124.47 (4.04)	145.50 (17.75)	192.60 (11.17)	146.02 (11.05)	100.40 (7.04)
β, hr^{-1}	0.040 (0.003)	0.067 (0.010)	0.047 (0.004)	0.051 (0.005)	0.035 (0.003)
$\beta_{t1/2}$, hr	17.33	10.34	14.74	13.59	19.80

*Distribution and elimination constants for unchanged isophosphamide in serum of these 5 patients determined from the biexponential decay function for plasma.
†From nonlinear least squares fit of $Ae^{-\alpha T} + Be^{\beta T}$.
‡Nos. in parentheses = ± SE.

TABLE 2.—Comparison of pharmacokinetic parameters for cyclophosphamide and isophosphamide

Parameters	Cyclophosphamide* (mean ± SD)	Isophosphamide (mean ± SD)
Distribution		
V_c, liters	21.6 ± 6.3	34.0 ± 2.5
K_{12}, hr^{-1}	2.9 ± 1.5	0.14 ± 0.04
K_{21}, hr^{-1}	4.2 ± 2.5	0.37 ± 0.16
Elimination		
K_{el}, hr^{-1}	0.29 ± 0.11	0.07 ± 0.02
k_m, † hr^{-1}	0.26 ± 0.10	0.03 ± 0.01
Cl, ml/min	10.7 ± 3.3	16.5 ± 8.0

*From ref 39.
†This is a hybrid metabolic rate constant as used by Cohen et al (39) and is distinguished from K_m, the Michaelis constant, as used elsewhere; k_m is derived from the Michaelis-Menten equation where K_m is assumed to be >> substrate concentration, therefore, $k_m = V_{max}/K_m$. The k_m derived from our nonlinear model is 0.034 (± 0.013).

Our working model is shown in figure 6. This model is described by the equations in figure 7. The first three equations were fitted simultaneously to unchanged isophosphamide in plasma and urine expressed as percent of dose. The transfer constants for these three equations were then held constant and the data for total metabolite (in plasma and urine) were then fitted to the remaining three equations. In order to adequately fit the data to the model, it was necessary to introduce an irreversible transfer factor (K_x) representing loss of radioactivity, either from its conversion to a volatile material or alkylation of the renal tract. The volume of distribution of the metabolites in plasma was also used as a parameter. We found the transfer constants for the distribution of metabolites to peripheral space to be on the order of 0.001 hour^{-1}. The parameters derived from fitting the model to the data are shown in table 3. The excretion rate constant for unchanged drug is small and relatively invariant; that for metabolite is larger but quite variable. There was also a large degree of variation between patients in the Michaelis constant for metabolism. Some further characteristics of the model for unchanged drug are shown in table 4. The large central compartment volume for unchanged isophosphamide represents plasma and easily perfused tissue space whereas the central compartment volume for the metabolites was found to be 2.8-7.5 liters and indicates limited diffusion from plasma. As shown in table 4, we found excellent agreement between the percent of metabolite recovered in the urine and that predicted by the model. The agreement between the data and the model is shown in figures 8A and 8B for unchanged drug and metabolite. In addition, we found that the concentration of isophosphamide in

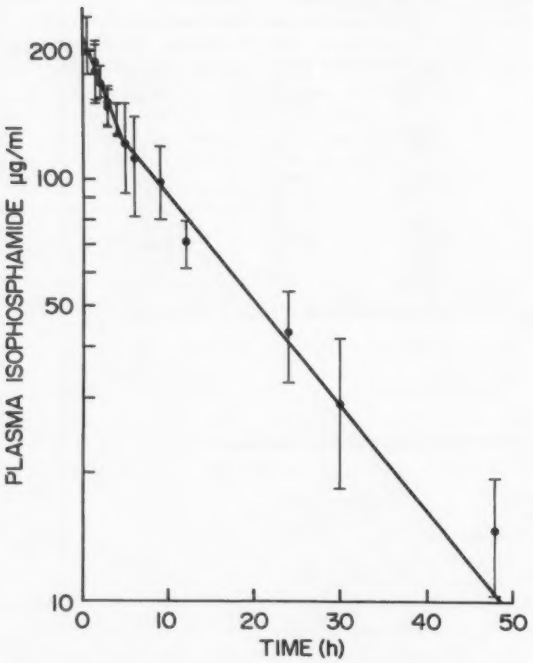

FIGURE 5.—Plasma decay of isophosphamide in patients receiving 5 g/m². Each point (•) represents a mean from 5 patients ± SD (from ref 37).

the cerebrospinal fluid in two patients agreed closely with the concentration predicted from the model to be in the peripheral space.

This model is now being used in our laboratory to predict plasma levels after repeat fractional doses of isophosphamide and to assess the influence of other drugs on the pharmacokinetics of isophosphamide.

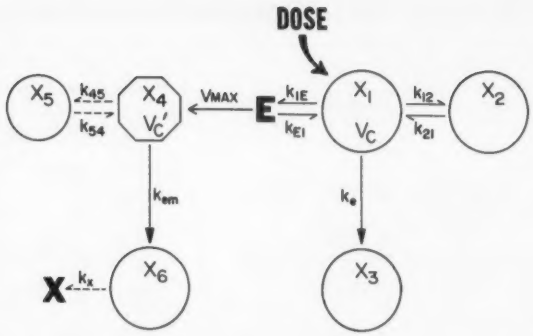

FIGURE 6.—Multicompartment pharmacokinetic model. X_1 and X_4, central compartments; X_3 and X_6, urine; and X_2 and X_5, peripheral compartments for isophosphamide and metabolite(s) respectively. V_{max} and k_{1E} and k_{E1} are constants for metabolism where E is the substrate-enzyme complex; k_x is the transfer rate constant (hr^{-1}) for irreversible biologic alkylation or drug decomposition; k_{ij} (i = 1,2,3...n, j = 1,2,3...m) are transfer rate constants (hr^{-1}) for drug transport into compartment j from compartment i. V_c and $V_{c'}$ are volumes of the central compartment for isophosphamide and metabolite(s) respectively.

$$\frac{dX_1}{dT} = k_{21} \cdot X_2 - (k_e + k_{12}) \cdot X_1 - \frac{V_M \cdot X_1}{K_M + X_1}$$

$$\frac{dX_2}{dT} = k_{12} \cdot X_1 - k_{21} \cdot X_2$$

$$\frac{dX_3}{dT} = k_e \cdot X_1$$

$$\frac{dX_4}{dT} = \frac{V_M \cdot X_1}{K_M + X_1} - (k_{em} + k_{45}) \cdot X_4 + k_{54} \cdot X_5$$

$$\frac{dX_5}{dT} = k_{45} \cdot X_4 - k_{54} \cdot X_5$$

$$\frac{dX_6}{dT} = k_{em} \cdot X_4 - k_x \cdot X_6$$

FIGURE 7.—Differential equations used for model shown in fig 6 where K_m is the Michaelis-Menten constant.

TABLE 3.—Summary of pharmacokinetic parameters for a multicompartmental model of isophosphamide in man*

Parameters	Patient No. and dose (mg)				
	1 (5320)	2 (6750)	3 (7750)	4 (9200)	5 (9500)
K_{12}, hr^{-1}	0.100 (0.010)	0.166 (0.040)	0.150 (0.024)	0.175 (0.12)	0.064 (0.008)
K_{21}, hr^{-1}	0.306 (0.053)	0.297 (0.104)	0.655 (0.142)	0.353 (0.041)	0.120 (0.035)
K_e, hr^{-1}	0.024 (0.001)	0.041 (0.003)	0.034 (0.001)	0.037 (0.001)	0.064 (0.002)
V_{max}, mg/ml/hr	0.022 (0.002)	0.041 (0.002)	0.017 (0.002)	0.008 (0.001)	0.024 (0.003)
K_m, mg/ml	1.040 (0.005)	0.965 (0.003)	0.711 (0.007)	0.151 (0.005)	0.808 (0.010)
K_{em}, hr^{-1}	8.92 (0.42)	0.662 (0.249)	0.134 (0.087)	18.27 (0.31)	3.62 (0.59)
k_x, hr^{-1}	0.007 (0.001)	0.007 (0.001)	0.008 (0.005)	0.006 (0.002)	0.006 (0.002)

*All values are followed by ± SE in parentheses.

TABLE 4.—Summary of pharmacokinetic parameters for isophosphamide in man

Parameters	Patient No. and body weight (kg)				
	1 (50)	2 (48)	3 (44)	4 (74)	5 (77)
Compartment volume (liters)					
Central (V_c)	33.4	31.9	32.0	34.8	37.9
Peripheral	10.9	17.9	7.3	17.3	20.2
Urine excretion, 72 hrs (%)*					
Isophosphamide (found)	47.7 (49.3)	47.7 (48.1)	57.1 (60.9)	41.1 (41.9)	66.0 (65.2)
Metabolites (found)	29.8 (30.1)	36.3 (33.5)	23.5 (24.0)	26.8 (27.8)	20.5 (20.1)
Renal clearance, Cl (ml/min)†	8.3	12.8	13.3	19.0	29.1

*Nos. in parentheses are percentages actually recovered; those preceding parentheses are percentages predicted by the model.

†This was determined experimentally from the slope of the line for the excretion rate plotted against the actual or interpolated plasma concentration at the midpoints of the urine excretion interval.

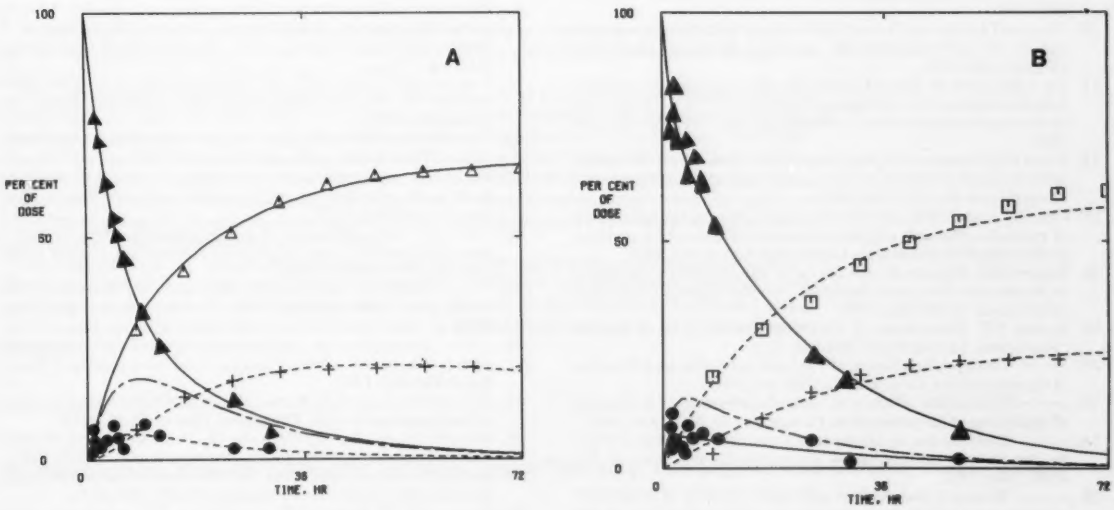

FIGURE 8.—Plots of percent of dose of isophosphamide or its metabolite(s) in the respective compartments of the pharmacokinetic model. A. Data points for patient No. 5 (9500 mg) were obtained experimentally from serum concentrations (▲) of isophosphamide and its metabolite(s) (●), and from urinary excretion rates (△) of isophosphamide and its metabolite(s) (+). (—) = theoretical levels of the drug in peripheral compartment X_2 of the model (see fig 6). B. Same as A but for patient No. 3 (7750 mg) where □= data points for isophosphamide in urine.

REFERENCES

1. Arnold H, and Bourseaux F. Synthese und Abbau cytostatisch wirksamer cyclischer *N*-Phosphamidester des Bis-(β -chlorathyl)-amins. Angew Chem 70:539-544, 1958.
2. Brock N. New *N*-mustard phosphamide ester compounds with cytostatic activity. *In* Proceedings of the 5th International Congress of Chemotherapy. Vienna, Verlag der Wiener Medizinischen Akademie, 1967, vol 2, p 45-51.
3. Gomori G. Histochemical demonstration of sites of phosphamidase activity. Proc Soc Exp Biol Med 69:407-409, 1948.
4. Brock N. Pharmacological studies with ifosfamide—a new oxazaphosphorine compound. *In* Advances in Antimicrobial and Antineoplastic Chemotherapy (Proceedings of the 7th International Congress of Chemotherapy, Prague, 1971) (Hejzlar M, Semonsky M, and Masak S, eds). Munich, Urban und Schwarzenberg, 1972.
5. ———.Pharmacologic characterization of cyclophosphamide (NSC-26271) and cyclophosphamide metabolites. Cancer Chemother Rep 51:315-325, 1967.
6. Brock N, and Hohorst HJ. Über die Aktivierung von Cyclophosphamid in Vivo and in Vitro. Arzneim Forsch 13:1021-1031, 1963.
7. ———. Metabolism of cyclophosphamide. Cancer 20:900-904, 1967.
8. Cohen JL, and Jao JY. Enzymatic basis of cyclophosphamide activation by hepatic microsomes of the rat. J Pharmacol Exp Ther 174:206-210, 1970.
9. Connors TA, Foster AB, Gilsenan AM, et al. Observations of the metabolism of cyclophosphamide. Biochem Pharmacol 21:1373-1376, 1972.
10. Connors TA, Grover PL, and McLoughlin AM. Microsomal activation of cyclophosphamide in vivo. Biochem Pharmacol 19:1533-1535, 1970.
11. Field RB, Gang M, Kline I, et al. The effect of phenobarbital or 2-diethylaminoethyl-2,2-diphenylvalerate on the activation of cyclophosphamide in vivo. J Pharmacol Exp Ther 180:475-483, 1972.
12. Foley GE, Friedman OM, and Droplet BP. Studies on the mechanism of action of Cytoxan: evidence of activation in vivo and in vitro. Cancer Res 21:57-63, 1961.
13. Hill DL, Laster WR, Jr. and Struck RF. Enzymatic metabolism of cyclophosphamide and nicotine and production of a toxic cyclophosphamide metabolite. Cancer Res 32:658-665, 1972.
14. Hohorst HJ, Ziemann A, and Brock N. Alkylierende Substanzen in Serum und Urin nach Injektion von Cyclophosphamid. Arzneim Forsch 15:432-434, 1965.
15. Sladek NE. Metabolism of cyclophosphamide by rat hepatic microsomes. Cancer Res 31:901-908, 1971.
16. ———. Therapeutic efficacy of cyclophosphamide as a function of its metabolism. Cancer Res 32:535-542, 1972.
17. ———.Therapeutic efficacy of cyclophosphamide as a function of inhibition of its metabolism. Cancer Res 32:1848-1854, 1972.
18. ———. Evidence for an aldehyde possessing alkylating activity as the primary metabolite of cyclophosphamide. Cancer Res 33:651-658, 1973.
19. ———. Bioassay and relative cytotoxic potency of cyclophosphamide metabolites generated in vitro and in vivo. Cancer Res 33:1150-1158, 1973.
20. Struck RF, and Hill DL. Investigation of the synthesis of aldophosphamide (AP), a toxic metabolite of cyclophosphamide (CTX), Proc Am Assoc Cancer Res 13:50, 1972.
21. Struck RF, Kirk MC, Mellett LB, et al. Urinary metabolites of the antitumor agent cyclophosphamide. Mol Pharmacol 7:519-529, 1971.
22. Takamizawa A, Tochino Y, Hamashima Y, et al. Studies on cyclophosphamide metabolites and their related compounds. I. Chem Pharm Bull (Tokyo) 20:1612-1616, 1972.
23. Bakke JE, Feil VJ, Fjelstul CE, et al. Metabolism of cyclophosphamide by sheep. J Agric Food Chem 20:384-388, 1972.
24. Bakke JE, Feil VJ, and Zaylskie RG. Characterization of the major sheep urinary metabolites of cyclophosphamide, a defleecing chemical. J Agric Food Chem 19:788-790, 1971.
25. Hohorst HJ, Ziemann A, and Brock N. 4-Ketocyclophosphamide, a metabolite of cyclophosphamide. Formation, chemical and biological properties. Arzneim Forsch 21:1254-1257, 1971.
26. Alarcon RA, and Meienhofer J. Formation of the cytotoxic aldehyde acrolein during in vitro degradation of cyclophosphamide. Nature [New Biol] 233:250-252, 1971.
27. Alarcon RA, Meienhofer J, and Atherton E. Isophosphamide as a new acrolein-producing antineoplastic isomer of cyclophosphamide. Cancer Res 32:2519-2523, 1972.
28. Colvin M, Padgett CA, and Fenselau C. A biologically active metabolite of cyclophosphamide. Cancer Res 33:915-918, 1973.
29. Brock N. Pharmacologische untersuchungen mit neun N-chloroathylphosphoraureester-diamiden. *In* Proceedings of the 5th International Congress of Chemotherapy (Spitky KH, and Haskek H, eds). Vienna, Verlag der Wiener Medizinischen Akademie, 1967, vol 2, p 1155.
30. Scheef W. Problems, experience, and results of clinical investigations with ifosfamide. *In* Advances in Antimicrobial and Antineoplastic Chemotherapy (Proceedings of the 7th International Congress of Chemotherapy, Prague, 1971) (Hejzlar M, Semonsky M, and Masak S, eds). Munich, Urban und Schwarzenberg, 1972.
31. Van Dyk JJ, Falkson HC, van der Merwe AM, et al. Unexpected toxicity in patients treated with iphosphamide. Cancer Res 32:921-924, 1972.
32. Cohen MH, and Mittelman A. Initial clinical trials with isofosfamide. Proc Am Assoc Cancer Res 14:64, 1973.
33. Allen LM, and Creaven PJ. Activation of the antineoplastic drug isophosphamide by rat liver microsomes. J Pharm Pharmacol 24:585-586, 1972.
34. ———. In vitro activation of isophosphamide (NSC-109724), a new oxazaphosphorine, by rat liver microsomes. Cancer Chemother Rep 56:603-610, 1972.
35. ———. Effect of microsomal activation on interaction between isophosphamide and DNA. J Pharm Sci 61:2009-2011, 1972.
36. ———. Interaction of mechlorethamine and isophosphamide with bovine serum albumin and rat liver microsomes. J Pharm Sci 62:854-856, 1973.
37. Creaven PJ, Allen LM, Alford DA, et al. Clinical pharmacology of isophosphamide. Clin Pharmacol Ther 16:77-86, 1974.
38. Mellett LB, el - Dareer SM, Luce JK, et al. Activation of cyclophosphamide in various species. Pharmacologist 11:273, 1969.
39. Cohen JL, Jao JY, and Jusko WJ. Pharmacokinetics of cyclophosphamide in man. Br J Pharmacol 43:677-680, 1971.
40. Bagley CM, Jr, Bostick FW, and DeVita VT, Jr. Clinical pharmacology of cyclophosphamide. Cancer Res 33:226-233, 1973.

ANNOUNCEMENTS

Medical Oncology Course

The University of Texas System Cancer Center M. D. Anderson Hospital and Tumor Institute at Houston
in cooperation with The University of Texas Health Science Center at Houston, Division of Continuing Education

September 8, 9, and 10, 1975

This comprehensive intensive course is designed to review current concepts of the natural history, diagnosis, therapy, and clinical management of the spectrum of malignant disease cared for by the medical oncologist. The course will consist of 24 hours of didactic lectures with time for discussion.

Your attention is directed to the revised dates of September 8, 9, and 10, 1975, for this course.

For further information write: **The Office of the Director, The University of Texas Health Science Center at Houston, Division of Continuing Education, PO Box 20367, Houston, Tex 77025.**

Memorial Sloan-Kettering Cancer Center Nursing Symposium

New York City, New York, September 3-5, 1975

An international symposium on nursing care of the patient with cancer, sponsored by the Memorial Sloan-Kettering Cancer Center (MSKCC), will be held at the Americana Hotel, New York City, New York, on September 3-5, 1975.

This symposium is designed for nurses and others involved in planning, managing, and providing care for patients with cancer. The 3-day seminar will highlight the emerging specialty of oncology nursing and will include: The Management of Families in Crisis; Helping the Child Cope With Cancer; Trends in the Diagnostic and Treatment Spectrum of Breast Cancer; The Multidisciplinary Approach to Rehabilitation; The Fourth Modality—Immunotherapy; New Hope for the Patient With Leukemia; Bone Marrow Transplantation; Improving the Quality of Life; Plastic and Prosthetic Reconstruction After Radical Surgery; The Integrated Patient Care Audit—The Consumer's Point of View.

The registration fee is $100.00; please include name and address (state or country) with a check for $100.00 (U.S.) for each registrant payable to MSKCC and forward to: MSKCC, Nursing Symposium, 850 3rd Ave, 21st floor, New York, NY 10022 (212 421-6900).Additional information and preview programs, as well as details on special hotel rates, may be obtained upon request.

Symposium on Modern Concepts in Brain Tumor Therapy: Laboratory and Clinical Investigation

Sheraton Biltmore, Atlanta, Georgia, February 26-28, 1976

This Symposium is sponsored by the Clinical Investigations Branch and the Cancer Clinical Investigation Review Committee of the National Cancer Institute. The program will include discussion of: Animal Models and Screening; Pharmacodynamics; Neuropathology; Multimodal Therapy and Unusual Methods of Treatment; Cooperative Clinical Trials; and Criteria of Evaluation and Problems of Analysis.

The Program Committee: Audrey E. Evans, **Children's Hospital of Philadelphia, Pa;** ***Cornelia Dettmer,*** **Christ Hospital, Cincinnati, Ohio;** ***Michael D. Walker,*** **Baltimore Cancer Research Center, Md;** ***Charles Wilson,*** **University of California at San Francisco; and** ***Giulio J. D'Angio,*** **Memorial Sloan-Kettering Cancer Center, New York, NY,** ***Chairman.***

This symposium is open to members of the medical and allied health professions. ***Advance registration requested, no registration fee.***

For information write to: **Audrey E. Evans, MD, The Children's Hospital of Philadelphia, One Children's Center 3400 Civic Center Blvd, Philadelphia, Pa 19104.**

Postgraduate Course on "Immunology for the Practicing Physician"

October 16-17, 1975, Kaiser Center Auditorium, Oakland, California

This course is designed to be the first in a yearly series to aquaint practicing physicians with the sometimes esoteric concepts of immunology. The presentations will be geared towards individuals who have limited experience with the vocabulary and general principles of immunology. The course will begin with very basic principles in immunology and progress through subjects of general interest to specific areas of new immunology research and how it relates to the physicians and their everyday practice of medicine. The course will end with discussions of representative cases of common diseases and the impact of immunologic evaluation of the ultimate establishment of a diagnosis and treatment.

This program is presented by the Department of Dermatology and Extended Programs in Medical Education, University of California School of Medicine, San Francisco and in cooperation with Western Pathology Laboratories, Oakland, California. It is acceptable for 21 hours of Category I credit towards the certificate in Continuing Education for the California Medical Association and the American Medical Association.

Registration will be on Thursday, October 16, 1975, at the Kaiser Center Auditorium, 300 Lakeside Drive, Oakland, California. The fee will be $100.00. For further information and applications for enrollment please contact Extended Programs in Medical Education, Rm C-135G, University of California, San Francisco, Calif 94143.

CORRECTION

Due to a printer's typographical error, an incorrect heading appears in table 3 of the article "Comparative Studies of Cyclocytidine (NSC-145668) and Cytosine Arabinoside (NSC-63878) in Mice" by Robert H. Liss and Gary L. Neil (Cancer Chemother Rep, Vol 57, No. 3, May/June 1975, p 514). The first group of numbers in the body of the table should be labeled *Cytosine arabinoside*. Only the second half of the table pertains to cyclocytidine.

U.S. DEPARTMENT OF
HEALTH, EDUCATION, AND WELFARE
PUBLIC HEALTH SERVICE
NATIONAL INSTITUTES OF HEALTH
BETHESDA, MARYLAND 20014

OFFICIAL BUSINESS
PENALTY FOR PRIVATE USE, $300

If your address has changed and you wish to continue receiving this publication, please check here , enclose old address from this publication, and fill in your new address below.

If you do not wish to continue receiving this publication, please check here and enclose your name and address from this publication. Clip out this notice and return to:

Cancer Chemotherapy Reports, National Cancer Institute, National Institutes of Health, Bethesda, Maryland 20014.

U.S. Department of Health, Education, and Welfare
Public Health Service **National Institutes of Health**
DHEW Publication No. 75-22